2018

Behaviour of high strength concrete (HSC) columns reinforced with steel equal angle (SEA) sections under different loading conditions

Ayoob Abbas Ibrahim
University of Wollongong

SCHOOL OF CIVIL, MINING AND ENVIRONMENTAL ENGINEERING

BEHAVIOUR OF HIGH STRENGTH CONCRETE (HSC) COLUMNS REINFORCED WITH STEEL EQUAL ANGLE (SEA) SECTIONS UNDER DIFFERENT LOADING CONDITIONS

A THESIS SUBMITTED IN FULFILMENT

OF THE REQUIREMENTS FOR THE AWARD OF THE DEGREE OF

DOCTOR OF PHILOSOPHY

BY

AYOOB ABBAS IBRAHIM

2018

ABSTRACT

The main objectives for the design of reinforced concrete (RC) columns are to satisfy strength and ductility requirements. High strength concrete (HSC) has been widely used in buildings, bridges and other structures due to its advantages over normal strength concrete (NSC). The use of HSC in lower storey RC columns of high rise buildings leads to the reduction of column sizes. However, the main problem associated with the use of HSC in the construction of RC columns is the lower ductility of the HSC column compared to the ductility of the NSC column for the same amount of confinement reinforcement. This is mainly because the ductility of the concrete decreases with the increase in the compressive strength. A new method of reinforcing concrete columns with steel equal angle (SEA) sections has been investigated in this study. For the same cross-sectional area, a SEA section has a higher second moment of area than a conventional steel bar, which leads to a higher bending stiffness of the SEA reinforced concrete member. In addition, the area of confined concrete is higher in SEA reinforced concrete members than in steel bar reinforced concrete members, which results in higher strength and ductility. It is noted that SEA sections have been extensively used in the construction of the steel structure. However, the influences of the SEA section as longitudinal reinforcement on the behaviour of square HSC columns have not been investigated yet. This study investigates experimentally and analytically the behaviour of square HSC columns reinforced longitudinally with SEA sections under different loading conditions.

The main experimental program of this study included the testing of 32 square high strength concrete (HSC) specimens subjected to different loading conditions. Also, 15 pullout test specimens were constructed to investigate the bond behaviour between reinforcing steel (steel bars and SEA sections) and surrounding concrete.

The experimental program included 32 square HSC specimens and was divided into two sets. The specimens in the first set of the experimental program were tested to investigate the behaviour of square HSC column specimens reinforced longitudinally with SEA sections under different loading conditions. The first set of the experimental program involved the testing of 20 square HSC specimens under concentric axial load, eccentric axial load and four-point bending. The specimens were reinforced longitudinally with either four N12 (12 mm diameter deformed steel) bars or four SEA sections and transversely with R10 (10 mm diameter plain steel) bars. The specimens were 210 mm × 210 mm square cross-section with 800 mm high. Fifteen specimens were tested under either concentric or eccentric axial load. The remaining five specimens were tested under four-point bending. The effects of the type of longitudinal reinforcement, the spacing of transverse reinforcement and loading condition on the behaviour of HSC specimens were investigated and discussed. In addition, analytical axial load-bending moment interactions of the tested specimens using the equivalent rectangular stress block and the layer-by-layer numerical integration methods were developed.

In the second set of the experimental program, the specimens were tested to evaluate the influence of the spacing of transverse ties on the performance of square HSC column

specimens reinforced longitudinally with SEA sections under axial compression. In this set of the experimental program, a total of 12 square HSC column specimens (210 mm sides and 600 mm height) reinforced longitudinally with either steel bars or SEA sections were cast and tested. The specimens were divided into three groups of four specimens. The specimens in the first group were reinforced longitudinally with four N12 (12 mm diameter) deformed steel bars. The specimens in the second group were reinforced longitudinally with four A30 SEA (29.1 mm × 29.1 mm × 2.25 mm) sections. The specimens in the third group were reinforced longitudinally with four A40 SEA (39.3 mm × 39.3 mm × 3.7 mm) sections. The lateral tie spacing in each group of specimens varied from 50 mm to 400 mm. The influences of the type of longitudinal reinforcement and the spacing of lateral ties on the behaviour of HSC specimens under axial compression were investigated. In addition, analytical axial load-axial deformation behaviours of the tested specimens were investigated and discussed.

The experimental results showed that the use of the SEA sections as longitudinal reinforcement in HSC column specimens led to significant improvements in the axial load carrying capacity and ductility compared to the corresponding HSC column specimens reinforced longitudinally with steel bars. Also, the use of the SEA sections as longitudinal reinforcement in HSC column specimens can reduce the need for a large amount of transverse ties in HSC columns. It has been found that the welding of small steel bar pieces at the ends of the SEA sections improved the pullout behaviour of SEA sections embedded in the HSC.

Analytical investigations were carried out to study the axial load-axial deformation and axial load-bending moment interactions of the HSC columns reinforced with SEA sections.The analytical axial load-axial deformation behaviours and axial load-bending moment interactions were in good agreement with the experimental results of the tested specimens.

ACKNOWLEDGEMENTS

I would like to express my gratitude to Associate Professor Muhammad N. S. Hadi and Associate Professor. M. Neaz Sheikh for their endless patience, continuous support and guidance during my study. I feel quiet lucky to have studied with them. I also want to thank Mr. Fernando Escribano, Mr. Ritchie Mclean and other technical staff for their help in the experimental program of this study.

I acknowledge the financial support from the Higher Committee for Education Development in Iraq for sponsoring my study at the University of Wollongong.

Finally, I would like to thank my wife Lina, my son Hussein and my daughters Fatimah and Rose and my son Mohammed for their love and continuous support and motivation during all stages of my PhD study.

LIST OF PUBLICATIONS

Journal Publications

1. Hadi, M. N. S., Ibrahim, A. A., Sheikh, M. N. (2018). "Behavior of High Strength Concrete Columns Reinforced with Galvanized Steel Equal Angle (GSEA) Sections under Different Loading Conditions", ***Journal of Structural Engineering (ASCE)*. 144(7), 04018070.**

2. Ibrahim, A. A., Sheikh, M. N., and Hadi, M. N. S. (2018). "Axial Compressive Behavior Of SEA Section Reinforced Square HSC Column" ***ACI Structural Journal*. 115(5), 1-12**.

Conference Publications

1. Ibrahim, A. A., Sheikh, M. N., and Hadi, M. N. S. (2017). "Behaviour of Square HSC Columns Reinforced with SEA Sections under Axial Compression" 28th Biennial National Conference of the Concrete Institute of Australia, Adelaide, Australia.
2. Ibrahim, A. A., Sheikh, M. N., and Hadi, M. N. S. (2017). "Performance Evaluation of Square High Strength Concrete (HSC) Columns Reinforced with Steel Equal Angle (SEA) Sections under Axial Compression" Proc. 1st International Conference on Structural Engineering Research (iCSER 2017), Western Sydney University, Sydney, Australia.
3. Ibrahim, A. A., Sheikh, M. N., and Hadi, M. N. S. (2017). "Axial Load and Bending Moment Behaviour of Square High Strength Concrete (HSC) Columns

Reinforced with Steel Equal Angle (SEA) Sections" Proc. 1st International Conference on Structural Engineering Research (iCSER 2017), Western Sydney University, Sydney, Australia.

TABLE OF CONTENTS

LIST OF FIGURES

LIST OF TABLES

ABBREVIATIONS

a	Depth of equivalent rectangular stress block, mm
A_{ch}	The concrete core area of column measured to the outside of the transverse reinforcement, mm^2
A_b	Area of transverse steel bar, mm^2
A_{CC}	Area of core concrete column enclosed by centre to centre of ties
A_{eff}	Effective confined area of concrete, mm^2
A_g	Gross area of concrete cross-section of column, mm^2
A_{SEA}	Area of longitudinal steel equal angle (SEA) section, mm^2
A_S	Area of longitudinal reinforcement, mm^2
b	Width of concrete cross-section of column, mm^2
b_t	Leg width of steel equal angle section, mm^2
c	Depth of neutral axis, mm^2
C_c	Resultant concrete compressive force, kN
C_x	Lateral dimension of the column core in x-axis, mm
C_y	Lateral dimension of the column core in y-axis, mm

D_c	The least lateral dimension of concrete column, mm^2
e	Eccentricity of applied load, mm^2
E_c	The elastic modulus of the concrete, GPa
E_s	Modulus of elasticity of longitudinal reinforcement, GPa
f_c	Compressive concrete stress
f_{cc}	Confined concrete strength, MPa
f_{co}	Unconfined concrete strength, MPa
f_c'	cylinder concrete compressive strength at 28 days, MPa
f_l	Lateral confinement pressure, MPa
f_l'	Effective lateral confining pressure, MPa
f_s	Axial stress in steel reinforcement, MPa
f_y	Yield strength of transverse reinforcement, MPa
h	Height of test specimen, mm
I_s	The modulus of elasticity of longitudinal reinforcement, mm^4
k_e	Effective confinement coefficient
P_{ecc}	Theoretical strength of concrete column under eccentric axial load, kN

P_{max}	Maximum axial load carried by test specimen, kN
P_o	Theoretical strength of concrete column under concentric axial load, kN
s	Tie spacing, mm
s'	Clear spacing between transverse ties, mm
w_i	The clear horizontal spacing between the longitudinal reinforcement, mm
$\alpha_2; \beta$	Equivalent rectangular stress block parameters
ε_c	Axial strain corresponding to f_c
ε_{cc}	Axial strain of concrete compressive corresponding to f_{cc}
ε_c'	Unconfined concrete compressive strain corresponding to f_c
ε_{co}	Unconfined concrete strain corresponding to f_{co}'
ε_{cu}	Ultimate confined concrete strain
ε_s	Axial strain of steel corresponding to f_s
ε_{sy}	Yield strain of steel corresponding to f_{sy}
ρ_c	The area ratio of the longitudinal reinforcement to the column core section
ρ_s	Volumetric ratio of transverse reinforcement
ρ_b	Volumetric ratio of longitudinal steel bars to column cross-section

ρ_{SEA}	Volumetric ratio of longitudinal steel equal angle (SEA) sections to column cross-section
μ	Ductility of test specimens

1 INTRODUCTION

1.1 Preamble

In recent years, high strength concrete (HSC) has been used widely in reinforced concrete constructions, especially for high-rise buildings and bridges (Ozbakkaloglu and Saatcioglu 2004; Hong et al. 2006a; Sharma et al. 2007; Begum et al. 2013; Hadi et al. 2017). The use of HSC in lower storey reinforced concrete (RC) columns of high rise buildings leads to the reduction of column sizes (Mendis and Panagopoulos 2000; Junior and Giongo 2004; Bastami 2010; Ho et al. 2010). In addition, strength and durability of RC columns can be increased by using HSC (Attard and Setunge 1996; Foster and Attard 2001; Li and Hadi 2003; Cladera and Mari 2005; Campione and Minafò 2010). However, the main concern regarding the use of HSC in the construction of columns is the lower ductility of the HSC column than the ductility of the NSC column for the same amount of confinement reinforcement (Hsu and Hsu 1994; Kwan et al. 2006; Lam et al. 2009; Subramanian 2011). Therefore, the ductility and the strength of HSC columns were extensively investigated in the literature (Mendis et al. 2000; Woods et al. 2007; Kwan and Ho 2010; Bai and Au 2011; Shih et al. 2013). In general, more lateral reinforcement is required in HSC columns than in NSC columns to achieve a similar ductility (Mendis et al. 2000; Sharma et al. 2005; Awati and Khadiranaikar 2012).

One of the effective methods for enhancing the ductility and the strength of an RC column is to confine the concrete core of the column adequately with transverse ties or

helices. The magnitude of the improvement in the strength and ductility of RC columns is influenced by various parameters including the compressive strength of concrete, volumetric ratio and spacing of transverse reinforcement, and cross-sectional geometry. The efficiency of the confinement provided by the transverse reinforcement decreases with the increase in the compressive strength of concrete (Bjerkeli et al. 1990; Razvi and Saatcioglu 1994; Bayrak and Sheikh 1998; Sharma et al. 2005; Paultre et al. 2010). For achieving a similar ductility, HSC columns need to be confined significantly more than NSC columns (Soliman and Yu 1967; Mendis et al. 2000; Awati and Khadiranaikar 2012). Moreover, circular columns confined with helices exhibit better strength and ductility than the corresponding square columns confined with square ties (Sheikh 1982; Mander et al. 1988a; Mander et al. 1988b; Bjerkeli et al. 1990; Cusson and Paultre 1995; Bhowmick et al. 2006).

Longitudinal reinforcement also contributes to the confinement of the concrete core of the columns. A minimum number of longitudinal reinforcement is needed for the stability of steel cages as well as for providing confinement to the transverse expansion of the concrete core. To investigate the contribution and the influence of longitudinal reinforcement bars on the ductility of high strength concrete (HSC) columns, a number of studies were carried out in the literature (Yong et al. 1988; Sheikh and Yeh 1990; Awati and Khadiranaikar 2012). It was reported that the distribution of the longitudinal reinforcement influenced the ductility of HSC columns. It was also reported that, for a given area of steel reinforcement, the ductility of the HSC column increases with the increase of the number of longitudinal bars (Campione and Minafò 2010).

Composite columns are usually used in high-rise buildings due to their high strength, stiffness, ductility, and seismic resistance (Ricles and Paboojian 1994; Mirza et al. 1996; Shanmugam and Lakshmi 2001; Dundar et al. 2008; Ellobody and Young 2011) of composite columns. There are two main types of composite columns: concrete encased steel section and concrete filled hollow steel section. Encased composite columns (concrete encased steel section) are being increasingly used as structural members because of their higher fire resistance compared to the concrete filled hollow steel sections, which require protection against fire (Ellobody and Young 2011). Also, in the encased composite column, the local buckling resistance of encased steel section is higher which increases the seismic resistance of the column (Hunaiti et al. 1994; Shanmugam and Lakshmi 2001; Weng and Yen 2002). In addition, the use of encased steel sections in composite columns reduces the cross-sectional dimensions and increases the strength-to-weight ratio of columns (Ellobody and Young 2011).

1.2 Research Significance

Concrete columns are commonly reinforced longitudinally with conventional steel bars and laterally with either steel ties or steel helices. For concrete columns reinforced with lateral steel ties, the area of the effectively confined concrete core is less than the total area of the concrete core, which results in lower strength and ductility of the square RC columns. This study proposes to use steel equal angle (SEA) sections as the longitudinal reinforcement in HSC columns. It is noted that SEA sections have been extensively used in the construction of steel structures. However, no previous study investigated the use of SEA sections in reinforcing HSC columns. The use of SEA sections in HSC

columns as longitudinal reinforcement may increase the area of the confined concrete core and delay the buckling of longitudinal reinforcement, as a SEA section has a higher second moment of area than a steel bar for the same cross-sectional area.

Columns are structural members that are usually subjected to combined axial compression and bending moment, rather than pure axial compression as flexural effects may be created by construction errors and position of the column in the structure (Hadi 2006; Hadi et al. 2016b). A number of research studies investigated the behaviour of the HSC columns under axial compression. However, a few research studies investigated the behaviour of high strength concrete (HSC) columns under eccentric axial loads. The most important factor that affects the performance of the columns is the value of initial eccentricity of the axial load. The effectiveness of lateral confinement on the ductility and the strength of RC columns decreases when the initial eccentricity of the axial load increases (Kottb et al. 2015). It was also seen that the effectiveness of the lateral confinement decreased as the compressive strength and spacing of lateral reinforcement increased (Foster and Attard 1997). However, an increase in the ratio of lateral reinforcement or closer tie spacing may improve the strength and ductility of reinforced concrete columns under eccentric axial load (Canbay et al. 2006). According to a detailed literature review, no study is available in the literature that deals with high strength concrete (HSC) columns reinforced with steel equal angle (SEA) sections. This study investigates the experimental and analytical behaviour of square HSC columns reinforced longitudinally with SEA sections under concentric axial load, eccentric axial load and four-point bending.

1.3 Scope of the Study

The experimental program of this study was carried out to investigate the behaviour and performance of square high strength concrete (HSC) columns reinforced longitudinally with steel equal angle (SEA) sections. The experimental program included testing 32 specimens cast and tested under different loading conditions. The experimental program was divided into two sets. In the first set, twenty specimens were reinforced longitudinally with either steel bars or SEA sections and tested under concentric and eccentric axial loads and four-point bending (flexural). These specimens had a cross-section of 210 mm × 210 mm and a height of 800 mm. In the second set, twelve specimens reinforced longitudinally with either steel bars or SEA sections were tested under concentric axial load. These specimens had a cross-section of 210 mm × 210 mm and a height of 600 mm.

1.4 Research Objectives

The main objective of this study is to investigate the behaviour and performance of square high strength concrete (HSC) columns reinforced longitudinally with steel equal angle (SEA) sections through experimental and analytical investigations. The specific objectives of this study can be briefly summarised as below.

• To assess experimentally the effects of using SEA sections as longitudinal reinforcement on the axial load-axial deformation behaviour and the failure modes of the HSC column specimens reinforced with SEA sections under different loading conditions.

• To assess the influence of the spacing of transverse ties on the behaviour of square HSC column specimens reinforced with SEA sections under concentric axial load.

• To evaluate whether replacing the steel bars with the SEA sections increases the strength and ductility of the square HSC columns.

• To evaluate the influence of different loading conditions such as concentric and eccentric axial loads, and four-point bending on the square HSC columns reinforced longitudinally with SEA sections.

• To investigate the analytical axial load-axial deformation responses of specimens reinforced longitudinally with SEA sections tested under concentric axial load.

• To construct the analytical axial load-bending moment interaction diagrams of square HSC columns reinforced longitudinally with SEA sections with different spacing of transverse ties using equivalent stress block method.

• To construct the analytical axial load-bending moment interaction diagrams of square HSC columns reinforced longitudinally with SEA sections with different spacing of transverse ties using the layer-by-layer integration method.

1.5 Structure of the Thesis

This thesis consists of eleven chapters, the contents of this thesis are summarised briefly in this section as follows:

In Chapter 1, the background, research significant, scope of the research and research objectives of this study were presented above (Chapter 1).

In Chapter 2, a review of literature related to previous research on tied concrete columns reinforced longitudinally with either steel bars or steel sections are reported.

In Chapter 3, The requirements of confined concrete by transverse ties according to available design codes are presented. The factors affecting the behaviour of the confined concrete column are also demonstrated. Furthermore, a review of the available stress-strain models of square confined and unconfined concrete is presented.

In Chapter 4, an experimental investigation is presented about 15 pullout specimens reinforced with either steel bars or SEA sections. The preparing, fabrication, placement and curing process of the pullout specimens are also reported. Also, the test results of the pullout specimens tested under the direct pullout test are presented and discussed.

In Chapter 5, details of the experimental program for specimens with 800 mm height (20 square HSC columns), fabrication of the test specimens, placement and curing process of the specimens are presented. The properties of materials used in the casting of the specimens are also presented. Also, the instrumentation and the test program of specimens under concentric and eccentric axial loads and four-point bending are reported.

In Chapter 6, test results of the preliminary material testing conducted to determine the mechanical properties of concrete, steel equal angle (SEA) sections and steel bars are demonstrated. Also, the experimental results of the specimens with 800 mm height that were tested under concentric and eccentric axial loads and four-point bending are presented and discussed.

In Chapter 7, details of the experimental program for specimens with 600 mm height (12 square HSC columns), fabrication of the test specimens, placement and curing

process of the specimens are described. Also, the instrumentation and the test program of specimens under concentric axial compression are presented.

In Chapter 8, the experimental results of the specimens with 600 mm height that were tested under concentric axial compression are reported and discussed.

In Chapter 9, the nominal axial load capacity of specimens tested under concentric and eccentric axial loads are calculated and compared with the corresponding experimental results. The maximum spacing of transverse ties for specimens reinforced with SEA sections is evaluated and discussed. The axial load-axial deformation behaviours of the square HSC columns reinforced longitudinally with either steel bars or SEA sections are established using a stress-strain model for concrete.

In Chapter 10, the axial load-bending moment interaction diagrams of the square HSC specimens reinforced longitudinally with either steel bars or SEA sections constructed using the equivalent rectangular stress block and the layer-by-layer numerical integration methods are presented and discussed.

In Chapter 11, major findings in this study are reported. Recommendations for the future investigations are also presented.

2 Review Studies on Concrete Columns Reinforced by Ties

2.1 Introduction

Steel bars are commonly used in reinforced concrete (RC) structural members as a reinforcement material. However, a concrete encased steel section is also usually used in high-rise buildings due to their high strength, stiffness, ductility, and seismic resistance of composite columns. In this chapter, a comprehensive review of studies on reinforced concrete columns under concentric and eccentric axial loads, which include concrete columns reinforced longitudinally with either conventional steel bars or steel sections is presented.

2.2 Concrete Columns Reinforced Longitudinally with Steel Bars

Mander et al. (1988a) conducted an experimental study on confined reinforced concrete columns to study their stress-strain behaviour. They presented results from a test of 31 columns specimens with different cross sections which included circular, rectangular and square. All specimens were subjected to axial compressive loads. The compressive strength of concrete ranged from 26 MPa to 43 MPa. The main variables of the experiment were distribution and ratio of longitudinal reinforcement and amount of transverse reinforcement ratio. It was found that for all different cross sections of column specimens, the ratio of transverse reinforcement was the most important variable that influenced the shape of the stress-strain relationship. It was also reported that the strength and the ductility of circular specimens confined with helices were

greater than the strength and ductility of rectangular or square specimens confined with transverse ties.

Yong et al. (1988) carried out an experimental study on the behaviour of high strength concrete (HSC) column specimens. A total of 24 HSC specimens were tested under axial compressive loads. The specimens were either 133 mm × 133 mm or 152 mm × 152 mm in cross-section with a height of 457 mm. The main parameters considered in this experimental study included the cover of concrete, the volumetric ratio of transverse reinforcement and distribution of longitudinal reinforcement. Concrete cylinder strength of concrete ranged between 83.6 to 93.5 MPa. The study reported that the increase of transverse reinforcement ratios resulted in enhancement of the behaviour of high strength concrete. The study found that the use of confinement did not affect the column when using transverse ties with spacing equal to the transverse dimension of the column. It was indicated that the improvement in ductility of high strength concrete occurred with using transverse ties, and the degree of improvement based on concrete strength, volumetric ratios of transverse and longitudinal reinforcement and spacing of ties. They also suggested that to gain enhancements for confined high strength concrete, the spacing of transverse reinforcement should be less than the lateral dimension of the column. The study proposed that by using spacing of transverse reinforcement less than the lateral dimension of the columns has advantages such as increase strength and ductility of high strength concrete. This may be because the effectively confined area of the concrete core can be increased.

Bjerkeli et al. (1990) conducted an experimental study on the behaviour of high strength concrete (HSC) column specimens subjected to an axial compressive load. The parameters in this experimental study included the aggregate, the geometry and size of column cross section, height of concrete columns, the volumetric ratio of transverse reinforcement, the yield strength of transverse reinforcement, distribution, number and size of longitudinal reinforcement and eccentricity of loading. The specimens were cast with different concrete strengths (ranging between 60 to 115 MPa). The specimens were made with either circular (150 mm × 500 mm), square (150 mm × 150 mm in cross-section and 500 mm height) or rectangular (300 mm × 500 mm in cross-section and 2000 mm height). The results indicated that the ductility of high strength concrete columns could enhance with the use of sufficient amount of transverse reinforcement as confinement. It was also found that the number of longitudinal reinforcement had a significant effect on the ductility of high strength concrete (HSC) columns. This may be because closer spacing of transverse reinforcement increases the effectiveness of confined concrete core of columns. In contrast, increasing the size of longitudinal reinforcement had a slight influence on the ductility of HSC columns. The study reported that the columns reinforced transversely with circular helices exhibited better performance than columns reinforced transversely with square ties. It was also found that the influence of confinement resulted in improving the strength of the tested specimens.

Sheikh and Yeh (1992) showed results from a test of 15 normal strength concrete (NSC) columns to study the behaviour of columns confined transversely by ties reinforcement. The strength of concrete was 27.6 MPa. All specimens were subjected for the test under

a constant axial compressive load and then increased applied flexural loads. The main variables of the experiment were a different level of axial compressive load, the ratio of transverse reinforcement, spacing the of transverse reinforcement (54 mm to 173 mm) and distribution of longitudinal reinforcement. The results showed that the most important factor affecting the behaviour of columns were the ratio of transverse reinforcement and the level of axial load. It was also noticed that the higher flexural strength and ductility for specimens caused by using a smaller spacing of transverse reinforcement.

Polat (1992) carried out an experimental program on twelve square reinforced concrete column specimens under monotonically axial compressive loads. All the column specimens were 230 mm × 230 mm in cross-section with a height of 1500 mm. The parameters considered in the study included the concrete compressive strength, yield strength and ratio of transverse reinforcement and the height of the axial strain gauge (300 mm and 450 mm). The cylinder compressive strengths varied from 36 MPa to 85 MPa. All specimens had longitudinal reinforcement that consisted of eight 10M (11.3 mm diameter deformed steel bars). The specimens were reinforced transversally with two different volumetric ratios (1.08% and 2.29%). The results of this investigation illustrated that the use of transverse reinforcement led to increasing the strength and ductility of the normal and high strength concrete columns. The results also reported that decreasing the spacing of transverse reinforcement by half could significantly enhance the strength and ductility of the high strength concrete columns. Also, they reported that for a given transverse reinforcement, the increase of the strength of

transverse reinforcement led to improving the strength and ductility of the concrete columns.

An experimental study on square high strength concrete (HSC) column specimens was carried by Cusson and Paultre (1994). A total of 27 specimens were tested under axial compressive load to investigate the effect of HSC on the confined concrete columns by transverse ties. All specimens had a cross-section of 235 mm × 235 mm and a height of 1400 mm. The main parameters considered in the experimental study included the concrete compressive strength and concrete cover of column specimens, the volumetric ratio of longitudinal reinforcement and the spacing and distribution of transverse reinforcement. Concrete compressive strength ranged between 53 MPa to 116 MPa. The percentage of longitudinal reinforcement ranged from 2.2% to 3.6%. The volumetric ratio of transverse reinforcement ranged between 1.4% and 4.9%, and the spacing of transverse ties was either 50 mm or 100 mm. Details of test specimens are presented in Figure 2.1.

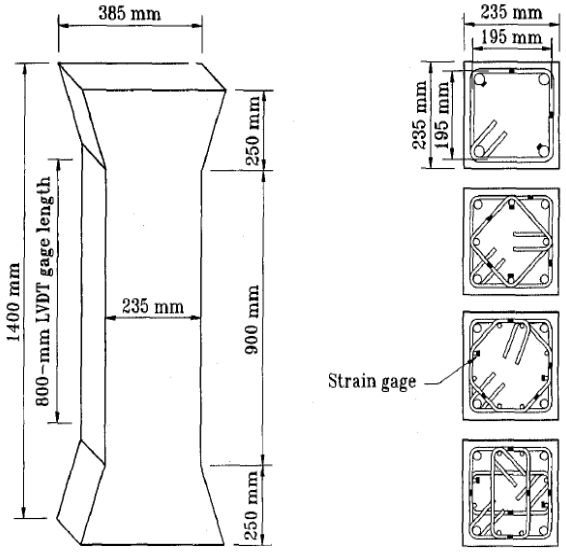

Figure 2.1 Details of test specimens (Cusson and Paultre 1994)

The study found that the effectively confined area of the concrete core can be increased by using the proper distribution of longitudinal reinforcement around the concrete core of column. The study reported that early spalling of cover concrete was observed during testing. It was also reported that the ratio of transverse reinforcement was the most significant variable that affected the stress-strain behaviour of confined concrete. A reduction in the transverse tie spacing resulted in improving in both strength and ductility of columns. They recommended that when computing the axial load carrying capacity of HSC columns, only the area of the concrete core can be considered.

Lloyd and Rangan (1995) conducted tests to investigate the behaviour of high strength concrete (HSC) column specimens. A total of thirty-six concrete specimens were tested under eccentric axial compressive loads. The specimens were either 175 mm × 175 mm or 300 mm × 100 mm in cross-section with an effective height of 1680 mm. The main parameters in this study were the concrete compressive strength, the geometry of cross-section, the ratio of longitudinal reinforcement and the eccentricity of the axial load. The concrete compressive strength of the tested specimens was either 58 MPa, 92 MPa or 97 MPa. Longitudinal reinforcement consisted of four and six steel bars for square and rectangular specimens, respectively. The eccentricities of axial load ranged between 0.086 and 0.4 times the overall specimen depth. They point out that the transverse steel reinforcements were insufficient to generate ductile behaviour for reinforced concrete columns with small applied load eccentricity. However, the results also indicated that the columns with larger load eccentricity ($e>0.3h$) were less brittle behaviour than columns with small load eccentricity.

Saatcioglu and Razvi (1998) presented results from a test of 26 square concrete column specimens. The specimens were 250 mm × 250 mm in cross sections and a height of 1500 mm. All specimens were tested under axial compression. The main parameters considered in the experimental study included concrete compressive strength, volumetric ratio and distribution of longitudinal reinforcement, configuration, strength and spacing of transverse reinforcement. Concrete cylinder strength of the specimens ranged between 60 MPa and 124 MPa. It was reported that columns with high strength concrete exhibited extremely brittle manner except for the specimens that had adequately high transverse confinement pressure. It was reported that with increasing compressive strength of concrete leads to decreasing of the ductility of the columns. They proposed that to improve the ductility of high strength concrete columns by using transverse reinforcement to confined concrete. Therefore, the researchers concluded that at approximately 70 % of the unconfined concrete strength, the concrete cover spalled off, and this mode of failure was more noticeable in columns with closely spaced transverse reinforcement. They predicted that instability of the concrete at compressive stress could lead to earlier spalling of cover concrete. It was also reported that there are many factors that can affect the spalling of concrete column cover, which includes cover thickness, concrete strength and type of reinforcement grid.

Mendis et al. (2000) conducted a theoretical study on the design of transverse reinforcement for high strength concrete columns subjected to axial compressive load. The main parameters considered in this theoretical study included the compressive strength of concrete, the buckling of longitudinal bars and fracture of transverse reinforcement and spacing of transverse reinforcement. The study reported that the

decrease of transverse reinforcement spacing in the high strength concrete column was not required to prevent buckling of longitudinal steel bars. It was also found that decrease in tie spacing was required when increasing compressive strength to maintain ductility of high strength concrete. They also recommended that additional study is essential for comparison and verification of the theoretical results with experimental results.

A comprehensive experimental study on the behaviour of short reinforced high strength concrete (HSC) columns was conducted by Li et al. (2000). A total of 30 reinforced concrete (RC) specimens were tested under axial compression. The main parameters considered in this experimental study involved concrete compressive strength, the configuration of lateral confinement and strength of transverse reinforcement. The specimens were either circular cross section (240 mm in diameter) or square cross section (240 mm × 240 mm) and 720 mm in height. The concrete compressive strength of the tested specimens ranged between 52 MPa and 75 MPa. All specimens had internal steel reinforcement that consisted of either 4 or 8 steel bars, 12 mm in diameter as longitudinal reinforcement and either 6 mm or 6.4 mm in diameter steel bar spacing at 20 mm, 35 mm, 50 mm or 65 mm as transverse reinforcement, as shown in Figure 2.2. The result of this investigation explained that the compressive strength of the concrete core was significantly increased when the strain rate was increased. The study also reported that the efficiency of the lateral confinement decreased when the spacing of the transverse reinforcement increased.

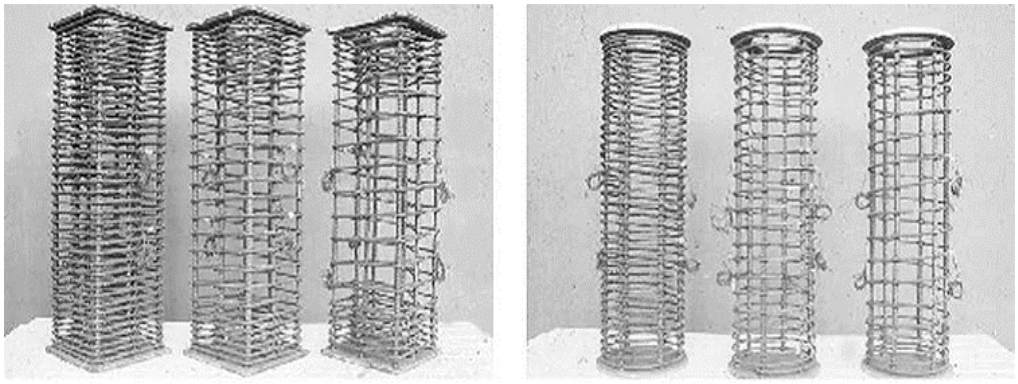

Figure 2.2 Typical reinforcement cages for specimens (Li et al. 2000)

Foster and Attard (2001) presented results from a test of 68 square columns, which were normal and high strength concrete, under eccentric loading. All columns had a square cross-section with 150 mm side width. The primary parameters considered were the strength of concrete, which ranged from 40 to 90 MPa, the applied load eccentricity, the volumetric ratio of longitudinal reinforcement and spacing of transverse reinforcement. The results showed that confining concrete by the transverse reinforcement increased the ductility of concrete. The magnitude increase in ductility of concrete depended on the concrete strength, the ratio of transverse reinforcement, spacing and yield strength of transverse reinforcement and the configuration of longitudinal reinforcement.

Chung et al. (2002a) investigated 65 square concrete column specimens under monotonically increasing axial compressive loads to determine the strength improvement of reinforced concrete columns confined by transverse ties. All the specimens were 200 mm × 200 mm in cross-section with a height of 600 mm with a concrete cover of 17 mm. The parameters considered included the concrete compressive strength, arrangement of longitudinal reinforcement, and amount, configuration and

strength of transverse ties. The specimens were made of concrete strengths between 20 MPa and 54 MPa. The study reported that columns made of high strength concrete (HSC) exhibited lower lateral expansion than columns made of normal strength concrete (NSC). Also, it was found that the columns made with HSC show lower post-peak deformation than columns with NSC. Therefore, in comparison with columns made with NSC, columns made with HSC need more transverse reinforcement to improve its post-peak deformation. They also reported that the specimens with closely spaced transverse reinforcement obtained higher strength and ductility than the specimens with widely spaced transverse reinforcement. This was because the decrease in the spacing of transverse reinforcement resulted in increasing the effectiveness of confined concrete core of columns. Also, they reported that the reduction in the spacing of transverse reinforcement led to the inhibited buckling of longitudinal reinforcement.

Ros et al. (2003) investigated the influence of transverse reinforcement on high strength concrete (HSC) column specimens. A total of 224 specimens made with either square or circular cross-section and were tested under axial compressive loads. The study investigated the influence of geometry and size of the specimen, the strength of concrete and volumetric ratio of transverse reinforcement. The square specimens were either 100 mm × 100 mm, 150 mm × 150 mm or 200 mm × 200 mm in the square section. The height of the square specimens ranged between 200 mm and 400 mm. The circular specimens were either 100 mm, 150 mm or 200 mm in diameter. The height of The circular specimens was either 200 mm, 300 mm or 400 mm. Concrete with an average compressive strength between 25 MPa and 100 MPa. The results of this experimental study indicated that the axial peak strain of the confined concrete specimens increases

as the degree of transverse confinement increases and these increase were higher in cylindrical specimens than prismatic specimens. They also noted that the increase in the strength of concrete resulted in decreasing the strain of concrete, leading to a more brittle post-peak behaviour. Based on the results of this study it was recommended that to consider concrete as confined concrete, the spacing of transverse reinforcement should be less than the lateral dimension (diameter or side width) of the specimen.

An experimental study on the behaviour of HSC column confined by either circular helices or square ties was conducted by Sharma et al. (2005). A total of 44 concrete specimens were tested under axial compressive load, eight plain concrete specimens and 36 reinforced concrete specimens. For all reinforced specimens, the concrete cover was 10 mm. The effects of geometry of cross section, the strength of concrete, volumetric ratio of longitudinal reinforcement, spacing, volumetric ratio, configuration and yield strength of transverse reinforcement were investigated. The specimens were either 150 mm × 150 mm in square section or 150 mm in diameter circular section with a height of 600 mm. The specimens were cast with two different concrete strengths (58.03 MPa and 76.8 MPa). The results of this investigation showed that when the strength of concrete increased, the ductility of concrete columns was decreased. Also, they reported that the early spalling of the concrete cover was more pronounced in HSC columns, which led to a sudden drop in the strength of columns. The results also indicated that to obtain similar ductility, high strength concrete columns required more amount of transverse reinforcement than normal strength concrete.

An experimental study on square high strength (HSC) concrete column specimens confined with low transverse reinforcement ratio was carried out by Hong et al. (2006b). A total of 30 square HSC specimens were tested under concentric axial load. The tested specimens had a square cross-section of 250 mm and 750 mm height. The 31 of specimens were longitudinally reinforced with four steel bars while the remaining 9 specimens were plain concrete specimens. All specimens were prepared without concrete cover. Three parameters influencing the behaviour of the stress-strain curve of confined concrete were investigated. These parameters were the concrete compressive strength, volumetric ratio and strength of transverse reinforcement (ties). The compressive strength of concrete ranged between 46.3 MPa and 128.0 MPa. The specimens were confined with square ties spaced at 25 mm, 50 mm, 100 mm and 150 mm with a volumetric ratio ranging between 0.32% and 1.92% (Figure 2.3). The results of this investigation showed that under axial compression, high strength concrete columns showed less lateral expansion than normal strength concrete (NSC) columns. Also, when the compressive strength of concrete columns increases, the concrete columns exhibited more brittleness. Also, when the compressive strength of concrete columns increases, the concrete columns exhibited more brittleness. The test results also showed that the effect of the increased yield tensile strength of transverse ties was insignificant on the confinement effect of the columns.

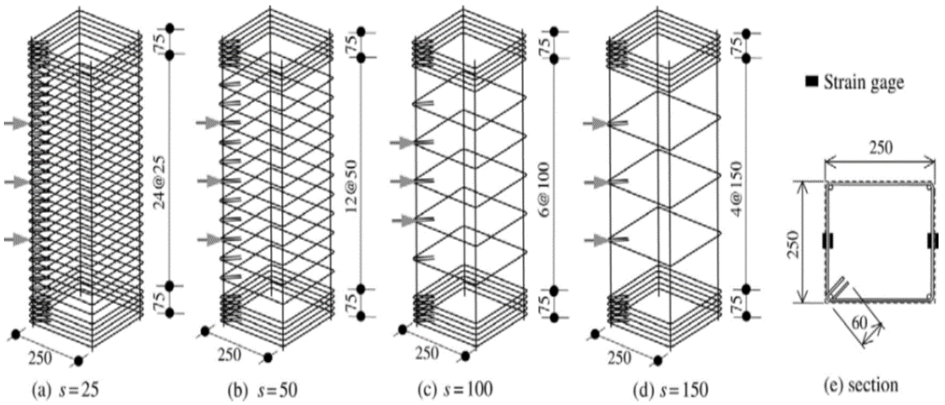

Figure 2.3 Details of test columns (Hong et al. 2006b)

Han and Shin (2006) developed an experimental program to investigate the influence of transverse ties in the reinforced concrete columns under monotonically increasing concentric compressive loading. A total of 18 column specimens were tested to study the effects of concrete strength, configurations of transverse reinforcement, amount of transverse reinforcement, the spacing of transverse reinforcement (40 mm to 150 mm) and spalling of concrete cover on the behaviour square reinforced concrete columns. The column specimens had a square cross-section of 260 mm with 1200 mm height and were cast with concrete with strengths of 22.1 MPa to 49 MPa. The column specimens were reinforced longitudinally with steel bars with a volumetric ratio of longitudinal reinforcement of 0.25% to 2.36%. The yield tensile strength of longitudinal reinforcement ranged from 436.4 MPa to 500 MPa. It was seen from the experimental results that as the transverse reinforcement increases, the buckling of longitudinal reinforcements occurred earlier and was more critical around the corner than interior longitudinal reinforcement. The results also indicated that compared with normal strength concrete columns, the buckling of longitudinal reinforcements was more

critical for high strength concrete columns. Also, they concluded that the configuration of transverse reinforcement resulted in increasing the ductility of specimens.

Woods et al. (2007) conducted tests to investigate the bending ductility of the square HSC column specimens. A total of eight square HSC column specimens were tested under axial compressive load. All the specimens were 203 mm × 203 mm in cross-section with a height of 2030 mm. In the study, the 28 days concrete strength of 69 MPa was used. The main parameters considered in the experimental study included the spacing and volumetric ratio of transverse reinforcement. The spacing of transverse reinforcement ranged between 66 mm to 193 mm. The volumetric ratios of transverse reinforcement ranged from 0.3% to 1.87%. The study reported that the increase in the spacing of transverse reinforcement resulted in decreased ductility of specimens due to reducing buckling capacity of the longitudinal reinforcement. The study also concluded that different parameters such as spacing and amount of transverse reinforcement could affect the ductility and load carrying capacity in the post-peak response of concrete column specimens.

A comprehensive experimental study on the behaviour of square concrete columns was conducted by Awati and Khadiranaikar (2012). A total of 62 square concrete specimens including four plain concrete specimens were tested under monotonic concentric axial load. All tested specimens were either 125 mm × 125 mm or 150 mm × 150 mm in square cross sections with a height of 750 mm and 900 mm, respectively. The concrete cover, the effects of the concrete compressive strength, the ratio of longitudinal reinforcement, spacing and the ratio of transverse reinforcement were investigated. The

concrete strength ranged between 61.0 MPa and 115.6 MPa. The 125 mm square reinforced concrete specimens were longitudinally reinforced with either four or eight 10 mm in diameter steel bars with volumetric ratios of 2% and 4%, respectively. The 150 mm square reinforced concrete specimens were longitudinally reinforced with either four or eight 12 mm in diameter steel bars with volumetric ratios of 2% and 4%, respectively. All reinforced concrete specimens were transversely reinforced with 8 mm in diameter steel bars using two types of arrangements and spaced at 30 mm, 50 mm, 75 mm or 100 mm.

Based on the results of this study it was realised that increasing the amount of the transverse reinforcement and decreasing the spacing of transverse reinforcement resulted in slightly increasing the strength (up to 10%) but significantly improved the ductility (ranging between 50% to 70%). For concentrically loaded column, early spalling of the concrete cover from the concrete core of columns was also noted. In addition, they reported that increasing the yield tensile strength of longitudinal reinforcement led to improving the post-peak behaviour and ductility of reinforced concrete columns. Also, they found that increasing the yield tensile strength of longitudinal reinforcement did not significantly improve the axial load capacity of columns but postponing the transfer of lateral pressure to the transverse reinforcement, causing an enhanced post-peak behaviour of columns.

Leite et al. (2013) investigated 32 rectangular cross-section columns under eccentric axial load. The effects of concrete strength, the ratio of longitudinal reinforcement, the slenderness of the specimens and the ratio between eccentricities at the ends were

investigated. The columns were either 100 mm × 200 mm or 150 mm × 200 mm in cross-section with a height of 3000 mm. The concrete compressive strength of the specimens ranged between 28.2 MPa and 93.3 MPa. The columns were reinforced longitudinally with either four or six steel bars of 12 mm diameter and transversely with 4 mm diameter steel bars. The slenderness ratios of the specimens were either 20 or 30. Three eccentricities related to the smallest dimension of the column had been selected (0.1, 0.2 and 0.4). The result of this investigation showed that the ductility of the specimens improved when the ratio of longitudinal reinforcement increased. The test results also reported that the increase of the eccentricity led to decreasing the axial load capacity of columns.

An experimental study by Jin et al. (2017) was conducted to investigate the effect of ratio, arrangement and strength of transverse steel ties on the size effect and failure of reinforced concrete columns. A total of 26 column specimens were tested under axial compression. The cross-section of columns ranged from 267 mm × 267 mm to 600 mm × 600 mm and the height varied from 800 mm to 1800 mm. The concrete strength of the specimens at 28 days was 42.8 MPa. All specimens were reinforced longitudinally with four steel bars (the longitudinal reinforcement ratio of 0.28%), and the yield tensile of longitudinal reinforcement ranged from 458 MPa to 1044 MPa. The result of this investigation showed that the transverse reinforcement ratio had significantly affected the failure modes of the reinforced concrete (RC) columns. When the ratio of transverse reinforcement increases, the failure of the RC columns became less brittle. Also, the configuration of transverse reinforcement had an important enhancement on the load carrying capacity of the RC columns. Furthermore, they found that as the strength or the

ratio of transverse reinforcement increases, the strength and ductility of the tested RC columns increases.

2.3 Concrete Columns Reinforced Longitudinally with Steel Sections

Composite columns are usually used in high-rise buildings due to high strength, stiffness, ductility, and seismic resistance of composite columns (Ricles and Paboojian 1994; Mirza et al. 1996; Shanmugam and Lakshmi 2001; Ellobody and Young 2011). There are two main types of composite columns: concrete encased steel section and concrete filled hollow steel section, as presented in Figures 2.4 and 2.5, respectively. Encased composite columns (concrete encased steel section) are being increasingly used as structural members because of their higher fire resistance compared to the concrete filled hollow steel sections, which require protection against fire (Weng and Yen 2002; Ellobody and Young 2011; Kim et al. 2012). Also, in the encased composite column, the local buckling resistance of encased steel section is higher (Hunaiti et al. 1994; Shanmugam and Lakshmi 2001; Weng and Yen 2002). In addition, the use of encased steel sections in composite columns reduces the cross-sectional dimensions and increases the strength-to-weight ratio of the columns (Ellobody and Young 2011).

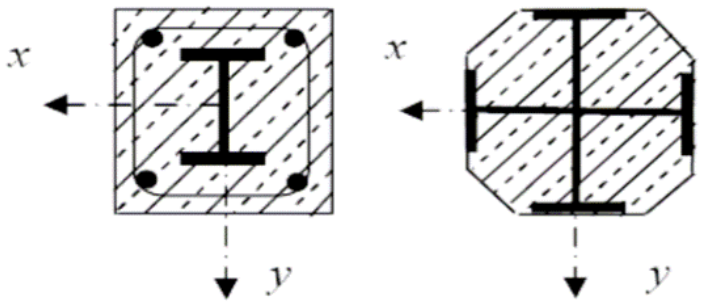

Figure 2.4 Concrete encased steel sections

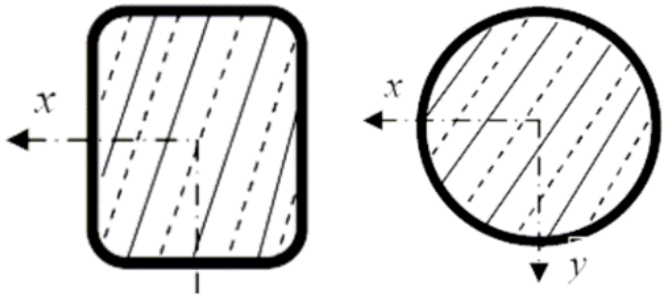

Figure 2.5 Concrete filled hollow steel sections

Chen and Lin (2006) investigated analytically the behaviour of concrete encased steel composite stub columns subjected to axial loading. They have developed an analytical model to predict the axial carrying capacity and to examine the relationship of load-deformation for composite columns. The variables considered were differenced steel member section and also ratio of transverse reinforcement. Based on the results of this study it was realised that by using the analytical model for the most of the composite stub columns could accurately predict the axial compressive load. The test results also showed that the shape of steel section encased in concrete affected on the confinement of concrete where the I-shape had low confined concrete compared with the cross-shaped steel section encased in concrete columns.

Zhao et al. (2010) tested ten concrete encased steel section composite columns under eccentric axial load. The tested composite column specimens were 160 mm × 180 mm in cross-section with heights 2.8 m, 3.2 m, 3.5 m and 4.1 m. The effects of different concrete strength, slenderness ratio of specimens (L/r) and the applied load eccentricities were investigated. The specimens were made of cubic concrete strength

ranging between 43.3 MPa and 67.0 MPa. The test specimens were designed with slenderness ratio (L/r) of 61, 62, 76 and 89. The eccentricities of the applied axial load ranged between 0 and 60 mm. The specimens were reinforced longitudinally with I-steel section (100 mm × 68 mm × 4.5 mm × 7.6 mm) and four steel bar (12 mm in diameter). The 6 mm in diameter steel bars were used as transverse reinforcement for all test specimens with a spacing of 150 mm and a clear cover of 15 mm. The result of this investigation showed that the load carrying capacity of composite columns decreased and the failure mode became sudden, and explosive as the slenderness ratios of the specimen increased from 61 to 89. The results also indicated that the compressive strength of concrete had an important influence on the ultimate strength of the composite column specimens under concentrically loading. They reported that the effect of compressive strength was not clear with specimens subjected to eccentric loading. However, they pointed out that the strength of the specimens was influenced significantly by the magnitude of eccentricity. Therefore, the strength of the specimens decreased with an increase of the eccentricity of the applied load.

Munoz and Hsu (1997) conducted an experimental program to investigate the behaviour of concrete encased steel section composite columns. The experimental program consisted of four composite column specimens that were tested under combined axial compressive and bending loads. One specimen was tested as a short column, and the three remaining specimens were tested as slender columns. All the test specimens had a square cross-section with a side width of 63.5 mm with either 812 mm or 1210 mm height. The study investigated the influence of slenderness ratio (42.7 and 64) and the loading condition. The specimens were made with a compressive strength of concrete

ranging between 25.83 MPa and 36.77 MPa. The test specimens were reinforced longitudinally with I-steel section and four steel bars (6.35 mm in diameter) and transversely with smooth wires. It was reported that the maximum compressive strength and its corresponding maximum compressive strain were the main factors that affect the strength and the curvature of the composite column. It was also reported that by using the analytical method, it could be studied the behaviour of composite columns with a wide range of varying such as a short and slender column, a different cross section of the column, and different load conditions (uniaxial and biaxial). The results also indicated that the failure of all specimens happened by concrete material failure at a level of load near the ultimate compressive strength while the steel elements did not yield during all stages of loading. This may be because the longitudinal reinforcement buckled before reaching its yield strength, which resulted in significant damage in the concrete core of reinforced concrete columns.

Ellobody and Young (2011) developed a nonlinear 3D finite element model to examine the behaviour of concrete encased steel section composite columns subjected to pin ended axial compression. They verified their finite elements model, by comparing with previously published experimental results. The influence of different shaped steel sections, the volumetric ratio of longitudinal reinforcement, the compressive strength of concrete (20 MPa to 110 MPa), volumetric ratio and spacing of transverse reinforcement and slenderness ratio of specimens were investigated. The specimens were either 240 mm × 240 mm, 160 mm × 160 mm, 165.1 mm × 177.8 mm or 280 mm × 280 mm in cross-section. The 240 mm × 240 mm specimens were reinforced longitudinally with only H-shaped steel section (140 mm × 140 mm × 7 mm × 12 mm).

The 160 mm × 160 mm specimens were reinforced longitudinally with H-shaped steel section (100 mm × 100 mm × 6 mm × 8 mm) and four 6 mm in diameter steel bars and transversely reinforced with 4 mm in diameter steel bars spaced at 75 mm. The 165.1 mm × 177.8 mm specimens were reinforced longitudinally with UB-shaped steel section (127 mm × 114 mm × 29.76 mm) and four 6 mm in diameter steel bars and transversely reinforced with 4 mm in diameter steel bars spaced at 75 mm. The 280 mm × 280 mm specimens were reinforced longitudinally with H-shaped steel section (150 mm × 150 mm × 7 mm × 10 mm) and twelve 12 mm in diameter steel bars and transversely reinforced with 8 mm in diameter steel bars spaced at 35 mm, 75 mm or 140 mm. The concrete compressive strength of specimens ranged between 18 MPa to 110 MPa. The yield tensile strength of the steel sections ranged between 275 to 690 MPa.

The authors also examined the bond behaviour between steel section, transverse reinforcement, longitudinal reinforcement and concrete material. The comparison between the experimental and numerical results has shown that the finite element model can predict the behaviour of concrete encased steel composite columns. They also compared the strength of encased composite column, which was computed by finite element model, with the results obtained by AISC (2005) and Eurocode 4 (1994). The study reported that for concrete strength of 30 MPa and yield strength of steel section varying from 275 to 460 MPa, the strength of composite columns predicted by Eurocode 4 (1994) method more accuracy than the AISC (2005) method.

The research program that was done by Kim et al. (2012) included testing 7 encased steel section composite columns under eccentric axial loads. The columns were cast with two different concrete strengths (94 MPa and 113 MPa). The parameters considered in the research program were full or partial concrete encased steel section, the eccentricity of the axial load (60 mm and 120 mm) and spacing, volumetric ratio and yield strength of transverse reinforcement. The 5 specimens were fully concrete encased steel sections and 2 specimens were partially concrete encased steel sections. The full concrete encased steel section specimens were reinforced longitudinally with a wide flange section (H-section) and transversely with D10 (9.5 mm diameter) steel bars at different volumetric ratios (1%, 2.19% and 2.59%), different spacings (either 50 mm or 130 mm) and different yield strength (either 560 MPa or 703 MPa). The remaining two specimens were partially concrete encased steel section specimens (260 mm × 260 mm cross-section with a height of 900 mm) that were reinforced longitudinally with only a wide flange section (H-section). The details of the cross-section of the specimens and reinforcement are presented in Figure 2.6. The result of this investigation showed that the amount of transverse confinement did not significantly influence the first peak load. The authors also indicated that after the first peak load, the fully encased composite specimens experienced a second peak axial load when they were well confined by transverse reinforcement. However, after the first peak load, the load capacity of the partially encased composite specimens continued to decrease. This may be because with the increase of applied load, the lateral expansion of concrete core increases and that can result in early buckling of the longitudinal reinforcement. The authors also recommended that to avoid the premature concrete crushing of the column, it should be

provided good lateral confinement or by locating the steel flanges close to the column surface.

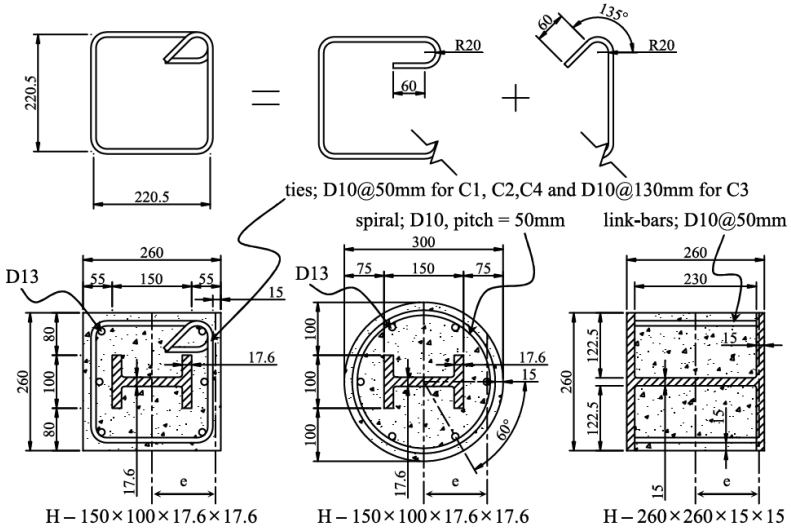

Figure 2.6 Details of test specimens (Kim et al. 2012)

An experimental study on square concrete encased concrete columns was carried by Hsu et al. (2009). A total of 24 concrete encased steel composite specimens were tested under different loading conditions. The tested specimens were 370 mm × 370 mm in the square section with concrete cylinder strength of 38 MPa. The effects of various sizes of encased steel sections and loading conditions were investigated. The tested specimens were reinforced longitudinally with four #6 (19.05 mm diameter) deformed steel bars and six different sizes of H-sections (H100 × 100 × 6 × 8, H150 × 100 × 6 × 9, H200 × 100 × 5.5 × 8, H150 × 150 × 7 × 10, H200 × 150 × 6 × 9 and H200 × 200 × 8 × 12) and transversely with #3 (9.5 mm diameter) deformed steel bars at a spacing of 100 mm within the confined region. The results of this experimental study indicated that the deterioration rates of load carrying capacity increased when the strength ratios of the

steel members in the weak axis were increased. This may be because the increased buckling resistance of steel members in the weak axis, which resulted in providing more confinement area to the concrete core of the columns. It was also observed from the experimental results that strength ratios of steel in the weak and strong sectional directions be adequately adjusted so that high member performance could be achieved.

Chen et al. (2014) studied the behaviour of concrete encased steel composite columns under seismic load. A total of 26 concrete encased steel composite column specimens were tested under cyclic reversed loading. Eighteen of the specimens were reinforced longitudinally with H-shaped steel sections and 10 mm steel bars while the remaining eight specimens were reinforced longitudinally with cross-shaped steel section, as shown in Figure 2.7. The effect of the amount transverse reinforcement, the axial compression ratio, encased depth ratio and geometry of encased steel section were investigated. The amount of transverse reinforcement ratio ranged between 0.95% and 2.4%. The axial compression ratios were 0.5, 0.65 and 0.75 with encased depth ratio of 2, 2.5 and 3. Based on the results of this study it was realised that the ductility decreased significantly when the concrete compressive strength increased. However, the ductility improved when the volumetric ratio of the transverse reinforcement increased. Also, they found that the ductility of specimens reinforced with a cross-shaped steel section was higher than the ductility of specimens reinforced with H-shaped steel section for the same condition. Therefore, they concluded that the seismic behaviour of steel-concrete composite specimens reinforced with cross-shaped steel section was better than the specimens reinforced with H-shaped steel section. This may be because the use of cross-

shaped steel section can increase the buckling resistance of longitudinal reinforcement thus providing more confinement area to the concrete core.

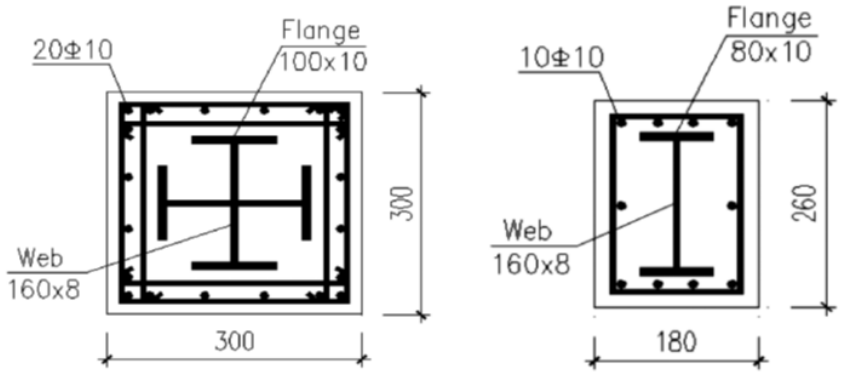

Figure 2.7 Details of test specimens (Chen et al. 2014)

An experimental study on concrete columns reinforced with steel section was carried by Wang et al. (2016) . A total of 5 square concrete specimens were tested under compression-bending. The specimens were 250 mm × 250 mm in cross-section and the concrete cover was 20 mm. One specimen was reinforced longitudinally with enlarging cross-shaped steel. Three specimens reinforced longitudinally with diagonal cross-shaped steel. The remaining specimen was reinforced with cross-shaped steel. Also, all specimens were reinforced with four longitudinal steel bars (14 mm diameter) and 6 mm diameter transverse reinforcement. The specimens were cast with 51.5 MPa. It was observed from the experimental results that as the compressive strength of concrete increased, the shear capacity increased and the deformability and ductility decreased due to brittle manner. The test results also showed that as the transverse reinforcement ratio reduced from 0.98% to 0.49%, the load carrying capacity of the specimens decreased by 16.8% and 10.0% for the specimens reinforced with enlarging and

diagonal cross-shaped steel, respectively. Also, the increased ductilities of the specimens reinforced with enlarging cross-shaped steel sections and diagonal cross-shaped steel sections were 11.5% and 7.2%, respectively. This may be because when the amount of transverse reinforcement decreased, the confinement area to the concrete core of columns also decreased.

2.4 Summary

This chapter has presented a review of studies on the behaviour of concrete columns reinforced longitudinally with either steel bars or steel sections. This review suggested that the longitudinal and transverse reinforcement are the most important factors that affect the behaviour of concrete columns. Also, the confining concrete area of the reinforced concrete (RC) columns is affected by the shape of steel section encased in concrete. According to a detailed literature review carried out herein, no study is available in the literature that deals with high strength concrete (HSC) columns reinforced with steel equal angle (SEA) sections.

The next chapter explains the transverse reinforcement detailing requirements for reinforced concrete tied columns in AS 3600 (2009) and ACI 318 (2014). In addition, the effects of different factors such as longitudinal reinforcement, transverse reinforcement, concrete strength, column geometry and eccentricity that influence the behaviour of RC columns are also presented. Furthermore, a review of the available stress-strain models of square confined and unconfined concrete is also reported

3 Confinement of Concrete Columns

3.1 Introduction

The main philosophy of using transverse reinforcement in concrete columns is to prevent buckling of longitudinal reinforcement and to restrict the lateral expansion of concrete due to Poisson's effect. The presence of the transverse reinforcement in concrete columns can improve the performance of concrete columns in terms of carrying capacity and deformability. On the other hand, the influence of transverse reinforcement is more pronounced in enhancing the ductility and after peak-stress deformability rather than load carrying capacity.

A review of literature related to previous research studies on tied concrete columns reinforced longitudinally with either steel bars or steel sections are presented in Chapter two. In this chapter, the transverse reinforcement detailing requirements for reinforced concrete tied columns in AS 3600 (2009) and ACI 318 (2014) are summarised. Also, the effect of different significant parameters such as the volumetric ratio, distribution and buckling of longitudinal reinforcement, the volumetric ratio, diameters, and spacing of transverse reinforcement, concrete compressive strength, column geometry and applied load eccentricity are also discussed in this chapter. Also, this chapter presents a detailed review of some previous analytical stress-strain models for concrete columns, which include unconfined and confined square concrete columns.

3.2 Design Code Requirements for Confinement of Reinforced Concrete Columns

The concept of concrete confined with transverse reinforcement was investigated by many researchers such as Sheikh and Uzumeri (1982), Mander et al. (1988b), Razvi and Saatcioglu (1994), Razvi and Saatcioglu (1999), Ros et al. (2003), Paultre and Légeron (2008) and Somma and Pieretto (2016). The investigation results of these researchers revealed that the ductility of the concrete columns improved with an increase in the lateral pressure.

As shown in Figure 3.1, the concrete in the core is restricted from expansion by the tie reinforcement, leading to the confinement of the concrete core and the separation of the concrete cover from the concrete core (Foster et al. 1998; Awati and Khadiranaikar 2012). After that, the load carrying capacity of the concrete core of columns is strongly affected by the confinement and can be expected to be greater than that of plain concrete. However, the improvements obtained from lateral confinement based on the spacing, strength and volumetric ratio of transverse reinforcement (Cusson and Paultre 1994; Sharma et al. 2005; Awati and Khadiranaikar 2012). Hence, it is reported that ductility is affected by the transverse reinforcement. Consequently, design codes such as the Australian Standard AS 3600 (2009) and the ACI 318 (2014) require various requirements for detailing of reinforcement in concrete columns.

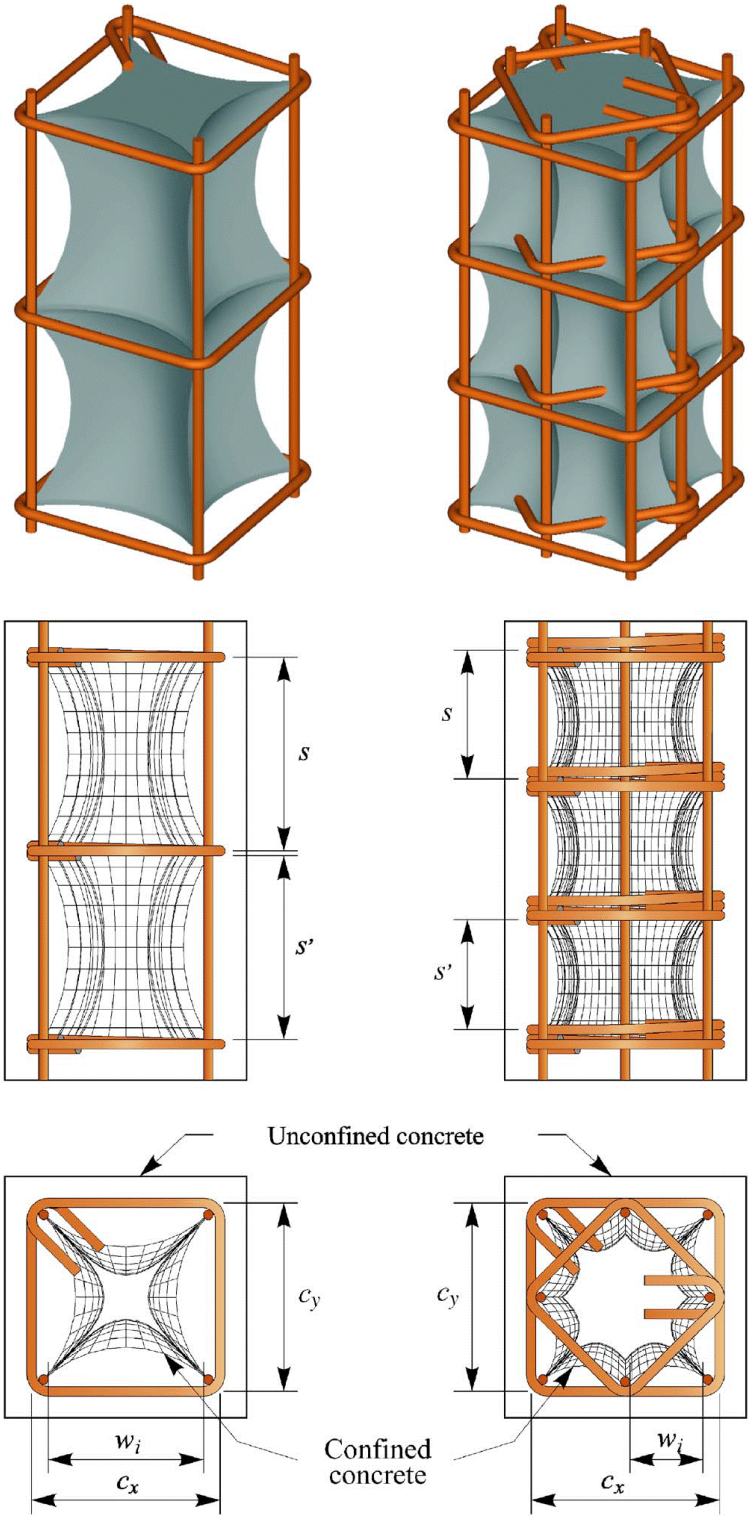

Figure 3.1 Confinement of reinforced concrete in square columns (Paultre and Légeron 2008)

3.2.1 **Determination of Required Spacing of Transverse Ties Based on AS 3600 (2009)**

The purpose of specifying minimum confinement of ligaments in the Australian Standard AS 3600 (2009) is to attempt to ensure ductility behaviour in concrete columns. To avoid premature buckling of longitudinal reinforcement, the transverse ties requirement is provided by AS 3600 (2009). The detailing requirements for transverse reinforcement in AS 3600 (2009) standard take into account the compressive strength of concrete. The maximum spacing of transverse ties for low to medium strength concrete ($f_c' \leq 50\,MPa$) according to AS 3600 (2009) is based on the column geometry and longitudinal reinforcement size. For concrete columns that are reinforced longitudinally with steel bars, AS 3600 (2009) requires that the spacing of transverse ties does not exceed 15 longitudinal steel bar diameters or the least lateral dimension of the concrete column.

For the concrete columns made of high strength concrete ($f_c' > 50\,MPa$), AS 3600 (2009) requires that the spacing of transverse reinforcement not exceed the smaller of $0.8D_c$ (D_c is the least lateral dimension of concrete column), 300 mm and the requirement of the spacing of transverse ties for low to medium strength concrete ($f_c' \leq 50\,MPa$). Also, according to AS 3600 (2009), the requirement to provide an effective confining pressure of $0.01f_c'$ is considered to be satisfied by giving spacing as follows:

For rectangular sections $$s \leq \frac{15nA_b f_y}{f_c'\sqrt{A_{cc}}} \tag{3.1}$$

where A_b is area of one leg of the transverse ties, f_y is the yield tensile stress of the transverse ties limited to 800 MPa, A_{cc} is the cross-sectional area of the core bounded by the centreline of the outermost confining bars and n is the number of transversely restricted longitudinal reinforcement.

3.2.2 **Determination of Required Spacing of Transverse Ties Based on ACI 318 (2014)**

The ACI 318 (2014) requires that the vertical spacing of transverse ties shall not exceed 16 longitudinal steel bar diameters, 48 transverse steel bar diameters or the smaller dimension of the compression member. Also, ACI 318 (2014) requires that the volumetric transverse reinforcement for square or rectangular reinforced concrete (RC) columns shall be not less than the value given by:

$$\rho_s = 0.3\left(\frac{A_g}{A_{ch}} - 1\right)\frac{f_c'}{f_y} \tag{3.2}$$

or

$$\rho_s = 0.09\frac{f_c'}{f_y} \tag{3.3}$$

where A_g is the gross area of concrete column section, A_{ch} is the concrete core area of column measured to the outside of the transverse reinforcement, f_y is the yield tensile strength of the transverse reinforcement.

3.3 Factors Affecting the Confined Concrete Column Behaviour

The factors that influence on the strength and ductility of reinforced concrete (RC) columns are discussed herein. These factors including the most significant parameters such as volumetric ratio, distribution, strength and buckling of longitudinal reinforcement, spacing, volumetric ratio, strength and configuration of transverse reinforcement, concrete compressive strength, column geometry and eccentricity, can influence the behaviour of concrete columns in terms of strength, ductility and failure modes.

3.3.1 **Longitudinal Reinforcement**

The presence of longitudinal reinforcement could enhance the confinement mechanism, strength and ductility of the reinforced concrete columns (Ho et al. 2010; Leite et al. 2013; Bing et al. 2001). A limit of 1% was determined for longitudinal reinforcement ratio in concrete columns AS 3600 (2009) and ACI 318 (2014). The presence of the minimum requirement longitudinal reinforcement for concrete columns was to prevent passive yielding of reinforcement, which results from creep and shrinkage deformation in the concrete (Cloyd 1998; Ziehl et al. 1998; CSA 2004; AS 2009; ACI 2014). Also, a minimum number of longitudinal reinforcement is required for the stability of steel cages as well as for providing confinement to the transverse expansion of the concrete core. Thereby, a number of investigations were carried out in the literature to study the contribution and the influence of longitudinal reinforcement bars on the ductility of high strength concrete (HSC) columns.

An experimental study by Foster and Attard (1997) was carried out on normal and high strength concrete columns. A total of 68 concrete column specimens were tested under eccentric compressive loads. All column specimens had a cross-section of 150 mm × 150 mm. The concrete compressive strength of the tested specimens ranged between 40 MPa and 90 MPa. It was observed from the experimental results that the arrangement of the longitudinal reinforcement in reinforced concrete could improve the confinement of the concrete core. This can lead to improving the ductility of reinforced concrete columns (Bing et al. 2001).

The research program that was done by Nagashima et al. (1992) including testing of 26 HSC specimens with 225 mm square cross section and a height of 716 mm. The specimens were reinforced longitudinally with steel bars (10 mm in diameter), which had different distributions and different strengths. All specimens were tested under monotonic axial load. They observed that for the same configuration ties, the load carrying capacity of the confined concrete of columns was independent of the number of longitudinal steel bars. They also reported that the strength of longitudinal steel bars had a slight influence on the stress-strain response of the columns.

Mander et al. (1988a) observed that the number of the longitudinal reinforcement had a slight effect on the stress-strain response of the concrete columns. A similar result was also reported by Hwee and Rangan (1990) when they carried out an experimental program on 12 high strength concrete (HSC) columns with different deformed steel bar diameters of either 12 mm or 6 mm. All columns had a cross-section of 150 mm × 150 mm and 800 mm height. The columns were cast with concrete strength ranging between

59 MPa and 68 MPa. The results also showed that the amount of longitudinal reinforcement had little effect on the axial stress-stress behaviour of the HSC columns. However, the amount of longitudinal reinforcement can enhance the effective confinement of the concrete core area (Campione and Minafò 2010). Also, it was reported that the effective confinement of reinforced concrete columns could be improved as the number of longitudinal reinforcement increases as well as when using a good distribution of longitudinal reinforcement around the perimeter of the concrete column section (Paultre et al. 2010). This may be because the amount and distribution of longitudinal reinforcement have significantly improved the buckling resistance of longitudinal reinforcement leading to more confinement area to the concrete core of the column, which results in improving the strength and stiffness of reinforced concrete columns.

In an analytical study by Claeson (1999), it was conducted to investigate the effect of the yield strength of longitudinal steel bars on the behaviour of reinforced concrete columns. He reported that the strength of longitudinal reinforcement had a slight effect on the post-peak behaviour of columns.

Sharma et al. (2005) studied the effects of the different amount of longitudinal reinforcement on the behaviour of reinforced concrete columns. As shown in Figure 3.2, the amount of longitudinal reinforcement has only a slight influence on the behaviour of the reinforced concrete column.

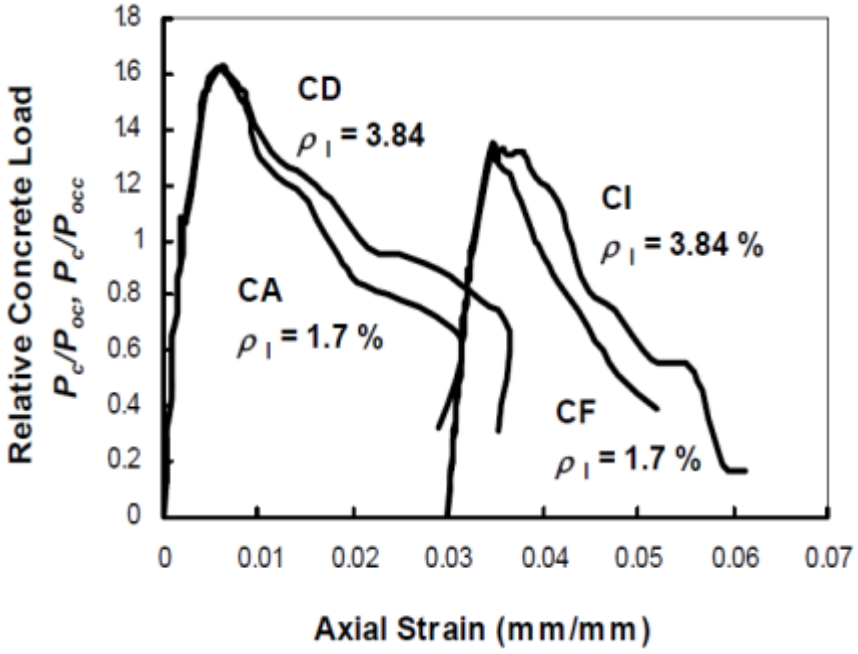

Figure 3.2 Effect of longitudinal reinforcement ratio on the behaviour of reinforced concrete columns (Sharma et al. 2005)

In relation to the buckling of longitudinal reinforcement in reinforced concrete (RC) columns under axial compression, a number of studies have investigated the influence of buckling on the behaviour of concrete columns. Reinforced concrete (RC) members, which were designed to resist significant forces and deformations under compression or large tensile strains followed by compression such as seismic forces, should account for potential loss of resistance generated by the buckling of longitudinal reinforcement (Massone and López 2014). Deformability of concrete after the ultimate stress is importantly influenced by the behaviour of longitudinal reinforcement (Saatcioglu and Razvi 1992).

According to Cusson and Paultre (1994) and Sharma et al. (2005), the use of large diameter of longitudinal steel bar in concrete columns resulted in marginal improving of the strength of concrete columns, whereas the large diameter of longitudinal reinforcement would prevent premature buckling of longitudinal reinforcement. Also, the buckling of longitudinal reinforcement resulted in significant damage in the concrete core of reinforced concrete columns (Hong et al. 2006b). Sato and Yamaguchi (2000) observed that after buckling of longitudinal reinforcement in reinforced concrete columns, the strength and stiffness of reinforced concrete columns significantly decreased. Also, it was found that the increased buckling resistance of longitudinal reinforcement resulted in providing more confinement area to the concrete core, whereas the outward buckling of longitudinal reinforcement from the core led to a significant decrease in the confinement of the concrete core (Campione and Minafò 2010).

3.3.2 **Transverse Reinforcement**

One of the functions of transverse reinforcement (helices or ties) is to provide passive lateral confining pressure to the concrete core by restricting lateral expansion of the concrete core. This passive confining pressure is then dependent on the spacing, volumetric ratio, configuration and strength of transverse reinforcement as well as the properties of longitudinal reinforcement. According to Bresler and Gilbert (1961), the confinement of concrete core provided by transverse ties was not effective all in improving the strength of reinforced concrete columns as the spacing of transverse ties was twice the concrete core cross-section. A similar observation was reported by Sheikh and Uzumeri (1982).

Sheikh and Yeh (1990) carried out tests on 15 square concrete columns (305 mm × 305 mm × 2740 mm) under flexural and axial load. The columns were cast with concrete compressive strength ranging between 25.9 MPa and 34.2 MPa. Based on test results it was noted that the amount of transverse reinforcement had significant effects on the column behaviour. Also, test results showed that before crushing of unconfined concrete, the transverse ties had little effects on the behaviour of the reinforced concrete columns. They also reported that when the spacing of transverse ties decreased, the confinement of concrete increased. However, the concrete cover in columns with a small spacing of transverse ties started to crush and spall off earlier than the columns with a larger spacing of transverse ties.

The configuration of transverse reinforcement has also been shown to influence column strength and ductility. Twenty-six high strength concrete with square (225 mm × 225 mm) cross section concrete columns were tested under monotonic axial compression by Nagashima et al. (1992), to investigate the effect of transverse reinforcement on the behaviour of columns. They reported that the load carrying capacity of the concrete columns increased when the spacing of transverse ties decreased. They also observed that the configuration of transverse reinforcement affected the behaviour of reinforced concrete columns. The magnitude of the improvements in the strength and ductility of RC columns provided by transverse reinforcement based on the type of configuration.

Chung et al. (2002b) investigated the effect of strength and ratio of transverse reinforcement on the behaviour of reinforced concrete columns. The columns were 200 mm × 200 mm in cross-section and 600 mm height. Increase in the spacing of

transverse reinforcement decreases the ductility of reinforced concrete columns for same longitudinal reinforcement ratio. Also, it was reported that the effectiveness of the confinement provided by transverse reinforcement decreased as the spacing of transverse ties increased and when the transverse tie spacing equal to the column cross-section, the effects of transverse reinforcement did not develop any confinement (Antonius and Imran 2012).

Suzuki et al. (2004) investigated the effect of transverse reinforcement by testing 27 specimens with the same longitudinal reinforcement. The volumetric ratio of transverse reinforcement ranged between 0.32% and 1.92%. Also, three different yield tensile strengths (317 MPa, 1028 MPa and 1288 MPa) were used for transverse ties. They observed that the transverse ties did not yield when using high strength concrete or high strength ties. They also reported that the increase of yield tensile strength of transverse tie had little effect on the improvement of transverse confinement in reinforced concrete columns. This is because the stress of transverse ties at maximum load is less than 50% of the yield tensile strength of ties. Also, test results showed that when the volumetric ratio of transverse reinforcement increased, the maximum stress and the corresponding strain of reinforced concrete columns increased, as illustrated in Figure 3.3.

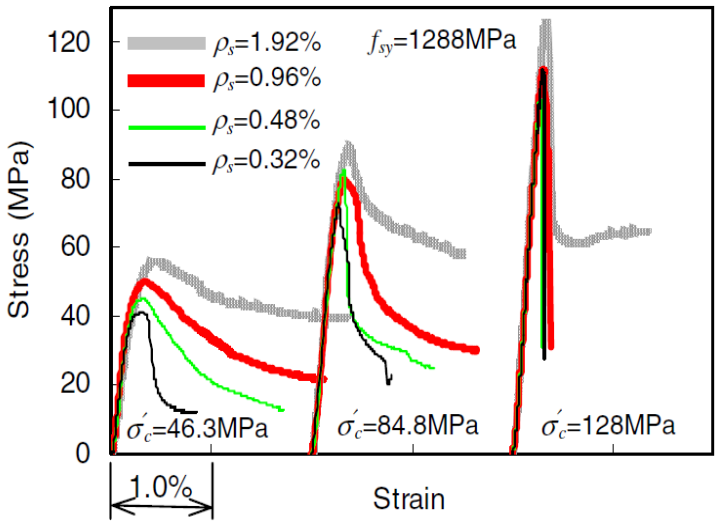

Figure 3.3 Effect of transverse reinforcement ratio (Suzuki et al. 2004)

Hong et al. (2006a) tested square reinforced concrete columns under concentric axial load. The concrete columns had three different compressive strengths (40 MPa, 80 MPa and 120 MPa). The transverse reinforcement ratios of the columns were 0.32%, 0.48%, 0.51%, 0.96%, 1.01%, and 1.92%. They reported that the high strength transverse ties in high strength concrete (HSC) columns did not yield at the maximum axial load (Figure 3.4). Based on test results it was also noted that when increasing the strength of transverse ties, the lateral confinement provided by lateral steel ties did not significantly enhance.

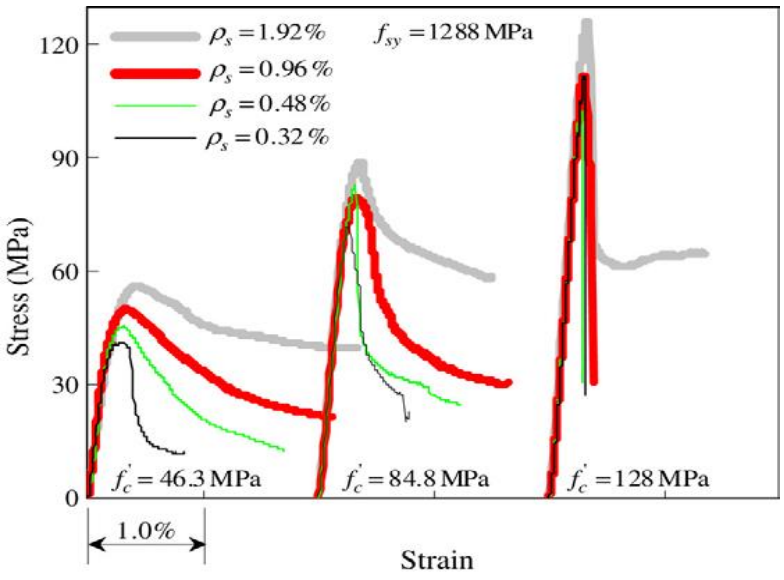

Figure 3.4 Effect of transverse reinforcement ratio (Hong et al. 2006a)

An experimental study by Yang and Kim (2016) was conducted to investigate the effect of transverse reinforcement on the behaviour of 14 columns under concentric axial load. They reported that the confinement providing from using transverse ties with a 90-degree hook was not effective compared to the confinement providing from using transverse ties with 135-degree hooks or rectangular hoops. They also observed that after the peak axial load and with increase axial deformation of reinforced concrete (RC) columns, the 90-degree hooks were gradually opened due to the lateral expansion of concrete core. This can result in early buckling of the longitudinal reinforcement and a severe crushing of the concrete core of RC columns.

3.3.3 **Concrete Strength**

Several researchers examined the influence of concrete strength on the behaviour of the confined core. The use of high strength concrete (HSC) in the construction of concrete

structures has been increased over the last few decades. The main problem associated with the use of HSC in the construction of columns is the lower ductility of the HSC column than the ductility of the normal strength concrete (NSC) column for the same amount of confinement reinforcement (Sharma et al. 2005; Husem et al. 2016). This is because the ductility of concrete decreases with the increase in the compressive strength of concrete (Ozbakkaloglu and Saatcioglu 2004; Kwan and Ho 2010; Leite et al. 2013). It was also observed that the failure mode of NSC was different from the HSC. The failure of NSC columns was gradually after the peak axial load, while the failure of HSC columns was exploded at the peak axial load (Hsu and Hsu 1994).

The efficiency of the confinement provided by the transverse reinforcement decreases with the increase in the compressive strength of concrete (Bayrak and Sheikh 1998). For achieving a similar ductility, HSC columns need to be confined significantly more than NSC columns (Mendis et al. 2000). This is because HSC shows small lateral expansion under axial compression than NSC as well as the HSC has a higher modulus of elasticity and lower internal microcracking (Cusson and Paultre 1994; Suzuki et al. 2004; Sharma et al. 2005; Hong et al. 2006a). Thereby, the transverse reinforcement comes into play later in the process, and the efficiency of passive confinement of HSC would be decreased (Cusson and Paultre 1994).

3.3.4 **Column Geometry**

The form of transverse reinforcement also affects the confining pressure produced in a concrete core. The superiority of circular helices comes from the geometric shape,

which creates a uniform and continuous pressure around the perimeter of the core. Whereas, rectilinear ties create a nonuniform pressure which peaks at locations of transverse legs of ties (Saatcioglu and Razvi 1992). Therefore, the helices reinforcement provides a better confining of the concrete core, as shown in Figure 3.5 (a). However, transverse tie reinforcement provides effective confining pressure only at the corners of the concrete core, which are the locations at the longitudinal steel bars, as shown in Figure 3.5 (b). Thereby, transverse tie reinforcement will provide less confining effect than transverse helix reinforcement even with the same volumetric ratio.

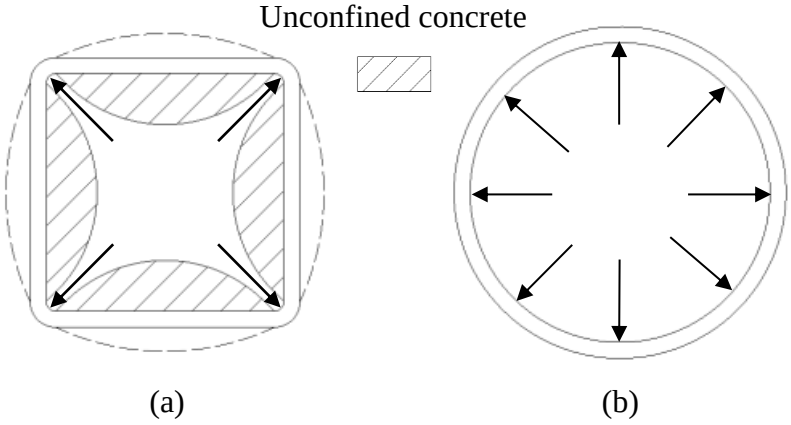

Figure 3.5 Confinement with transverse reinforcement: (a) Square tie and (b) Helix (Park and Paulay 1975)

Saatcioglu and Razvi (1998) investigated the effect of column geometry on the behaviour of reinforced concrete (RC) columns with different geometries (square and circular) that were tested under monotonically increasing axial compression. The square and circular concrete columns had a compressive strength of 124 MPa and were reinforced laterally with steel bar reinforcement ratio of about 3%. They reported that

the failure of square columns was in brittle behaviour, whereas the failure of circular columns was more ductile behaviour than square columns. Also, test results reported that when the volumetric ratio of transverse reinforcement in square columns was 64% higher than the volumetric ratio of transverse reinforcement in circular columns, the square and circular columns achieved a similar behaviour.

An experimental study by Sharma et al. (2005) was conducted to examine the influence of section geometry on the behaviour of high strength concrete (HSC) columns. Eighteen HSC columns with square (150 mm × 150 mm) cross section reinforced with lateral steel ties and eighteen HSC columns with circular (150 mm diameter) concrete column reinforced with lateral steel helices were tested under monotonically increasing axial compression. Both the square and circular columns were reinforced laterally with a similar amount of transverse reinforcement. Based on test results it was noted that the columns with helices were better effective than the columns in terms of strength and ductility. As presented in Figure 3.6, at the peak axial load, the axial strains of square columns were 0.42% and 0.51%, whereas the axial strains of circular columns were developed to 0.74% and 0.81%. Also, test results showed that for a given transverse reinforcement ratio, the strength and ductility of circular concrete columns were 28% and 66%, respectively, higher than the strength and ductility of square columns. Thus, they recommended that more transverse reinforcement ratio is required in square columns to achieve the desired strength and ductility as in circular columns.

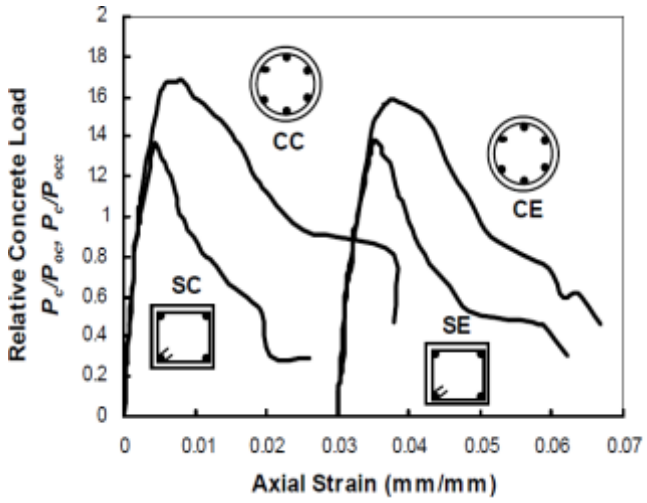

Figure 3.6 Effect of column geometry on the behaviour of reinforced concrete columns (Sharma et al. 2005)

3.3.5 **Eccentricity**

Columns are structural members subjected to combined axial compression and bending moment, rather than pure axial compression as flexural effects may be created by construction errors and lateral forces (Hadi 2006; Hadi et al. 2016b). A number of researchers have studied the behaviour of the HSC columns under axial compression. However, a few research studies were carried out on the behaviour of the high strength concrete (HSC) columns under eccentric axial loads. The most important factor is the value of initial eccentricity of the axial load that affects the performance of the columns. Under eccentric axial load, reinforced concrete (RC) columns might not be subjected to the same concrete cover stability problem, as the concrete cover on the compression surface of the RC columns tends to buckle towards the concrete core of the columns, which gives adequate transverse restraint against the instability of the concrete cover (Saatcioglu and Razvi 1998).

Lloyd and Rangan (1996) tested 36 rectangular/square columns to study the behaviour of high strength concrete (HSC) subjected to eccentric loading. The results indicated that when the initial eccentricity less than 30% of the lateral dimension of the cross-section of the column, the transverse reinforcement in concrete columns had little effect on the ductile behaviour of columns. Foster and Attard (1997) tested sixty-eight square normal and high strength concrete columns under eccentric compression. They reported that the ductility behaviour of RC columns was based on the confining pressure supplied by transverse reinforcement. Also, they found that the effectiveness of transverse reinforcement was influenced by factors such as compressive concrete strength and the spacing of ties. Lee and Son (2000) tested 32 RC columns with concrete compressive strength ranged between 55 MPa to 65 MPa and subjected to different eccentric loads. It was reported that as the initial eccentricity decreased the concrete cover spalling area increased. Canbay et al. (2006) tested eleven 250 mm × 250 mm × 1500 mm high strength reinforced concrete columns to examine the behaviour of columns confined laterally with ties under eccentric axial load. They concluded that an increase in the ratio of transverse reinforcement or closer tie spacing might result in improving the strength and ductility of reinforced concrete columns under eccentric axial load. Kottb et al. (2015) tested ten square RC columns to investigate the behaviour of high strength concrete columns under eccentric axial loads. They reported that as eccentricity increased, the strength of columns decreased (Figure 3.7).

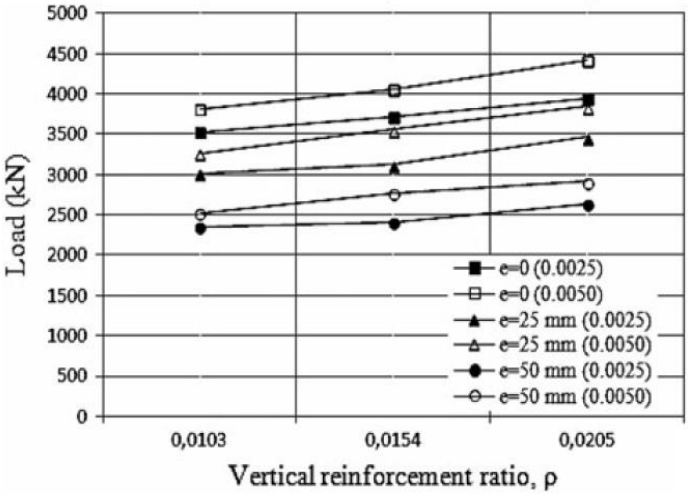

Figure 3.7 Effect of eccentricity on the strength of concrete columns (Husem et al. 2016)

3.4 Stress-Strain Model of Concrete

Several experimental studies were conducted in the past to propose the stress-strain relationship of unconfined concrete and confined concrete by transverse reinforcement. The earlier stress-strain relationship models were based on the experimental results with normal strength concrete (NSC). Some of these models can be used to cover both normal strength concrete and high strength concrete. The stress-strain behaviour of concrete changes with the changing of concrete compressive strength (Ozbakkaloglu and Saatcioglu 2004). In general, the ascending and descending branches of the stress-strain curve becomes steeper as the compressive strength of concrete increases (Tsai 1988; Hsu and Hsu 1994). Therefore, the stress-strain models of NSC columns may be not adequate for HSC columns (Cusson and Paultre 1995). It has been noted in a comprehensive literature review that most of the earlier studies focused on the stress-strain behaviour of confined NSC columns (Richart et al. 1928; Richart et al. 1929;

Chan 1955; Popovics 1973; Sheikh and Uzumeri 1982; Mander et al. 1988a; Mander et al. 1988b; Saatcioglu and Razvi 1992). However, a few studies carried out on the stress-strain behaviour of confined HSC columns (Yong et al. 1988; Bjerkeli et al. 1990; Cusson and Paultre 1994; Cusson and Paultre 1995). From a review of the literature, it can be concluded that generally, the ascending branch of the stress-strain behaviour for the HSC is more linear than for the NSC. Also, the NSC columns gradually fail after reaching the maximum axial load, whereas the HSC columns explode at the maximum axial load (Hsu and Hsu 1994).

3.4.1 **Stress-Strain Models for Unconfined Concrete**

Popovics (1973) suggested a single equation to predict stress-strain relationship for unconfined concrete. There are three main parameters (f'_{co}, E_c) used to control the ascending and descending branches behaviour of stress-strain curve. The mathematical expression for the ascending branch of the stress-strain relationship is given below.

$$f_c = \frac{f'_c \left(\frac{\varepsilon_c}{\varepsilon'_c}\right) r}{r - 1 + \left(\frac{\varepsilon_c}{\varepsilon'_c}\right)^r} \qquad \text{for} \qquad \varepsilon_c \leq \varepsilon'_c \tag{3.4}$$

The parameter r determines the initial slope and the curvature of the ascending branch of the stress-strain curve.

where $$r = \frac{E_c}{E_c - E_{sec}} \tag{3.5}$$

The secant modulus of elasticity of confined concrete can be expressed as follows:

$$E_{sec} = \frac{f_c'}{\varepsilon_c'} \tag{3.6}$$

The modulus of elasticity of unconfined concrete can be expressed as follows:

$$E_c = 3320\sqrt{f_c'} + 6900 \tag{3.7}$$

The stress-strain relationship of Popovics (1973), which is applicable for NSC, was modified by Thorenfeldt et al. (1987) to be applicable for HSC. The post-peak part of the model becomes steeper with an increase in the compressive strength of concrete. The authors proposed the following equation for the unconfined concrete stress-strain relation

$$f_c = f_c' \left(\frac{\varepsilon_c}{\varepsilon_c'}\right) \frac{n}{\left[n - 1 + \left(\frac{\varepsilon_c}{\varepsilon_c'}\right)^{nk}\right]} \tag{3.8}$$

$$k = 1 \qquad \text{when} \qquad \frac{\varepsilon_c}{\varepsilon_c'} \leq 1 \tag{3.9}$$

or

$$k = 0.67 + \frac{f_c'}{62} \qquad \text{when} \qquad \frac{\varepsilon_c}{\varepsilon_c'} \geq 1 \tag{3.10}$$

where

$$n = 0.8 + \frac{f_c'}{17} \tag{3.11}$$

$$E_c = 3320\sqrt{f_c'} + 6900 \text{ (MPa)} \tag{3.12}$$

The strain ε_c' is defined below.

$$\varepsilon_c' = \frac{f_c'}{E_c}\left(\frac{n}{n-1}\right) \tag{3.13}$$

where f_c and ε_c are the axial compressive concrete stress and axial concrete strain, respectively; f_c', ε_c' are the unconfined compressive concrete strength and unconfined concrete strain, respectively, and E_c is the elastic modulus of concrete.

3.4.2 **Stress-Strain Models for Concrete Confined by Tie Reinforcement**

Sheikh and Uzumeri (1982) had developed an analytical stress-strain model for concrete confined laterally with steel ties. The stress-strain model was derived from test data obtained from previous studies. One of the significant characteristics of the proposed model is the concept of the concrete effectively confined within the concrete core surrounded by the centre line of the perimeter ties. The proposed stress-strain curve consists of three parts. The first part (ascending branch) is a second-degree parabola, while the second and third parts are straight lines, as shown in Figure 3.8. The mathematical expression for the stress-strain relationship is given below.

$$f_c = f_{cc}'\left[2\left(\frac{\varepsilon_c}{\varepsilon_{cc}}\right) - \left(\frac{\varepsilon_c}{\varepsilon_{cc}}\right)^2\right] \quad \text{for} \quad \varepsilon_c \le \varepsilon_{cc1} \tag{3.14}$$

The mathematical expression for the horizontal branch of the stress-strain relationship is given below.

$$f_c = K_s f_{co}' \quad \text{for} \quad \varepsilon_{cc1} < \varepsilon_c \le \varepsilon_{cc2} \tag{3.15}$$

$$K_s = 1.0 + \frac{b_c^2}{140 P_{occ}} \left[\left(1 - \frac{nC^2}{5.5 b_c^2} \right) \left(1 - \frac{s}{2b_c} \right)^2 \right] \sqrt{\rho_s f_s'} \tag{3.16}$$

The mathematical expression for the descending branch of the stress-strain relationship is given below.

$$f_c = f_{cc}'[1 - Z(\varepsilon_c - \varepsilon_{cc})] \quad \text{for} \quad \varepsilon_{cc2} < \varepsilon_c \leq \varepsilon_{cc30} \tag{3.17}$$

where

$$Z = \frac{0.5}{\frac{3}{4}\rho_s \sqrt{\frac{b_c}{s}}} \tag{3.18}$$

where f_{cc}', $\varepsilon_{cc1}$and ε_{cc2} are defined below.

$$f_{cc}' = K_s f_{co}' \tag{3.19}$$

$$\varepsilon_{cc1} = 80 K_s f_c' \times 10^{-6} \tag{3.20}$$

$$\varepsilon_{cc2} = \varepsilon_{co} \left[1 + \frac{248}{C} \left[1 - 5.0 \left(\frac{s}{b_c} \right)^2 \right] \frac{\rho_s f_s'}{\sqrt{f_c'}} \right] \tag{3.21}$$

where b_c is the width of confined concrete core (centre-to-centre of transverse ties), A_{cc} is the area of confined concrete core, K_s is the magnification factor, the f_s' is the stress of the transverse ties. and C is the distance between longitudinal reinforcement.

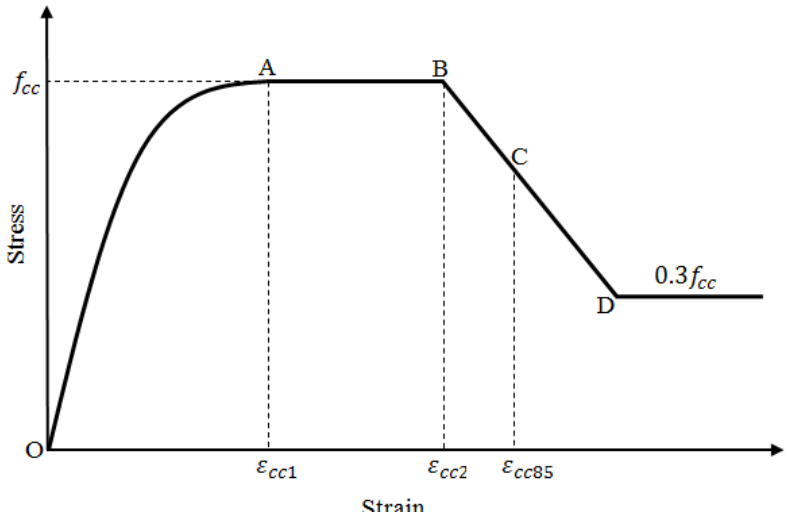

Figure 3.8 Stress-strain curve of concrete (Sheikh and Uzumeri 1982)

Fafitis and Shah (1985) suggested a stress-strain relationship for confined concrete. The authors proposed two equations for the ascending and descending parts of the stress-strain curve as Equations (3.22) and (3.23), respectively.

$$f_c = f_{cc}\left[1 - \left(1 - \frac{\varepsilon_c}{\varepsilon_{cc}}\right)^A\right] \qquad \text{for} \quad 0 \le \varepsilon_c \le \varepsilon_{cc} \qquad (3.22)$$

$$f_c = f_{cc}exp[-k(\varepsilon_c - \varepsilon_{cc})^{1.15}] \qquad \text{for} \quad \varepsilon_{cc} \le \varepsilon_c \qquad (3.23)$$

The equations for the constant A and k:

$$A = \frac{E_c\varepsilon_{cc}}{f_{cc}} \qquad (3.24)$$

$$k = 0.17f_{cc}exp(-0.01f_l) \qquad (3.25)$$

where f_{cc} and ε_{cc} can be found using the following equations:

$$f_{cc} = f' + \left(1.15 + \frac{3048}{f_c'}\right) f_l \tag{3.26}$$

$$\varepsilon_{cc} = 1.027 \times 10^{-7} f_c' + 0.0296 \frac{f_l}{f_{cc}} + 0.00195 \tag{3.27}$$

where f_l represents the confinement pressure and is given by the following equations:

For circular columns $$f_l = \frac{2A_{st} f_{yh}}{s d_s} \tag{3.28}$$

For square columns $$f_l = \frac{2A_{st} f_{yh}}{s d_e} \tag{3.29}$$

$d_s$is the core diameter of the column and d_e is the equivalent diameter.

3.5 Summary

This chapter has presented a review of the transverse reinforcement detailing requirements for concrete columns confined by ties in AS 3600 (2009) and ACI 318 (2014). Also, the influences of different factors such as longitudinal reinforcement, transverse reinforcement, concrete strength, column geometry and eccentricity that affect the behaviour of confined concrete columns were also presented. Also, in this chapter stress-strain relationship for unconfined and confined concrete columns presented. This review suggested that by using high strength concrete with concrete structures have advantages such as decrease cross-section and increase strength, which leads to economic structures. However, high strength concrete (HSC) has some

deficiencies; such as a more sudden failure, brittleness and low ductility as compared with normal strength concrete (NSC). Also, it was reported that; high strength concrete columns need more amount of transverse reinforcement than normal strength concrete to achieve similar ductility. Moreover, it has shown that the effective confined concrete area in columns reinforced laterally with square ties is less than the core area of the columns, which means that the strength capacity and ductility of confined columns decrease. The extensive review of literature in Chapters two and three exhibited that there is a gap in the existing knowledge about the behaviour of concrete columns reinforced longitudinally with SEA sections.

The next chapter explains the details of the experimental investigation of pullout specimens. The preparing, fabrication, placement and curing process of the pullout specimens are also presented. Also, the test results of the pullout specimens tested under the direct pullout test are reported and discussed.

4 EXPERIMENTAL INVESTIGATION OF PULLOUT SPECIMENS

4.1 General

In order to better understand the behaviour of steel equal angle (SEA) sections in high strength concrete, it is essential to design a new procedure to improve pullout resistance of steel equal angle (SEA) sections embedded in HSC. For this aim, an experimental investigation is performed in this chapter to assess the pullout behaviour of N12 deformed steel bars and SEA sections in HSC. This is because this study proposed to use the SEA sections as longitudinal reinforcement in HSC columns. A total of fifteen pullout specimens with different types of longitudinal reinforcement (deformed steel bars or plain SEA sections) embedded in HSC pullout specimens were tested under direct tensile pullout test. All pullout specimens were cast and tested at the High Bay Laboratories, University of Wollongong, Australia. Finally, the experimental results of the pullout specimens were presented and discussed.

4.2 Pullout Specimens

4.2.1 **Description of the Pullout Specimens**

In this section, a new procedure was proposed to improve pullout resistance of steel equal angle (SEA) sections embedded in high strength concrete (HSC), as SEA sections were required to use as longitudinal reinforcement. The main objective of this study is the use of SEA sections instead of steel bars in reinforcing square HSC columns. As the

surfaces of the SEA sections were smooth, it was essential to design a new procedure to improve the pullout resistance of steel equal angle (SEA) sections embedded in HSC. For this aim, an experimental investigation is described in this chapter to assess the pullout behaviour of N12 deformed steel bars and SEA sections in HSC. The test variables in the pullout test investigation were reinforcing type and size (N12 steel bars, A30 and A40 SEA sections). The test matrix of pullout specimens was developed to investigate the pullout load-slip response of SEA sections embedded in HSC. A total of 15 pullout specimens were cast and tested, as reported in Table 4.1. The pullout specimens were divided into five groups with three specimens in each group. The first group (Group PN12) was considered as a reference group. The pullout specimens in Group PN12 were reinforced with embedded N12 deformed steel bars (12 mm diameter). The specimens in the second group (Group PA30) were reinforced with A30 SEA sections (29.1 mm × 29.1 mm × 2.25 mm). The specimens in the third group (Group PA30W) were reinforced with A30 SEA section with welded small steel bar pieces at the embedded end. The specimens in the fourth group (Group PA40) were reinforced with A40 SEA sections (39.3 mm × 39.3 mm × 3.7 mm). The specimens in the fifth group (Group PA40W) were reinforced with A40 SEA section with welded small steel bar pieces at the embedded end. For Specimens in Groups PA30W and PA40W, two small steel bars were welded at the embedded end of the SEA section, as shown in Figure 4.1(a). At first, one small steel bar with 8 mm diameter and 40 mm length was welded transversely between the legs of SEA section. Second, one short steel bar with 16 mm diameter and 70 mm length was welded at the embedded end of SEA sections (Figure 4.1(a)). The reason for using two short steel bars (at the embedded

end) was to prevent slippage of steel equal angle (SEA) sections, as the surfaces of the SEA sections were smooth.

Table 4.1 Details of pullout specimens

Group	Specimen	Reinforcement type	Welded steel bar pieces	Size of specimens mm × mm × mm
N12	N12-1	N12 deformed steel bars	-	100 × 100 × 100
	N12-2			
	N12-3			
PA30	PA30-1	A30 SEA sections	-	100 × 100 × 100
	PA30-2			
	PA30-3			
PA30W	PA30W-1	A30 SEA sections	Yes	100 × 100 × 100
	PA30W-2			
	PA30W-3			
PA40	PA40-1	A40 SEA sections	-	150 × 150 × 150
	PA40-2			
	PA40-3			
PA40W	PA40W-1	A40 SEA sections	Yes	150 × 150 × 150
	PA40W-2			
	PA40W-3			

All pullout specimens were cast on the same day at the laboratories of the School of Civil, Mining and Environmental Engineering at the University of Wollongong, Australia. The full details and results of the used materials (steel bars, SEA sections and concrete) are reported in Chapters five and six. For clarity, the compressive strength of concrete tests was used to determine the concrete performance according to AS 3600 (2009). The average compressive strength of the concrete used in the pullout test specimens was 68.5 MPa. Tensile tests were performed to determine the tensile behaviour of the deformed N12 steel bars, A30 and A40 SEA sections according to AS 1391 (2007). The average yield tensile strengths of A30 and A40 SEA sections were 374 MPa and 473 MPa, respectively.

Wooden cubes of 100 mm × 100 mm ×100 mm were used as formwork for the N12 deformed steel bars and the A30 SEA specimens. Wooden cubes of 150 mm × 150 mm × 150 mm were used as formwork for the A40 SEA specimens. The steel bars and SEA sections were placed vertically along a central axis in each wooden cube. The cubic size of pullout specimens was based on the steel bar diameter according to RILEM (1983). The steel bar is rounded cross-section while the SEA section is equal angle section. Therefore, to fabricate pullout specimens for SEA sections, the equivalent diameter for each SEA sections was used to determine the dimensions of the wooden formwork. All the reinforcing deformed steel bars and the SEA sections were placed in a vertical position within the wooden formworks before pouring concrete. Before pouring concrete, small wood pieces were used on the top face of the cubes to fix the single embedded reinforcement in a vertical position inside the wooden formworks, as shown in Figure 4.1(b). Afterwards, the concrete was poured inside the wooden formwork

(cubes). The external electrical vibrator was used to compact the concrete of the pullout specimens (Figure 4.1(c)). After the concrete was cast, pullout specimens were left for 24 hours inside the lab. Then wooden moulds were removed, and pullout specimens were cured by placing in water tank up to 28th day till testing (Figure 4.2)

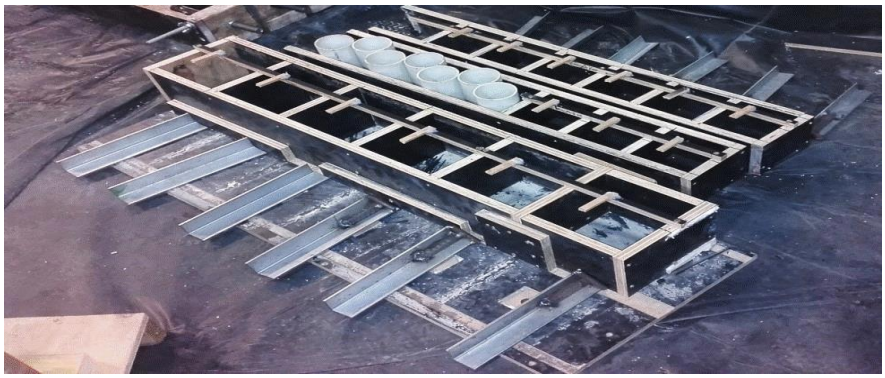

(a)

(b)

(c)

Figure 4.1 Preparing, Pouring, compacting and finalising the placement process of concrete of pullout specimens

Figure 4.2 Curing of pullout specimens in water tank

4.3 Test Procedure of the Pullout Specimens

All the pullout test specimens were tested using a 500 kN Instron testing machine. The applied load to the pullout tested specimens continued until the longitudinal reinforcement pulled out cubic concrete or when the cubic concrete was splitting. A load cell measurement was used to record the applied load to the pullout test specimen during testing. Reinforcing N12 steel bar was rounded cross-section while A30 and A40 SEA were equal angle cross-sections. However, the 500 kN Instron testing machine was not designed to grip equal angle cross-section (SEA section). Thus, to test specimens with the SEA sections, a piece of steel bar was welded at the free end of each SEA section pullout specimens for the gripping purpose, as shown in Figure 4.3. The small steel bar wasused in the section for gripping and does not affect on the bond behaviour

of SEA sections as they are fully welded at the free end of the SEA sections. The free end of the longitudinal reinforcement was connected to the grips of the 500 kN Instron testing machine utilised for direct tensile tests, whereas the portion of the longitudinal reinforcement embedded in the concrete cube was fixed by a rigid steel frame, which was fixed to the lower portion (basement) of the testing machine. The rigid Steel frame consisted of two steel plates, which connected using four threaded bolts (Figure 4.4). The top steel plate was a rectangular shape with a size of 250 mm × 375 mm × 10 mm, and it was a puncture in the centre to allow the longitudinal reinforcement to be fixed to the upper grips of the testing machine. The bottom steel plate was also a rectangular shape with a size of 610 mm × 160 mm × 50 mm and was fixed to the lower grip of the 500 kN Instron testing machine by a special steel cylinder, as shown in Figure 4.4. The pullout test specimens were position between the top and bottom steel plates of the steel frame. To prevent the friction between the pullout the specimen and the top plate of the steel frame, rubber layer of 375 mm × 250 mm × 5 mm was placed on the top surface of pullout specimen and the top steel plate of steel frame to reduce the premature failure (Figure 4.4).

Figure 4.3 Welding small steel bar at free end of SEA section for gripping purpose

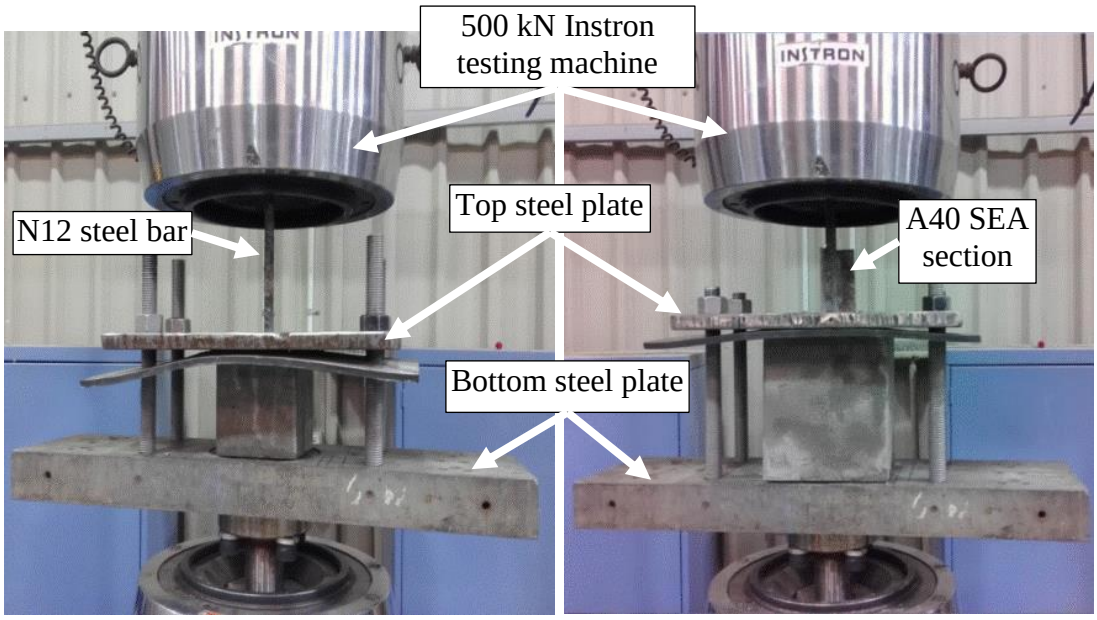

(a) (b)

Figure 4.4 Typical pullout test set up: (a) N12 steel bar pullout specimens and (b) A40 SEA pullout specimen

4.4 Test results of pullout Specimens

Figures 4.5 to 4.9 present the pullout load-slip behaviour response of the pullout specimens. The pullout specimens with N12 steel bars obtained pullout load with an average of about 24.9 kN. All the pullout specimens with N12 steel bars failed by splitting of the concrete in the zone where the N12 steel bar was placed in the concrete cube, as shown in Figure 4.10. Six pullout specimens were used to investigate the pullout behaviour of A30 SEA sections, three specimens (PA30-1, PA30-2 and PA30-3) were reinforcing with A30 SEA section without short steel bars at embedded ends. The reaming three specimens (PA30W-1, PA30W-2 and PA30W-3) were welded short steel bars at embedded ends.

Table 4.2 presents the test results of pullout specimens. The pullout Specimens PA30-1, PA30-2 and PA30-3 obtained pullout load with an average of about 18.0 kN. However, the pullout specimens PA30W-1, PA30W-2 and PA30W-3 achieved pullout load with an average of about 23.3 kN. Also, it was observed that different failure pattern was observed in pullout specimens reinforcing with A30 SEA sections with and without welded short steel bars at the embedded end, as shown in Figure 4.11. Specimens PA30-1, PA30-2 and PA30-3 failed by pull-out of the A30 SEA section without obvious interlocking of the aggregates. Whereas, Specimens PA30W-1, PA30W-2 and PA30W-3 failed by splitting.

The pullout specimens PA40-1, PA40-2 and PA40-3 achieved pullout loads with an average of about 41.3 kN. However, the pullout specimens PA40W-1, PA40W-2 and PA40W-3 attained pullout loads with an average of about 47.9 kN. Also, it was observed that different failure pattern was seen in pullout specimens reinforcing with A40 SEA sections with (splitting failure mode) and without (pullout failure mode) welded short steel bars at embedded ends, as shown in Figure 4.11.

Based on the results of pullout specimens it was realised that the use welded small steel bar piece at embedded ends for SEA sections resulted in improved pullout behaviour of specimens. The reason for these improvements was because that the interlocking between welded small steel bar pieces and surrounding concrete provided the resistance to the slippage movement. The pullout load resistance was provided by friction between

welded small steel bar pieces and surrounding concrete. Hence, It can be concluded that the proposed method (welding small steel bar pieces at embedded ends) to improve the pullout behaviour of plain SEA sections embedded in HSC can be increased pullout load capacity, which can reduce the influence of the absence of ribs in the SEA sections.

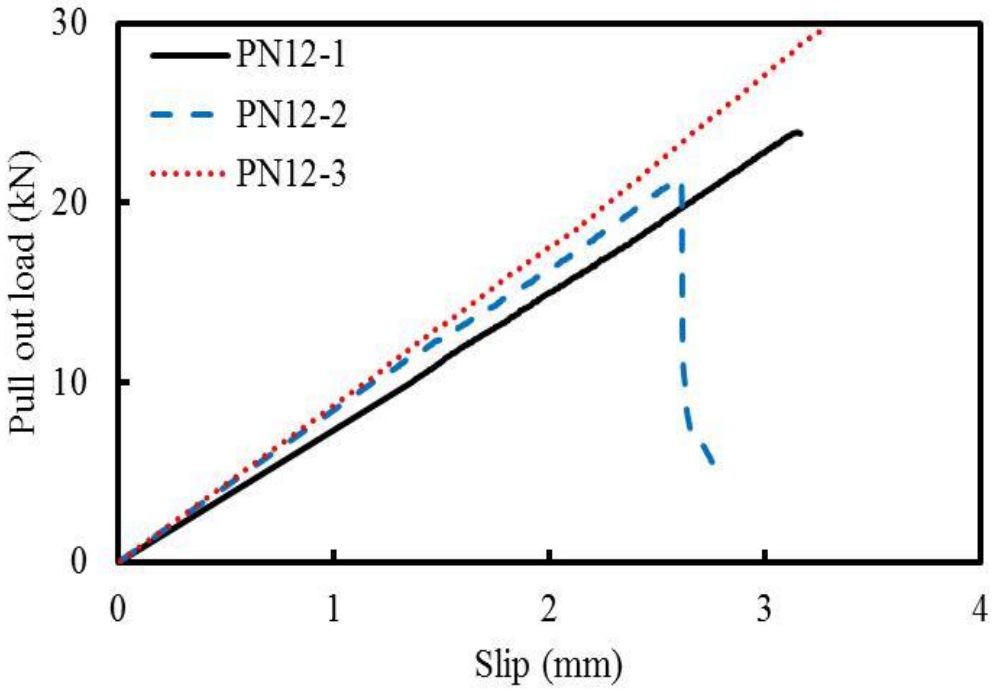

Figure 4.5 Pullout load-slip behaviour for specimens in Group N12

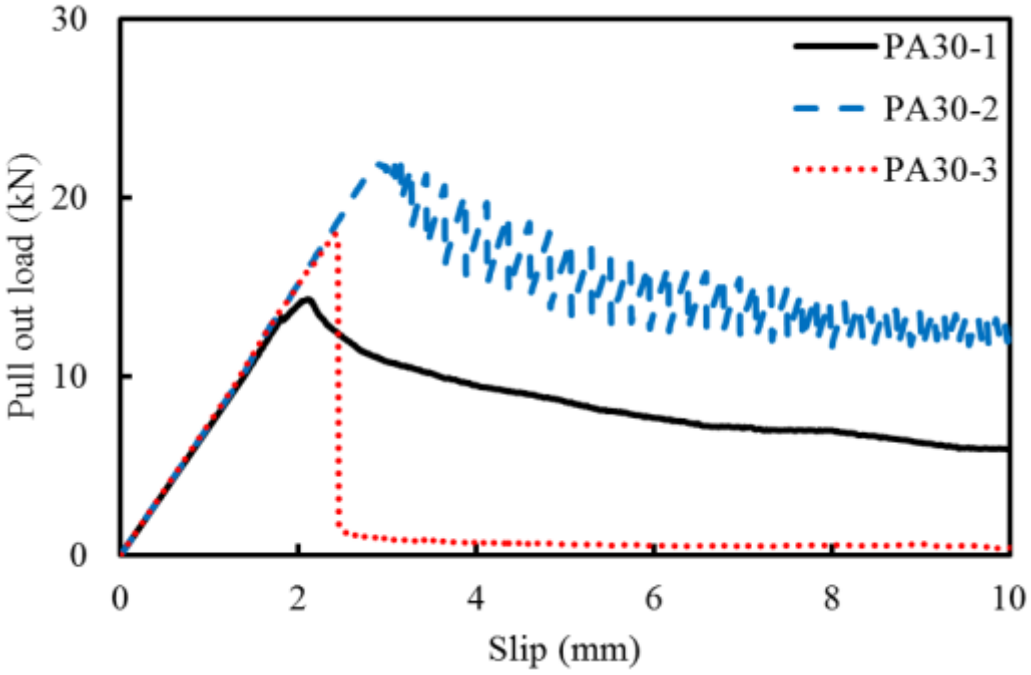

Figure 4.6 Pullout load-slip behaviour for specimens in Group PA30

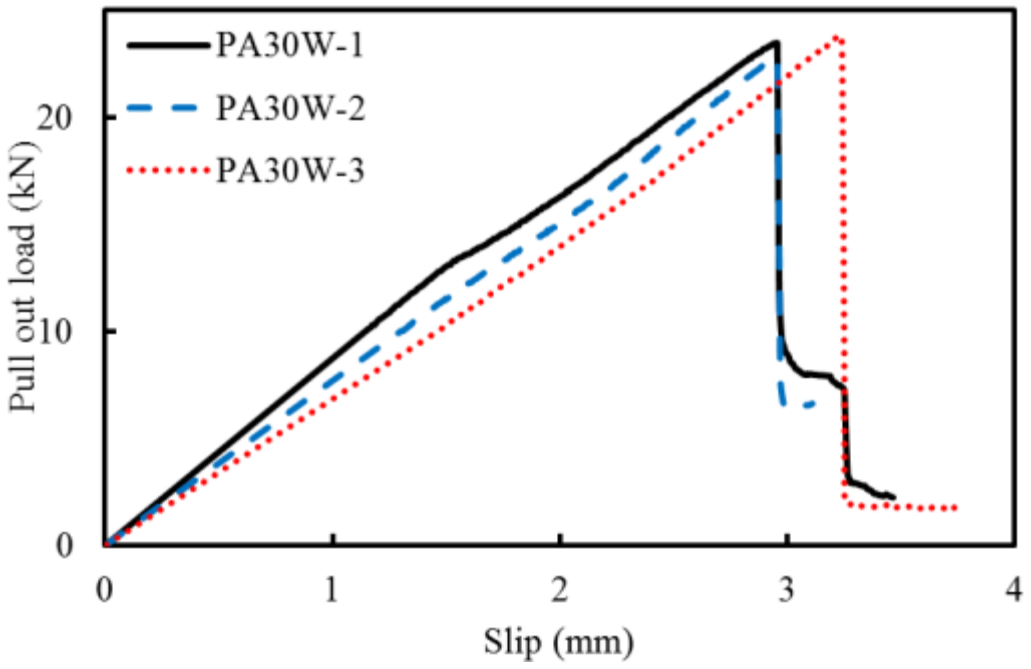

Figure 4.7 Pullout load-slip behaviour for specimens in Group PA30W

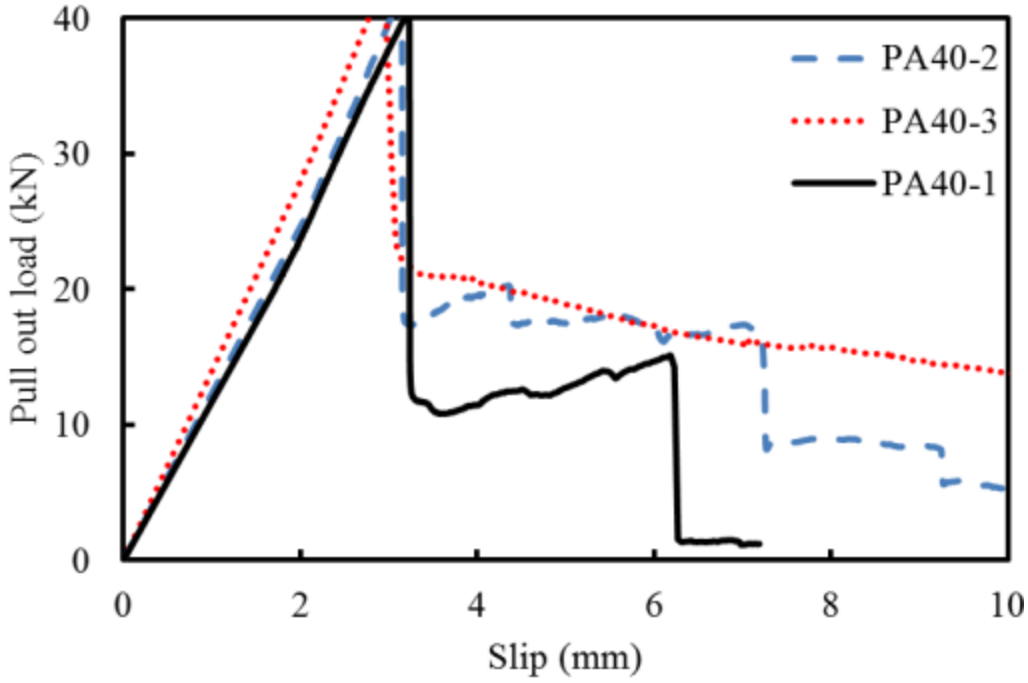

Figure 4.8 Pullout load-slip behaviour for specimens in Group PA40

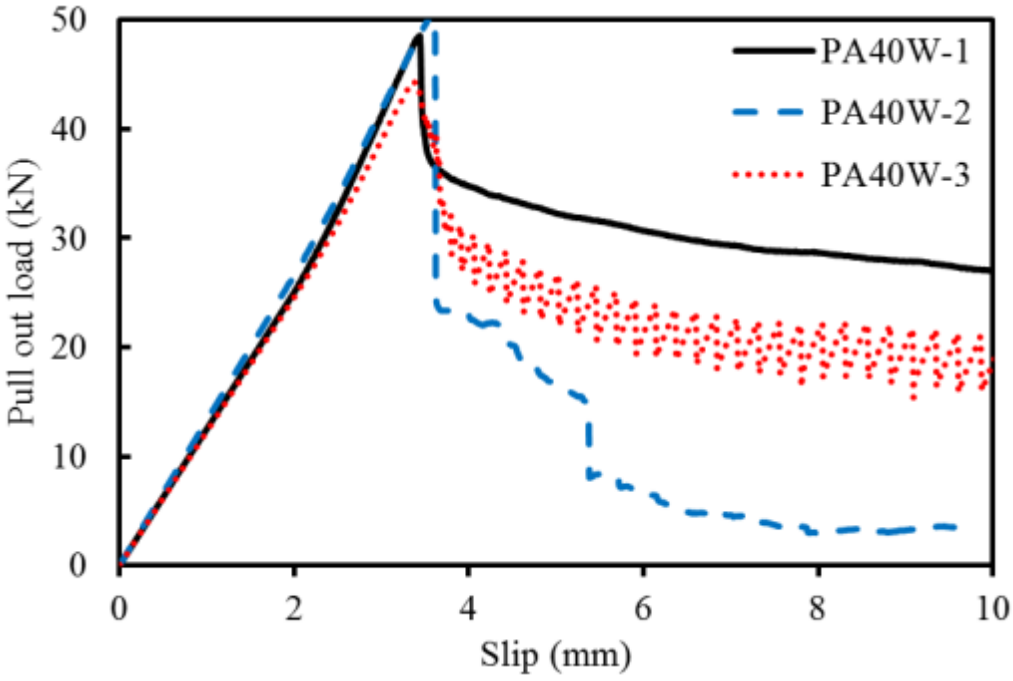

Figure 4.9 Pullout load-slip behaviour for specimens in Group PA40W

Table 4.2 Test results for pullout specimens

Group	Specimen	Reinforcement type	Welded steel bar pieces	Pullout load kN	Average Pullout load kN	Failure Mode
PN12	PN12-1	N12 steel bars	-	23.9	24.9	Splitting
	PN12-2			21.3		Splitting
	PN12-3			29.6		Splitting
PA30	PA30-1	A30 SEA sections	-	14.3	18.0	Pullout
	PA30-2			21.9		Pullout
	PA30-3			17.9		Pullout
PA30W	PA30W-1	A30 SEA sections	Yes	23.4	23.3	Splitting
	PA30W-2			22.8		Splitting
	PA30W-3			23.8		Splitting
PA40	PA40-1	A40 SEA sections	-	40.4	41.3	Pullout
	PA40-2			41.7		Pullout
	PA40-3			41.8		Pullout
PA40W	PA40W-1	A40 SEA sections	Yes	48.5	47.9	Splitting
	PA40W-2			50.8		Splitting
	PA40W-3			44.3		Splitting

Figure 4.10 Typical failure mode of N12 steel bar pullout specimen with failure by splitting

(a) (b)

Figure 4.11 Typical failure mode of SEA pullout specimen: (a) without welding small steel bar pieces at embedded end and with failure by pullout (b) with welding small steel bar pieces at the embedded end with failure by splitting

4.5 Summary

Detailed descriptions of designing and testing fifteen cubic concrete pullout specimens reinforced with either deformed steel bars of steel equal angle (SEA) sections are presented in this chapter. The pullout specimens were divided into five groups of three specimens based on reinforcing types (steel bar or SEA section), size of SEA sections and welding small steel bar pieces at the embedded end. For all groups, the pullout specimens were tested under the direct tensile pullout test. Based on the test results presented in this chapter, the welding of small steel pieces at the embedded end of the SEA section resulted in improving the pullout behaviour of the SEA section embedded in high strength concrete compared to the deformed steel bar embedded in high strength concrete.

The next Chapters 5, 6, 7, 8 exhibit that the experimental program included two sets with different parameters. The first set of the experimental program involved testing of 20 square HSC specimens under concentric axial load, eccentric axial load and four-point bending. While, in the second set of the experimental program, the specimens were tested to evaluate the influence of the spacing of transverse ties (ranged from 50 mm to 400 mm) on the performance of square HSC column specimens reinforced longitudinally with SEA sections under axial compression. Therefore, the use 600 mm height for the specimens in the second set is sufficient to investigate the influence of the spacing of transverse ties, which were varied from 50 mm to 400 mm.

5 EXPERIMENTAL PROGRAM OF SPECIMENS WITH 800 mm HEIGHT

5.1 General

A comprehensive experimental program is designed in this chapter to study the behaviour of square high strength concrete (HSC)specimens with 800 mm height reinforced longitudinally with either steel bars or steel equal angle (SEA) sections and transversally with plain steel bars (ties). Twenty specimens were cast and tested at High Bay Laboratories, University of Wollongong, Australia. Test specimens were conducted to investigate the effect of main parameters of using SEA sections as longitudinal reinforcement, transverse reinforcement spacing (50 mm and 75 mm), longitudinal reinforcement ratios (ranged from 1.03% and 2.41%) and different load conditions (0, 25 mm and 50 mm eccentricity and four-point bending). Also, in this chapter, the details of the used materials in the experimental program are presented. Then the details of the test specimens, formwork setup, placement of strain gauges and curing process of the specimens are also presented. The test program used to test the specimens under different load conditions is also described. Finally, all the details of the experimental program are presented in the following sections.

5.2 Material Properties

Three main materials were used in this experimental program; these materials are the concrete, steel equal angle (SEA) sections and steel bars. The details of these materials are presented in the following sections.

5.2.1 **Concrete**

All the concrete used in this experimental program was provided by a local concrete supplier. Concrete samples were made of high strength concrete (HSC) with a maximum aggregate size of 10 mm. The design compressive strength of concrete was 70 MPa. Fifteen plain concrete cylinder samples of 100 mm diameter and 200 mm height were cast according to AS 1012.9 (1999) in order to determine the required compressive strength of concrete (Figure 5.1(a)). Three samples of 150 mm diameter and 300 mm height were cast according to AS 1012.10 (2000) in order to determine the indirect tensile strength of concrete (Figure 5.1(b)). In addition, three prismatic samples with a square cross section of 100 mm × 100 mm and length of 500 mm were constructed to investigate the direct tensile strength of concrete (Figure 5.1(c)). To determine the modulus of rupture of concrete, three plain concrete beam samples with a square section of 100 mm side dimension and 500 mm in length were made according to AS 1012.11 (2000), as shown in Figure 5.1(d). Table 5.1 presents the plain concrete samples.

Table 5.1 Plain concrete samples

Type of Test	Sample No.	Sample Size (mm)	Testing Age (Day)
Compression	3	100 × 200	7
	3		28
	3		56
Indirect tensile	3	150 × 300	28
Direct tensile	3	100 × 100 × 500	28
Flexural (Modulus rupture)	3	100 × 100 × 300	28

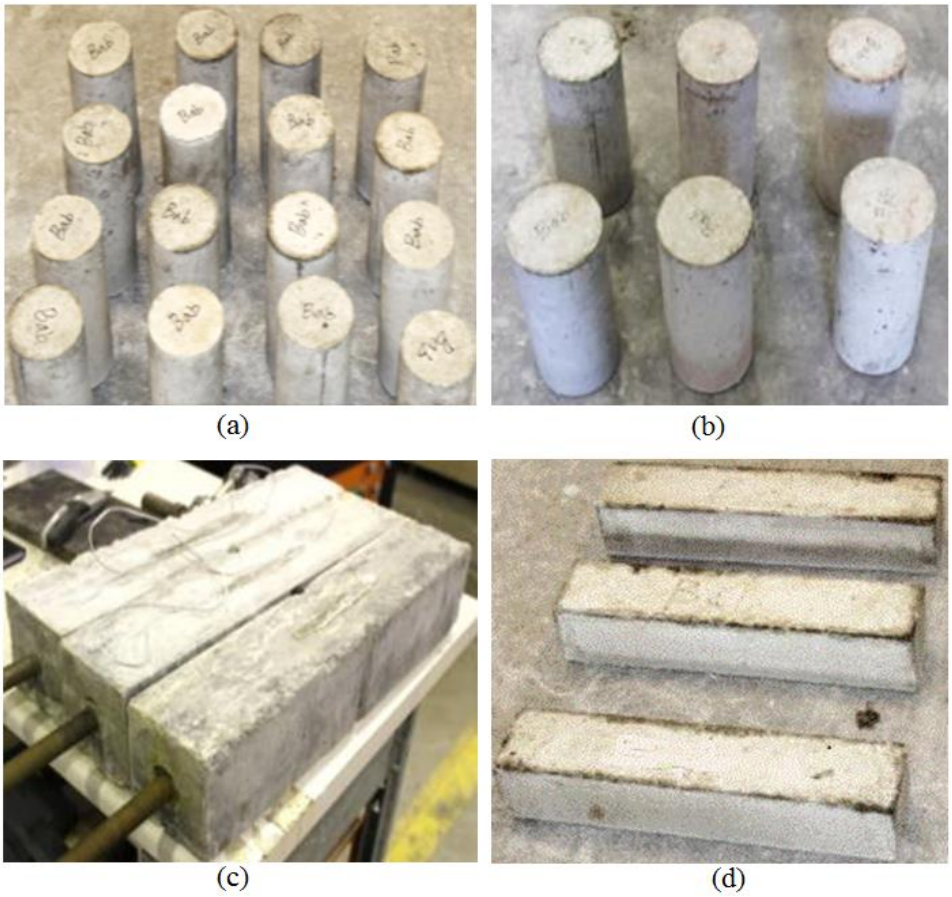

(a) (b) (c) (d)

Figure 5.1 Plain concrete samples: (a) Compression; (b) Indirect tensile strength of concrete; (c) Direct tensile strength of concrete and (d) Modulus rupture of concrete

5.2.2 **Steel Equal Angle (SEA) Sections**

In the experimental program, two cross sections of the steel equal angle (SEA) were used to reinforce the specimens as longitudinal reinforcement. These SEA sections were supplied by OneSteel (2010). The A30 SEA had a nominal leg width of 30 mm and a nominal thickness of 2.5 mm with a nominal yield tensile strength of 350 MPa (Figure 5.2(a)). The A40 SEA section had a nominal leg width of 40 mm and a nominal thickness of 4 mm with a nominal yield tensile strength of 450 MPa (Figure 5.2(b)). Before measuring the actual dimensions of SEA sections, zinc coating was removed by sandpaper and then the dimensions were measured. The nominal and measured dimensions of SEA sections are shown in Table 5.2.

Table 5.2 Dimensions and properties of steel equal angle (SEA) sections

Steel Equal Angle (SEA) Section	Leg Width (mm)	Thickness (mm)	Area (mm^2)
Nominal			
A30	30	2.5	132
A40	40	4.0	280
Measured (average)			
A30	29.1	2.25	122.6
A40	39.3	3.70	268.3

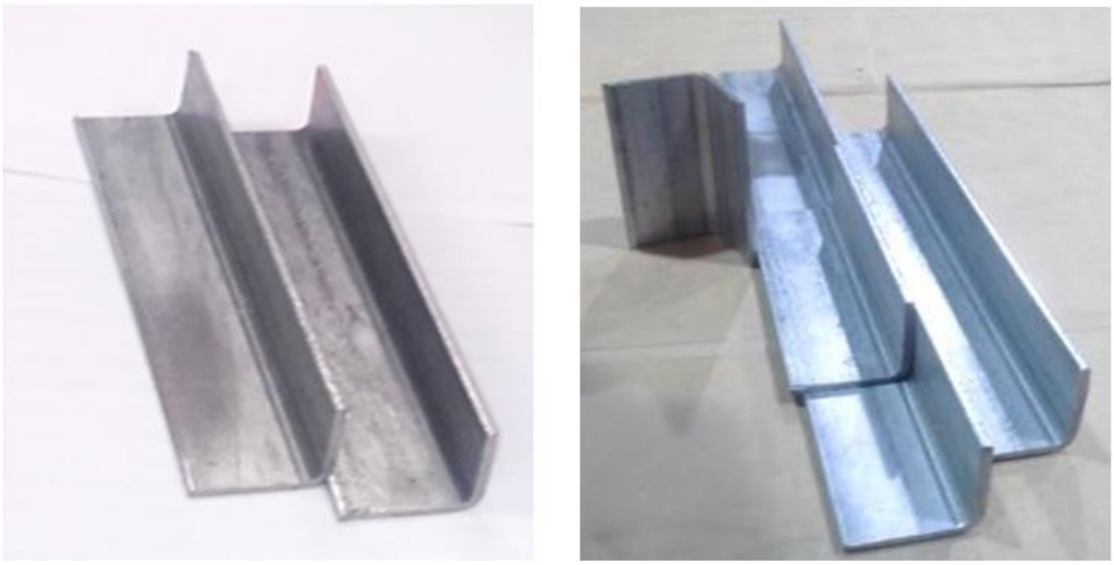

Figure 5.2 Steel equal angle (SEA) sections used in the experimental program: (a) A30 SEA sections and (b) A40 SEA sections

5.2.3 **Steel Bars**

Two types of steel bars were used in this experimental program. The N12 steel bars (deformed steel bars of 12 mm diameter and 500 MPa nominal yield tensile strength) were used as longitudinal reinforcement in the reference specimens. Plain R10 steel bars (plain steel bars of 10 mm diameter and 250 MPa nominal yield tensile strength) were used as transverse ties for all specimens.

5.3 Fabrication of the Test Specimens

5.3.1 **Details of Test Specimens**

In this study, the test matrix of HSC specimens was developed to examine the influence of the type of longitudinal reinforcement (steel bars or SEA sections) and the spacing of transverse reinforcement on the behaviour of high strength concrete (HSC) specimens under different loading conditions (concentric and eccentric axial loads and four-point bending). Twenty HSC specimens with 210 mm × 210 mm square cross-section and 800 mm height were cast and tested.

The dimensions of the specimens were selected to be appropriate for the requirement and capacity of the available testing machine in the lab. It is noted that vertical support with height to side width (l/b) ratio of higher than or equal to 2.5 is considered as a column according to AS 3600 (2009) and CAN/CSA S6 (2006). The (l/b) ratio of the specimens was equal to about 4. Also, it is seems that the slenderness ratio of the specimens was 16, which is within the limit of a short concrete column. Also, according to ACI 318 (2014), the height of the specimens was sufficient to provide an adequate development length for the longitudinal reinforcement.

The test matrix is shown in Table 5.3. The specimens were divided into five groups. The first group (Group R-S50) was considered as a reference group. The specimens in Group R-S50 (reference specimens) were reinforced longitudinally with four N12 bars (deformed steel bars of 12 mm diameter and 500 MPa nominal yield tensile strength) and transversely reinforced with R10 bars (plain steel bars of 10 mm diameter and 250

MPa nominal yield tensile strength) at 50 mm centres. The specimens in the second group (Group A30-S50) were reinforced longitudinally with four A30 SEA sections and transversely with R10 plain bars at 50 mm centres. The specimens in the third group (Group A30-S75) were reinforced longitudinally with four A30 SEA sections and transversely with R10 plain bars at 75 mm centres. The specimens in the fourth group (Group A40-S50) were reinforced longitudinally with four A40 SEA sections and transversely with R10 plain bars at 50 mm centres. The specimens in the fifth group (Group A40-S75) were reinforced longitudinally with four A40 SEA sections and transversely with R10 plain bars at 75 mm centres. The A30 SEA section had a leg width of 29.1 mm and a thickness of 2.25 mm and A40 SEA section had a leg width of 39.3 mm and a thickness of 3.7 mm. Each group contained four specimens. The first specimen of each group was tested under concentric axial load. The second specimen of each group was tested under 25 eccentric axial load. The third specimen of each group was tested under 50 mm eccentric axial load. The last specimen of each group was tested under four-point bending to investigate the flexural behaviour. The details and the designs of each group of specimens are shown in Figure 5.3.

5.3.2 **Specimen Identification**

In this experimental program, the specimens were labelled with three parts as shown in Table 5.3. The first part refers to the type of longitudinal reinforcement in which R represents N12 steel bars and A30 and A40 refer to SEA sections. The second part indicates the centre-to-centre spacing of transverse ties in which S50 and S75 refer to 50 mm and 75 mm spacing, respectively. The third part indicates the mode of loading condition in which C refers concentric axial load, E25 refers to 25 mm eccentric axial

load, E50 refers to 50 mm eccentric axial load and F refers to four-point bending. For example, Specimen A30-S75-E25 is reinforced longitudinally with A30 SEA sections and confined with transverse ties at 75 mm centres, which was tested under 25 mm eccentric axial load. Also, Specimen R-S50-F is reinforced longitudinally with N12 steel bars and confined with transverse ties at 50 mm centres and tested under four-point bending (flexural).

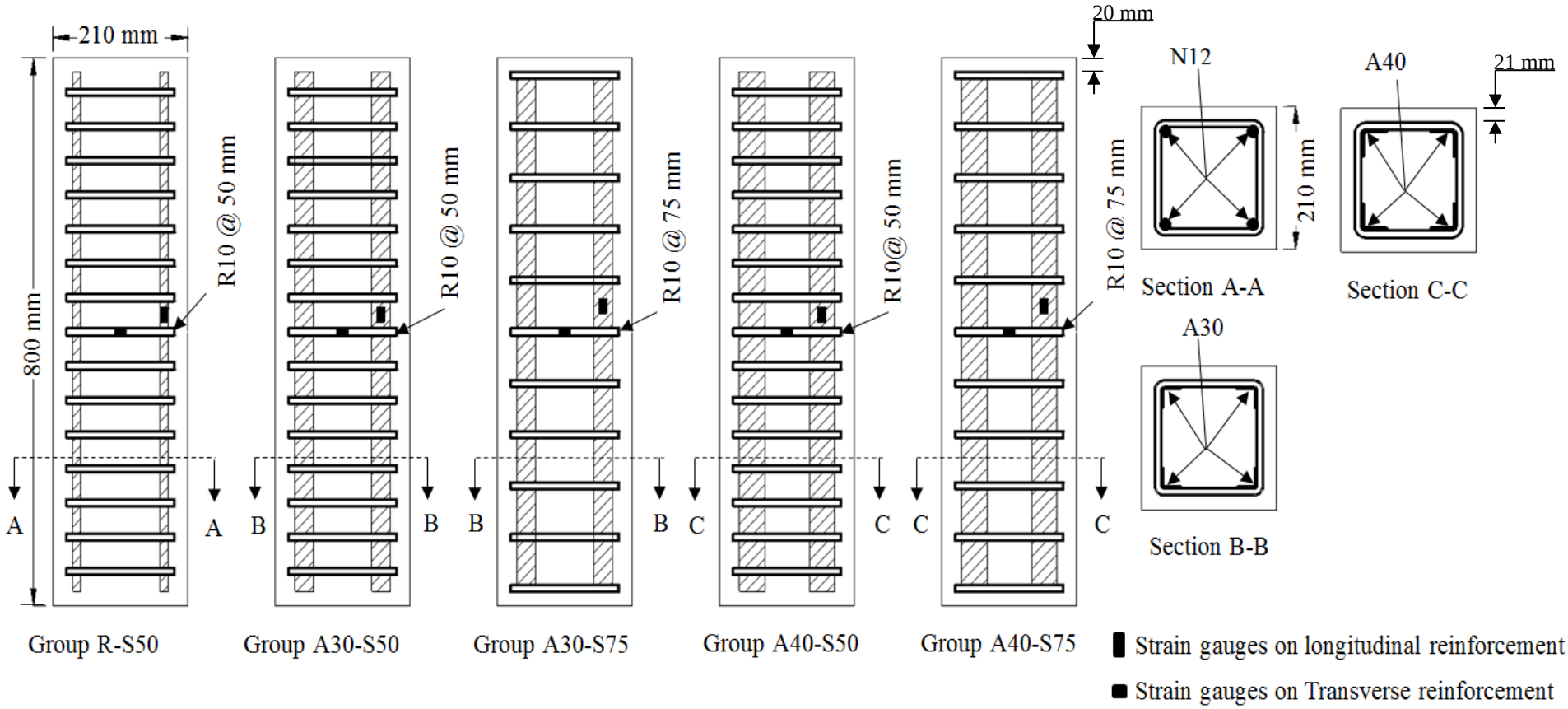

Figure 5.3 Dimension and reinforcement arrangements of the test specimens with 800 mm height

Table 5.3 Test Matrix of Specimens with 800 mm Height

Group ID	Longitudinal Reinforcement								Transverse Reinforcement		Load eccentricity
	Reinforcement Type	Number	Steel Bar			Steel Equal Angle (SEA) Section			Diameter (mm)	Spacing (mm)	
			Diameter (mm)	ρ_b %	f_y (MPa)	Dimension (mm)	ρ_{SEA} %	f_y (MPa)			
R-S50	Steel Bar	4	12	1.03	556	-	-	-	10	50	0 25 mm 50 mm Flexural
A30-S50	Steel Equal Angle (SEA) Section	4	-		-	29.1 × 2.25	1.11	374	10	50	0 25 mm 50 mm Flexural
A30-S75		4	-		-	29.1 × 2.25	1.11	374	10	75	0 25 mm 50 mm Flexural
A40-S50		4	-		-	39.3 × 3.7	2.43	473	10	50	0 25 mm 50 mm Flexural
A40-S75		4	-		-	39.3 × 3.7	2.43	473	10	75	0 25 mm 50 mm Flexural

Note: ρ_b represents volumetric ratio of longitudinal reinforcement bars

ρ_{SEA} represents volumetric ratio of longitudinal reinforcement SEA sections

5.3.3 **Formwork Setup**

The formwork used for casting the concrete specimens was fabricated by 17 mm thick plywood. The combined formwork included five groups of small formwork. Each group was used for casting four specimens. The small formwork was fabricated using two large sheets of plywood (985 mm x 800 mm x 17 mm) and five small sheets of plywood (220 mm x 800 mm x 17 mm), as shown in Figure 5.4. Afterwards, the formwork was prepared by placing the plywood sheets together by screws. Then, pieces of timber were also used vertically and transversely to fix the formwork before pouring the concrete (Figure 5.5). All The small formworks were then placed on the large plywood sheets to prevent contact between concrete and floor of the lab. At each end, four pieces of Styrofoam (polystyrene) were attached at the corners inside the formwork. Every piece of Styrofoam was 100 mm long (Figure 5.5). The Styrofoam was used to create smooth rounded edges (20 mm radius) at each end of the specimen so that the specimen ends could be wrapped with Carbon Fibre Reinforced Polymer (CFRP) to prevent stress concentrations at the ends during testing.

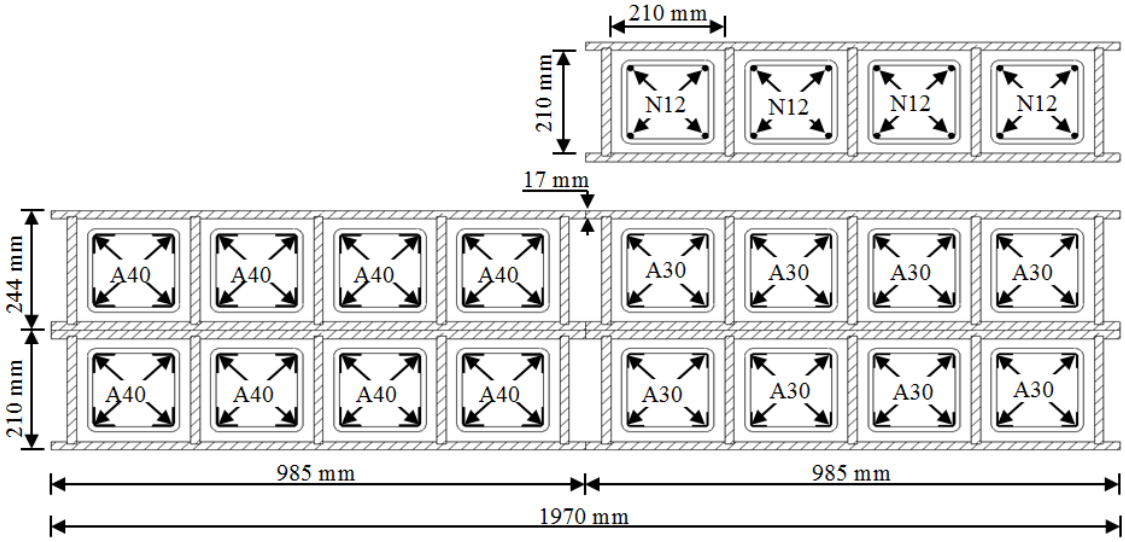

Figure 5.4 Plan view of wooden formwork

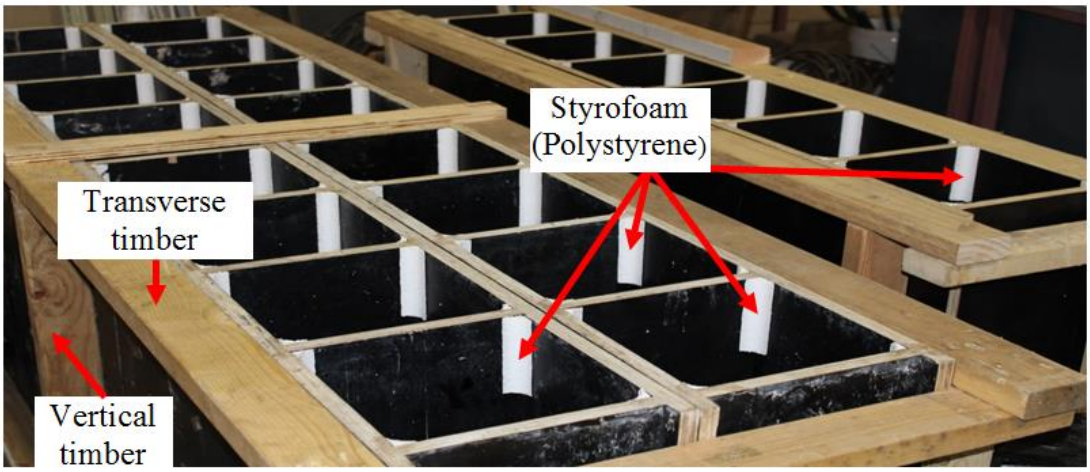

(a)

(b)

Figure 5.5 Fabrication and preparation of the specimens: (a) Wooden formwork and (b) Steel cages inside the formwork

5.3.4 **Steel Cages**

The longitudinal steel bars and SEA sections were cut into a length of 760 mm in order to maintain a 20 mm clear cover at the top and bottom of the specimen. For all specimens, the square transverse ties were fabricated in the lab from plain R10 bars to have 21 mm clear covers on the sides of the specimen. All transverse ties were bent in four corners with a radius of about 6 mm to fix the square transverse ties over the SEA

sections, as shown in Figure 5.6. For all specimens, the transverse ties were made with 90-degree hooks around one of the longitudinal reinforcement (steel bars or SEA sections) and extended with a minimum overlap of 80 mm at both ends, as shown in Figure 5.6. Afterwards, each tie was welded at three points on the hook corner to ensure adequate confinement by the transverse ties (Figure 5.6).

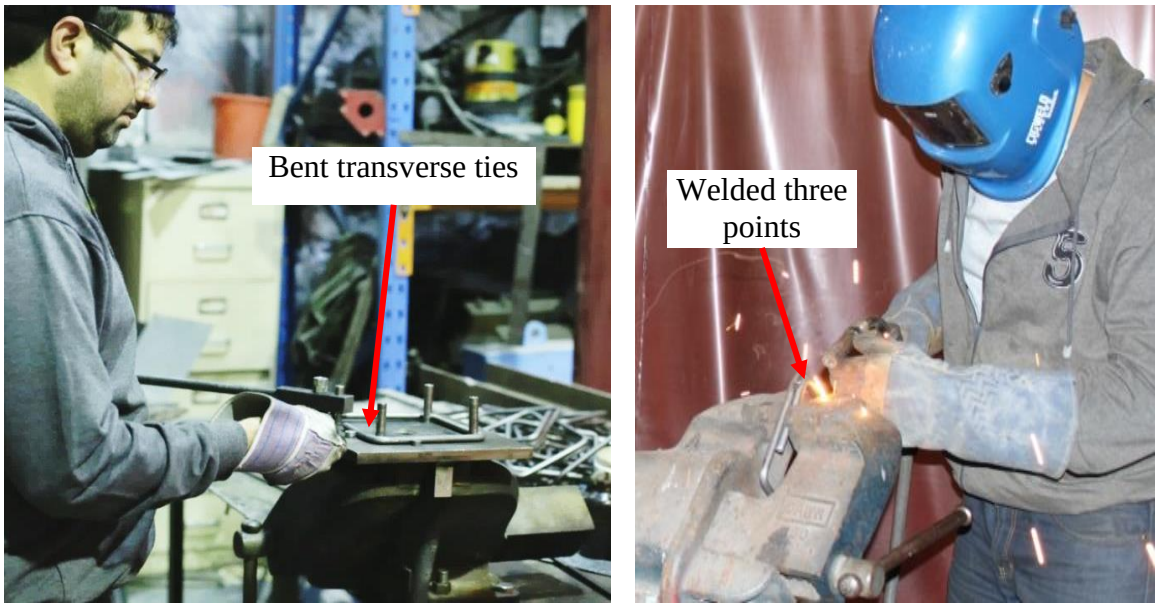

Figure 5.6 Fabrication of the transverse ties with 90-degree hooks

The SEA sections with smooth surfaces were used as longitudinal reinforcements. Due to the smooth surfaces of SEA sections, the slippage of the SEA sections during the test might occur. Therefore, to decrease the effect of slippage in the specimens that contained SEA sections, two small steel bars were welded at the top and bottom of the SEA sections. At first two small steel bars with 8 mm diameter and 40 mm length were welded transversely between the ends of SEA section. Second, two small steel bars with 16 mm diameter and 70 mm length were welded at the top and bottom of SEA sections.

To fabricate the reinforcement cages, two aluminium templates were made. One template was placed on top and another template on the bottom of steel cages. Both of these templates were designed to hold transverse ties with various spacing (Figure 5.7). Afterwards, all steel cages were prepared by placing the longitudinal and transverse reinforcement together, as shown in Figures 5.8 and 5.9.

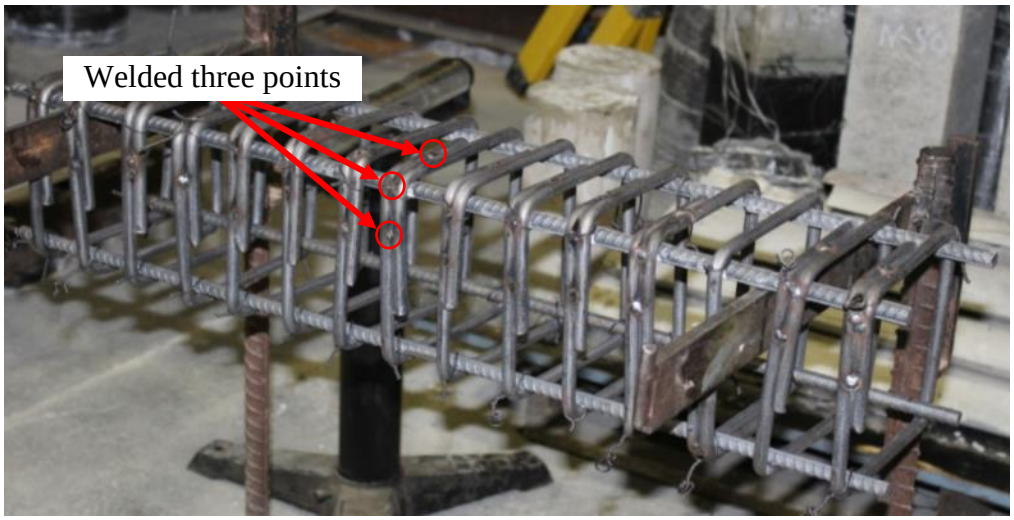

(a)

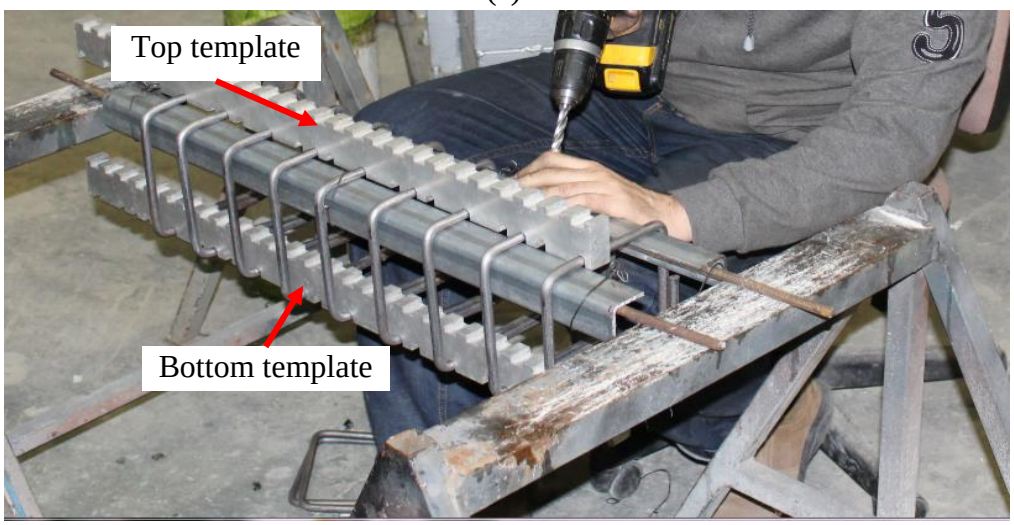

(b)

Figure 5.7 Placing the steel cages: (a) longitudinal steel bars and (b) longitudinal SEA sections

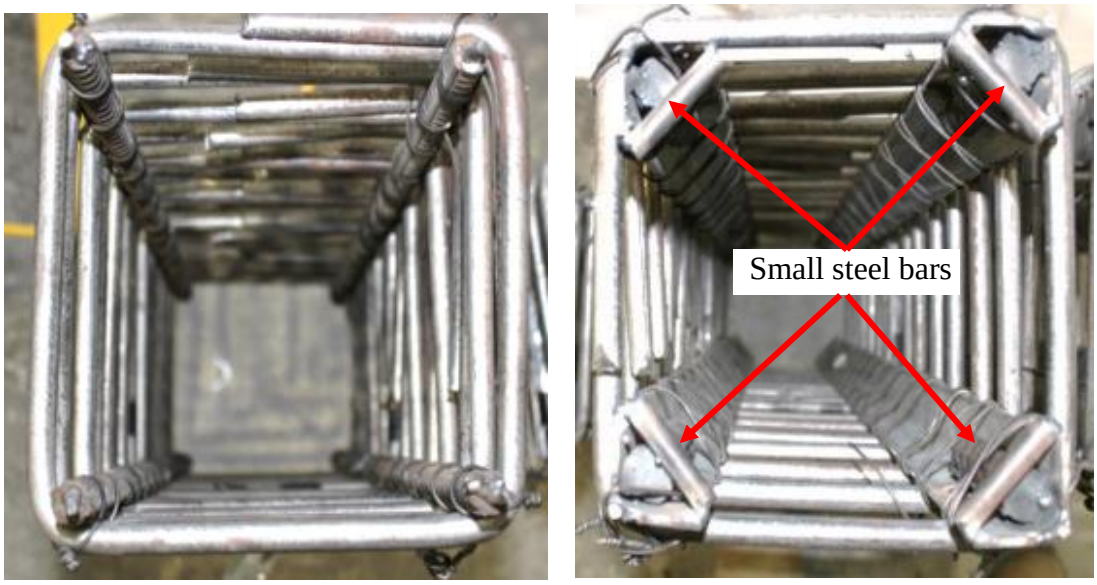

(a) (b)

Figure 5.8 Top view of steel cages with (a) longitudinal steel bars and (b) SEA sections

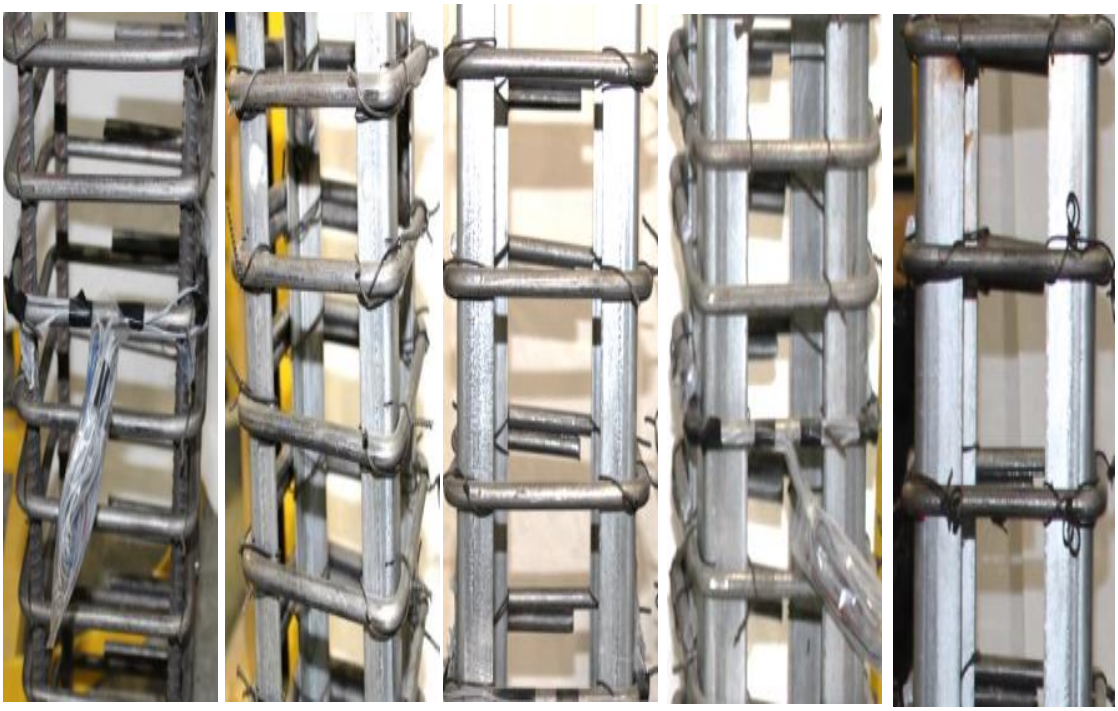

Group R-S50 Group A30-S50 Group A30-S75 Group A40-S50 Group A40-S75

Figure 5.9 Overview of the assembled steel cages

5.3.5 **Placement and Curing Process of the Specimens**

The test specimens were cast with high strength concrete, which was provided by a local ready-mixed concrete supplier. All specimens were cast vertically from one batch and at the same day. The concrete was poured into the formwork in three levels. An electric vibrator was used at every level to compact the concrete and remove air bubbles from the concrete (Figure 5.10). Then the surface of the test specimens was finished with a trowel (Figure 5.10). After 24 hours from pouring, all specimens were covered with wet clothes and watered three times a day until 28 days. This process was to maintain the specimens under moist conditions. The specimens were removed from the formwork after 14 days (Figure 5.11). The specimens were covered by wet clothes for 28 days after casting.

In addition to the test specimens, a number of control samples were also cast in order to investigate the mechanical properties of concrete. Fifteen small cylinders with 100 mm diameter and 200 mm height, three cylinders with 150 mm diameter and 300 mm height and three beam samples with 100 mm square cross-section and 500 mm length were cast. These control samples were removed from the moulds after 24 hours and then placed in a curing tube and left to cure until the testing day.

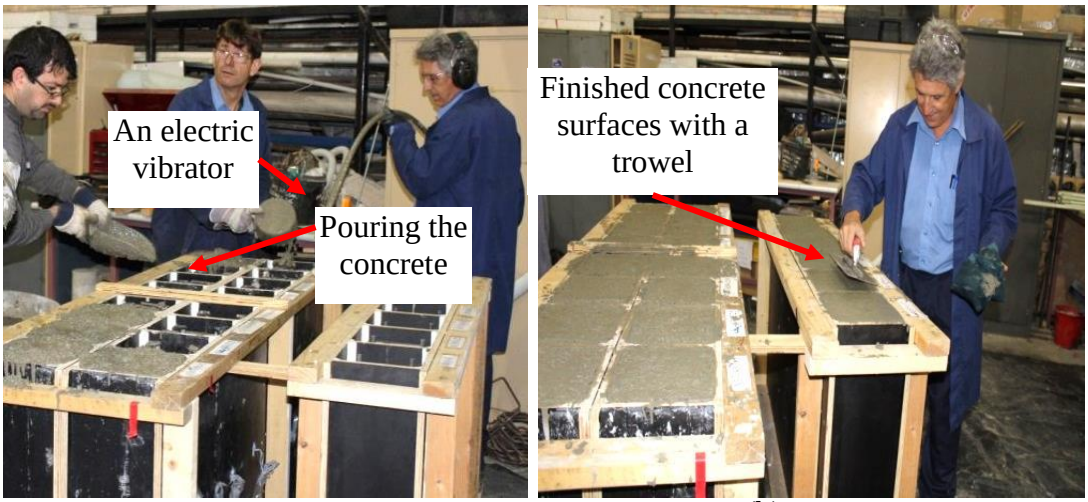

(a) (b)

Figure 5.10 Pouring, compacting and finishing the placement process of concrete

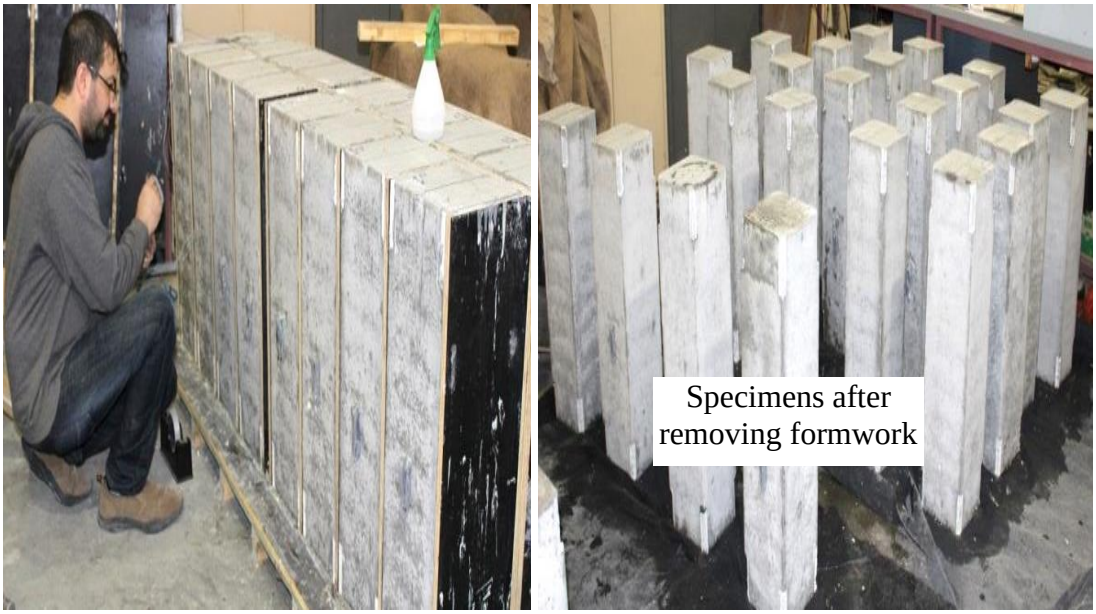

(a) (b)

Figure 5.11 Removal of the formwork and cast the column specimens

5.4 Instrumentation of Test Specimens

In this experimental program, the specimens were instrumented internally by strain gauges. The surfaces of steel cages were prepared for strain gauges by removing the zinc coating from the SEA sections using sandpaper and for the deformed steel bars by a grinder to achieve smooth and clean surfaces. Prior to pouring the concrete in the formwork, two electrical strain gauges were attached at the mid-height (the anticipated failure location) on the outside of two opposite longitudinal reinforcement (bars and SEA sections) to monitor the axial stress-axial strain responses of steel bars and SEA sections (Figure 5.12). In addition, two electrical strain gauges were bonded to the tie bar at the mid-height (the anticipated failure location) of the specimens in opposite directions to monitor strains in the transverse direction (Figure 5.12). Prior to inserting steel cages inside formwork, the strain gauges were sealed using non-corrosive silicon to avoid mechanical damage during the concrete cast. Electrical strain gauges were connected to a data logger and a computer.

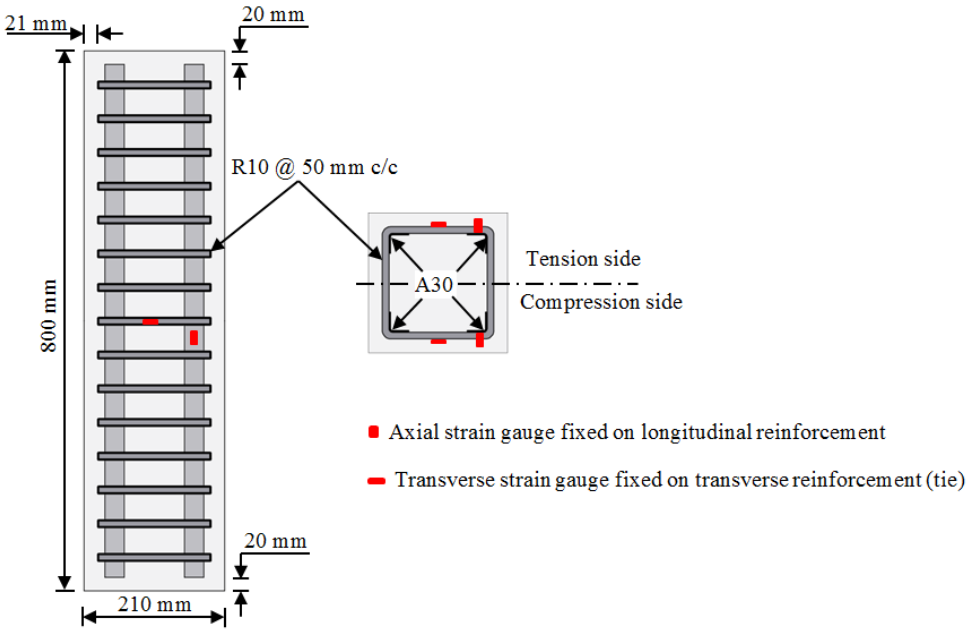

Figure 5.12 Location of strain gauges

5.5 Testing Program

5.5.1 Specimens Tested under Concentric and Eccentric Axial Loads

A total of twenty HSC specimens were cast and tested in the Structural Engineering laboratory of the School of Civil, Mining and Environmental Engineering at the University of Wollongong, Australia. The Denison compression testing machine with a load capacity of 5000 kN was used to test the specimens. Before testing, the top and bottom surfaces of the specimens to be tested under concentric and eccentric axial compression were capped with high strength plaster to provide a uniform load distribution during testing. Afterwards, the specimens were placed vertically between two loading plates of the 5000 kN Denison testing machine. The eccentric axial load was applied to the specimen by an eccentric loading head system manufactured at the University of Wollongong, Australia (Hadi and Widiarsa 2012). The loading head system is shown in Figure 5.13. The loading head system consisted of two square high strength steel loading heads and steel joints, which were attached at the top and the bottom ends of the specimens, as shown in Figure 5.13. For specimens tested under concentric axial loads, only the two square high strength steel loading heads were used to transfer the applied load of testing machine concentrically to the tested specimens, as shown in Figure 5.13.

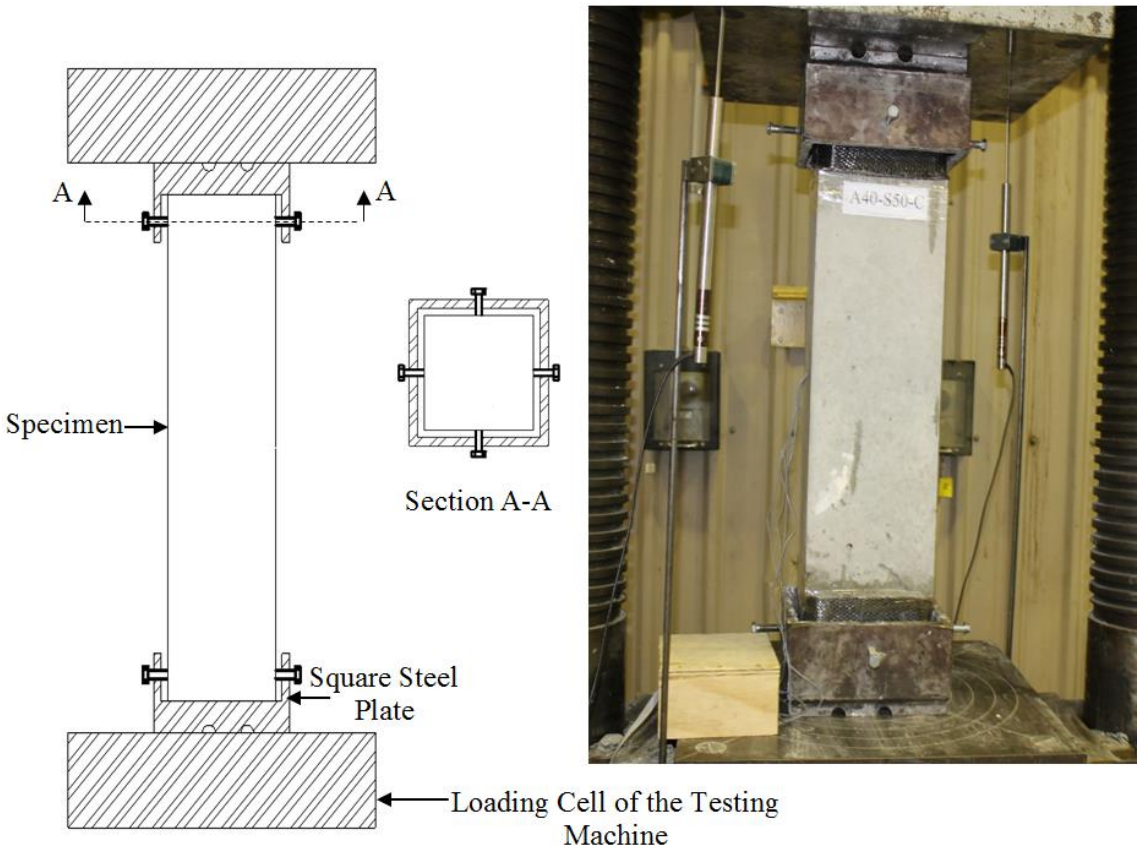

Figure 5.13 Typical test set up for specimen under concentric axial load

For specimens tested under eccentric axial loads, in addition to the two square high strength steel loading heads, the steel ball joints were used to transfer the applied load of the testing machine into 25 mm and 50 mm eccentric axial loads, as shown in Figure 5.14. All the specimens tested under concentric and eccentric axial loads were instrumented externally with two Linear Variable Displacement Transducers (LVDTs) to monitor the axial deformation for each specimen. The LVDTs were attached to the loading plate of the 5000 kN Denison testing machine at two diagonal corners. For specimens tested under eccentric axial load, in addition to the two LVDTs, a laser triangular was also attached at the mid-height of the tested specimens to capture the

transverse deflection (Figure 5.15). Electrical strain gauges, linear variable displacement transducers (LVDTs) and laser triangulation were connected to a data logger and a computer.

For specimens tested under concentric and eccentric axial load, the testing of specimens was started with an initial force-controlled preloading to about 10% of the expected maximum axial load of the specimens to regulate minor misalignments between the specimen and the compression testing machine heads. The load was then released to 30 kN at a similar rate. Afterwards, the test resumed under a displacement controlled loading at 0.3 mm per minute until the strength of the specimens dropped to about 40% of the maximum axial load.

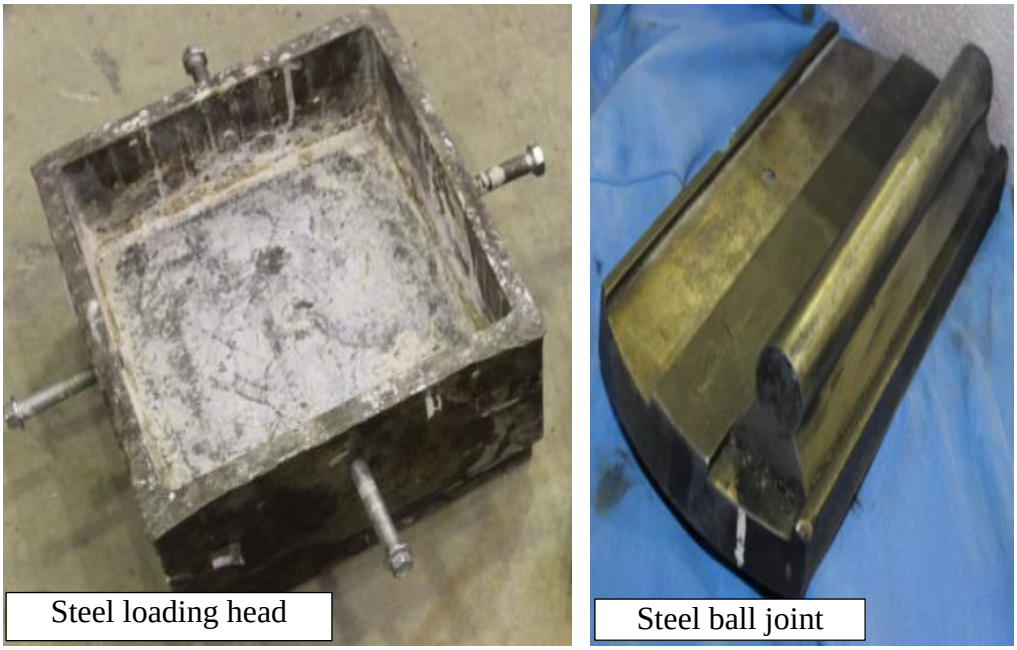

(a) (b)

Figure 5.14 Loading head and eccentric load system

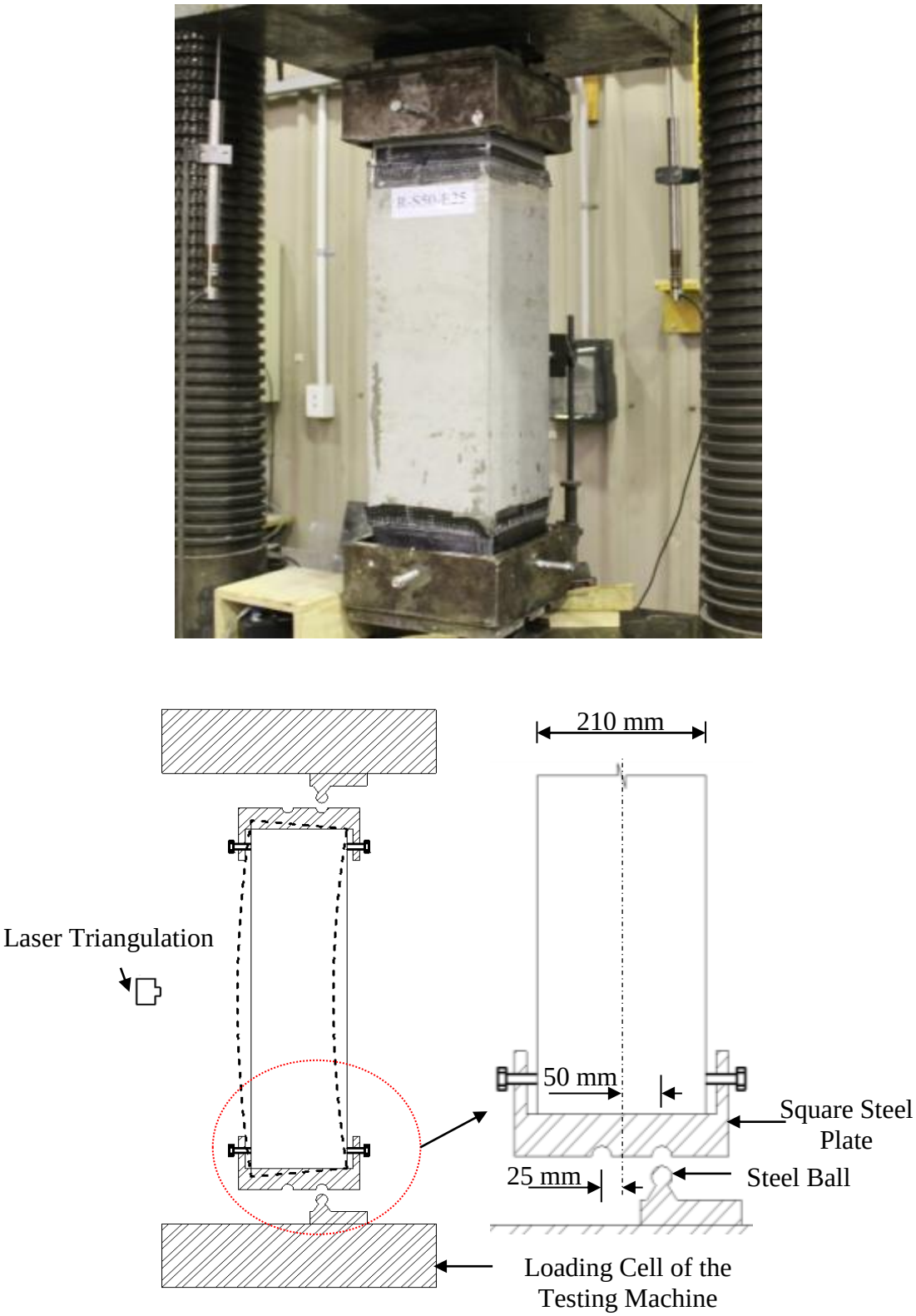

Figure 5.15 Typical test setup for specimen under eccentric axial load

5.5.2 **Specimens Tested under Four-Point Load**

A total of five specimens were tested under four-point bending with a clear span of 700 mm, as shown in Figures 5.16 and 5.17. The four-point bending system consisted of a set of two steel rigs, which were placed on the bottom (placed diagonally across the lower loading plate of the testing machine) and the top of the specimens tested under four-point bending. All the specimens tested under four-point loading were instrumented externally with two LVDTs to monitor the deflection for each specimen. The LVDTs were attached to the loading plate of the 5000 kN Denison testing machine at two diagonal corners. In addition to the two LVDTs, the midspan deflection was captured by a laser triangulation, which was placed vertically underneath the specimens tested under four-point bending. For specimens tested under four-point bending, the test was conducted under a displacement control loading at 0.3 mm per minute up to failure.

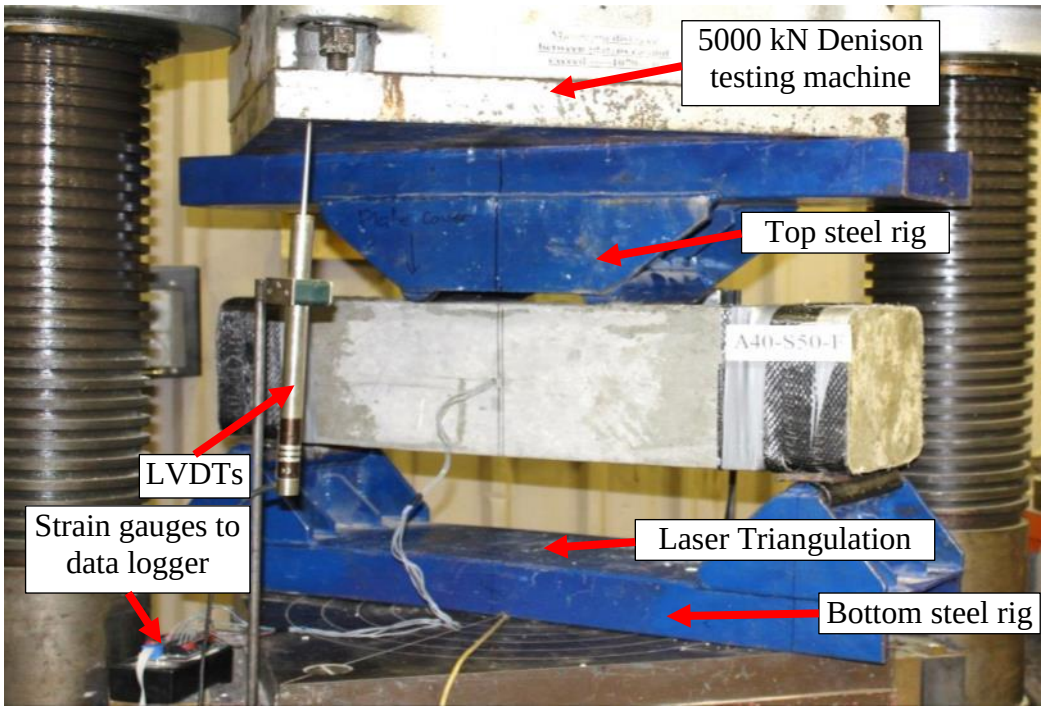

Figure 5.16 Typical testing set up of specimen under four-point bending

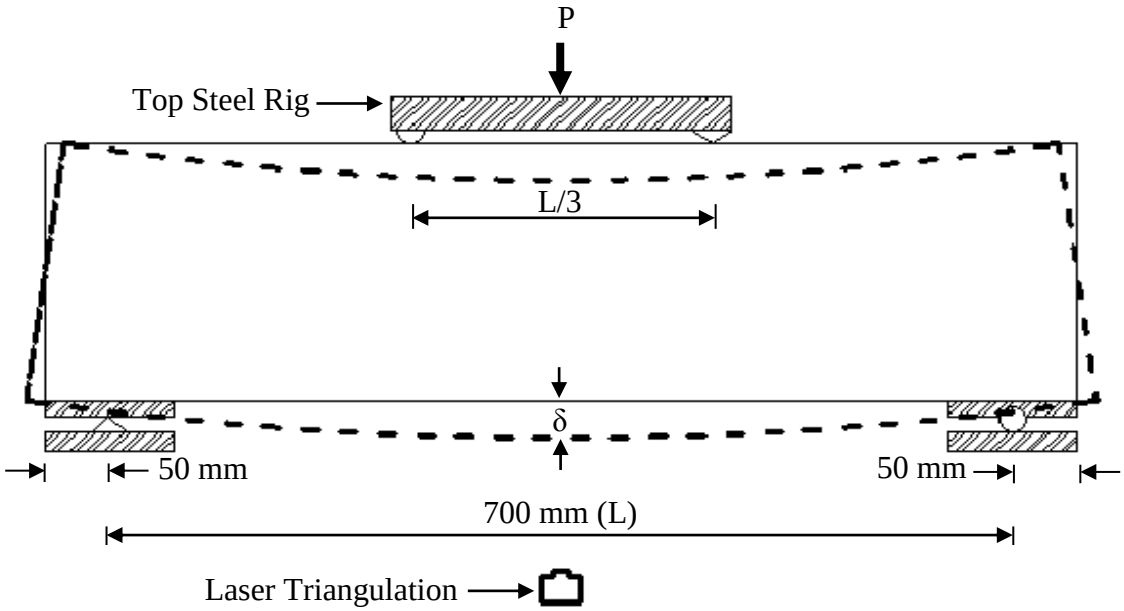

Figure 5.17 Schematic of specimen tested under four-point bending

5.6 Summary

In this chapter, the details of the experimental program for specimens with 800 mm height were discussed. The properties of the main materials included concrete, SEA sections and steel bars were presented. Also, the details of the fabrication, instrumentation and testing program of the HSC square specimens with 800 mm height under concentric and eccentric axial loads and four-point bending were also described. The experimental results from this experimental program (preliminary testing of materials and specimens with 800 mm) are presented in the next chapter.

6 EXPERIMENTAL RESULTS OF SPECIMENS WITH 800 mm HEIGHT

6.1 General

The experimental results of the twenty high strength concrete (HSC) specimens with 800 mm height and the preliminary material testing are presented and discussed in this chapter. Five reinforced concrete (RC) column specimens reinforced longitudinally with steel bars and fifteen RC column specimens reinforced longitudinally with SEA sections. The results of the test specimens are investigated to study the effect of type of longitudinal reinforcement (steel bars and SEA sections) and spacing of transverse ties on the behaviour of square HSC columns tested under concentric and eccentric axial load and four-point bending. In addition, the results of preliminary testing of materials included concrete testing (compressive, tensile and flexural test results), steel equal angle (SEA) sections (tensile test results) and steel bar testing (tensile test results) are also presented to define the response of constituent materials.

6.2 Preliminary Testing of Materials

The materials used in this experimental program were concrete, steel equal angle (SEA) sections and steel bars. Different testings were carried out to determine the influence of constituent material properties on the behaviour of square high strength concrete (HSC) specimens reinforced longitudinally with either steel bars or SEA sections. Also, the

results of preliminary testing of materials were used for analytical analysis of the tested specimens which are presented and discussed in Chapter seven.

6.2.1 **Concrete Testing**

Four types of concrete tests were conducted on the concrete in order to determine the concrete properties that were used in the experimental program. The tests included compressive strength test, indirect and direct tensile strength test and modulus of rupture test.

The compressive strength of concrete was conducted and determined in according with Australian Standard AS 1012.9 (1999). A total of 9 concrete cylinders with a diameter of 100 mm and a height of 200 mm were cast on the same day and tested at 7, 28 and 56 days to obtain the compressive strength of concrete. For each day of testing, three concrete cylinders were tested and the average was calculated. Prior to testing the concrete cylinders the rough surface face was capped with high strength plaster to ensure full contact between the loading plate of the compression testing machine and the specimen to prevent premature cracking. The compression testing was carried out on an 1800 kN Avery testing machine with the load applied at a rate of 17.5% until failure, which is equivalent to the 20 ± 2 MPa compressive stress per minute until no increase in force was sustained (Figure 6.1). The results of the compression testing are shown in Table 6.1. The average 7, 28 and 56 days concrete compressive strength of 53.6 MPa, 68.5 MPa and 70.7 MPa were achieved.

(a) (b)

Figure 6.1 Testing of cylinder compressive strength of concrete: (a) testing of sample and (b) sample after testing

Table 6.1 Test Results of the Compressive Strength of Concrete

Sample no.	Testing age (Day)	Diameter (mm)	Height (mm)	Maximum load (kN)	Compressive strength (MPa)	Average compressive strength (MPa)
1	7	101	200	422	52.7	53.6
2		102	200	436	53.3	
3		100	200	429	54.7	
1	28	100	200	543	69.2	68.5
2		101	200	547	68.4	
3		100	200	534	68.0	
1	56	102	200	573	70.1	70.7
2		100	200	554	70.6	
3		101	200	565	71.3	

The tensile strength of the concrete was obtained by performing an indirect tensile strength test (splitting test) according to the Australian Standard AS 1012.10 (2000). The samples were tested at 28 days after casting in the 1800 kN Avery compression testing machine using a typical testing jig as shown in Figure 6.2. Three concrete cylinders of 150 mm diameter and 500 mm height were cast on the same day. The test results of the indirect tensile testing of concrete are shown in Table 6.2. The average 28 days indirect concrete tensile strength was 5.5 MPa.

(a) (b)

Figure 6.2 Testing of indirect tensile strength of concrete (a) testing of sample and (b) sample after testing

Table 6.2 Concrete indirect tensile strength test results

Sample no.	Diameter (mm)	Length (mm)	Maximum load (kN)	Indirect tensile strength of concrete (MPa)	Average indirect tensile strength of concrete (MPa)
1	151	300	391	5.5	5.5
2	148	300	372	5.3	
3	152	300	400	5.6	

Three concrete samples were cast and tested to investigate the direct tensile strength of high strength concrete (HSC). After 28 days from casting, the samples were tested in the 500 kN Instron testing machine, as shown in Figure 6.3. Three prismatic samples of 100 mm × 100 mm cross section and 500 mm height were cast on the same day. The test results of the direct tensile testing of concrete are presented in Table 6.3. The average 28 days direct concrete tensile strength was 3.8 MPa.

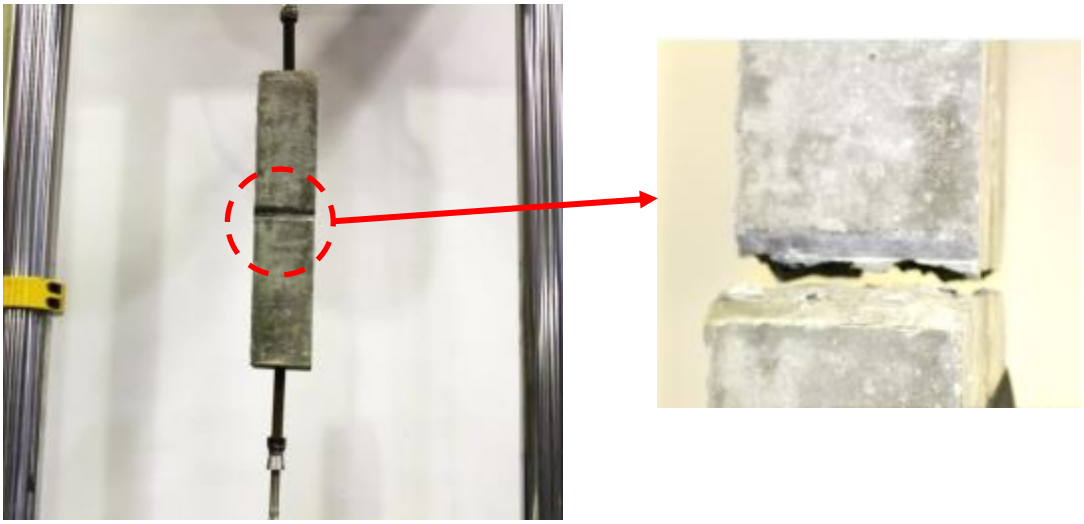

Figure 6.3 Testing of direct tensile strength of concrete

Table 6.3 Concrete Direct Tensile Strength Test Results

Sample no.	Width (mm)	Depth (mm)	Length (mm)	Maximum load (kN)	Direct tensile strength of concrete (MPa)	Average direct tensile strength of concrete (MPa)
1	100	101	500	35.0	4.3	3.8
2	101	100	500	28.5	3.5	
3	100	99	500	29.6	3.6	

Three concrete beam samples were cast and tested to find modulus of rupture (flexural strength) of the concrete according to the Australian Standard AS 1012.11 (2000). Three concrete beam samples of 100 mm × 100 mm cross section and 500 mm length were cast on the same day. The concrete beam samples were positioned in the 3000 kN Avery testing machine after 28 days after casting and tested under four-point bending until failure occurred within the middle third of the concrete beam samples, as shown in Figure 6.4. The results of the concrete flexural strength (modulus of rupture) test are shown in Table 6.4. The average 28 days modulus of rupture of concrete was 5.3 MPa.

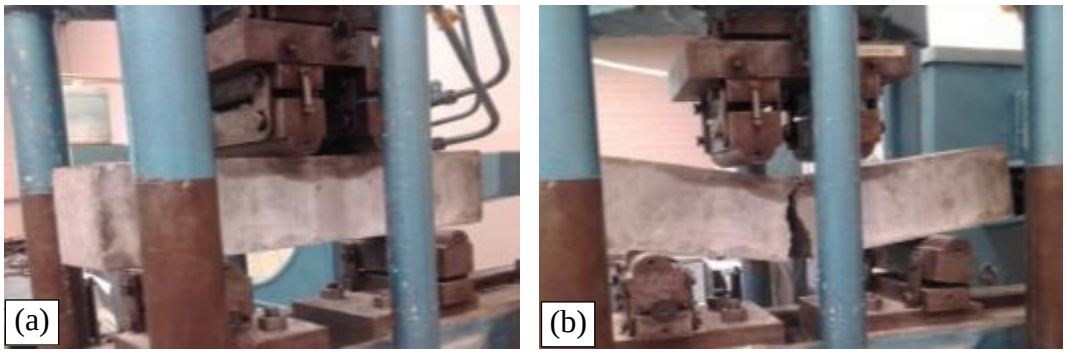

Figure 6.4 Testing of modulus of rupture of concrete: (a) Testing of sample and (b) Sample after testing

Table 6.4 Concrete Modulus of Rupture Test Results

Sample no.	Width (mm)	Depth (mm)	Length (mm)	Maximum load (kN)	Modulus of rupture of concrete (MPa)	Average modulus of rupture of concrete (MPa)
1	102	102	300	19	5.4	5.3
2	100	99	300	17	5.2	
3	99	100	300	18	5.3	

6.2.2 **Steel Equal Angle (SEA) Section Testing**

The steel equal angle (SEA) sections (A30 and A40) supplied by OneSteel (2010) were used in the specimens of Groups A30-S50, A30-S75, A40-S50 and A40-S75. The cross section of A30 SEA had a nominal leg width of 30 mm and a nominal thickness of 2.5 mm with a nominal yield tensile strength of 350 MPa. The A40 SEA section had a nominal leg width of 40 mm and a nominal thickness of 4 mm with a nominal yield tensile strength of 450 MPa. The tensile properties of the SEA sections were determined according to the Australian Standard AS 1391 (2007). For A30 and A40 SEA sections, tensile coupons were taken from the flange of the SEA sections, as shown in Figure 6.5. Three coupons from each of A30 and A40 sections were extracted and tested by using the 500 kN Instron testing machine according to the Australian Standard AS 1391(2007).

An extensometer was set-up at mid-height of the tensile coupons to determine the axial strain, as shown in Figure 6.6. The stress was calculated based on the load divided by the cross-sectional area at the middle of the samples. The test results of the SEA sections that were tested are shown in Figures 6.7 and 6.8. The average yield tensile strength for the A30 and A40 SEA sections was found to be 374 MPa and 473 MPa, respectively.

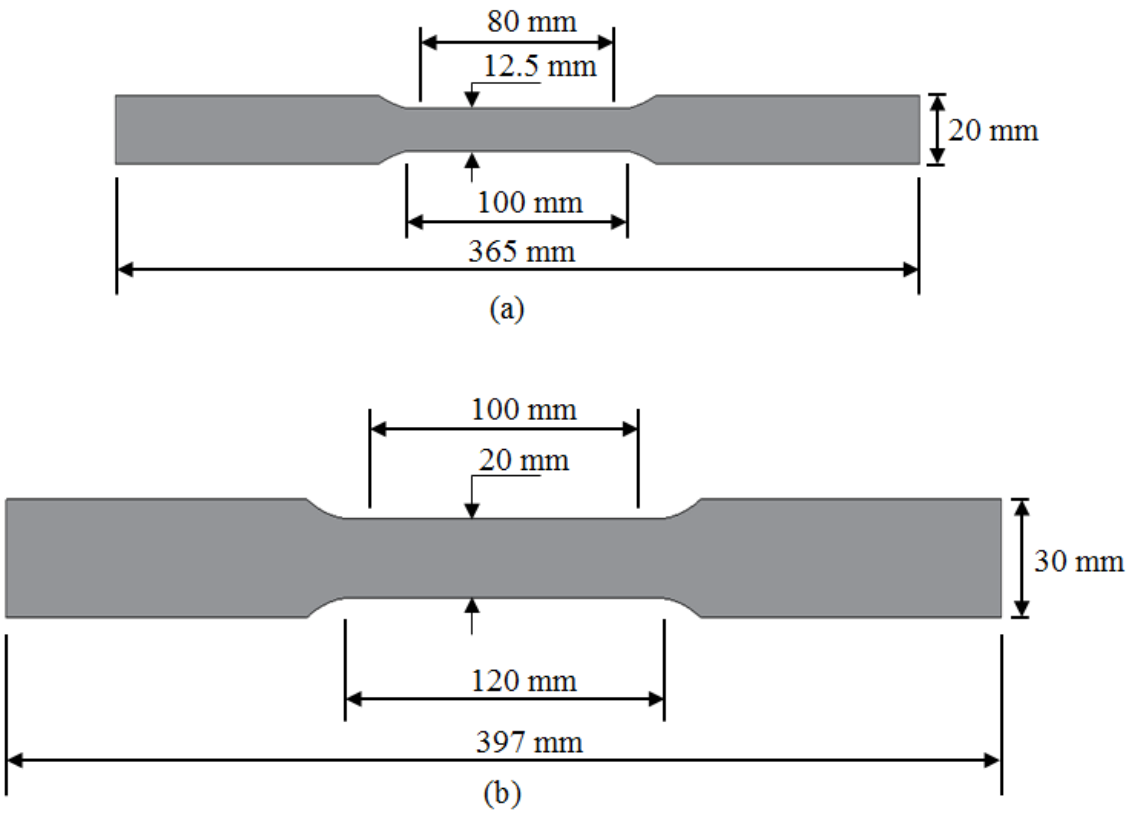

Figure 6.5 Details of tensile coupon specimens of steel equal angle (SEA) section: (a) A30 and (b) A40

Figure 6.6 Tensile test of the steel equal angle (SEA) sections: (a) A30 SEA and (b) A40 SEA

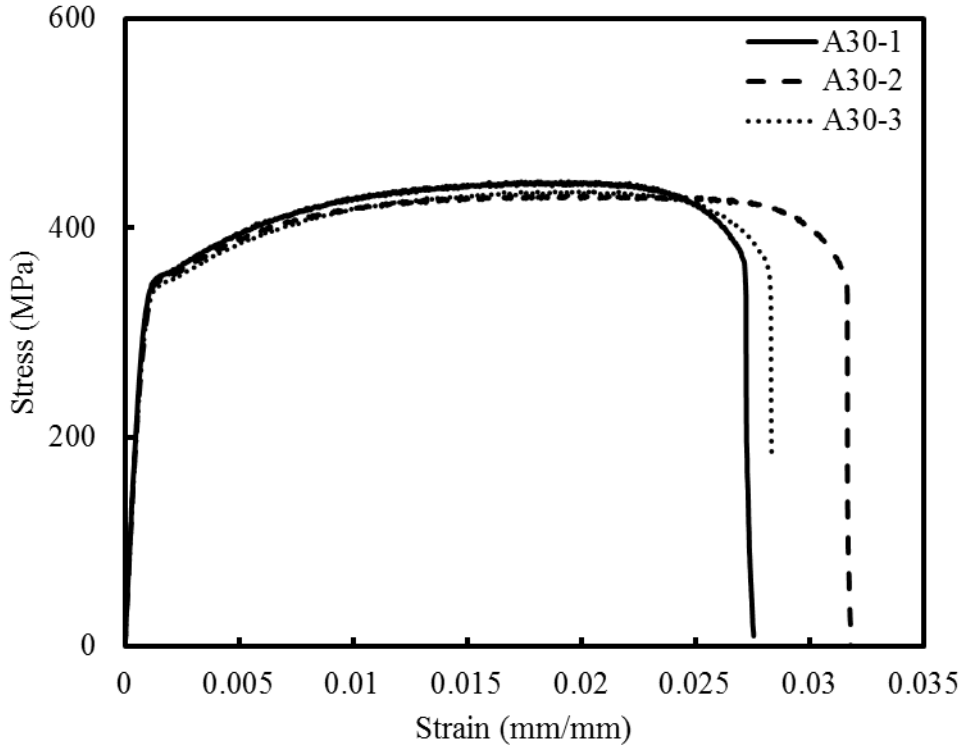

Figure 6.7 Stress-strain behaviour of A30 steel equal angle (SEA) sections

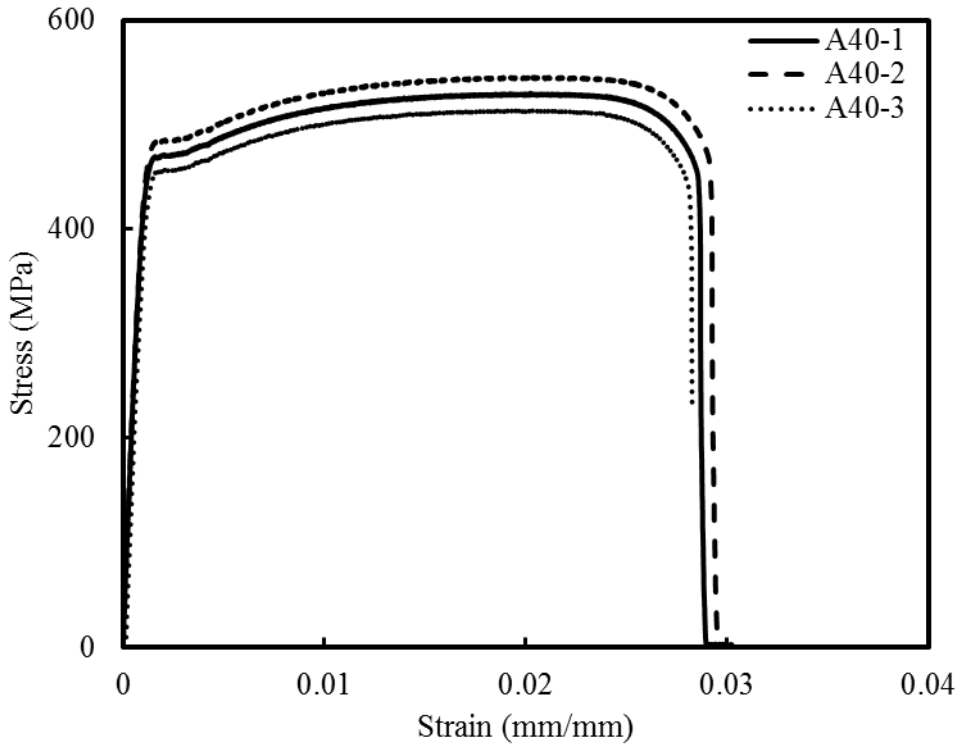

Figure 6.8 Stress-strain behaviour of A40 steel equal angle (SEA) sections

6.2.3 **Steel Bar Testing**

Deformed N12 steel bars were used as longitudinal reinforcement in Group R-S50 specimens. Plain steel R10 bars were used as transverse ties for all specimens. Three samples from each of N12 and R10 bars were tested by using the 500 kN Instron testing machine according to the Australian Standard AS 1391 (2007), as shown in Figure 6.9. An extensometer was set-up at mid-height of the steel bar to determine the longitudinal strain (Figure 6.9). The test results of the N12 and R10 bars are reported. The average yield tensile strengths were 556 MPa and 323 MPa for N12 and R10 steel bars, respectively. The axial stress-axial strain curves of N12 bars and R10 bars are presented in Figures 6.10 and 6.11.

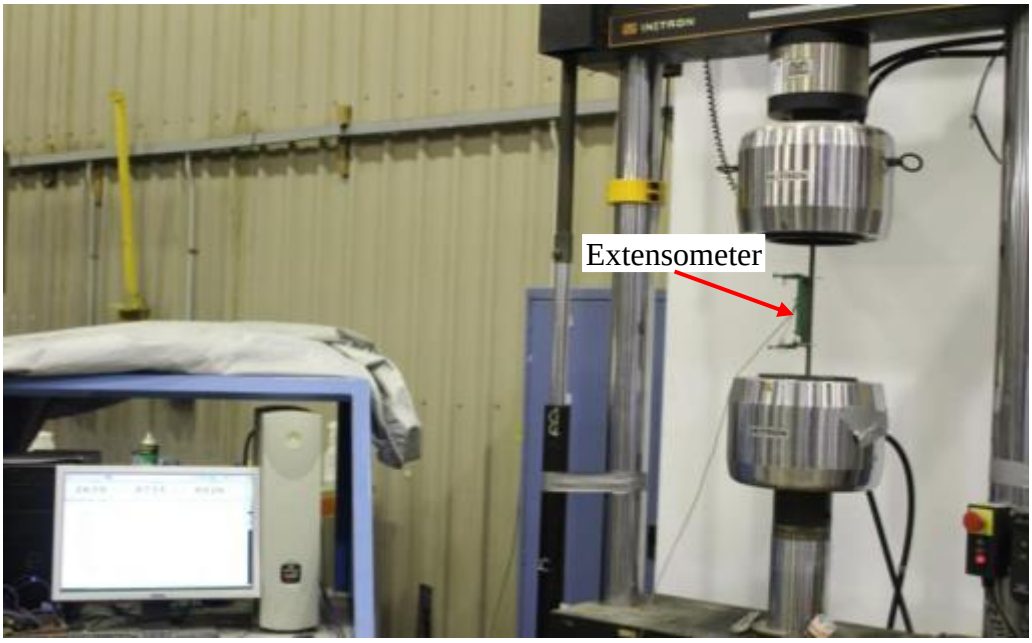

Figure 6.9 Tensile test of the steel bar using Instron machine

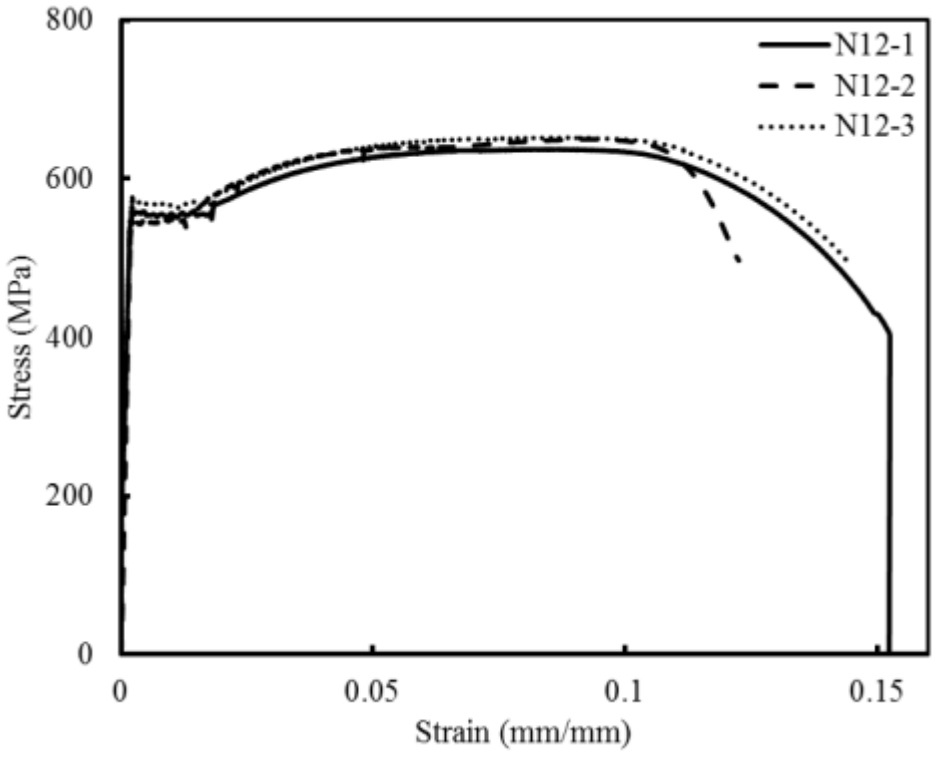

Figure 6.10 Stress-strain behaviour of N12 steel bars

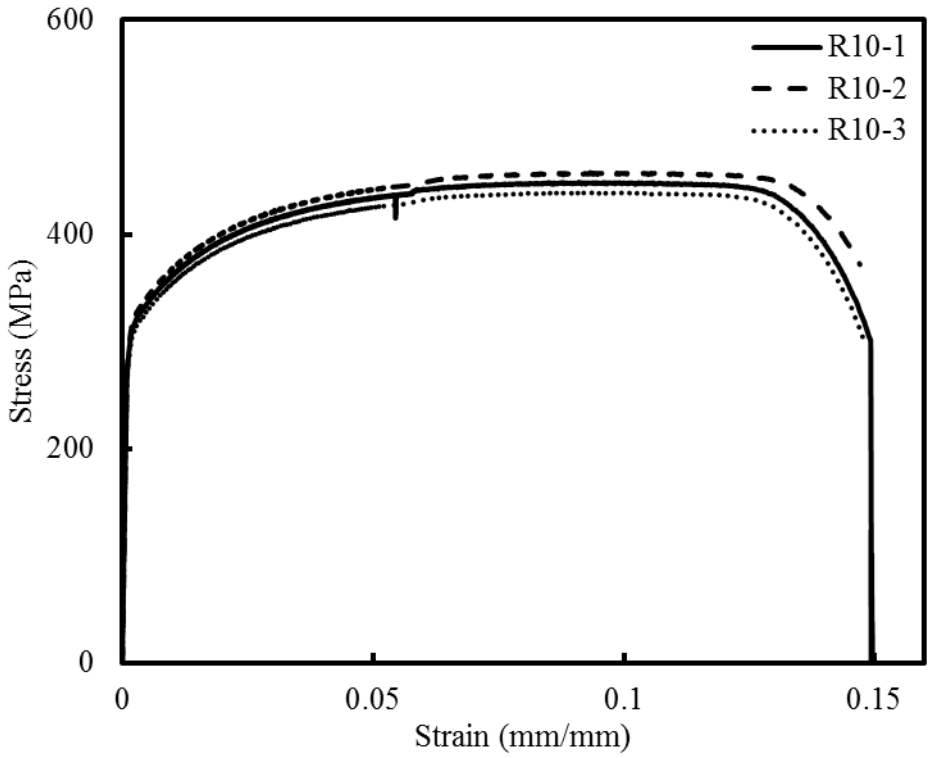

Figure 6.11 Stress-strain behaviour of R10 steel bars

6.3 Specimens Tested under Axial loads

In this section, a total of fifteen HSC specimens were tested under concentric and eccentric axial loads in order to examine the behaviour of square HSC columns under concentric and eccentric axial loads.

6.3.1 **Ductility of Tested Specimens**

In this study, the ductility (μ) of the tested column specimens was calculated based on the energy absorption capacity of the specimen. The ductility was calculated as the ratio of the area under the axial load-axial deformation curve up to the ultimate deformation

to the area up to the deformation corresponding to the yield load (Hadi and Youssef 2016; Hadi et al. 2016b).

$$\mu = \frac{A_u}{A_y} \tag{6.1}$$

where A_y and A_u are the areas under the axial load-axial deformation curves up to the yield deformation (Δ_y) and up to the ultimate deformation (Δ_u), respectively. The yield deformation (Δ_y) is taken as the axial deformation corresponding to the intersection point of an extension line through 75% of the maximum axial load and the horizontal line from the maximum axial load (Pessiki and Pieroni 1997). The ultimate deformation was measured as the axial deformation at an axial load equal to 80% of the maximum axial load in the descending branch of the axial load-axial deformation curve (Sheikh and Legeron 2014; Hadi and Youssef 2016), as shown in Figure 6.12.

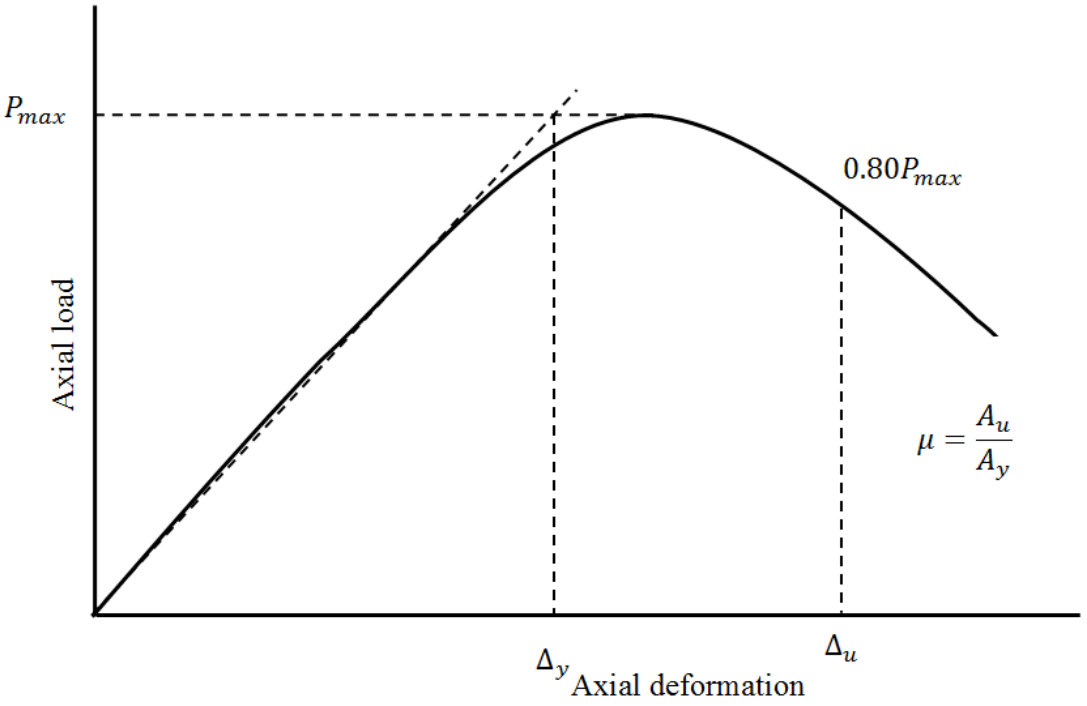

Figure 6.12 Ductility of tested column specimens

6.3.2 **Specimens Tested under Concentric Axial Load**

A total of five HSC specimens were tested under concentric axial compression. All the specimens were tested up to about 40% of the maximum axial load in the post-peak descending branch of the axial load-axial deformation response. The axial load-axial deformation behaviours of all specimens tested under concentric axial load showed similar behaviour up to the first peak axial load. Then the concrete cover spalled off, which led to a drop in the axial load of about 1.1% to 7.7% of the first peak axial load. Afterwards, the passive confinement of the concrete core of the specimen was activated and specimens exhibited an increase in the axial load carrying capacity up to the second peak axial load. The second peak axial load were either lower or higher than the first peak axial load depending on the conditions of the confined concrete core (Foster 1999; Hadi et al. 2016a). The first crack in Specimen R-S50-C was initiated at the top edge of the specimen (Figure 6.13), whereas the first crack in Specimens A30-S50-C appeared at the mid-height of the specimen, as shown in Figure 6.14.

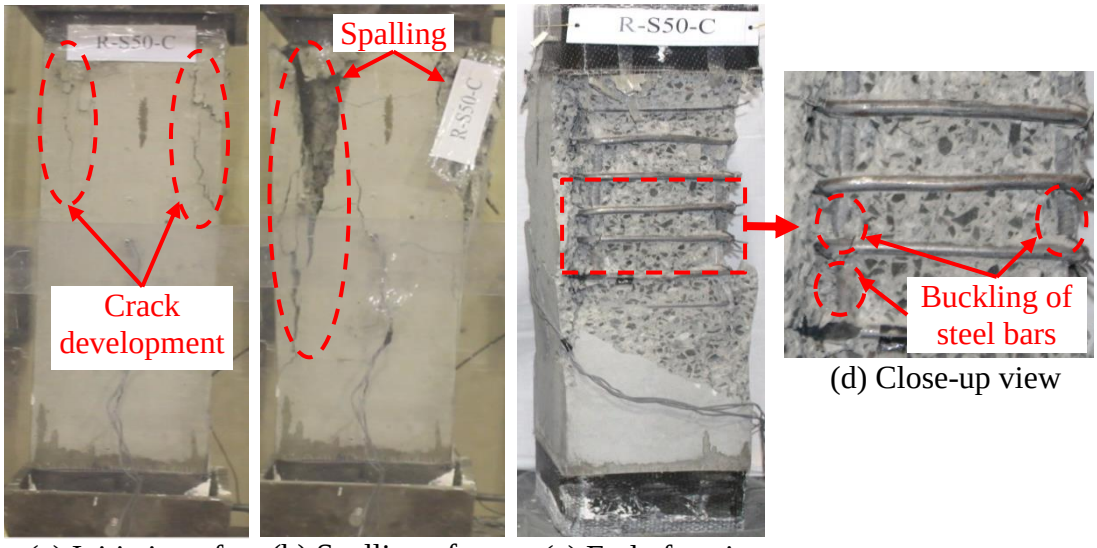

(a) Initiation of crack (b) Spalling of cover concrete (c) End of testing (d) Close-up view

Figure 6.13 Behaviour of Specimen R-S50-C during different stages of loading

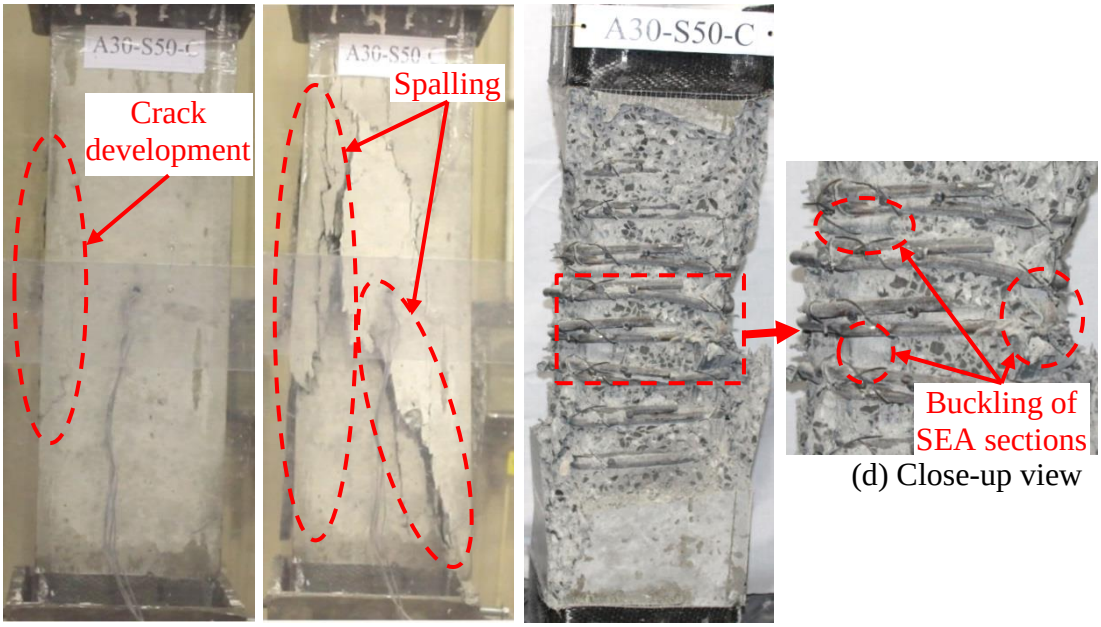

(a) Initiation of crack (b) Spalling of cover concrete (c) End of testing (d) Close-up view

Figure 6.14 Behaviour of Specimen A30-S50-C during different stages of loading

For Specimens A30-S75-C, A40-S50-C and A40-S75-C, the hairline cracks started at first around the mid-height and then extended near the top one-third height of the specimens (Figures 6.15, 6.16 and 6.17). At the first peak axial load, the strain in the longitudinal N12 steel bars in Specimen R-S50-C was 0.1%, while the average axial strains in the longitudinal A30 and A40 SEA sections were 0.08%. The reason for the low axial strain in the longitudinal reinforcement was because the HSC experienced low lateral expansion under axial compression. The low lateral expansion in the HSC is due to higher modulus of elasticity and lower internal micro cracking of the HSC than those of NSC (Cusson and Paultre 1994; Sharma et al. 2005). The failure of the specimens under concentric axial compression was due to the spalling of the concrete cover, followed by outward buckling of the longitudinal steel bars and SEA sections, as shown in Figures 6.15, 6.16 and 6.17.

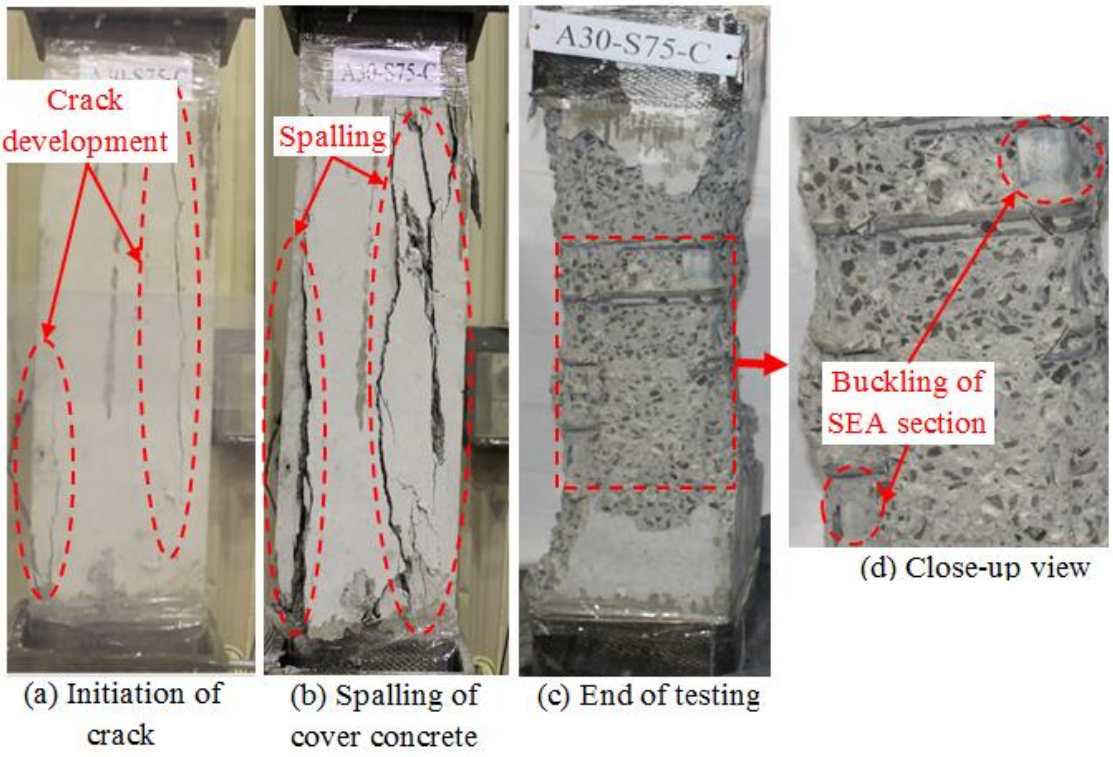

Figure 6.15 Behaviour of Specimen A30-S75-C during different stages of loading

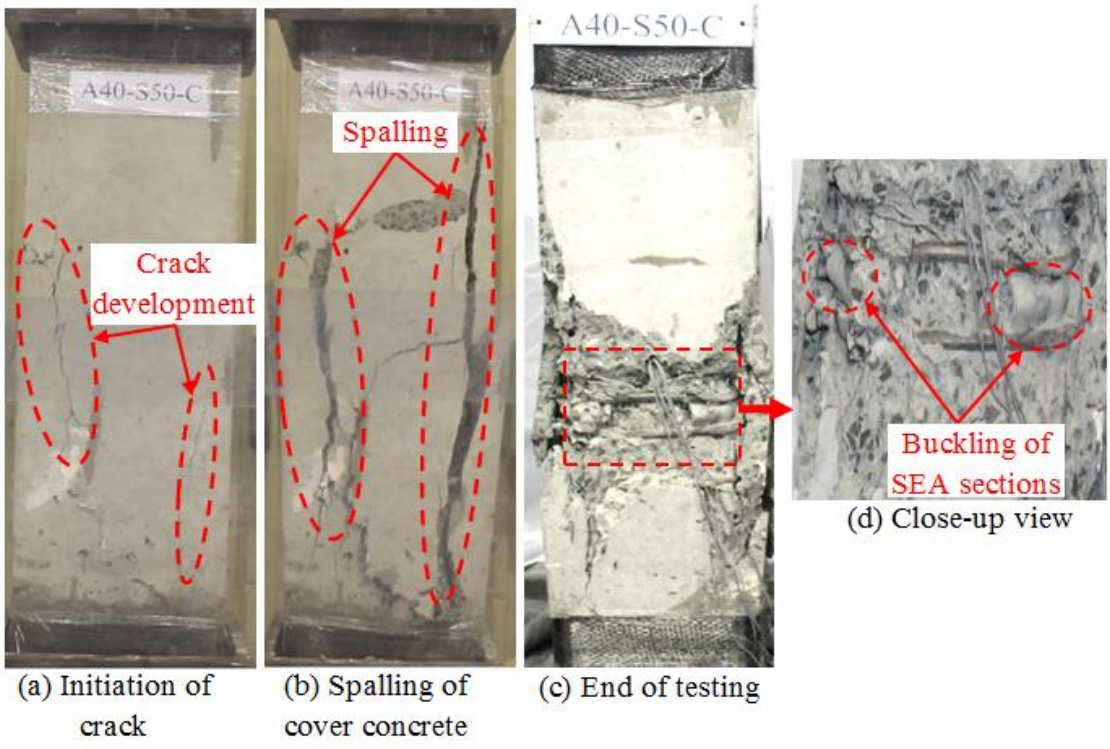

Figure 6.16 Behaviour of Specimen A40-S50-C during different stages of loading

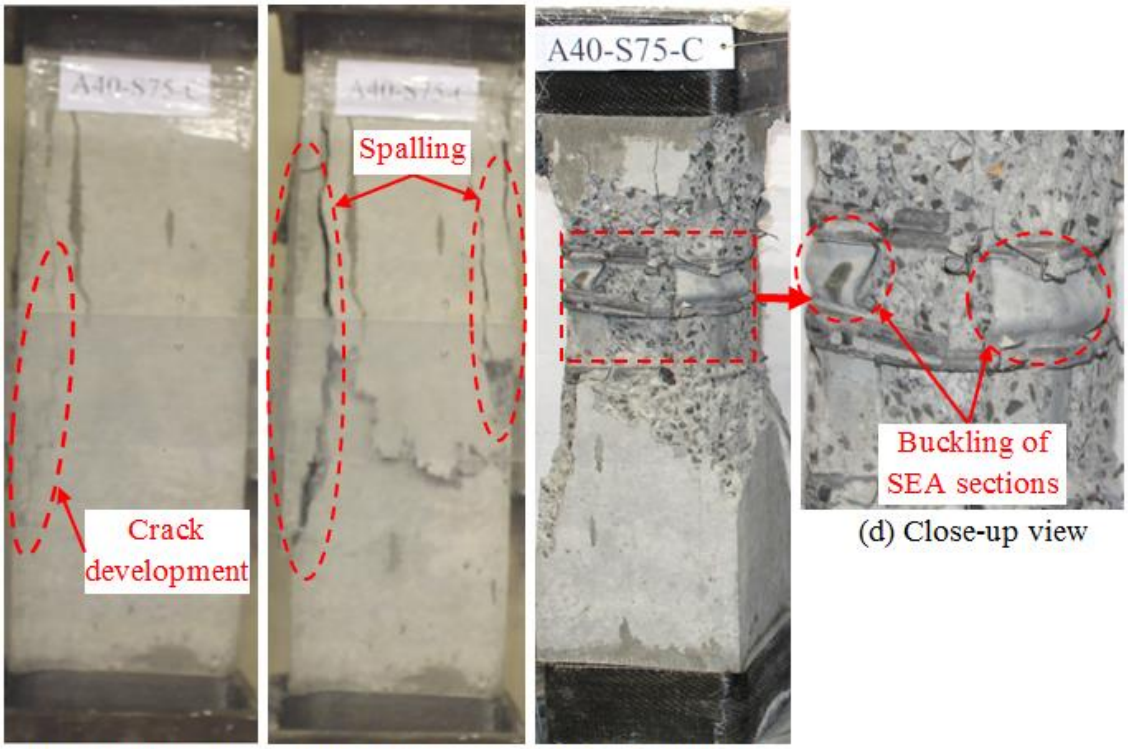

Figure 6.17 Behaviour of Specimen A40-S75-C during different stages of loading

Table 6.5 presents the experimental results of specimens tested under concentric axial loads in terms of the first and second peak axial loads and the corresponding axial deformations and ductility. For specimens tested under concentric axial loads, it can be observed that Specimens A30-S50-C, A40-S50-C and A40-S75-C had both first and second peak axial loads, whereas Specimens R-S50-C and A30-S75-C had only one peak axial load, as shown in Figure 6.18. This was because the longitudinal SEA sections were activated and confined the concrete core after cover spalling. For the specimens with the same spacing of transverse ties (50 mm) and with different types of longitudinal reinforcement (N12 steel bars, A30 and A40 SEA sections), Specimen

A30-S50-C exhibited lower first peak axial load, which was only 6.6% lower than the first peak axial load of Specimen R-S50-C. This lower peak axial load may be attributed to the fact that N12 steel bars had 49% higher yield tensile strength than A30 SEA sections. The second peak axial load of Specimen A30-S50-C was only 1% lower than the first peak axial load (Figure 6.18). In addition, the use of the SEA sections improved the performance of the specimens by enhancing the post-peak axial load-axial deformation behaviour, where Specimen A30-S50-C achieved an increase of about 56.3% in ductility compared to Specimen R-S50-C. These observations clearly indicated that by using SEA sections as the main reinforcement led to a significant increase in the confinement to the concrete core after the concrete cover spalled off. Although steel bars had 18% higher yield tensile strength than A40 SEA sections, it was observed that Specimen A40-S50-C achieved about 9.6% and 43.8% higher first peak axial load and ductility, respectively, than Specimen R-S50-C. The reason for the higher strength and ductility may be because the A40 SEA section more effectively confined the concrete core and also the cross-sectional area of the A40 SEA section was higher than the cross-sectional area of N12 steel bar.

For the specimens reinforced with A30 SEA sections with different spacing of transverse ties (50 mm and 75 mm), Specimen A30-S50-C exhibited lower first peak axial load, which was only 7.9% lower than the peak axial load of Specimen A30-S75-C. This lower first peak axial load is due to the development of a plane of weakness between the concrete core and concrete cover in Specimen A30-S50-C. The plane of weakness between concrete core and concrete cover led to the spalling of concrete cover at an early stage of loading (Cusson and Paultre 1994; Razvi and Saatcioglu 1994;

Pessiki and Pieroni 1997). However, Specimen A30-S50-C obtained about 47.1% higher ductility than Specimen A30-S75-C. The reason for this higher ductility was due to the increased confinement for the shorter spacing of transverse ties in Specimen A30-S50-C than the spacing of transverse ties in Specimen A30-S75-C.

For the specimens reinforced with A40 SEA sections with different spacing of transverse ties (50 mm and 75 mm), Specimen A40-S50-C showed higher first peak axial load, which was 8.4% higher than the first peak axial load of Specimen A40-S75-C. The reason is that the decrease in the spacing of transverse ties from 75 mm to 50 mm led to an increase in the effective confinement area of the concrete core. The second peak axial loads of Specimens A40-S50-C and A40-S75-C were 96.4% and 98.9%, respectively, of the corresponding first peak axial loads. This small difference between the first and second peak axial loads of Specimen A40-S50-C and Specimen A40-S75-C indicated that the use of SEA sections significantly increased the area of the confined concrete core. In addition, Specimen A40-S50-C obtained about 9.5% higher ductility than Specimen A40-S75-C. The increase in ductility was due to the decrease in the spacing of transverse ties from 75 mm to 50 mm, which led to a more effective confinement of the concrete core.

Table 6.5 Experimental Results of the Tested Specimens under Concentric Axial Loads

Specimen	First Peak		Second Peak		Ductility (μ)
	Axial load (kN)	Axial deformation (mm)	Axial load (kN)	Axial deformation (mm	
R-S50-C	2716	2.8	-	-	1.6
A30-S50-C	2548	2.6	2524	2.8	2.5
A30-S75-C	2749	2.6	-	-	1.7
A40-S50-C	2977	2.7	2873	3	2.3
A40-S75-C	2747	2.6	2716	2.7	2.1

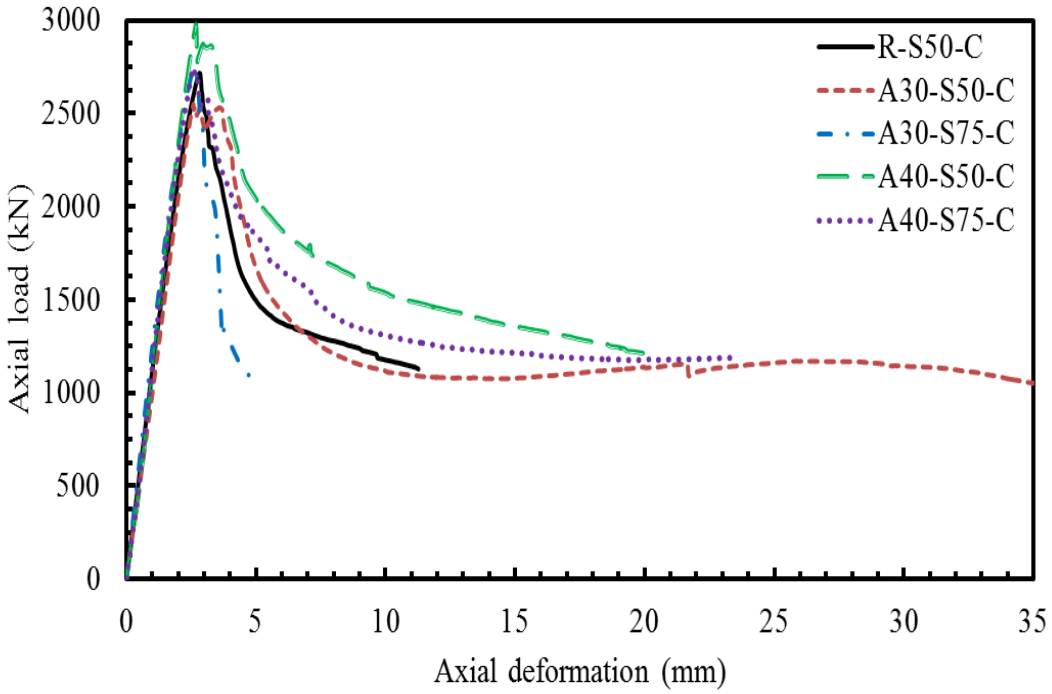

Figure 6.18 Axial load-axial deformation behaviour of specimens tested under concentric axial load

6.3.3 **Specimens Tested under 25 mm Eccentric Axial Load**

From each group, one specimen was tested under 25 mm eccentric axial load. All these specimens were tested. All the specimens were tested up to about 40% of the maximum axial load in the post-peak descending branch of the axial load-axial deformation response. The axial load-axial deformation behaviour for eccentrically loaded specimens experienced similar trends up to the maximum axial load. At first, the cracks started on the tension side at the mid-height of the specimens and then extended on all the four sides, as shown in Figures 6.19, 6.20 and 6.21. The failure of the specimens tested under eccentric axial loads was initiated by spalling of the concrete cover, followed by buckling of the longitudinal reinforcement and crushing of concrete in the compression zone (Figure 6.19). It was also observed from the readings of the strain gages attached on the longitudinal reinforcement that all specimens tested under eccentric axial loads were yielded on the compression side. However, the axial strain in Specimen A30-S50-E25 was not measured as the strain gages in Specimen A30-S50-E25 did not function properly during the test.

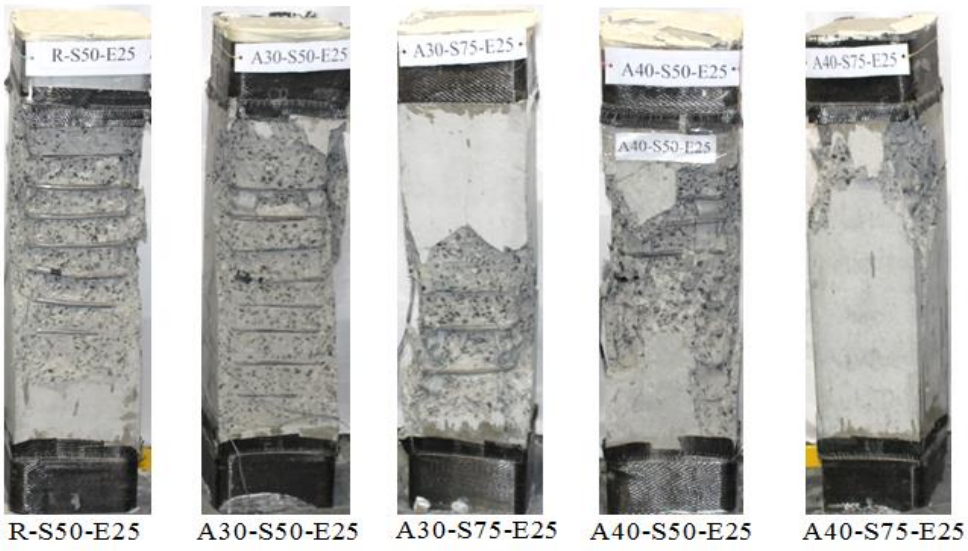

Figure 6.19 Behaviour of Specimens under 25 mm eccentric axial loads: Compression side

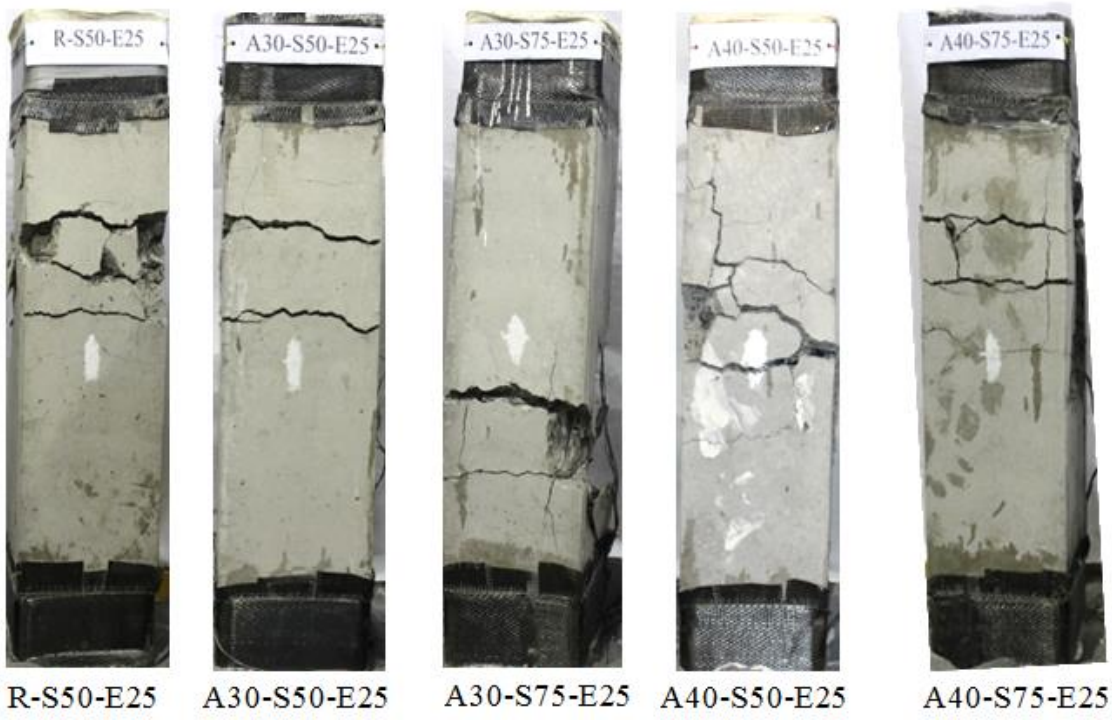

Figure 6.20 Behaviour of Specimens under 25 mm eccentric axial loads: Tension side

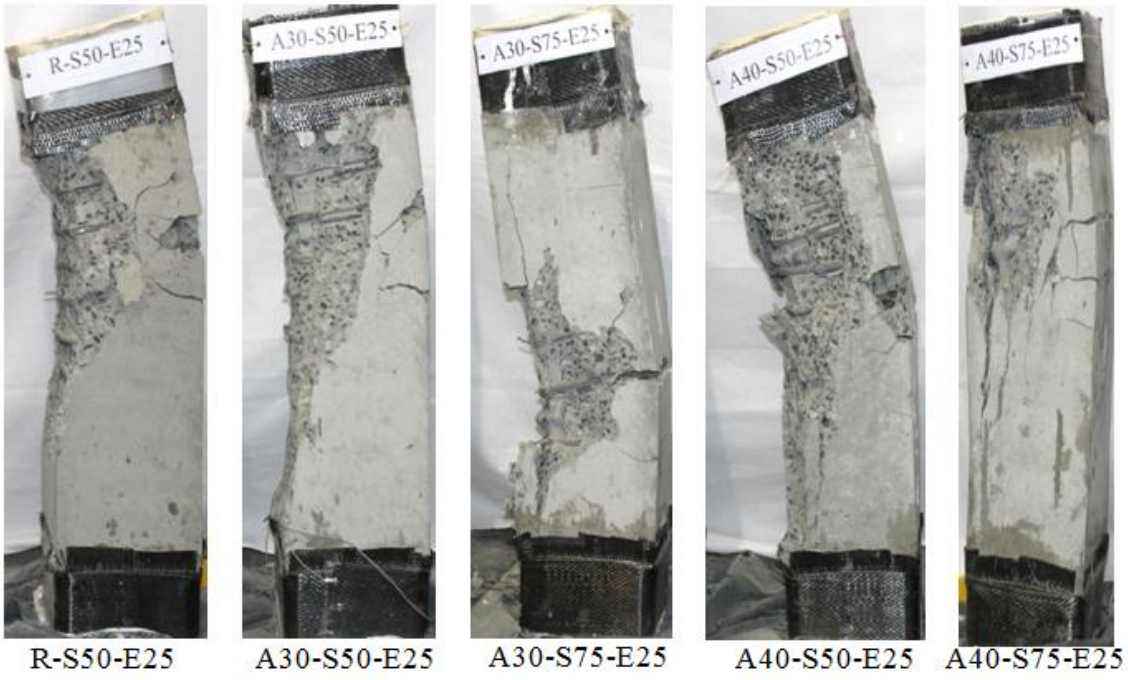

Figure 6.21 Behaviour of Specimens under 25 mm eccentric axial loads: Side view

Table 6.6 presents the experimental results of specimens tested under 25 mm eccentric axial load in terms of the yield axial load, the first and second peak axial loads and the corresponding axial deformations and ductility. For specimens tested under 25 mm eccentric axial loads, it can be observed that Specimens A30-S50-E25, A30-S75-E25, A40-S50-E25 and A40-S75-E25 had both the first and the second peak axial loads, whereas Specimen R-S50-E25 had only one peak axial load, as shown in Figure 6.22. This observation indicated that the longitudinal SEA sections were effectively activated to confine the concrete core after the concrete cover spalled off.

For the specimens with the same spacing of transverse ties (50 mm) and with different longitudinal reinforcements (N12 steel bars, A30 and A40 SEA sections), Specimen A30-S50-E25 exhibited lower first peak axial load, which was only 8.8% lower than the peak axial load of Specimen R-S50-E25. This may be attributed to the fact that steel bars had 49% higher yield tensile strength than A30 SEA sections. However, Specimen A30-S50-E25 obtained about 30.8% higher ductility than Specimen R-S50-E25 because the bending stiffness of a SEA section was greater than the bending stiffness of a steel bar. Although steel bars had 18% higher yield tensile strength than A40 SEA sections, it was observed that Specimens A40-S50-E25 obtained 3.3% and 46.2% higher first peak axial load and ductility, respectively, than Specimen R-S50-E25. The higher first peak axial load and ductility were because the A40 SEA section had a higher bending stiffness than the N12 steel bar.

For the specimens reinforced with A30 SEA sections with different spacing of transverse ties (50 mm and 75 mm), It can be observed that Specimen A30-S75-E25 had

the lowest axial load carrying capacity of 1457 kN, which might have resulted from premature failure or misalignments during testing. Therefore, the ductility and strength of Specimen A30-S75-E25 were not further analysed.

For the specimens reinforced with A40 SEA sections with different spacing of transverse ties (50 mm and 75 mm), Specimen A40-S50-E25 showed higher first peak axial load, which was 8.8% higher than the first peak axial load of Specimen A40-S75-E25. This may be because of the decreased spacing of transverse ties from 75 mm to 50 mm improved the confinement to the concrete core. The second peak axial loads of Specimens A40-S50-E25 and A40-S75-E25 were 78.3% and 82.4%, respectively, of the corresponding first peak axial loads. However, Specimens A40-S50-E25 and A40-S75-E25 showed very similar ductilities. This may be because the confinement effect from longitudinal SEA sections decreased under eccentric axial load. Another possible reason was that the use of A40 SEA sections led to the formation of dense cages, which might have caused the development of a plane of separation between the concrete cover and the concrete core at an early stage of loading.

Table 6.6 Experimental Results of the Tested Specimens under 25 mm Eccentric Axial Loads

Specimen	First Peak			Second Peak			Ductility (μ)
	Axial load (kN)	Axial deformation (mm)	Transverse deformation (mm)	Axial load (kN)	Axial deformation (mm)	Transverse deformation (mm)	
R-S50-E25	1967	2.7	1.2	-	-	-	1.3
A30-S50-E25	1808	2.9	2.2	1437	3.5	4.6	1.7
A30-S75-E25	1457	2.8	1.1	1307	3.8	4.7	-
A40-S50-E25	2032	2.8	1.3	1670	3.6	3.9	1.9
A40-S75-E25	1867	3.0	2.0	1587	3.8	4.2	1.9

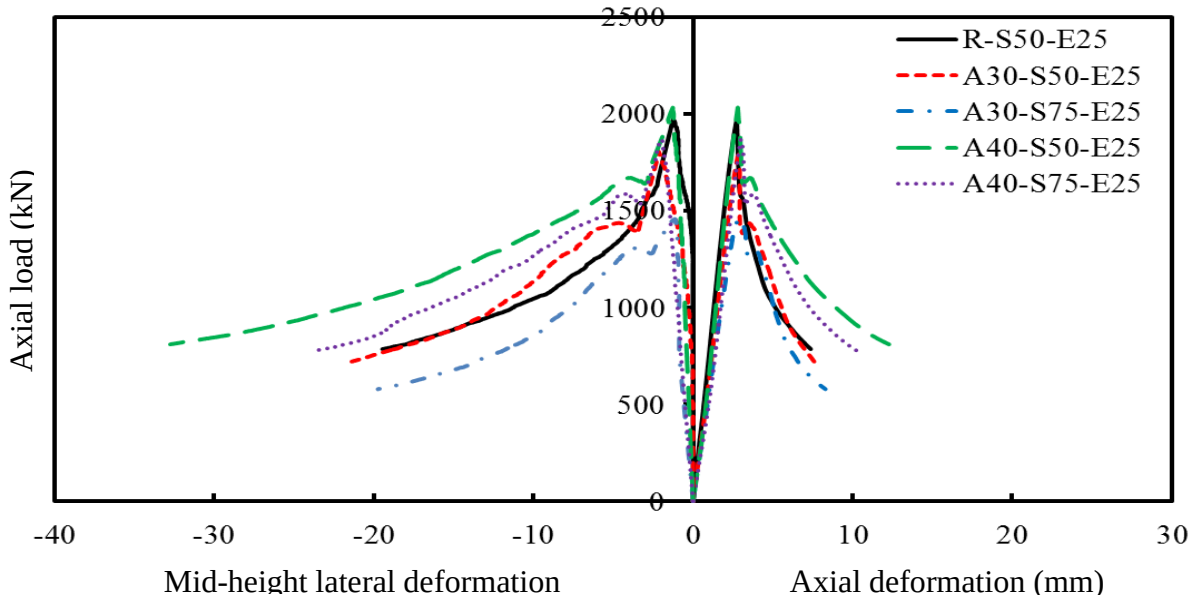

Figure 6.22 Axial load-axial deformation and axial load-mid-height lateral deformation behaviour of specimens tested under 25 mm eccentric axial load

6.3.4 **Specimens Tested under 50 mm Eccentric Axial Load**

From each group, one specimen was tested under 50 mm eccentric axial load. All the specimens were tested up to about 40% of the maximum axial load in the post-peak descending branch of the axial load-axial deformation response. The axial load-axial deformation behaviour for eccentrically loaded specimens experienced similar trends up to the maximum axial load. At first, the cracks started on the tension side at the mid-height of the specimens and then extended on all the four sides, as shown in Figures 6.23, 6.24 and 6.25. The failure mode of the specimens tested under eccentric axial loads was initiated by spalling of the concrete cover, followed by buckling of the longitudinal reinforcement and crushing of concrete in the compression zone, as shown in Figure 6.23.

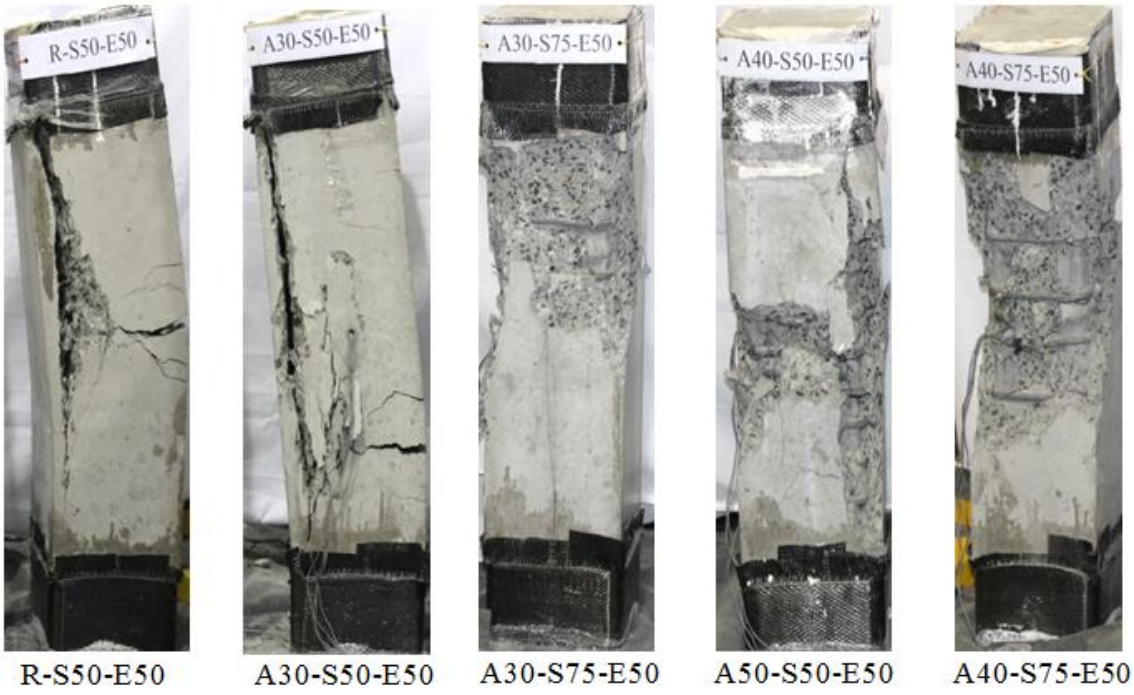

Figure 6.23 Behaviour of Specimens under 50 mm eccentric axial loads: Compression side

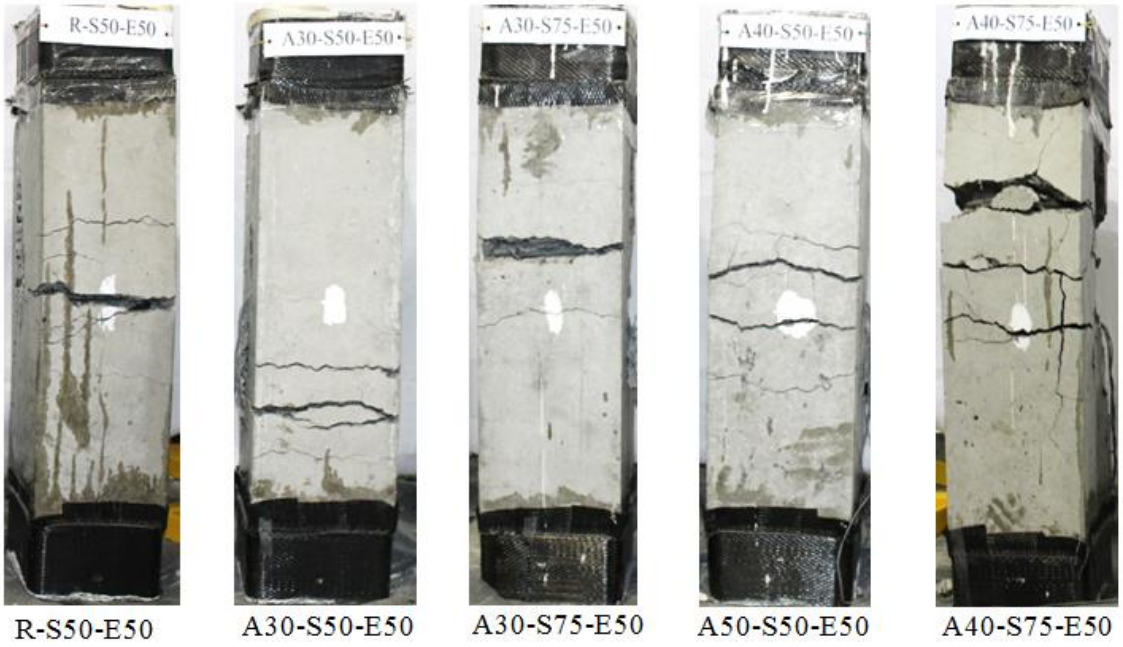

Figure 6.24 Behaviour of Specimens under 50 mm eccentric axial loads: Tension side

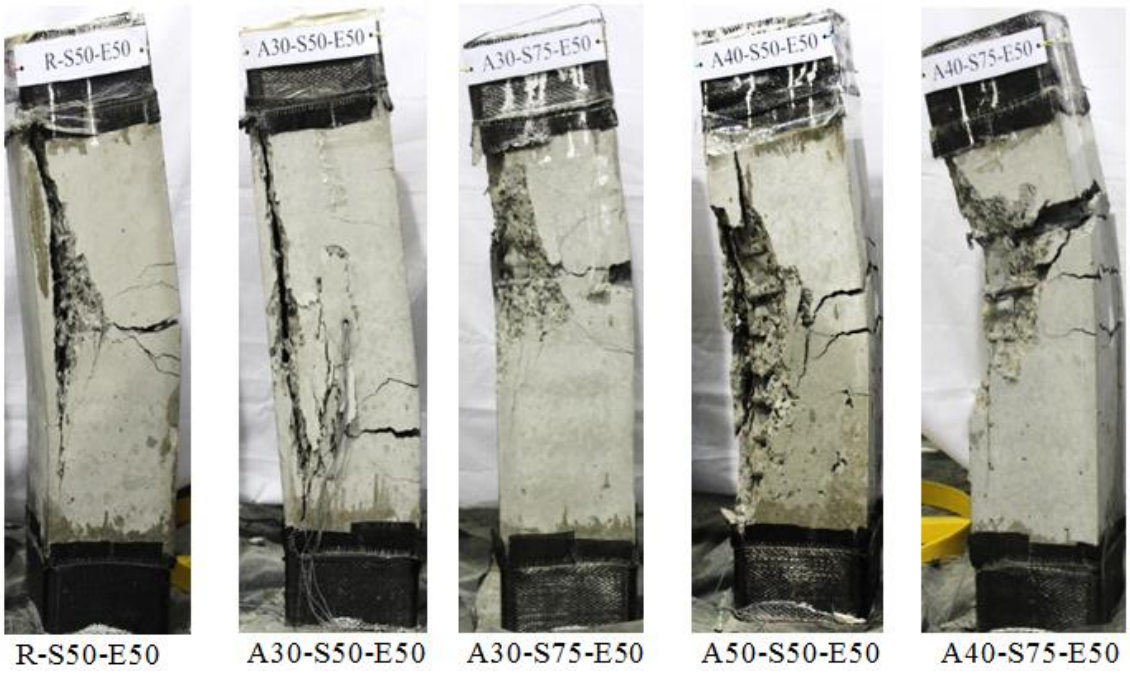

Figure 6.25 Behaviour of Specimens under 50 mm eccentric axial loads: Side view

Table 6.7 summarises the experimental results for specimens tested under 50 mm eccentric axial load in terms of the yield load, the first and second peak axial loads and the corresponding axial deformations and ductility. All the specimens were tested up to about 40% of the maximum axial load in the post-peak descending branch of the axial load-axial deformation response. For specimens tested under 50 mm eccentric axial loads, it can be observed that Specimens R-S50-E50, A30-S50-E50, A40-S50-E50, and A40-S75-E50 had both first and second peak axial loads, whereas Specimen A30-S75-E50 had only one peak axial load, as shown in Figure 6.26. In general, most of the specimens reinforced with SEA sections had second peak axial loads, which indicated that the longitudinal SEA sections were effectively activated to confine the concrete core after the concrete cover spalled off.

For specimens with the same spacing of transverse ties (50 mm) and with different longitudinal reinforcements (N12 steel bars, A30 or A40 SEA sections), Specimen A30-S50-E50 obtained 6.4% lower first peak axial load than Specimen R-S50-E50 (Figure 6.26). This lower first peak axial load may be attributed to the fact that N12 steel bars had 49% higher yield tensile strength than A30 SEA sections. The second peak axial loads of Specimens R-S50-E50 and A30-S50-E50 were 70.8% and 72.2%, respectively, of the corresponding first peak axial loads. It was observed that Specimen A30-S50-E50 obtained about 8.3% higher ductility than Specimen R-S50-E50. This slightly higher ductility for SEA reinforced specimens under 50 mm eccentric axial loads may be because of higher confinement effectiveness of SEA sections compared to steel bar specimens under 50 mm eccentric axial loads. Although steel bars had 18% higher yield tensile strength than A40 SEA sections, it was observed that Specimen A40-S50-C

obtained 8.8% higher first peak axial load than Specimen R-S50-E50. The reason for this higher first peak axial load was because the A40 SEA section had a much higher bending stiffness and a greater cross-sectional area than the N12 steel bar. In addition, Specimen R-S50-E50 exhibited 75.0% lower ductility than Specimen A40-S50-E50. The reason of the higher strength and ductility may be because the A40 SEA section had a higher bending stiffness and a greater cross-sectional area than the N12 steel bar.

For the specimens reinforced with A30 SEA sections with different spacings of transverse ties (50 mm and 75 mm), Specimen A30-S50-E50 showed lower first peak axial load, which was 2.9% lower than the peak axial load of Specimen A30-S75-E50, as shown in Figure 6.26. Also, Specimen A30-S50-E50 obtained about 7.7% higher ductility than Specimen A30-S75-E50.

For the specimens reinforced with A40 SEA sections with different spacings of transverse ties (50 mm and 75 mm), Specimen A40-S50-E50 showed lower first peak axial load, which was 2.4% lower than the first peak axial load of Specimen A40-S75-E50. The reason for this may be because the decrease in the spacing of transverse ties from 75 mm to 50 mm resulted in increased amount of steel reinforcement, which led to the development of a plane of separation between the concrete cover and the concrete core at an early stage of loading. The second peak axial loads of Specimens A40-S50-E50 and A40-S75-E50 were 77.7% and 74.6% respectively, of the corresponding first peak axial loads. Also, Specimen A40-S50-E50 showed 23.5% higher ductility than Specimen A40-S75-E50.

Table 6.7 Experimental Results of the Tested Specimens under 50 mm Eccentric Axial Loads

Specimen	First Peak			Second Peak			Ductility (μ)
	Axial load (kN)	Axial deformation (mm)	Transverse deformation (mm)	Axial load (kN)	Axial deformation (mm)	Transverse deformation (mm)	
R-S50-E50	1340	2.7	1.9	1037	3.4	4.5	1.2
A30-S50-E50	1260	2.5	1.1	986	3.2	3.2	1.3
A30-S75-E50	1297	2.5	3.0	-	-	-	1.4
A40-S50-E50	1457	2.7	3.4	1191	3.3	4.6	2.1
A40-S75-E50	1492	2.7	2.6	1190	3.4	5.1	1.7

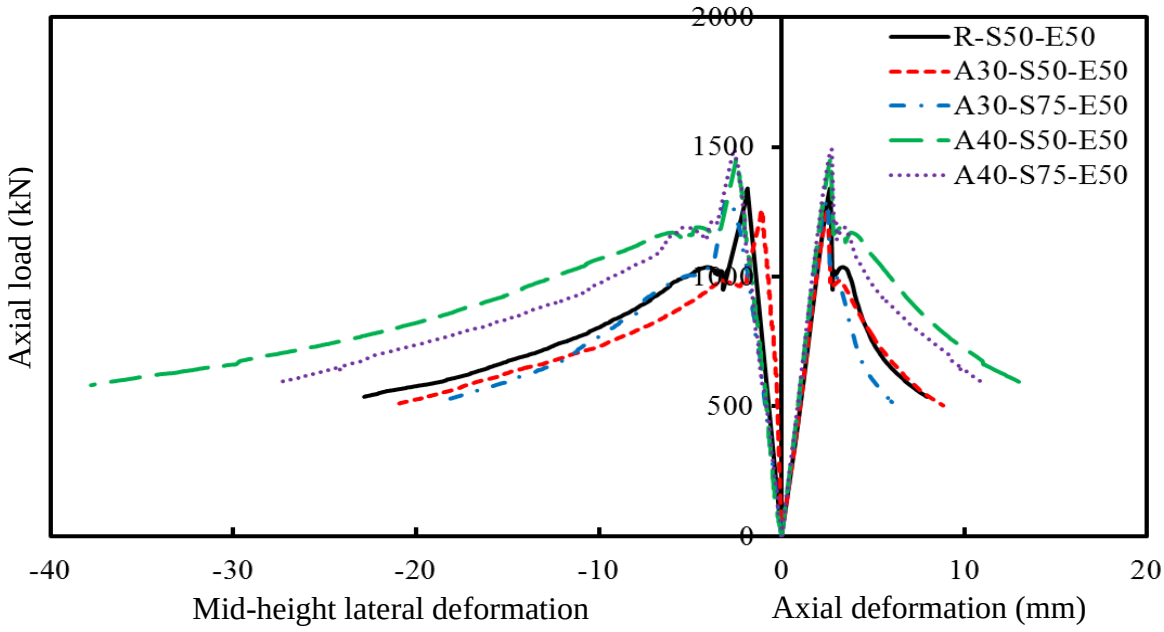

Figure 6.26 Axial load-axial deformation behaviour of specimens tested under 50 mm eccentric axial load

6.3.5 **Effect of Eccentricity on Strength and Ductility of the Tested Specimens**

Figure 6.27 shows the effect of eccentricity on the maximum axial loads of the specimens tested under concentric, 25 mm eccentric and 50 mm eccentric axial loads. Specimens R-S50-E25 and R-S50-E50 achieved 72% and 49%, respectively, of the first peak axial load achieved by Specimen R-S50-C. Specimens A30-S50-E25 and A30-S50-E50 achieved 71% and 49%, respectively, of the first peak axial load achieved by Specimen A30-S50-C. Specimen A30-S75-E50 achieved 47% of the first peak axial load achieved by Specimen A30-S75-C. Specimens A40-S50-E25 and A40-S50-E50 achieved 68% and 49%, respectively, of the first peak axial load achieved by Specimen A40-S50-C. Specimens A40-S75-E25 and A40- S75-E50 achieved 68% and 54%, respectively, of the first peak axial load achieved by Specimen A40-S75-C.

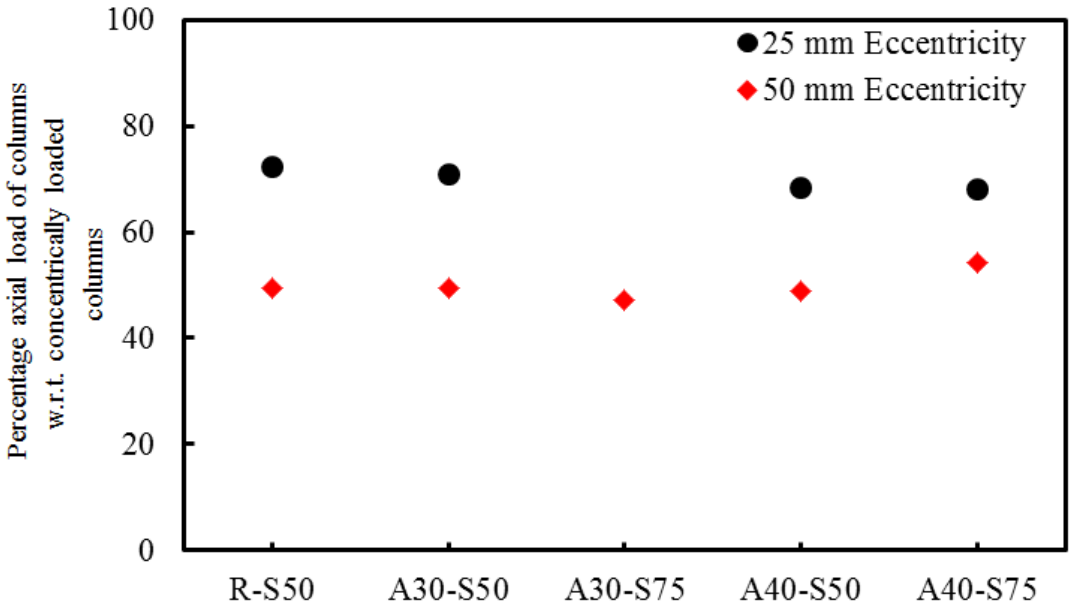

Figure 6.27 Influence of eccentricity on maximum axial load of tested specimens

Figure 6.28 shows the effect of eccentricity on the ductilities of the specimens tested under concentric, 25 mm eccentric and 50 mm eccentric axial loads. Specimens R-S50-E25 and R-S50-E50 achieved 81% and 75%, respectively, of the ductility achieved by Specimen R-S50-C. Specimens A30-S50-E25 and A30-S50-E50 achieved 68% and 52%, respectively, of the ductility achieved by Specimen A30-S50-C. Specimen A30-S75-E50 achieved 82% of the ductility achieved by Specimen A30-S75-C. Specimens A40-S50-E25 and A40-S50-E50 achieved 83% and 91%, respectively, of the ductility achieved by Specimen A40-S50-C. Specimens A40-S75-E25 and A40-S75-E50 achieved 90% and 81%, respectively, of the ductility achieved by Specimen A40-S75-C.

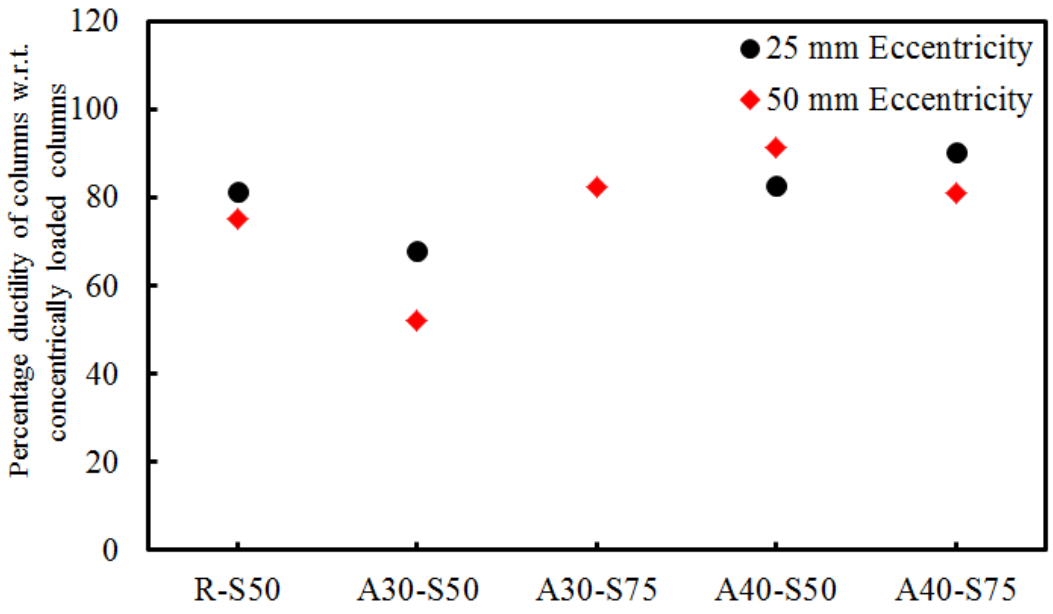

Figure 6.28 Influence of eccentricity on ductility of tested specimens

6.3.6 **Specimens Tested under Four-Point Bending**

One specimen from each group was tested under four-point bending. All specimens were tested to failure. As the load was applied, tension cracks started at midspan on the bottom side (tension surface) of the specimen. As the load increased, cracks became wider and extended to the side of the whole specimen, as shown in Figure 6.29. The failure of all specimens tested under four-point bending was due to the rupture of longitudinal reinforcement (steel bars and SEA sections) on the tension sides, as shown in Figure 6.30.

Figure 6.31 shows the load-midspan deflection behaviour of the specimens tested under four-point bending. It can be observed that all specimens showed similar behaviour in the elastic region. After the load reached the maximum value, a sudden decrease in the load occurred. The specimens still resisted the applied load with increasing displacement, while the failure of the specimen occurred by yielding and then rupture of the longitudinal tensile reinforcement (steel bars and SEA sections). The typical failure occurred for all tested specimens by the rupture of steel reinforcement (steel bars and SEA sections) on the tension side, as shown in Figure 6.30. It can also be observed from Figure 6.31 that all specimens reinforced with SEA sections exhibited better performances in terms of post-peak load-midspan deflection behaviour and load carrying capacity compared to the Specimen R-S50-F.

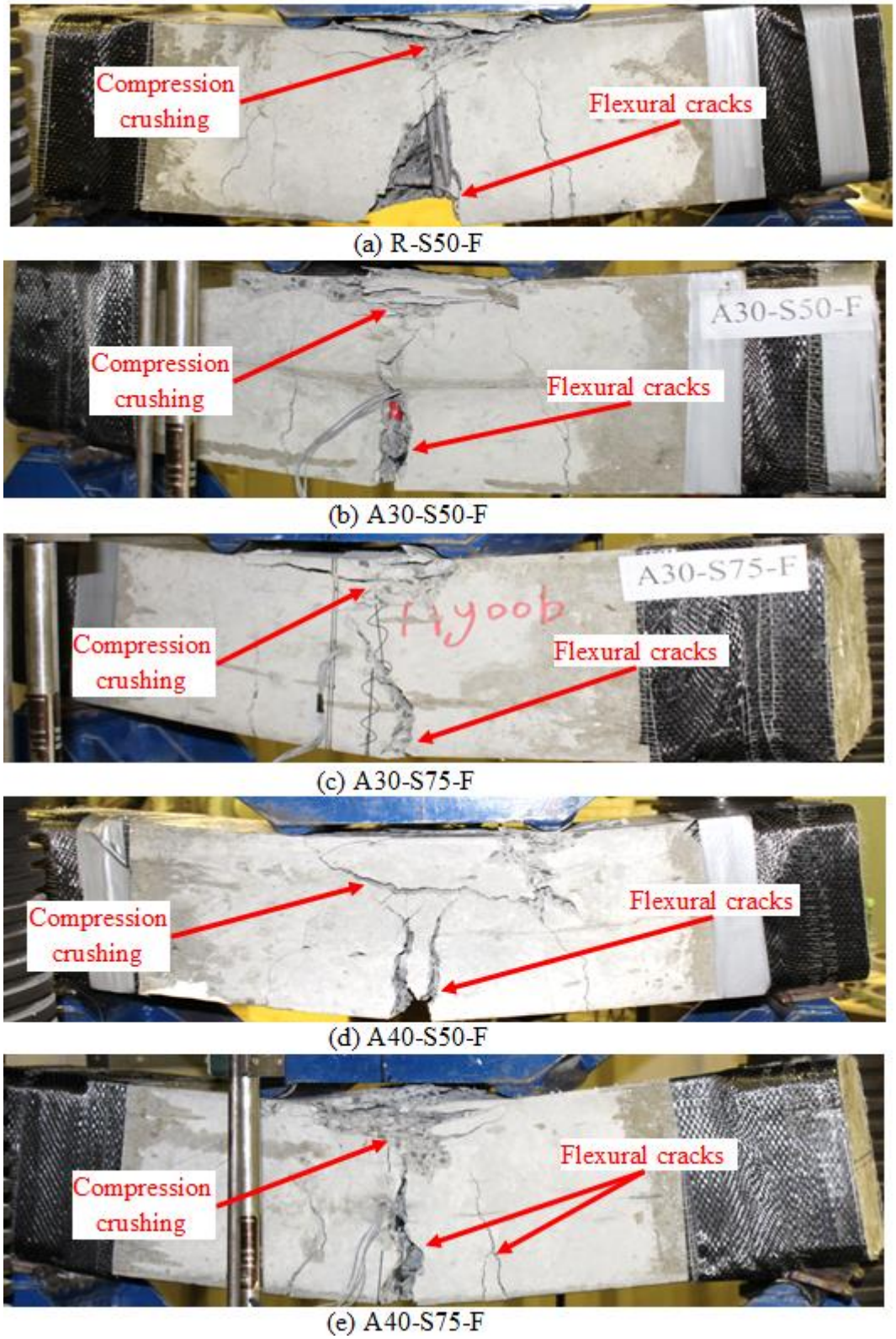

Figure 6.29 Failure modes of the tested specimens under four-point bending

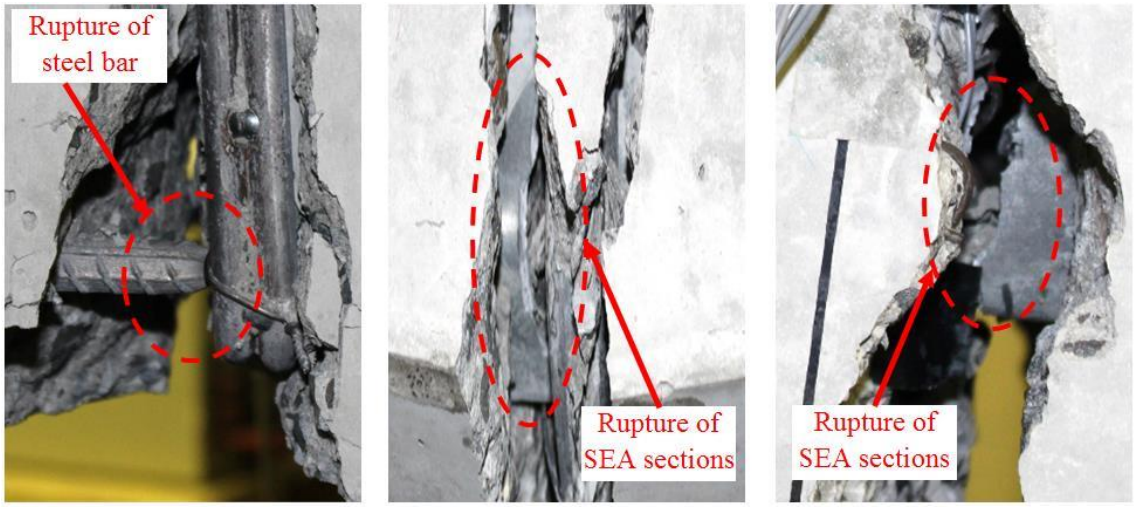

Figure 6.30 Close-up view of the typical failure under four-point bending: (a) R-S50-F; (b) A40-S50-F and (c) A40-S75-C

Table 6.8 summarises the experimental results of the tested specimens under four-point bending in terms of the yield load and maximum load, corresponding midspan deflections and ductility. For the specimens with the same spacing of transverse ties (50 mm) and with different longitudinal reinforcements (N12 steel bars, A30 and A40 SEA sections), it can be observed that although steel bars had 49% higher yield tensile strength than A30 SEA sections, Specimen A30-S50-F exhibited 6.3% higher maximum load than Specimen R-S50-F. It can also be observed that Specimen A30-S50-F achieved about 62.5% higher ductility than Specimen R-S50-F. The higher maximum load and ductility were because, for a similar longitudinal reinforcement area, the A30 SEA section had a higher bending stiffness than the N12 steel bar. Although the steel bars had 18% higher yield tensile strength than A40 SEA sections, the maximum load of Specimen A40-S50-F was about 100% higher than the maximum load of Specimen R-S50-F and the ductility of Specimen A40-S50-F was about 33.3% higher than the

ductility of Specimen R-S50-F. The increases in the maximum load and ductility were because the A40 SEA section had a much higher bending stiffness than the N12 steel bars. Another reason might be that the cross-sectional area of the A40 SEA section was greater than the cross-sectional area of the N12 steel bar, which provided increased bond effect between the longitudinal reinforcement and surrounding concrete.

For the specimens reinforced with A30 SEA sections and different spacings of transverse ties (50 mm and 75 mm), it can be observed that Specimens A30-S50-F and Specimen A30-S75-F exhibited similar maximum loads. It can also be observed that Specimens A30-S50-F achieved about 21.9% higher ductility than Specimen A30-S75-F. This may be because the smaller tie spacing of 50 mm led to better control of the shear crack width than the wider tie spacing of 75 mm.

For the specimens reinforced with A40 SEA sections with different spacings of transverse ties (50 mm and 75 mm), Specimens A40-S50-F and A40-S75-F exhibited similar maximum loads. This was because the confinement effect due to lateral reinforcement in the beams is not significant at the peak load. Similar observations were reported in Rashid and Mansur (2005) and Kwan et al. (2006). However, Specimens A40-S50-F showed about 4.7% lower ductility than Specimen A40-S75-F. The reason for the decrease in the ductility may be because Specimen A40-S50-F with closer transverse tie spacing (50 mm) had a higher amount of transverse steel reinforcement than A40-S75-F with wider transverse tie spacing (75 mm), which led to the development of a plane of separation between the concrete cover and the concrete core in the compression zone at an early stage of loading.

Table 6.8 Experimental Results of the Tested Specimens under Four-point Bending

Specimen	Maximum Load (P_{max}) (kN)	Midspan deflection at (P_{max}) (mm)	Ductility (μ)
R-S50-F	244	9.5	4.8
A30-S50-F	260	9.5	7.8
A30-S75-F	257	8.4	6.4
A40-S50-F	491	11.8	6.4
A40-S75-F	493	10.5	6.7

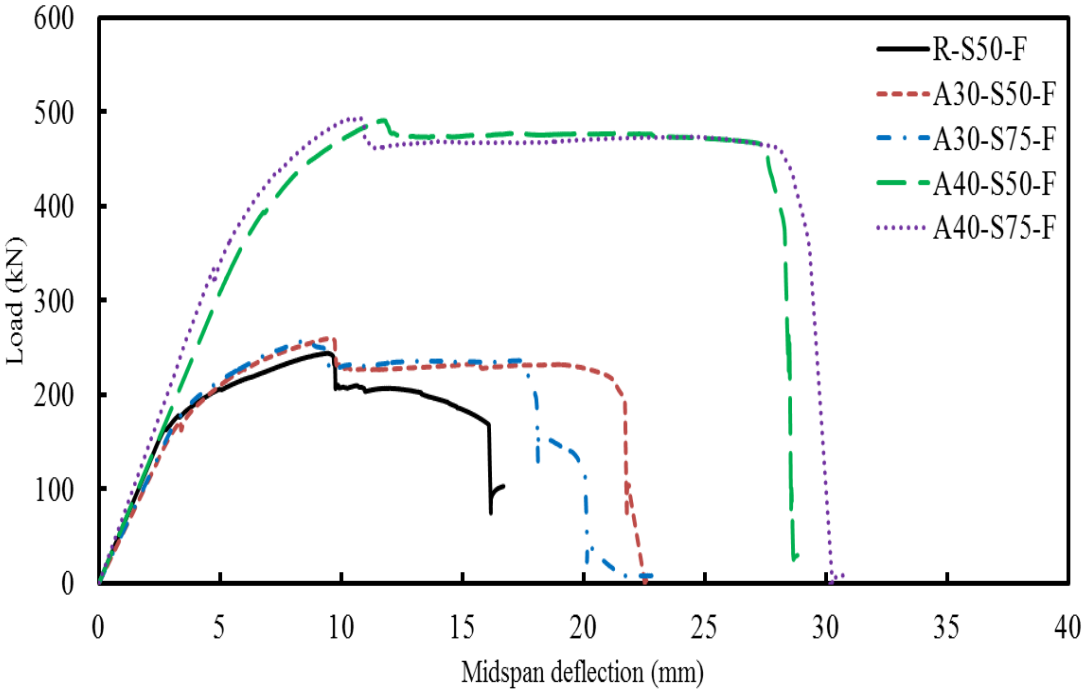

Figure 6.31 Load-midspan deflection behaviour of specimens tested under four-point bending

6.4 Summary

In this chapter, the test results of preliminary material that were used in this study are presented. Afterward, the experimental results of 20 concrete specimens with 800 mm height reinforced longitudinally with either steel bars or SEA sections and laterally with transverse ties are presented. The specimens were divided into five groups of four specimens. One specimen from each group was tested under concentric 25 mm and 50 mm eccentric axial loads and four-point bending to investigate the influence of the different type of longitudinal reinforcement (steel bars and SEA sections), the spacing of transverse ties and different size of SEA sections on the behaviour of square HSC columns.

Based on the experimental test results presented in this chapter, it was found that although the force contribution of SEA sections was much lower than the force contributions of steel bars for the similar cross-sectional area, the ductility of the HSC specimens reinforced longitudinally with SEA sections was significantly higher than the ductility of the specimens reinforced longitudinally with steel bars. The following chapter presents the details of the experimental program of specimens with 600 mm height.

7 EXPERIMENTAL PROGRAM OF SPECIMENS WITH 600 mm HEIGHT

7.1 General

The main focus of this experimental program is to investigate the behaviour of square high strength concrete (HSC) columns that were reinforced longitudinally with steel equal angle (SEA) sections and different spacing of transverse ties. In this chapter, the experimental program included testing of twelve square HSC specimens subjected to concentric axial load. The specimens in this experimental program were divided into three groups of four specimens (Groups B, A30 and A40). The test parameters included the type of longitudinal reinforcement (steel bars and SEA sections), size of SEA sections (A30 and A40 SEA sections) and spacing of transverse ties, which varied from 50 mm to 400 mm. The experimental program was conducted at the laboratories of the School of Civil, Mining and Environmental Engineering at the University of Wollongong, Australia. Finally, this chapter presents a brief description of the materials, fabrication of test specimens with 600 mm height and instrumentation and testing procedure.

7.2 Materials

In this experimental program, the materials were used in fabricating of specimens with 600 mm height were the same materials that were used in fabricating the specimens with 800 mm height. The full details and results of the used materials are reported in Chapters five and six. Below is a brief description of the materials. Three main materials were used in fabricating the test specimens, which were included concrete, steel bars and SEA sections. A ready mix high

strength concrete with a maximum aggregate size of 10 mm was used to cast the tested specimens. According to AS 1012.9 (1999), the compressive strength of concrete was determined by tests performed on three standard 100 mm x 200 mm concrete cylinders. The average compressive strength of the concrete at 28-days was 68.5 MPa.

Two different diameters of steel bars were used. Deformed N12 steel bars (12 mm diameter) were used as longitudinal reinforcement for specimens in Group B. Plain R10 steel bars (10 mm) were used as transverse ties for all specimens. Three samples from each of N12 and R10 bars were tested according to AS 1391(2007) using the 500 kN Instron testing machine. The average yield tensile strengths of the N12 steel bars and R10 steel bars were 556 MPa and 323 MPa, respectively. Two different steel equal angle (SEA) sections were used in this study. The SEA sections were supplied by OneSteel (2010). The tensile properties of the SEA sections were determined according to the Australian Standard AS 1391 (2007). For each SEA section, tensile coupon specimens were taken from the flat portion of the SEA section. Three samples from each of A30 and A40 SEA sections were tested using the 500 kN Instron testing machine. The average yield tensile strengths of A30 and A40 SEA sections were 374 MPa and 473 MPa, respectively.

7.3 Fabrication of the Test Specimens

7.3.1 **Details of Test Specimens**

The experimental program aimed at investigating the influence of the longitudinal reinforcement (steel bars and SEA sections) and the spacing of lateral reinforcement (ties) on the behaviour of square HSC column specimens under axial compression. As part of the research program, a total

of 12 square HSC column specimens with 210 mm × 210 mm cross-section and 600 mm height were cast and tested under concentric axial compression. The tested specimens are considered as columns as their height to least lateral side dimension is greater than 2.5 (Canadian Standards CAN/CSA S6-06 (CSA 2006) and Australian Standard AS 3600 (2009). The tested specimens were divided into three groups of four specimens, as presented in Table 7.1. The tie spacing in each group of specimens varied from 50 mm to 400 mm (Figure 7.1). The specimens in the first group (Group B) served as the reference specimens and were reinforced longitudinally with four N12 steel bars (12 mm diameter deformed steel bars with 500 MPa nominal yield tensile strength) and laterally with R10 steel bars (10 mm diameter plain steel bars with 250 MPa nominal yield tensile strength). In the second group (Group A30), the specimens were reinforced longitudinally with four A30 SEA sections (29.1 mm leg width and 2.25 mm thickness) and laterally with R10 steel bars. The specimens in the third group (Group A40) were reinforced longitudinally with four A40 SEA sections (39.3 mm leg width and 3.7 mm thickness) and laterally with R10 steel bars. The tie spacings of the specimens of each group were either 50 mm, 100 mm, 200 mm or 400 mm. The column specimens were designed according to Australian Standard AS 3600 (2009) requirements. However, Specimens B-S200, B-S400, A30-S200, A30-S400, A40-S200 and A40-S400 were prepared out of AS 3600 (2009) requirements for comparison purposes and to assess the buckling length of the longitudinal reinforcement with different spacing of transverse ties.

7.3.2 **Specimen Identification**

The tested column specimens were identified in two parts, as reported in Table 7.1. In the first part, B, A30 and A40 represents N12 steel bar, A30 SEA section and A40 SEA section, respectively. In the second part S50, S100, S200, and S400 represents the centre-to-centre tie spacing of 50, 100, 200 and 400 mm at centres, respectively. For instance, Specimen A30-S100

was reinforced longitudinally with four A30 SEA sections and laterally with R10 steel bars having a tie spacing of 100 mm at centres. Also, Specimen B-S400 was reinforced longitudinally with four N12 steel bars and laterally with R10 steel bars having a tie spacing of 400 mm at centres.

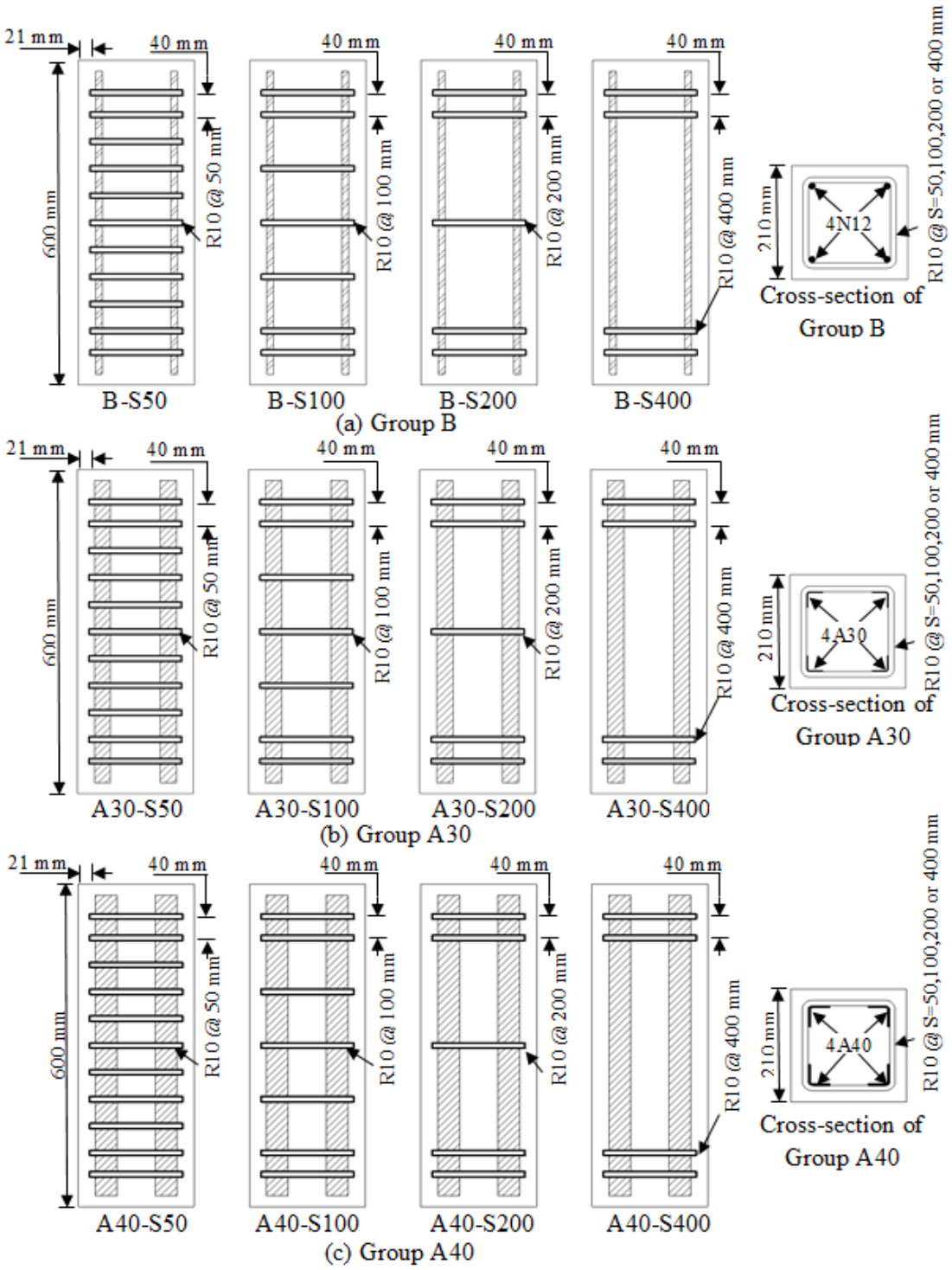

Figure 7.1 Geometry and reinforcement details of the tested specimens with 600 mm heigh

Table 7.1 Experimental Matrix of Specimens with 600 mm Height

Group ID	Specimen Labels	Longitudinal Reinforcement								Transverse Reinforcement	
		Reinforcement Type	Number	Bar			Steel Equal Angle (SEA) Section				
				Diameter (mm)	ρ_b %	f_y (MPa)	Dimension (mm)	ρ_{SEA} %	f_y (MPa)	Diameter (mm)	Spacing (mm)
B	B-S50	Steel Bar	4	12	1.03	556	-	-	-	10	50
	B-S100										100
	B-S200										200
	B-S400										400
A30	A30-S50	Steel Equal Angle (SEA) Section	4	-		-	29.1 X 2.25	1.11	374	10	50
	A30-S100										100
	A30-S200										200
	A30-S400										400
A40	A40-S50		4	-		-	39.3 X 3.7	2.43	473	10	50
	A40-S100										100
	A40-S200										200
	A40-S400										400

7.3.3 **Formwork Setup**

The formwork used for casting the concrete specimens was fabricated from 17 mm thick plywood. The formwork included two groups of small formwork. Each group was used for casting six specimens. The small formwork was fabricated using two large sheets of plywood (1439 mm x 600 mm x 17 mm) and seven small sheets of plywood (220 mm x 600 mm x 17 mm), as shown in Figure 7.2. The formwork was prepared by placing the plywood sheets together with screws. Afterwards, pieces of timber were also used vertically and transversely to fix the formwork before pouring the concrete (Figure 7.3). All the small formworks were then placed on the large plywood sheets to prevent contact between concrete and floor of the lab. At each end, four pieces of Styrofoam (polystyrene) were attached at the corners inside the formwork. Every piece of Styrofoam was 90 mm long, as shown in Figure 7.3. The Styrofoam was used to create smooth rounded edges (20 mm radius) at each end of the specimen so that the specimen ends could be wrapped with Carbon Fibre Reinforced Polymer (CFRP) to prevent stress concentrations at the ends during testing.

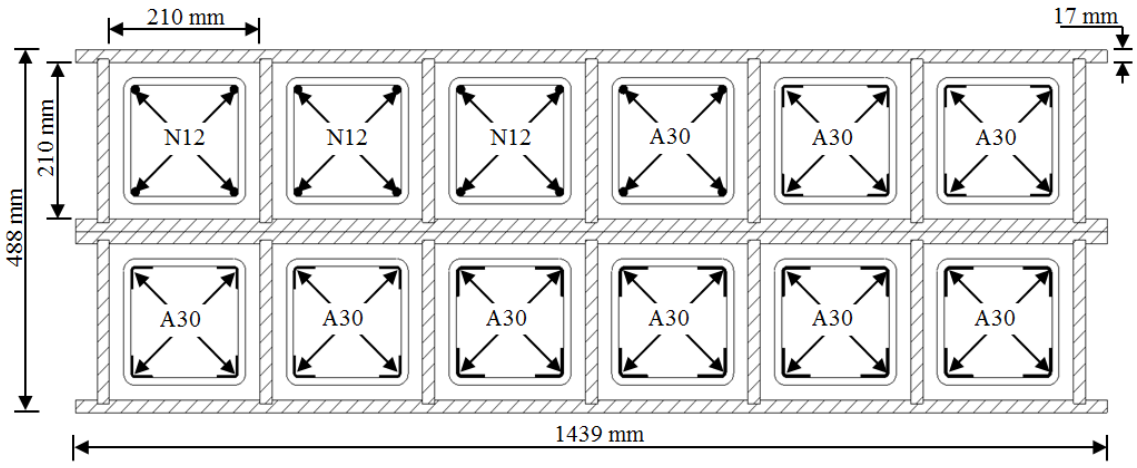

Figure 7.2 Plan view of wooden formwork for specimens with 600 mm height

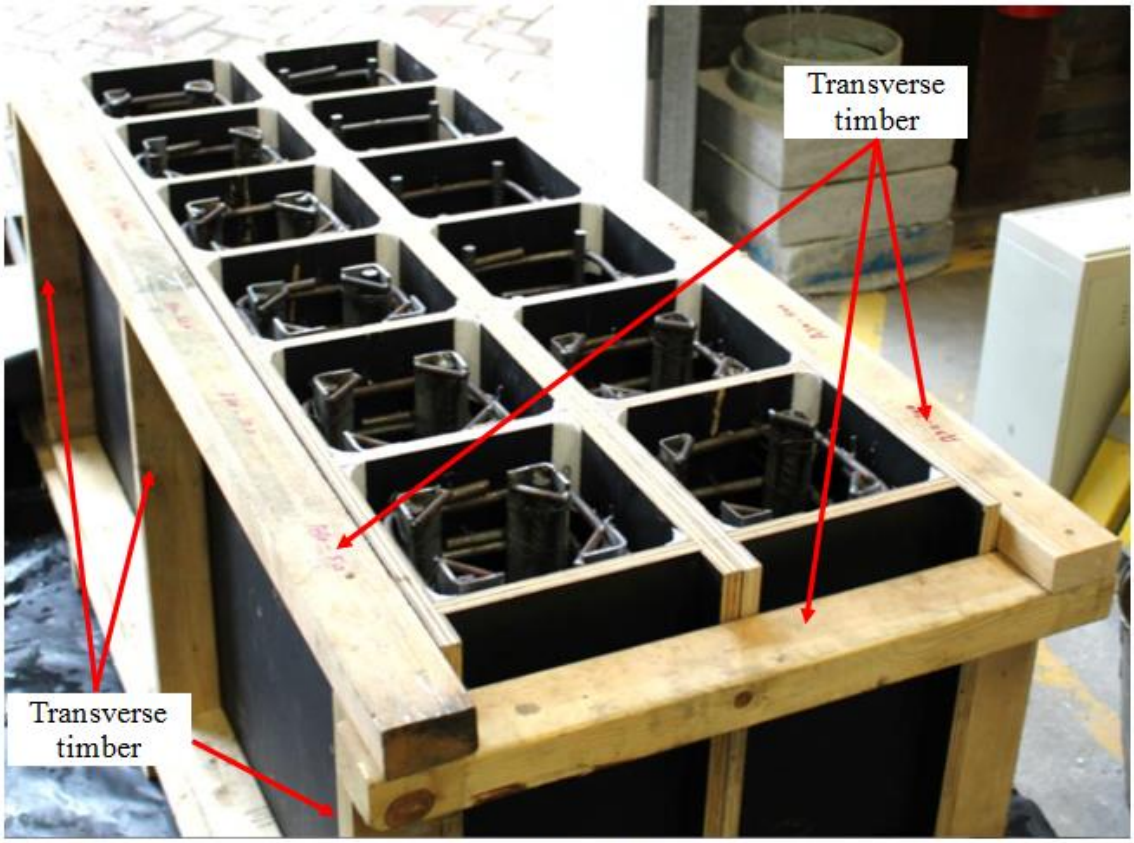

(a) Side view

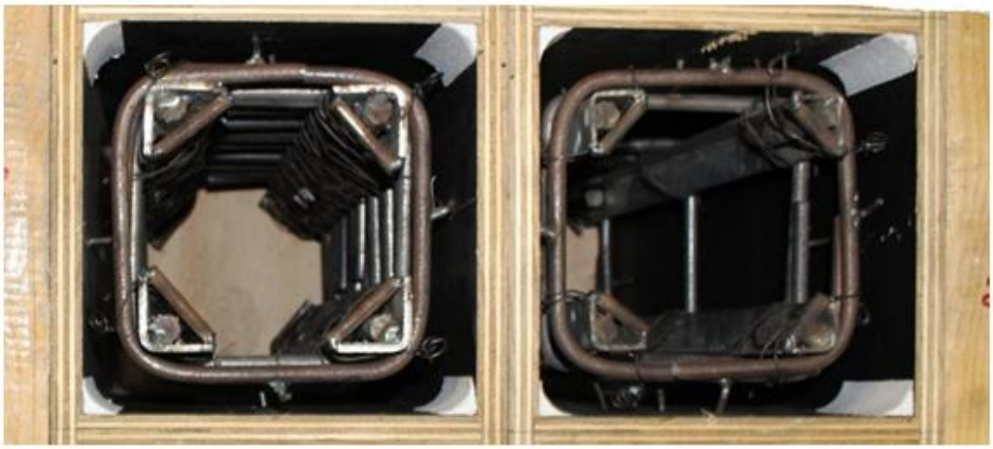

(b) Top view

Figure 7.3 Steel cages inside the formwork: (a) Side view and (b) Top view

7.3.4 **Steel Cages**

The longitudinal steel bars and SEA sections were cut into a length of 560 mm in order to maintain a 20 mm concrete clear cover at the top and the bottom of the specimens, to prevent direct loading of the longitudinal reinforcements during testing. For all specimens, the concrete side cover was 21 mm to the face of the transverse ties. Square ties were fabricated from R10 bars for all specimens. All ties were bent at four corners with a radius of 6 mm so that the ties could be placed over the SEA sections. Also, the ties were bent for 90-degree hooks around one of the longitudinal reinforcement and extended for an overlap of 80 mm at both ends. Each tie was welded at three points on the overlap. The spacing of transverse ties was 50 mm, 100 mm, 200 mm and 400 mm. For all specimens, the spacing of lateral ties was reduced to 40 mm at the end regions to prevent premature failures at the ends of the columns. The longitudinal and transverse reinforcement cages assembled for the specimens are shown in Figures 7.4 to 7.6.

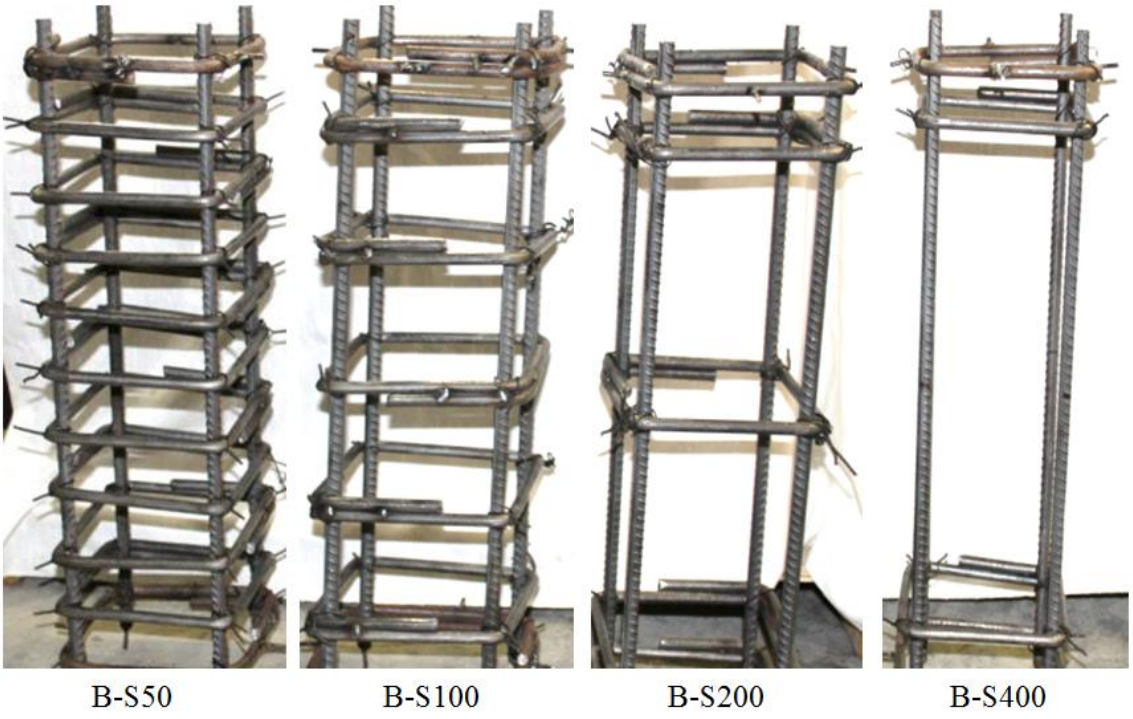

Figure 7.4 Overview of the assembled steel cages of Group B specimens

Figure 7.5 Overview of the assembled steel cages of Group A30 specimens

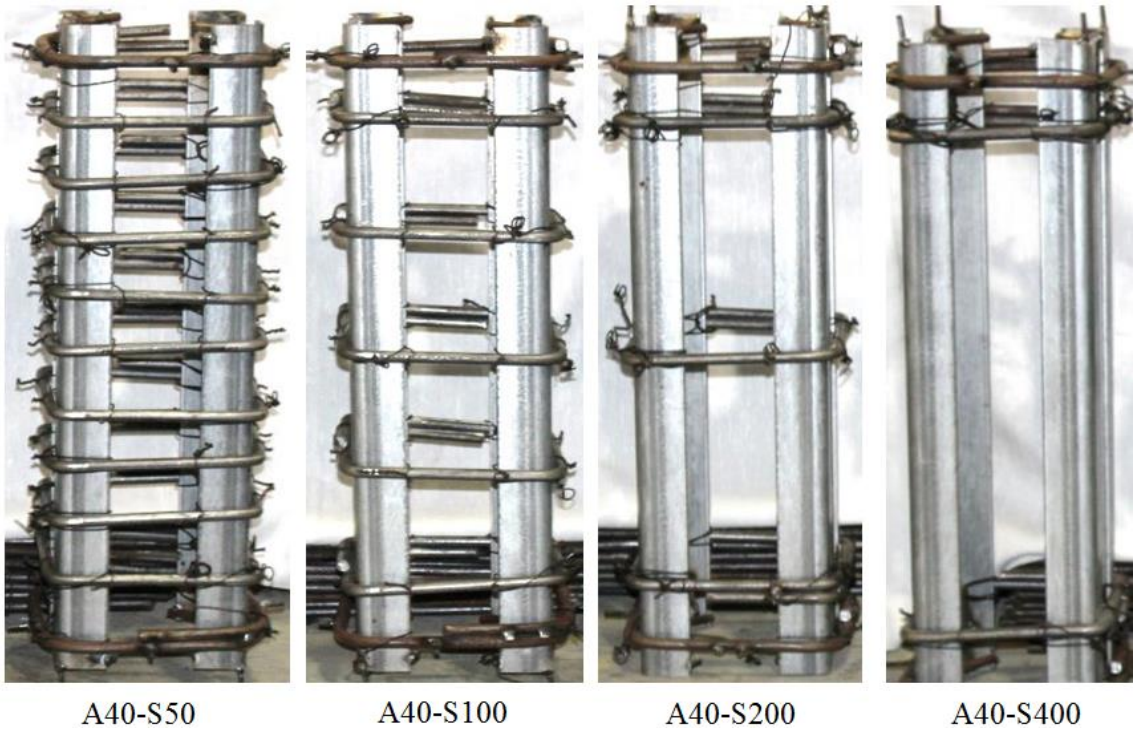

Figure 7.6 Overview of the assembled steel cages of Group A40 specimens

Deformed N12 steel bars and smooth SEA sections were used as longitudinal reinforcement. In order to decrease the possible slippage of the SEA sections in the specimens reinforced with SEA sections, two short plain steel bars (8 mm diameter and 40 mm long) were welded laterally between the ends of the SEA sections at the top and the bottom (Figure 7.7). In addition, two short steel bars (16 mm diameter and 70 mm length) were welded internally and axially at the top and bottom of each SEA section. Hence, the reason of using two steel 16 mm bars (one for each end) was to prevent slippage of longitudinal steel equal angle (SEA) sections, as the surfaces of the SEA sections were smooth. To fabricate the reinforcement cages, two aluminium templates were made. One template was placed on top and another template on the bottom of steel cages. Both of these templates were designed to hold transverse ties with various spacing (Figure 7.7). Afterwards, all steel cages were prepared by placing the longitudinal and lateral reinforcement together with steel wires, as shown in Figure 7.7.

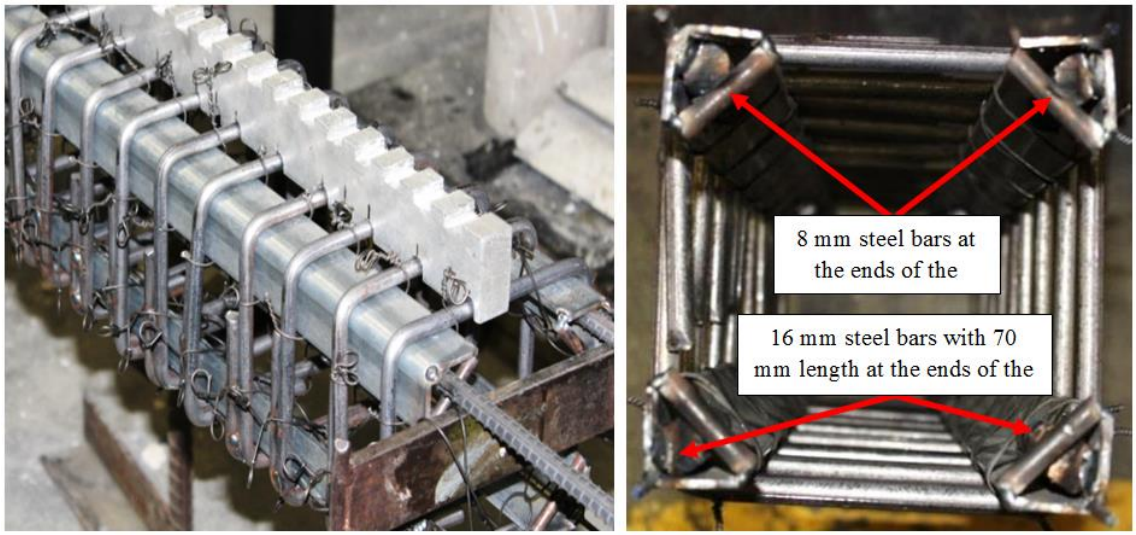

(a) Assemblage steel cage with SEA sections

(b) Top view with short steel bars at the ends of SEA sections

Figure 7.7 Reinforcement arrangements for specimens with 600 mm height

7.3.5 **Placement and Curing Process of the Specimens**

The column specimens were prepared for vertical casting using formwork built with 17 mm plywood. Prior to the concrete was poured into the formwork, the dust build up was removed by the aid of compressed air. All specimens were cast vertically to simulate typical construction practice of columns. Concrete was poured in the formwork directly from a concrete truck along a chute that was located on the truck, as shown in Figure 7.8. The concrete was poured into the formwork in three levels. An electric vibrator was used at every level to compact the concrete and remove air bubbles. After 24 hours, the specimens were covered with wet clothes for 28 days and were wet daily to ensure that the specimens remained under moist conditions and allowed for adequate curing. The specimens were removed from the formwork after 14 days from casting and kept covered with wet clothes until 28 days from casting, as shown in Figure 7.9.

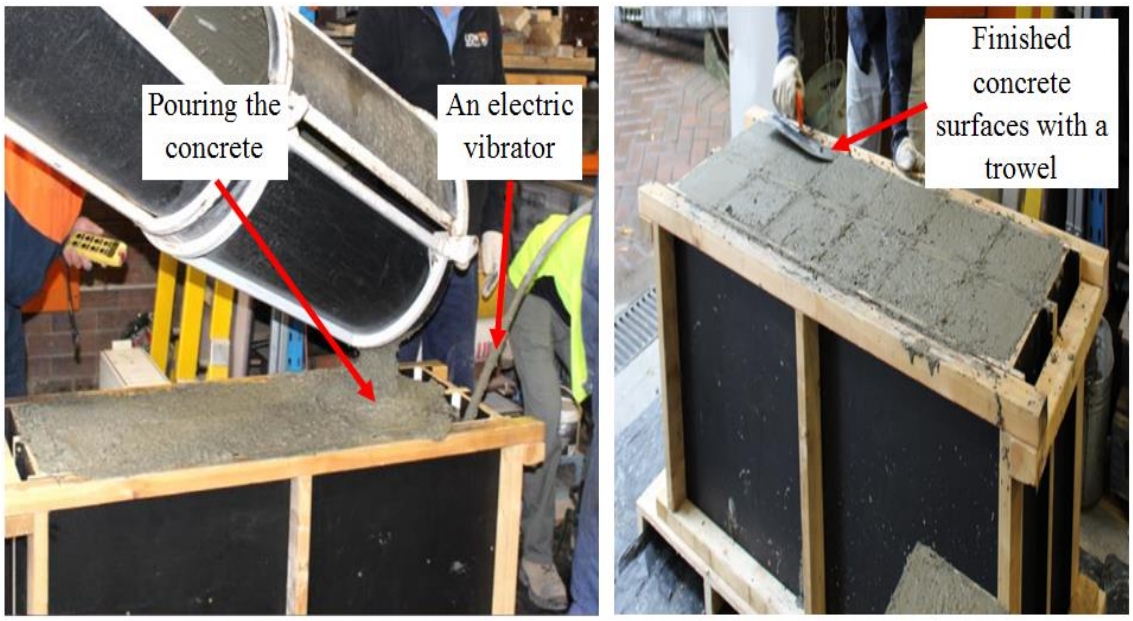

(a) Pouring concrete (b) Finishing concrete

Figure 7.8 Pouring and finishing the placing process of concrete

(a) During removal formwork (b) Curing column specimens

Figure 7.9 Removal of the formwork and curing process the column specimens with 600 mm height

7.4 Instrumentation and Testing Procedure

The column specimens were instrumented externally to capture the axial deformation of the specimens by using two linear variable differential transducers (LVDTs), as shown in Figure 7.10. The LVDTs were attached to the heads of the testing machine at two opposite corners to capture the axial deformation in the specimens (Figure 7.10). The axial compression was captured by the internal load cell of the testing machine.

To ensure that the load is applied uniformly, the top surface (rough surface) of the column specimens was capped with a thin layer of high strength plaster. To avoid premature failure in the end regions of the specimens during testing, the top and the

bottom ends of the column specimens were wrapped using two layers of Carbon Fibre Reinforced Polymer (CFRP) sheets with a width of 90 mm. The testing of the column specimens was carried out using the 5000 kN Denison compression testing machine in the Structural Engineering Laboratories at the University of Wollongong, Australia. The specimen was moved by fork lift, aligned in the centre of the lower plate in the testing machine, and then levelled. At the beginning of the test, each specimen was preloaded to about 10% of the expected maximum axial load of the specimens to prevent any movement in the specimens at the beginning of the test. Afterwards, the test resumed under a displacement controlled concentric axial loading at the rate of 0.3 mm/minute until the strength of the specimens dropped to about 20% of the maximum axial load. The LVDTs were connected to a data logger to record the data at every two seconds.

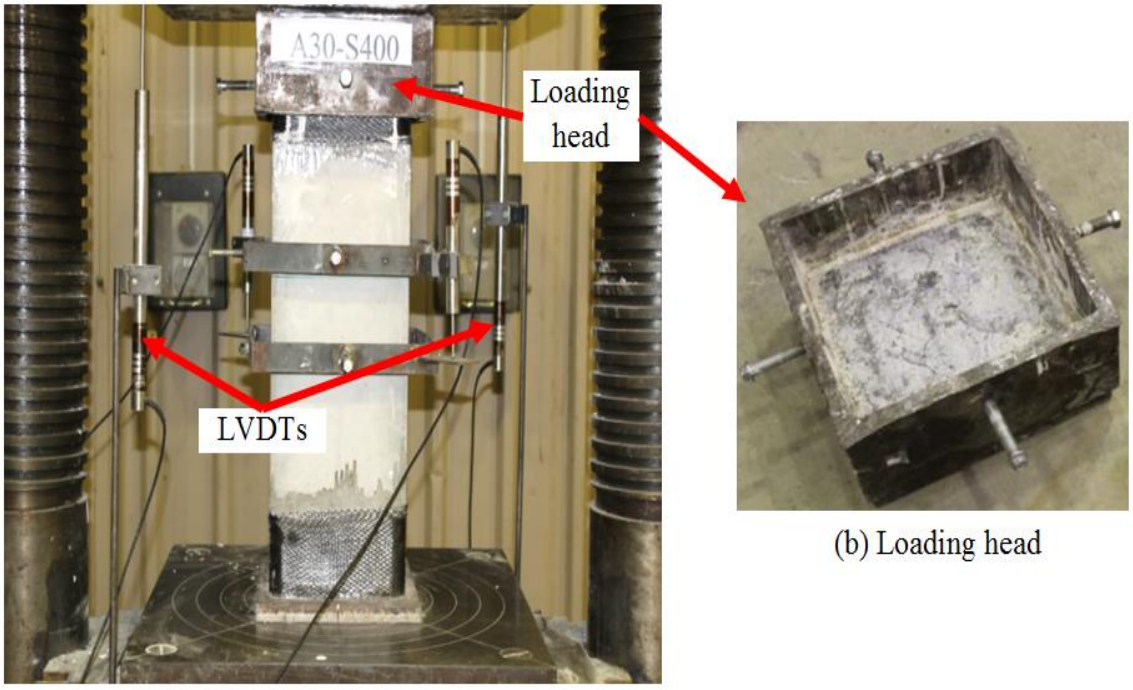

(a) Column specimen

(b) Loading head

Figure 7.10 Typical test setup of specimens with 600 mm height

7.5 Summary

This chapter describes the details of the experimental program for specimens with 600 mm height. The specimens were divided into three groups based on longitudinal reinforcement and spacing of transverse reinforcement. The details of the test specimen, steel cages, formwork setup, placement and process of the specimens and instrumentation and testing procedure are presented in this chapter. The next chapter presents and discusses the experimental results of specimens with 600 mm height that were tested under concentric axial load.

8 EXPERIMENTAL RESULTS OF SPECIMENS WITH 600 mm HEIGHT

8.1 General

In order to a better understand the behaviour of high strength concrete (HSC) columns reinforced longitudinally with steel equal angle (SEA) sections, it is necessary to extend the data base for HSC columns with different spacing of transverse ties. For this aim an experimental program is presented in this chapter to investigate the behaviour of square HSC columns reinforced with SEA sections and different spacing of transverse ties. As described in chapter seven, 12 square HSC column specimens with 600 mm height were cast and tested as part of the research program in this study to evaluate the use of SEA sections as longitudinal reinforcement. All specimens were tested under concentric axial load at the laboratories of the School of Civil, Mining and Environmental Engineering at the University of Wollongong, Australia. The test parameters included the type of longitudinal reinforcements (steel bars and SEA sections), size of SEA sections (A30 and A40 SEA sections) and spacing of transverse ties (50 mm, 100 mm, 200 mm and 400 mm). All columns were tested under concentric axial load.

8.2 Test Results of Specimens with 600 mm Height

In this chapter, the ductility (μ) of the tested column specimens was calculated based on the energy absorption capacity of the specimen. The ductility was calculated as the ratio of the area under the axial load-axial deformation curve up to the ultimate deformation

(80% of the maximum axial compressive load) to the area up to the deformation corresponding to the yield load. More details of the ductility method of the specimens are explained in chapter six.

8.2.1 **Behaviour of Column Specimens with 50 mm Tie Spacing**

Specimens B-S50, A30-S50, and A40-S50 were reinforced longitudinally with N12 steel bars, A30 SEA sections and A40 SEA sections, respectively. The spacing of transverse ties for B-S50, A30-S50, and A40-S50 was 50 mm at centres (centre-to-centre). All the specimens were tested up to about 20% of the maximum axial load in the post-peak descending branch of the axial load-axial deformation response. There were some visual cracks prior to the maximum axial load. The first hairline cracks in Specimens B-S50 and A30-S50 appeared at about 88% and 86%, respectively, of the corresponding maximum axial loads (Figures 8.1 and 8.2). These hairline cracks were observed at the mid-height of the specimens. As the axial load increased, the number, length and width of the cracks increased until the spalling of the concrete cover. The first hairline crack in Specimen A40-S50 was initiated at approximately 90% of the maximum axial load, as shown in Figure 8.3. This crack occurred at the top one-third height of the specimen and then the cracks appeared at the midheight of the specimen. Afterwards, the number, length, and width of the cracks increased until the spalling of the concrete cover. The failure of Specimens B-S50, A30-S50 and A40-S50 was attributed to the spalling of large pieces of the concrete cover, which was followed by outward buckling of the longitudinal reinforcement and fracture of transverse ties at welded points, as shown in Figures 8.1 to 8.3.

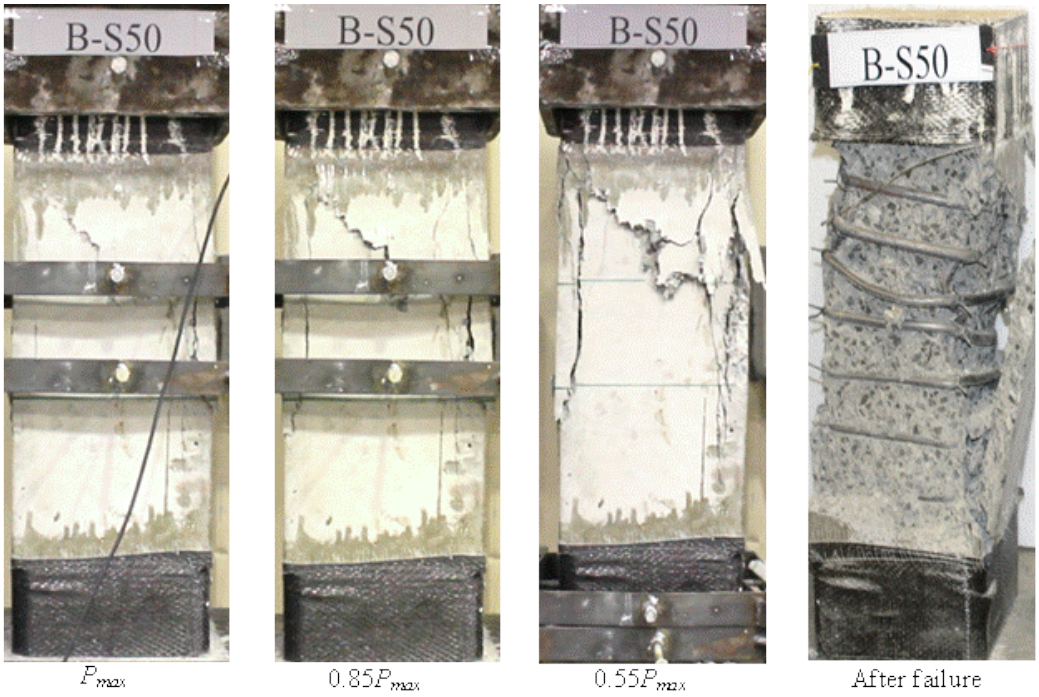

Figure 8.1 Overview of the test specimen B-S50: (a) during different stages of loading (after peak axial load) and (b) Close-up view of test region

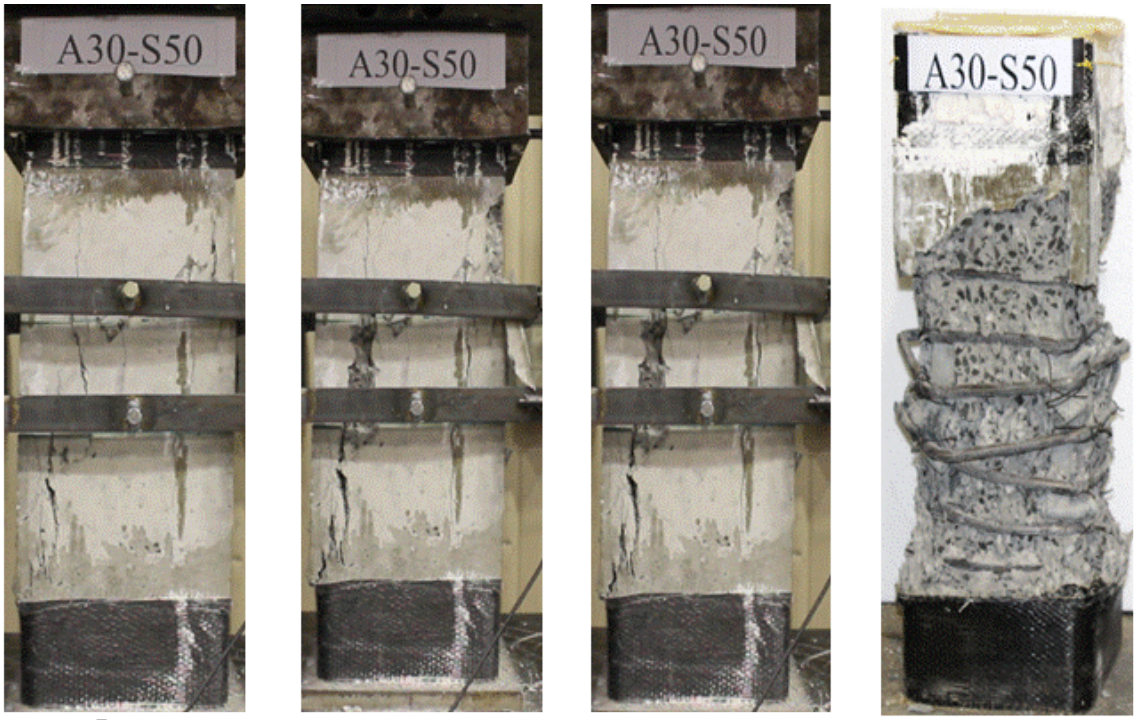

Figure 8.2 Overview of the test specimen A30-S50: (a) during different stages of loading (after peak axial load) and (b) Close-up view of test region

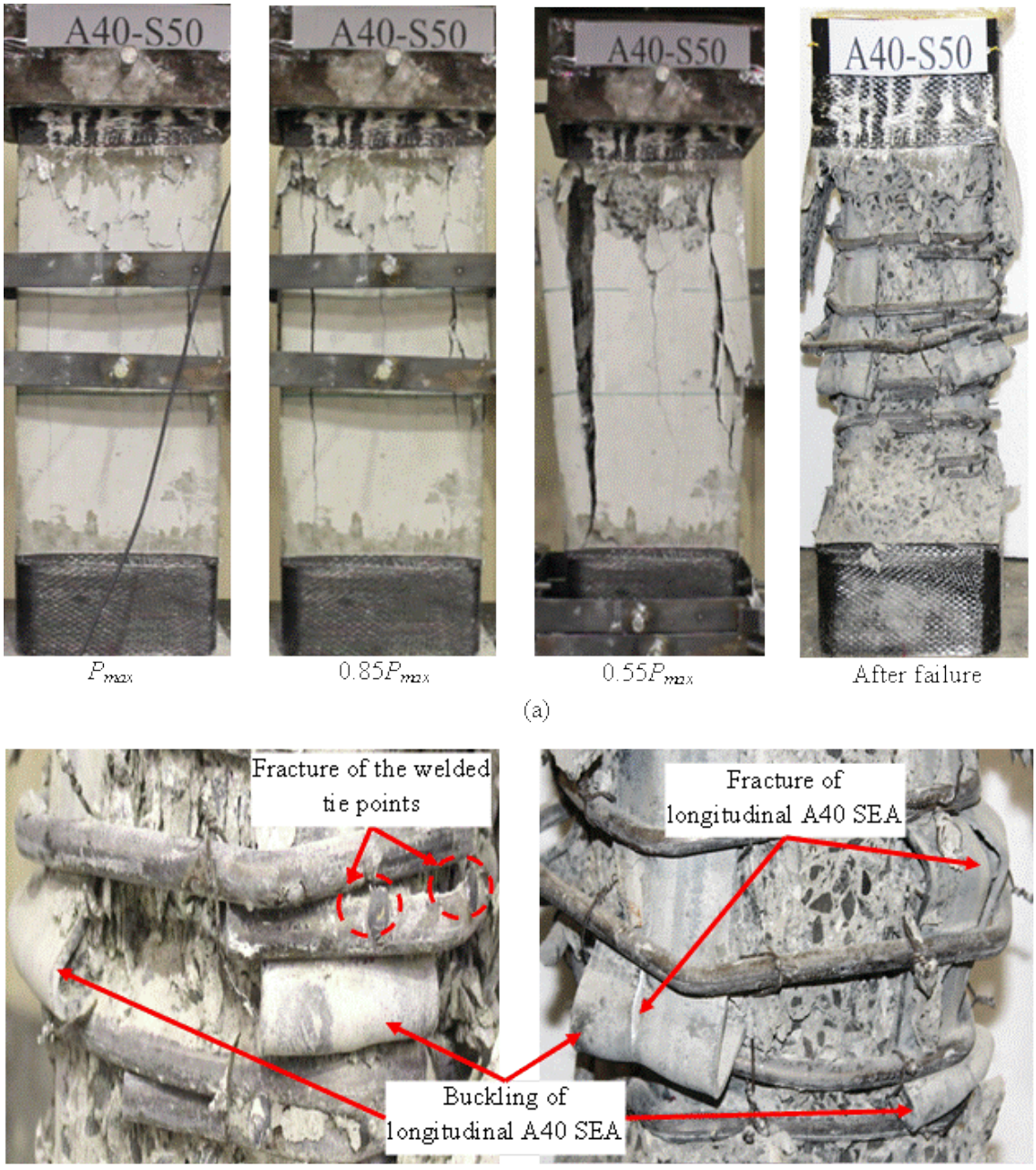

Figure 8.3 Overview of the test specimen A40-S50: (a) during different stages of loading (after peak axial load) and (b) Close-up view of test region

The maximum axial load and corresponding axial deformation of the Specimens B-S50, A30-S50 and A40-S50 are reported in Table 8.1. The maximum axial load represents

the axial load carried by the gross concrete cross-sectional area (concrete core and concrete cover) of specimens. The axial load-axial deformation responses of the specimens are shown in Figure 8.4. The maximum axial load carried by the reference Specimen B-S50 was 2929 kN, which is about 11.6% higher than the maximum axial load of Specimens A30-S50. The maximum axial load of Specimen B-S50 was higher because the average yield tensile strength of N12 steel bars was 49% higher than the average yield tensile strength of A30 SEA sections. At the maximum axial loads, the force contribution of N12 steel bars in Specimen B-S50 was 27% greater than the force contribution of A30 SEA sections in Specimen A30-S50. However, the ductility of Specimen A30-S50 was 44.4% greater than the ductility of Specimen B-S50. The greater ductility of Specimen A30-S50 indicates that SEA sections increased the area of the effectively confined concrete core after cracking occurred at the cover-core interface. The maximum axial load of Specimens A40-S50 was 2.7% higher than the maximum axial load of Specimen B-S50. Also, the ductility of Specimen A40-S50 was 50.0% higher than the ductility of Specimen B-S50. The reason for the higher maximum axial load and the ductility was attributed to the higher confinement to the concrete core provided by the A40 SEA sections. Another possible reason was that at the maximum axial load, the force contribution of A40 SEA in Specimen A40-S50 was about 50% higher than the force contribution of N12 steel bars in Specimen B-S50. The maximum axial load of Specimen A40-S50 was 14.6% higher than the maximum axial load of Specimen A30-S50. The reason for the higher maximum axial load was that at the maximum axial load, the force contribution of A40 SEA in Specimen A40-S50 was about 64% higher than the force contribution of A30 SEA sections in Specimen A30-S50. Also, Specimen A40-S50 achieved only 3.8% higher ductility than Specimen A30-

S50. The higher ductility for Specimen A40-S50 indicates that A40 SEA sections were more effective than A30 SEA sections in confining the concrete core of the specimen. Based on test results, it was reported that the ductility and confinement efficiency of square HSC columns could be significantly enhanced by using SEA sections as longitudinal reinforcement. Also, it was noted that the early spalling of the concrete cover was observed in the tested specimens. This phenomenon is more observed as the compressive strength of concrete increases and closely spacing of transverse reinforcement (Foster et al. 1998; Sharma et al. 2007; Awati and Khadiranaikar 2012).

Table 8.1 Summary of the Test Results of Column Specimens with 400 mm Tie Spacing

Specimen	Maximum concentric axial load, P_{max} (kN)	Axial deformation at P_{max} (mm)	Ultimate Axial Deformation Δ_{80}[a] (mm)	Ductility
B-S50	2929	2.3	3.1	1.8
A30-S50	2625	2.2	4.0	2.6
A40-S50	3009	2.2	3.9	2.7

Note: [a] represents the deformation corresponding to 80% of the maximum axial load in the descending branch of the axial load-axial deformation behaviour.

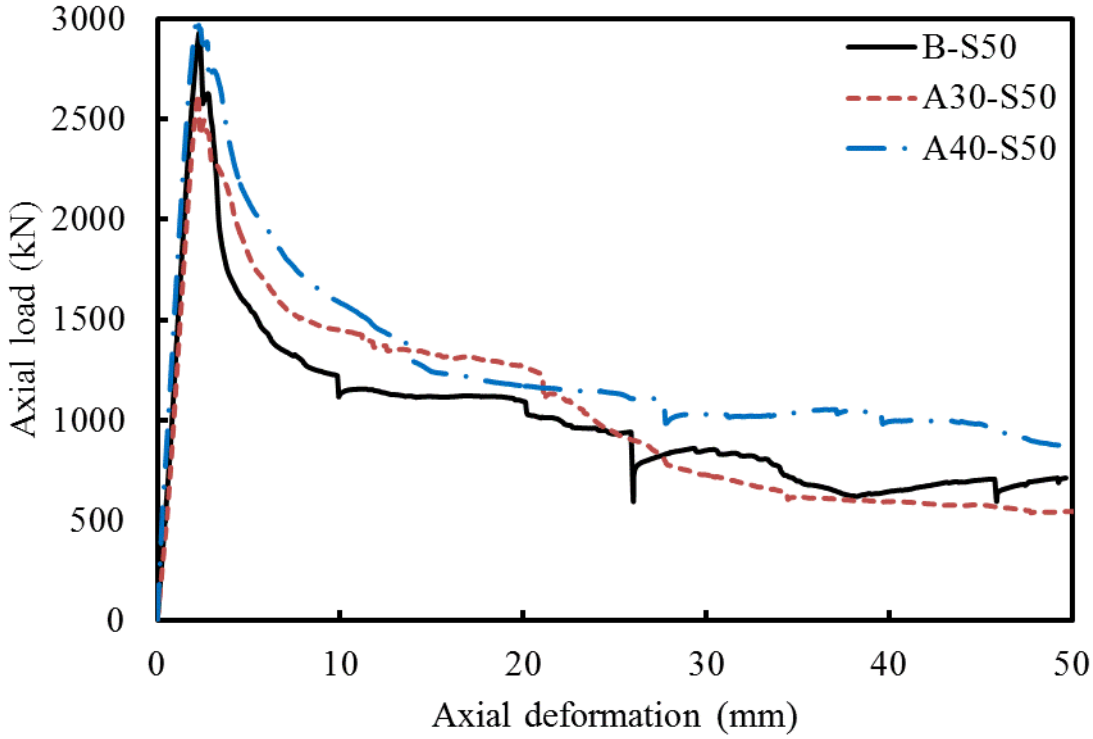

Figure 8.4 Axial load-axial deformation response of column specimens with tie spacing of 50 mm at centres

8.2.2 **Behaviour of Column Specimens with 100 mm Tie Spacing**

Specimens B-S100, A30-S100, and A40-S100 were reinforced longitudinally with N12 steel bars, A30 SEA sections, and A40 SEA sections, respectively. The spacing of transverse ties for B-S100, A30-S100, and A40-S100 was 100 mm at centres. All the specimens were tested up to about 20% of the maximum axial load in the post-peak descending branch of the axial load-axial deformation response.

The first hairline cracks in Specimen B-S100 appeared at approximately 90% of the corresponding maximum axial load, as shown in Figure 8.5. The first hairline cracks in Specimen A30-S100 appeared at about 82%of the corresponding maximum axial load,

as shown in Figure 8.6. The cracks occurred at the top one-third height of the specimens and then the cracks were observed at the midheight of the specimens. Afterwards, the number, length, and width of cracks continued to increase until the concrete cover spalled off. The hairline crack in Specimen A40-S100 was initiated at about 83% of the maximum axial load (Figure 8.7). These cracks were observed at the top one-third of the specimen and then the cracks extended downwards and continued to increase in number and size until the spalling of the concrete cover occurred. The failure of Specimen B-S100 was characterised by the spalling of the concrete cover, which was followed by outward buckling of the longitudinal reinforcement, as shown in Figure 8.5. For column specimens reinforced longitudinally with SEA sections, the failure of Specimens A30-S100 and A40-S100 was also characterised by the spalling of the concrete cover, which was followed by outward buckling of the longitudinal reinforcement, as shown in Figures 8.6 and 8.7. Also, it was observed that the early spalling of the concrete cover was observed in the tested specimens. This phenomenon is more observed when the specimens reinforced with closely longitudinal and transverse reinforcement. Also, the early spalling of the concrete cover was associated with high strength concrete columns. Similar behaviour was reported by Saatcioglu and Razvi (1998) and Ozbakkaloglu and Saatcioglu (2004).

Figure 8.5 Overview of the test specimen B-S100: (a) during different stages of loading (after peak axial load) and (b) Close-up view of test region

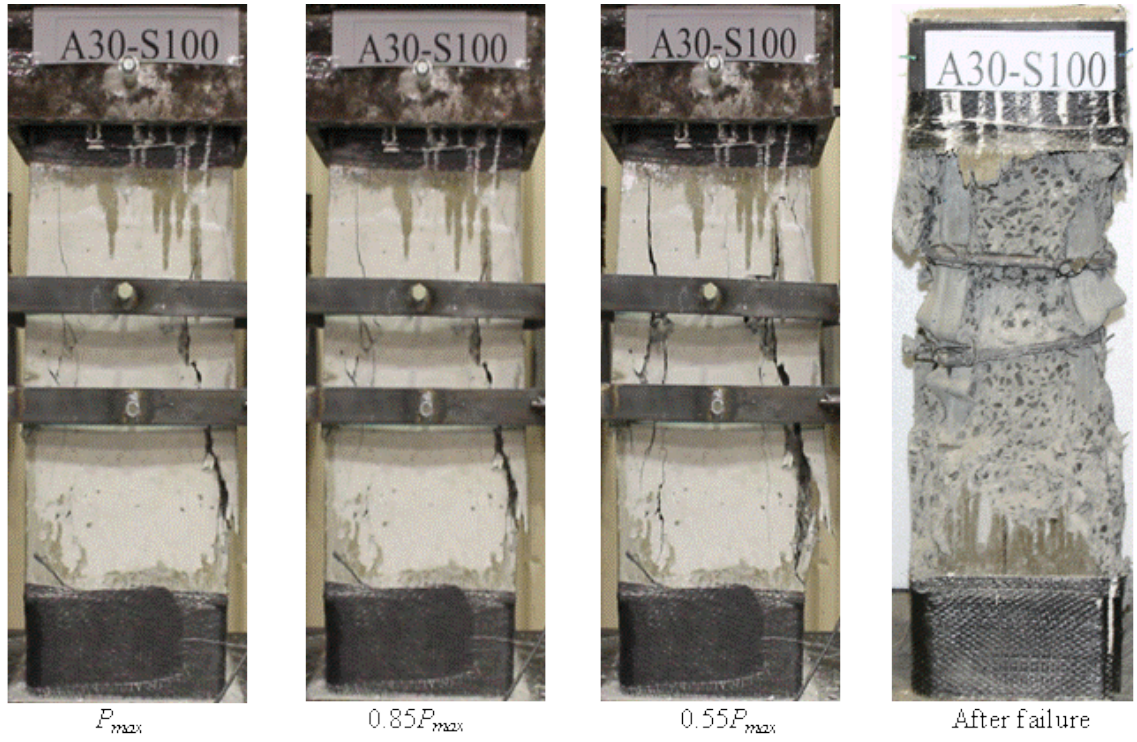

Figure 8.6 Overview of the test specimen A30-S100: (a) during different stages of loading (after peak axial load) and (b) Close-up view of test region

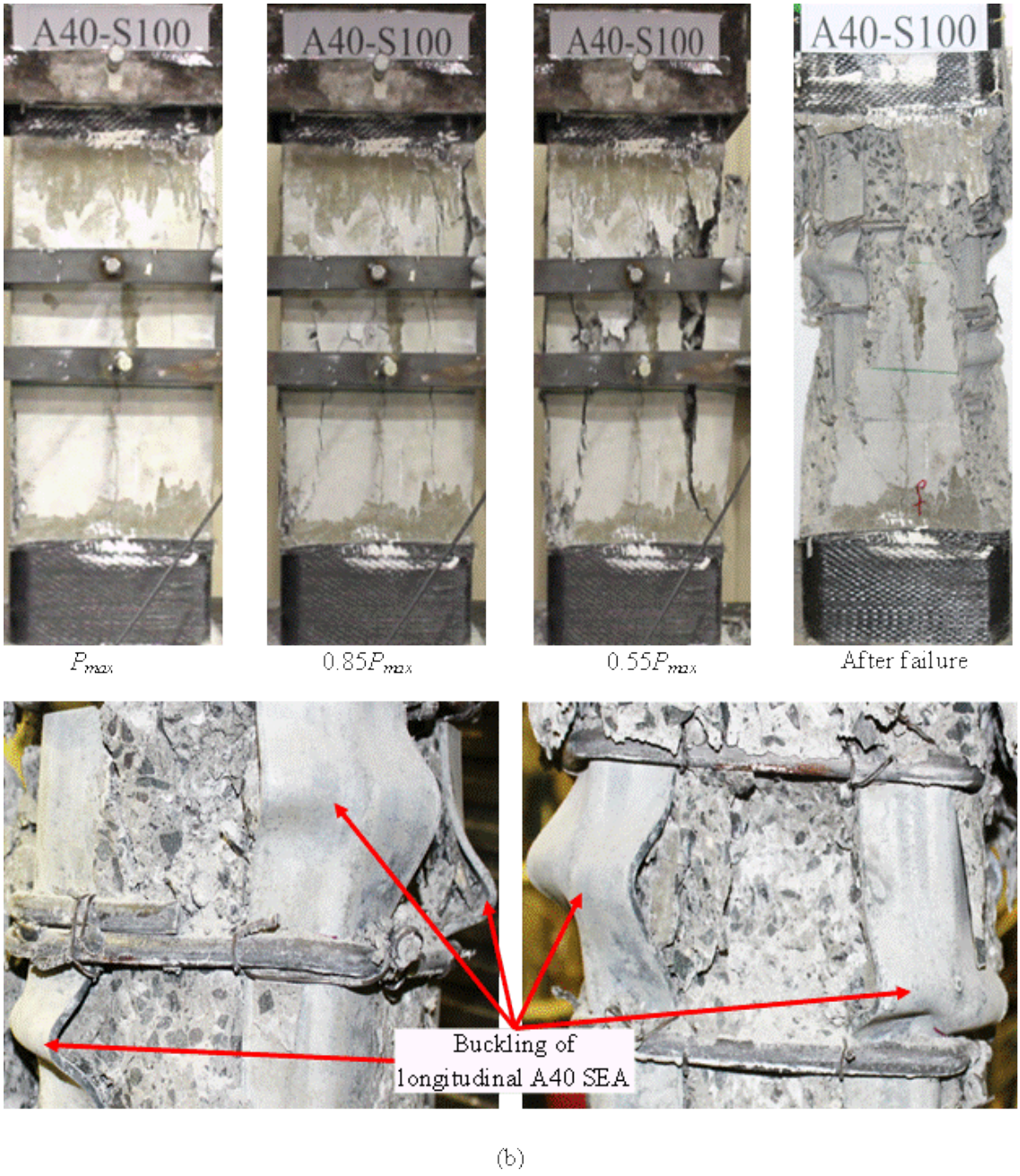

Figure 8.7 Overview of the test specimen A40-S100: (a) during different stages of loading (after peak axial load) and (b) Close-up view of test region

The test results of Specimens B-S100, A30-S100 and A40-S100 are reported in Table 8.2. The axial load-axial deformation responses of the specimens are shown in Figure 8.8. The maximum axial load of Specimen B-S100 was similar to the maximum axial

load of Specimen A30-S100, although, at maximum axial loads, the force contribution of N12 steel bars in Specimen B-S100 was 27% higher than the force contribution of A30 SEA sections in Specimen A30-S100. It was also observed that the ductility of Specimen A30-S100 was 12.5% higher than the ductility of Specimen B-S100. This indicates that the ductility of HSC columns can be better enhanced by using A30 SEA sections rather than using N12 steel bars because A30 SEA sections are a greater restraint against the buckling and provided large confinement of the concrete core in the post-peak behaviour. Specimen A40-S100 obtained 8.0% higher maximum axial load compared to Specimen B-S100. The reason for the higher maximum axial load was that at the maximum axial load, the force contribution of A40 SEA sections in Specimen A40-S100 was about 50% greater than the force contribution of N12 steel bars in Specimen B-S100. In addition, Specimen A40-S100 achieved 18.8% higher ductility than Specimen B-S100. The use of SEA sections as longitudinal reinforcement resulted in higher ductility compared to the conventional steel bar reinforced specimens due to the increased confinement of the concrete core provided by the SEA sections. The maximum axial load of Specimen A40-S100 was 8.3% higher than the maximum axial load of Specimen A30-S100. Also, Specimen A40-S100 achieved 5.6% higher ductility compared to Specimen A30-S100. This may be because the force contribution of A40 SEA in Specimen A40-S100 was about 64% greater than the force contribution of A30 SEA sections in Specimen A30-S100.

Table 8.2 Summary of the Test Results of Column Specimens with 100 mm Tie Spacing

Specimen	Maximum concentric axial load, P_{max} (kN)	Axial deformation at P_{max} (mm)	Ultimate Axial Deformation Δ_{80} [a] (mm)	Ductility
B-S100	2626	2.1	2.7	1.6
A30-S100	2619	2.3	2.8	1.8
A40-S100	2836	2.4	3.2	1.9

Note: [a] represents the deformation corresponding to 80% of the maximum axial load in the descending branch of the axial load-axial deformation behaviour.

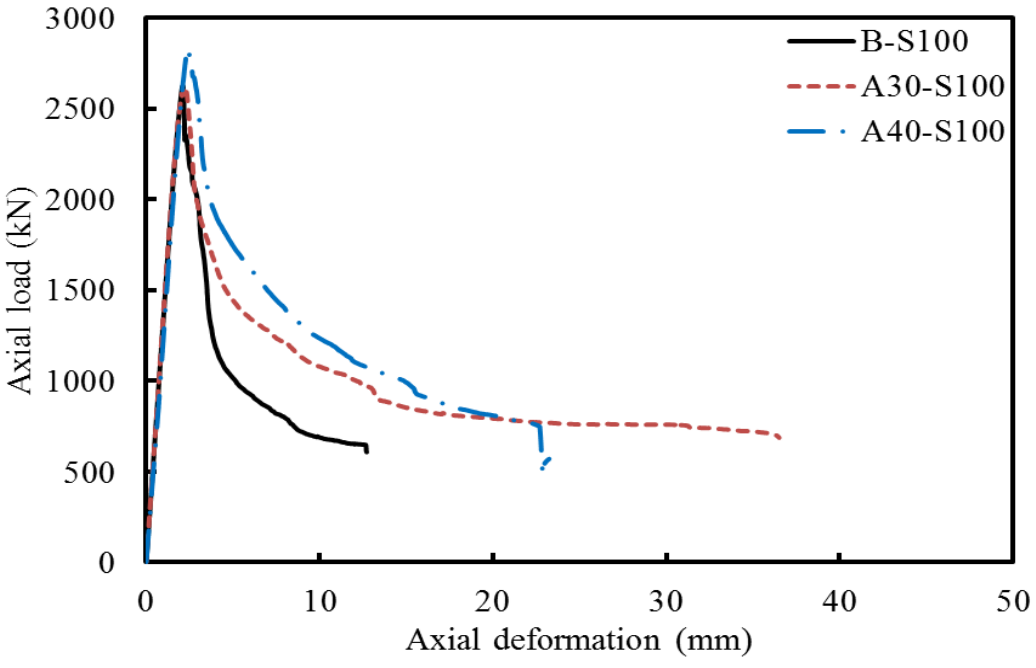

Figure 8.8 Axial load-axial deformation response of column specimens with tie spacing of 100 mm at centres.

8.2.3 **Behaviour of Column Specimens with 200 mm Tie Spacing**

Specimens B-S200, A30-S200, and A40-S200 were reinforced longitudinally with N12 bars, A30 SEA sections, and A40 SEA sections, respectively. The spacing of transverse ties for Specimens B-S200, A30-S200, and A40-S200 was 200 mm at centres. All these specimens were tested up to about 20% of the maximum axial load in the post-peak descending branch of the axial load-axial deformation response. For Specimen B-S200, the first hairline crack began at about 93% of the maximum axial load, as shown in Figure 8.9. This first crack occurred at the top one-third height of the specimens and then the cracks appeared at the midheight of the specimen. As the axial load increased close to the failure condition, the number and size of the cracks increased until spalling of the concrete cover was observed. Whereas, the first hairline cracks in Specimens A30-S200 and A40-S200 started at about 91% and 87%, respectively, of the corresponding maximum axial loads, as shown in Figures 8.10 and 8.11. These cracks were observed at the mid-height of the specimens. Afterwards, with the increase of the applied axial load, the number and size of the cracks increased and the concrete cover spalled off. The observed failure in Specimens B-S200 was attributed to the crushing of the concrete core due to the spalling of concrete cover and the instability of longitudinal reinforcements (Figure 8.9). The failure of Specimens A30-S200 and A40-S200 was attributed to the spalling of the concrete cover, which was followed by outward buckling of longitudinal SEA sections (Figures 8.10 and 8.11). Hence, it can be evident that use of SEA sections as longitudinal reinforcement may improve the failure of HSC columns because the buckling length of SEA sections was higher than the buckling length of steel bars for the similar cross-sectional area.

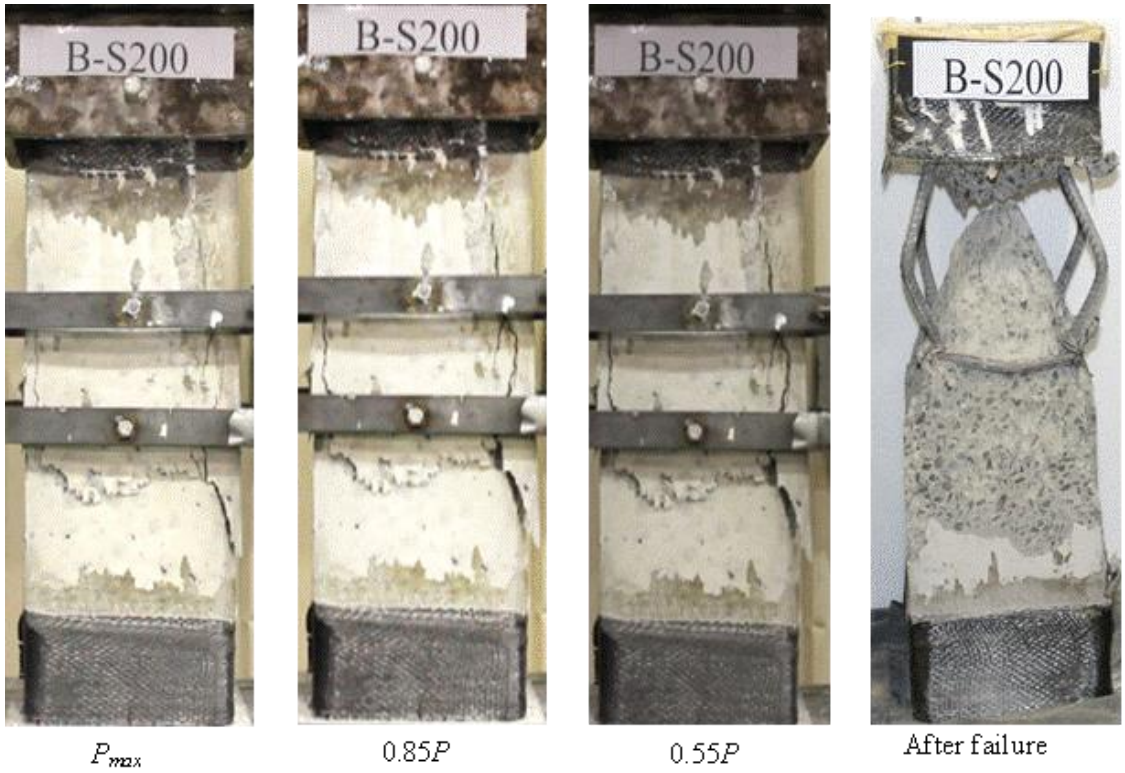

Figure 8.9 Overview of the test specimen B-S200: (a) during different stages of loading (after peak axial load) and (b) Close-up view of test region

Figure 8.10 Overview of the test specimen A30-S200: (a) during different stages of loading (after peak axial load) and (b) Close-up view of test region

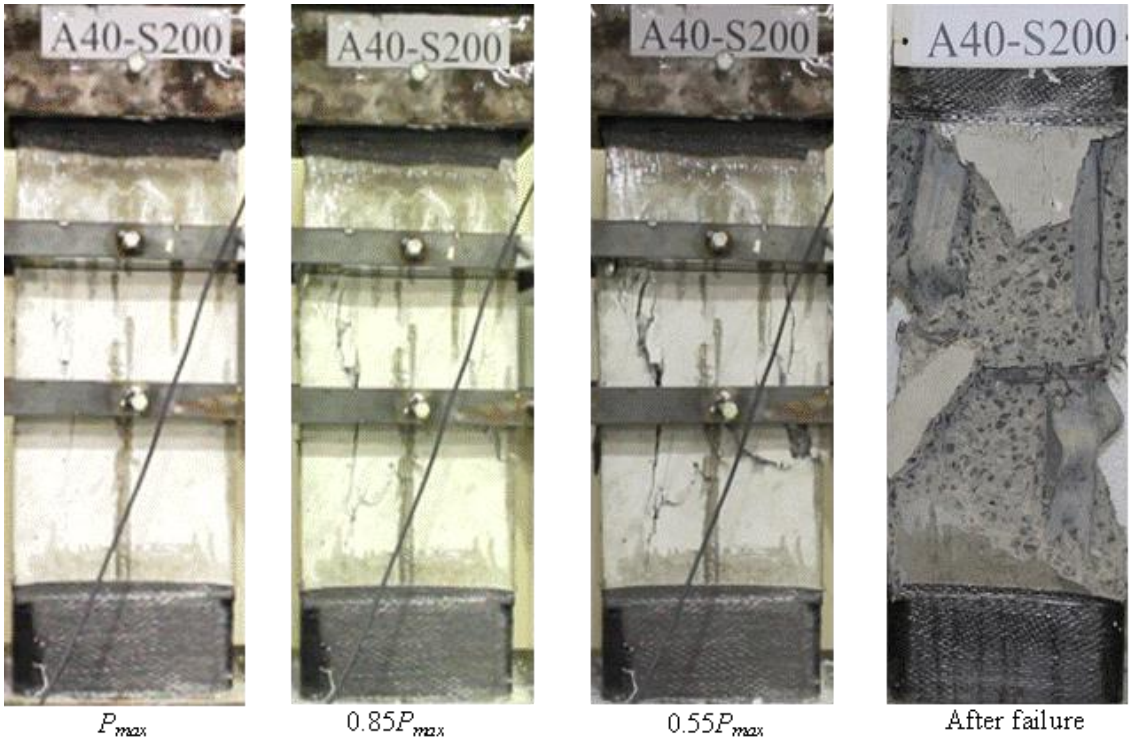

Figure 8.11 Overview of the test specimen A40-S200: (a) during different stages of loading (after peak axial load) and (b) Close-up view of test region

The test results of Specimens B-S200, A30-S200 and A40-S200 are reported in Table 8.3. The axial load-axial deformation responses of the specimens are shown in Figure

8.12. The maximum axial load of Specimen A30-S200 was 2.9% higher than the maximum axial load of Specimen B-S200. It is noted that the average yield tensile strength of steel bars was 49% higher than the average yield tensile strength of A30 SEA sections which resulted in 27% higher force contribution of N12 steel bars in B-S200 specimen compared to the force contribution of A30 SEA section in A30-S200 specimen at the maximum axial load. This increase in the maximum axial load in Specimen A30-S200 was because when the spacing of transverse ties increased, the failure of longitudinal reinforcement (steel bars or SEA sections) tended to be controlled by the buckling more than the yielding of the longitudinal reinforcement. The confinement provided by the transverse ties decreased with the increase in the spacing of transverse ties. The maximum axial load of Specimen A30-S200 was higher because A30 SEA section had a higher second moment of area and hence showed higher buckling load. In addition, Specimen A30-S200 obtained 6.7% greater ductility compared to Specimen B-S200. The reason of greater ductility in Specimen A30-S200 was that as the buckling load of longitudinal reinforcement increased, the confinement effect to the concrete core increased (Campione and Minafò 2010). The maximum axial load of Specimen A40-S200 was 16.3% greater than the maximum axial load of Specimen B-S200. The reason of higher maximum axial load might be because the N12 steel bars in Specimen B-S200 buckled before yielding, whereas the A40 SEA sections yielded before buckling due to higher buckling load of A40 SEA sections than the buckling load of N12 steel bars. Also, Specimen A40-S200 showed 13.3% higher ductility than Specimen B-S200. Hence, reinforcing specimens with SEA sections improved the performance of the specimens because of higher buckling load of SEA sections than the buckling load of steel bars and also because of the increase in the

effective confinement of concrete core. The higher buckling load for SEA sections was because the second moment of area of the SEA section was greater than the second moment of area of the steel bar for the similar cross-sectional area. Specimen A40-S200 showed only 13.0% higher maximum axial load compared to Specimen A30-S200. The higher maximum axial load in Specimen A40-S200 may be because A40 SEA sections in Specimens A40-S200 had higher force contribution than A30 SEA sections in Specimen A30-S200. Also, the ductility of Specimen A40-S200 was 6.2% higher than the ductility of Specimen A30-S200. The higher ductility in Specimen A40-S200 indicated that A40 SEA sections provided better confinement of the concrete core.

Table 8.3 Summary of the Test Results of Column Specimens with 200 mm Tie Spacing

Specimen	Maximum concentric axial load, P_{max} (kN)	Axial deformation at P_{max} (mm)	Ultimate Axial Deformation Δ_{80}[a] (mm)	Ductility
B-S200	2399	1.8	2.3	1.5
A30-S200	2469	1.9	2.4	1.6
A40-S200	2791	2.2	2.8	1.7

Note: [a] represents the deformation corresponding to 80% of the maximum axial load in the descending branch of the axial load-axial deformation behaviour.

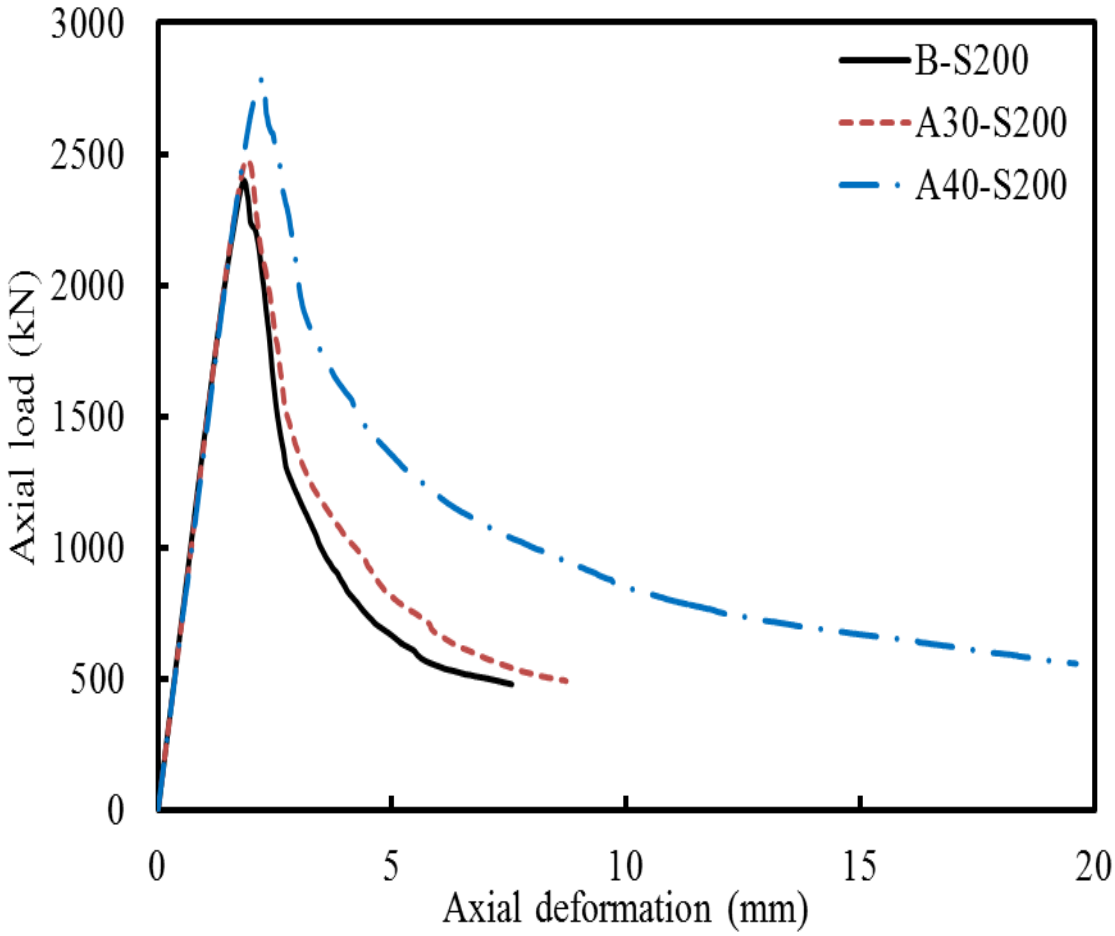

Figure 8.12 Axial load-axial deformation response of column specimens with tie spacing of 200 mm at centres

8.2.4 **Behaviour of Column Specimens with 400 mm Tie Spacing**

Specimens B-S400, A30-S400, and A40-S400 were reinforced longitudinally with N12 steel bars, A30 SEA sections, and A40SEA sections, respectively. The spacing of transverse ties for B-S400, A30-S400, and A40-S400 was 400 mm at centres. Specimens B-S400, A30-S400 and A40-S400 were prepared out of AS 3600 (2009) code requirements for comparison purposes and to evaluate the buckling length of the longitudinal reinforcement with different spacing of transverse ties.

The first hairline cracks in Specimens B-S400, A30-S400 and A40-S400 started at approximately 90%, 89%, and 88%, respectively, of their maximum axial loads, as shown in Figures 8.13 to 8.15. These cracks were observed at the mid-height of the specimens. As the applied axial load increased close to the maximum axial load, the cracks extended both upwards and downwards of the specimens. Afterwards, the number and size of the cracks increased and the concrete cover spalled off. The failure in Specimen B-S400 was characterised by the crushing of the concrete core, which occurred after the spalling of the concrete cover and outward buckling of longitudinal steel bars (Figure 8.13). The failure in Specimens A30-S400 and A40-S400 was characterised by outward buckling of longitudinal SEA sections without crushing of the concrete core (Figures 8.14 and 8.15). As a result, it can be observed from the comparisons of the failure behaviours shown in Figures 8.13 to 8.15 that the failure of Specimen B-S400 (N12 steel bar specimen with spacing of transverse ties of 400 mm) is much more brittle than the failure of Specimens A30-S400 (A30 SEA specimen with spacing of transverse ties of 400 mm) and A40-S400 (A30 SEA specimen with spacing of transverse ties of 400 mm) under concentric axial load. Hence, the presence of the longitudinal SEA sections improves the failure behaviour and enhances the post-peak behaviour of square high strength concrete (HSC) columns.

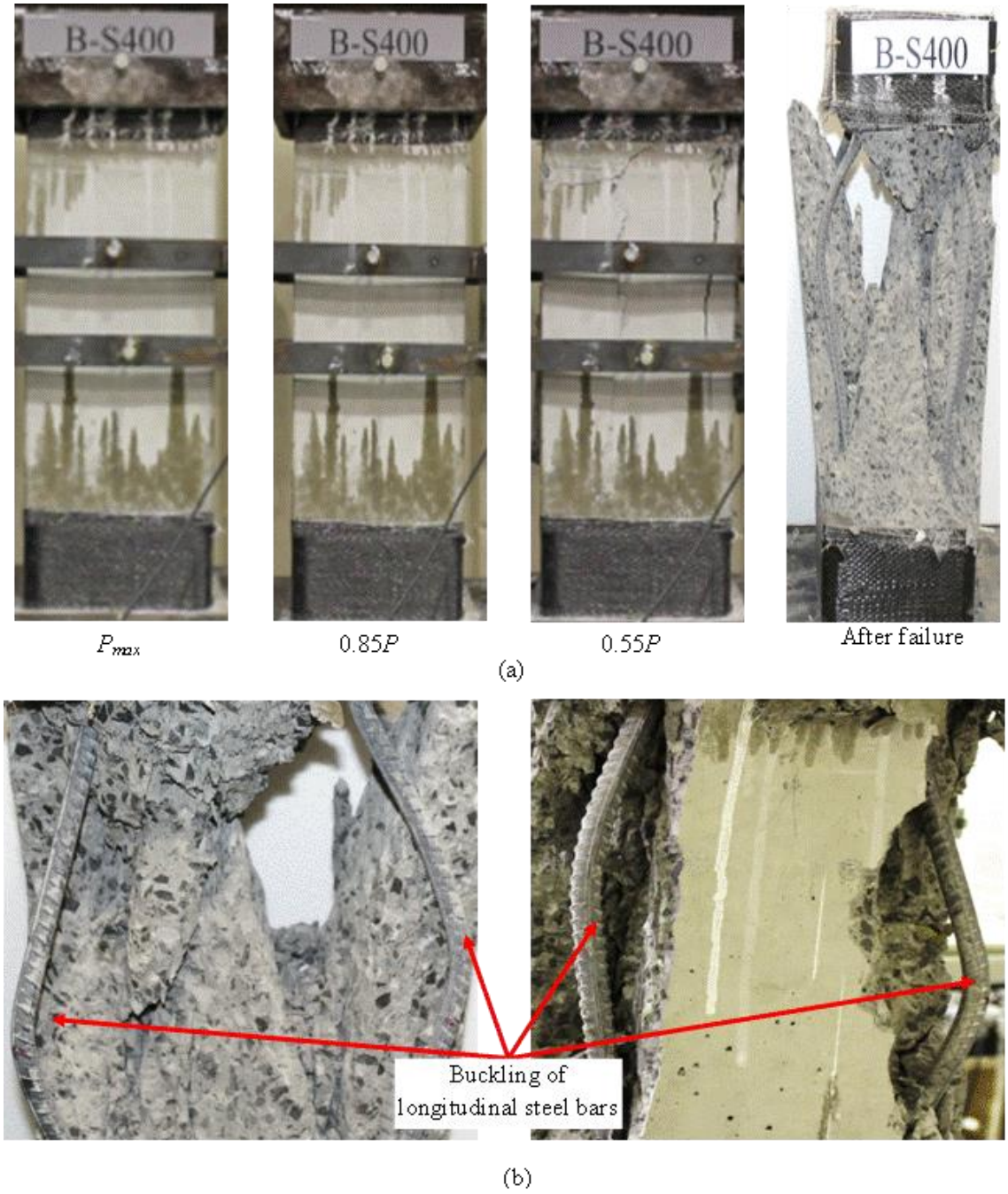

Figure 8.13 Overview of the test specimen B-S400: (a) during different stages of loading (after peak axial load) and (b) Close-up view of test region

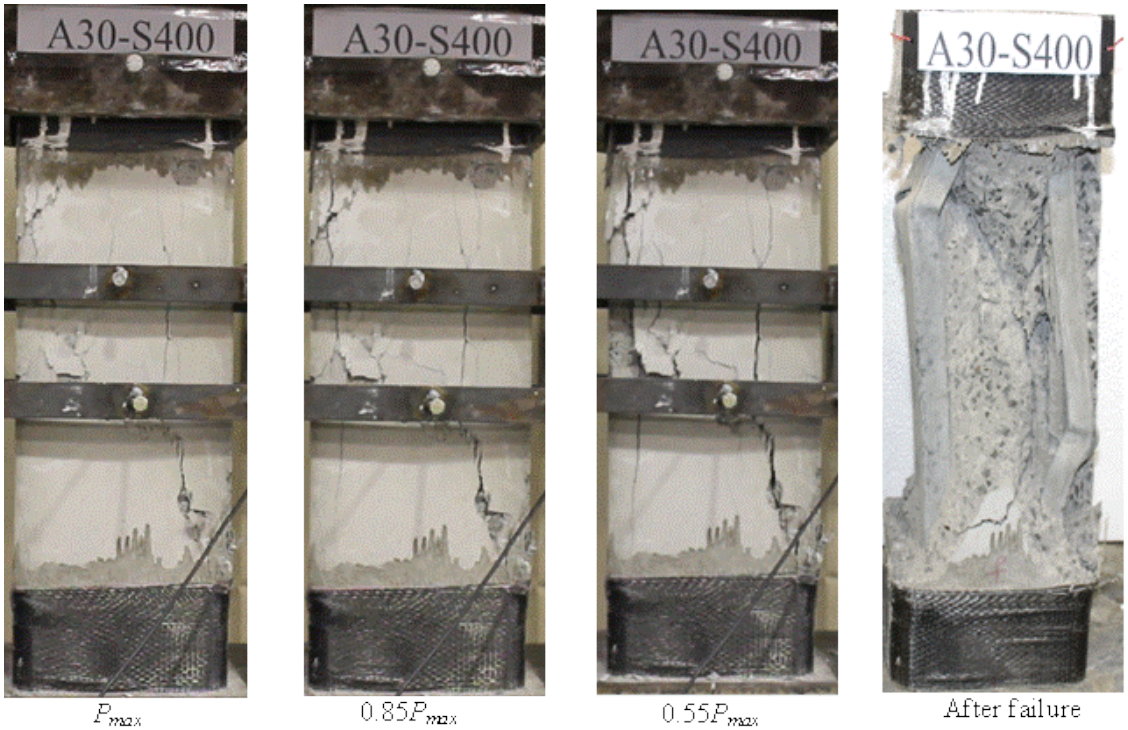

Figure 8.14 Overview of the test specimen A30-S400: (a) during different stages of loading (after peak axial load) and (b) Close-up view of test region

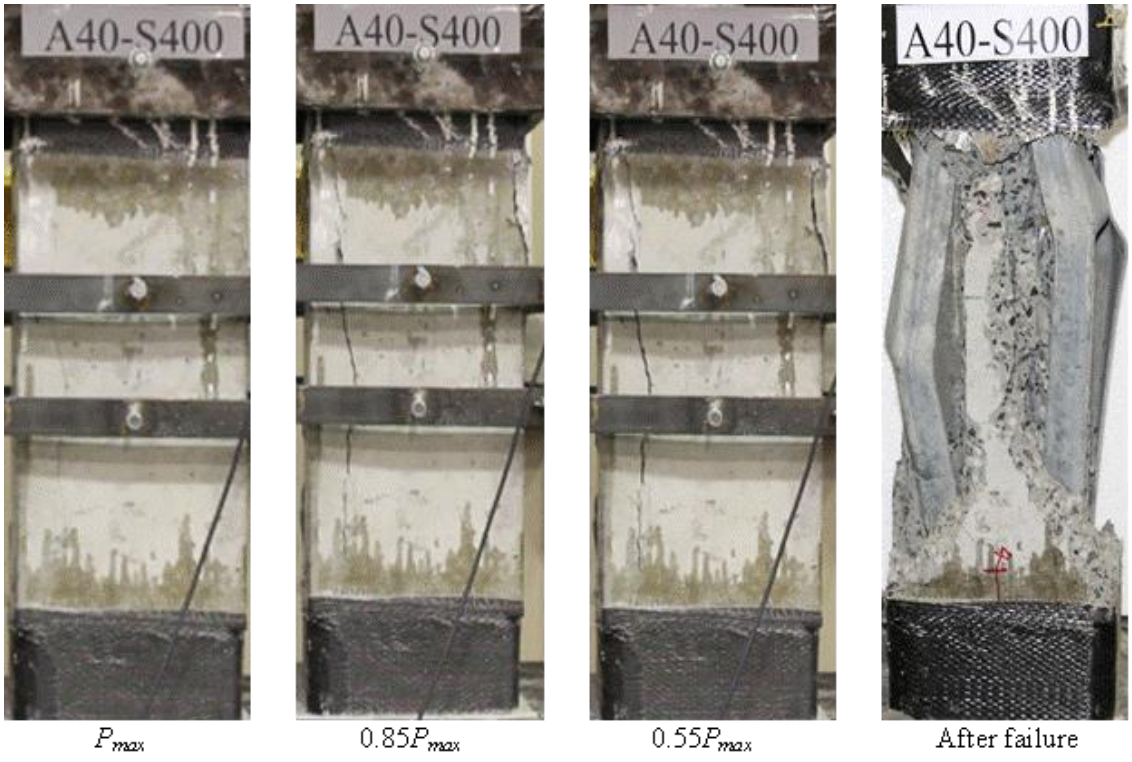

Figure 8.15 Overview of the test specimen A40-S400: (a) during different stages of loading (after peak axial load) and (b) Close-up view of test region

The test results of Specimens B-S400, A30-S400 and A40-S400 are presented in Table 8.4. The axial load-axial deformation responses of the specimens are shown in Figure 8.16. It is noted that the spacing of transverse ties in the Specimen B-S400 was higher than the required spacing of transverse ties recommended in ACI 318 (2014). Specimen B-S400 was designed to compare the behaviour of Specimens A30-S400 and A40-S400 in terms of failure mode, strength, and ductility. The maximum axial load of Specimens A30-S400 was 42.5% higher than the maximum axial load of Specimen B-S400. This may be because the use of SEA sections instead of steel bars in reinforcing square HSC column specimens significantly increased the buckling load of longitudinal reinforcement. The minimum second moment of area of the A30 SEA section was about 77% higher than the second moment of area of the conventional steel bar for the same cross-sectional area. In addition, the minimum radius of gyration of the A30 SEA section was about 50% greater than the radius of gyration of the conventional steel bar for the same cross-sectional area.

The lower axial load carrying capacity of Specimen B-S400 was due to the instability of longitudinal bars (buckling of longitudinal steel bars at an early stage of loading), which pushed out the concrete cover and created weakness planes between the concrete cover and the concrete core. Similar observations were also reported in Polat (1992) and Saatcioglu and Razvi (1998). Therefore, the ductility of Specimen B-S400 was not further analysed. The maximum axial load of Specimen A40-S400 was 52.2% higher than the maximum axial load of Specimen B-S400. This significantly high maximum axial load in Specimen A40-S400 was because the confinement efficiency of the concrete core of the specimens increased by using A40 SEA sections as longitudinal

reinforcement instead of N12 steel bars. Another possible reason is that at maximum axial load, the conventional steel bars in Specimen B-S400 reached buckling before yielding of the longitudinal steel bars. However, at maximum axial load, the A40 SEA sections in Specimen A40-S400 yielded before buckling as A40 SEA sections had much higher buckling load than N12 steel bars. The maximum axial load of Specimen A40-S400 was 6.9% higher than the maximum axial load of Specimen A30-S400. Also, the ductility of Specimen A40-S400 was 6.7% higher than the ductility of Specimen A30-S400. This indicates that the A40 SEA sections were more effective than the A30 SEA sections in confining the concrete core of the specimen.

Table 8.4 Summary of the Test Results of Column Specimens with 400 mm Tie Spacing

Specimen	Maximum concentric axial load, P_{max} (kN)	Axial deformation at P_{max} (mm)	Ultimate Axial Deformation Δ_{80}[a] (mm)	Ductility
B-S400	1717	1.8	-	-
A30-S400	2446	2.1	2.4	1.5
A40-S400	2614	2.2	2.7	1.6

Note: [a] represents the deformation corresponding to 80% of the maximum axial load in the descending branch of the axial load-axial deformation behaviour.

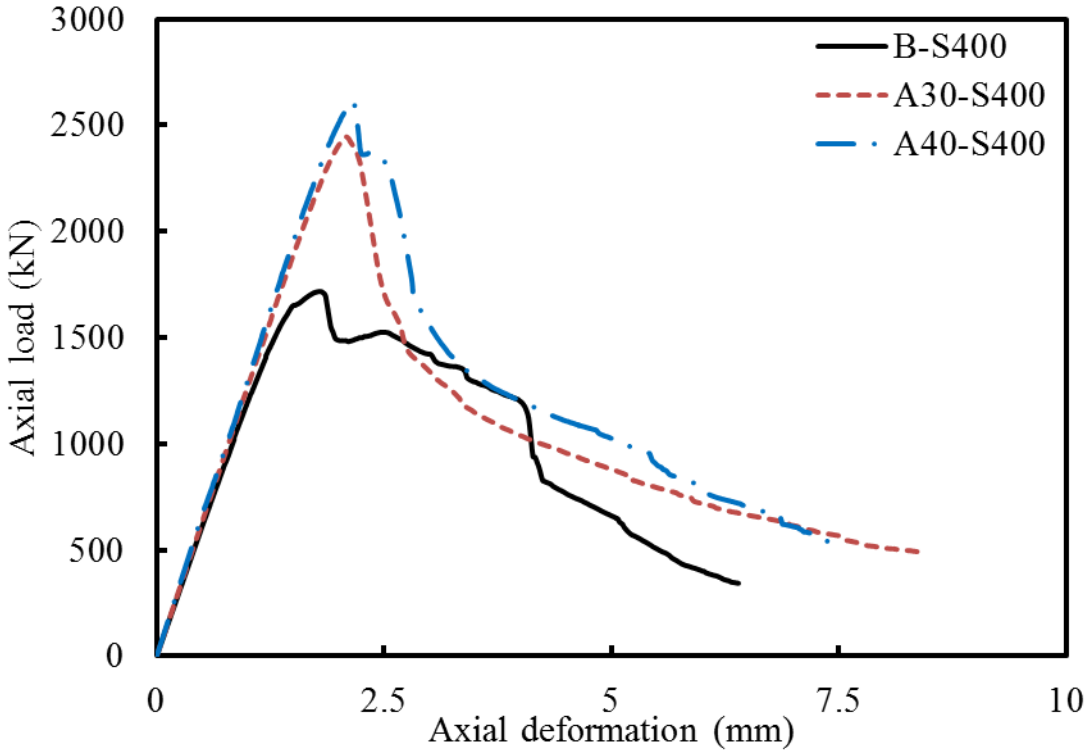

Figure 8.16 Axial load-axial deformation response of column specimens with tie spacing of 400 mm at centres

8.3 Influence of Transverse Tie Spacing on the Behaviour of the Tested Specimens

In this section, the influence of increasing the spacing of transverse ties from 50 mm to 400 mm in each group of specimens was investigated and discussed. The main aim is to investigate the effect of increasing transverse tie spacing on the strength, ductility and buckling load for each group of specimens. As discussed above, the use of SEA section as longitudinal reinforcement led to increased effective confinement of the concrete core and greater buckling load compared to the use of the N12 steel bars. Therefore, the improvements in the effective confinement of concrete core and buckling load for SEA

sections influenced the strength and ductility of the specimens particularly with the increase in the transverse tie spacing. The SEA section has more than one second moment of area and more than one radius of gyration due to unsymmetrical cross section, whereas the steel bar has one second moment of area and one radius of gyration due to symmetrical cross section. To be on the safe side, the minimum second moment of area and the minimum radius of gyration of the A30 and A40 SEA sections were selected to compare with the second moment of area and radius of gyration of N12 steel bars. The second moment of area and radius of gyration of N12 steel bar were about 1018 mm^4 and 3 mm, respectively. The minimum second moment of area and the minimum radius of gyration of A30 SEA section were about 4380 mm^4 and 6 mm. The minimum second moment of area and minimum radius of gyration of A40 SEA section were about 15700 mm^4 and 8 mm, respectively.

8.3.1 **Influence of Transverse Tie Spacing on Column Specimens of the B Group**

The Specimens B-S50, B-S100, and B-S200 and B-S400 were reinforced longitudinally with four N12 bars. The spacing of transverse ties for B-S50, B-S100, and B-S200 and B-S400 were 50 mm, 100 mm, 200 mm, and 400 mm, respectively. The test results of the specimens in Group B are reported in Tables 8.1 to 8.4. The axial load-axial deformation responses of the specimens are presented in Figure 8.17. The maximum axial load of Specimen B-S50 was 11.5% higher than the maximum axial load of Specimen B-S100. The ductility of Specimen B-S50 was 12.5% greater than the ductility of Specimen B-S100. Specimen B-S50 achieved 22.1% and 20.0% higher maximum axial load and ductility, respectively, compared to Specimen B-S200.

Furthermore, the maximum axial load of Specimen B-S50 was 70.6% higher than the maximum axial load of Specimen B-S400. The sharp decrease of the axial load of Specimen B-S400 indicates that the buckling load of longitudinal steel bars and the confinement of the concrete core significantly decreased as the spacing of transverse ties increased from 50 mm to 400 mm. Also, the ductility of the specimen with 400 mm transverse tie spacing, which exceeds the required spacing of transverse ties by ACI 318 (2014), was not calculated as the specimen failed prematurely. The premature failure of Specimen B-S400 was because the large transverse tie spacing of Specimen B-S400 resulted in buckling of the longitudinal reinforcement at an early stage of loading.

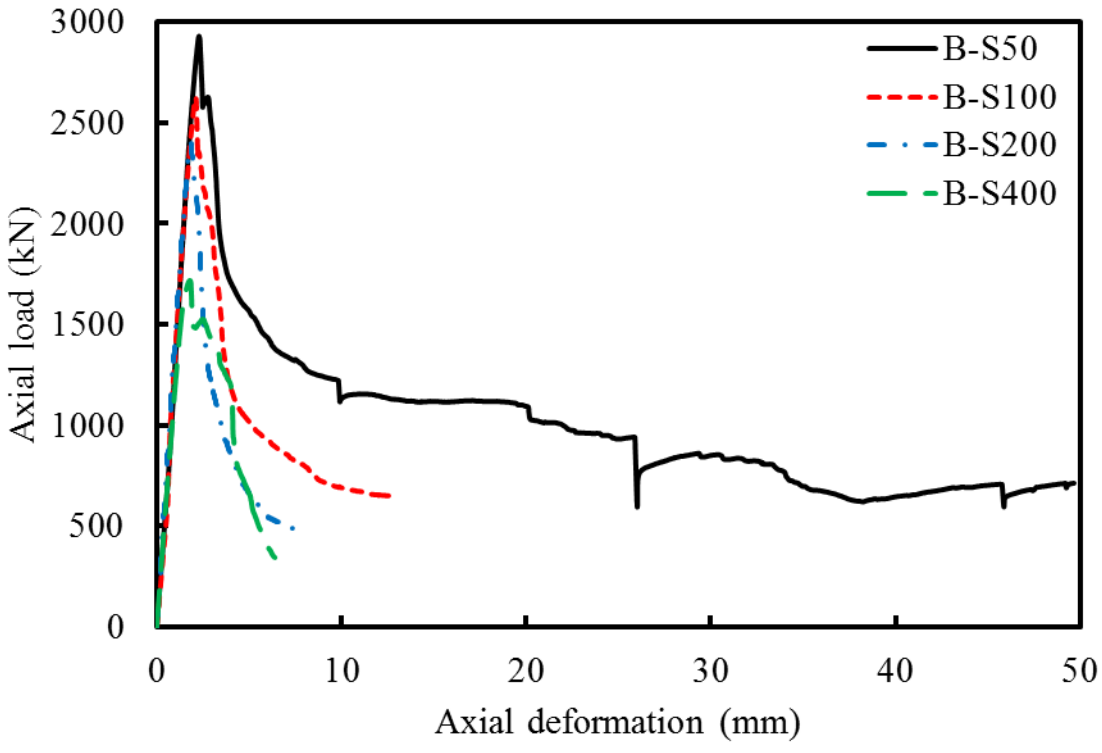

Figure 8.17 Axial load-axial deformation response of Group B specimens

8.3.2 **Influence of Transverse Tie Spacing on Column Specimens of the A30 Group**

The Specimens A30-S50, A30-S100, and A30-S200 and A30-S400 were reinforced longitudinally with four A30 SEA sections. However, the specimens A30-S50, A30-S100, and A30-S200 and A30-S400 were reinforced transversely with steel ties at 50 mm, 100 mm, 200 mm and 400 mm centre-to-centre spacing. The test results of the specimens in Group A30 are reported in Tables 8.1 to 8.4. The axial load-axial deformation responses of the specimens are presented in Figure 8.18. Compared to Specimen A30-S100, the maximum axial load of Specimen A30-S50 was only 0.2% higher. This may be because the formation of a natural separation plane between the cover and the concrete core caused the failure of concrete cover in Specimen A30-S50 due to the closely spaced transverse ties. Similar observations were also reported in Saatcioglu and Razvi (1998), Ozbakkaloglu and Saatcioglu (2004) and Awati and Khadiranaikar (2012). However, Specimen A30-S50 achieved 44.4% higher ductility than Specimen A30-S100. This increase in the ductility in Specimen A30-S50 was because the spacing of transverse ties of Specimen A30-S50 was closer than the spacing of transverse ties of Specimen A30-S100, which resulted in increasing lateral confining pressure with an improvement in the confined concrete core area. Specimen A30-S50 obtained 6.3% higher maximum axial load than Specimen A30-S200. In addition, the ductility of Specimen A30-S50 was 62.5% higher than the ductility of Specimen A30-S200. Specimen A30-S50 achieved 7.3% and 73.3% higher maximum axial load and ductility, respectively, than Specimen A30-S400. It is noted that the transverse tie spacing of Specimen A30-S50 was 50 mm and transverse tie spacing of Specimen A30-S400 was 400 mm.

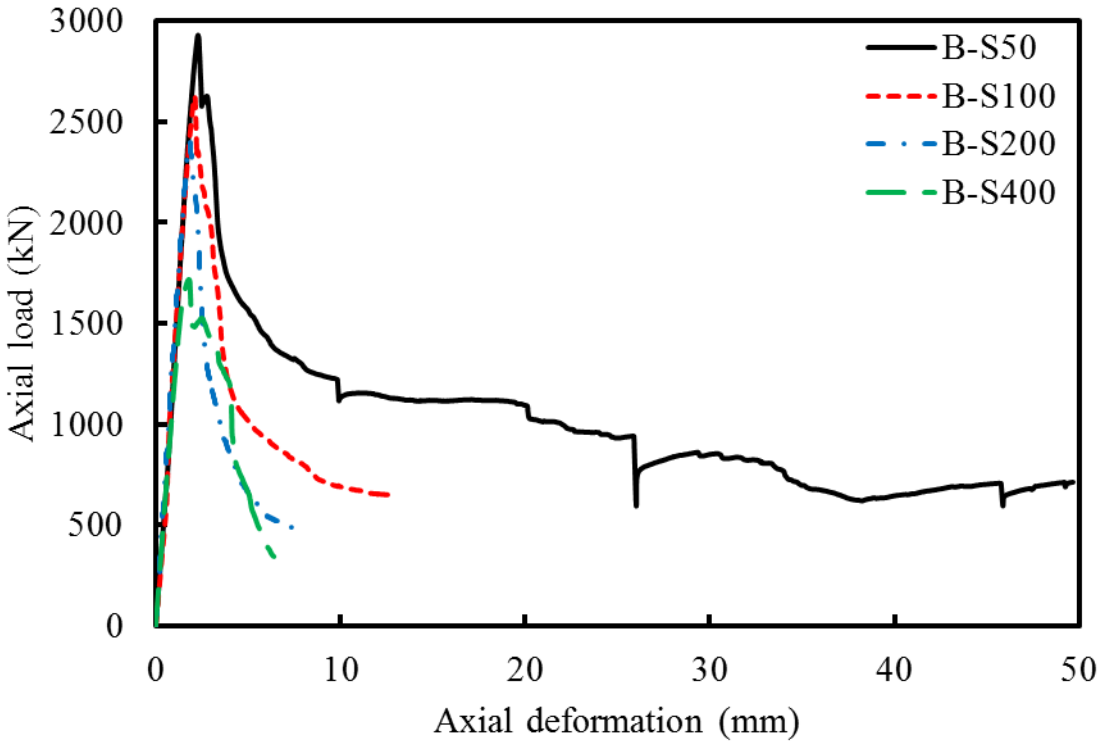

Figure 8.18 Axial load-axial deformation response of Group A30 specimens

8.3.3 **Influence of Transverse Tie Spacing on Column Specimens of the A30 Group**

The Specimens A40-S50, A40-S100, and A40-S200 and A40-S400 were reinforced longitudinally with four A40 SEA sections. The spacing of transverse ties for A40-S50, A40-S100, and A40-S200 and A40-S400 were 50 mm, 100 mm, 200 mm, and 400 mm, respectively. The test results of the specimens in Group A40 are reported in Tables 8.1 to 8.4. The axial load-axial deformation responses of the specimens are presented in Figure 8.19. The maximum axial load of Specimen A40-S50 was 6.1% greater than the maximum axial load of Specimen A40-S100. Moreover, the ductility of Specimen A40-S50 was 42.1% higher than the ductility of Specimen A40-S100. Specimen A40-S50

obtained 7.8% and 58.8% higher maximum axial load and ductility, respectively, compared to Specimen A40-S200. Also, Specimen A40-S50 obtained about 15.1% and 68.8% higher maximum axial load and ductility, respectively, compared to Specimen A40-S400. For the increase of the spacing of transverse ties from 50 mm to 400 mm, the maximum axial load and ductility of the specimens reinforced with A40 SEA sections decreased by about 15.1% and 68.8%, respectively. These decreases in the strength and ductility of specimens reinforced with A40 SEA were because the confinement of the concrete core decreased due to the increased spacing of transverse tie up to 400 mm. Under axial compression, the effect of transverse ties to restrain the expansion of concrete core decreases as the spacing of transverse ties increases, which results in decreasing the strength and ductility of the column.

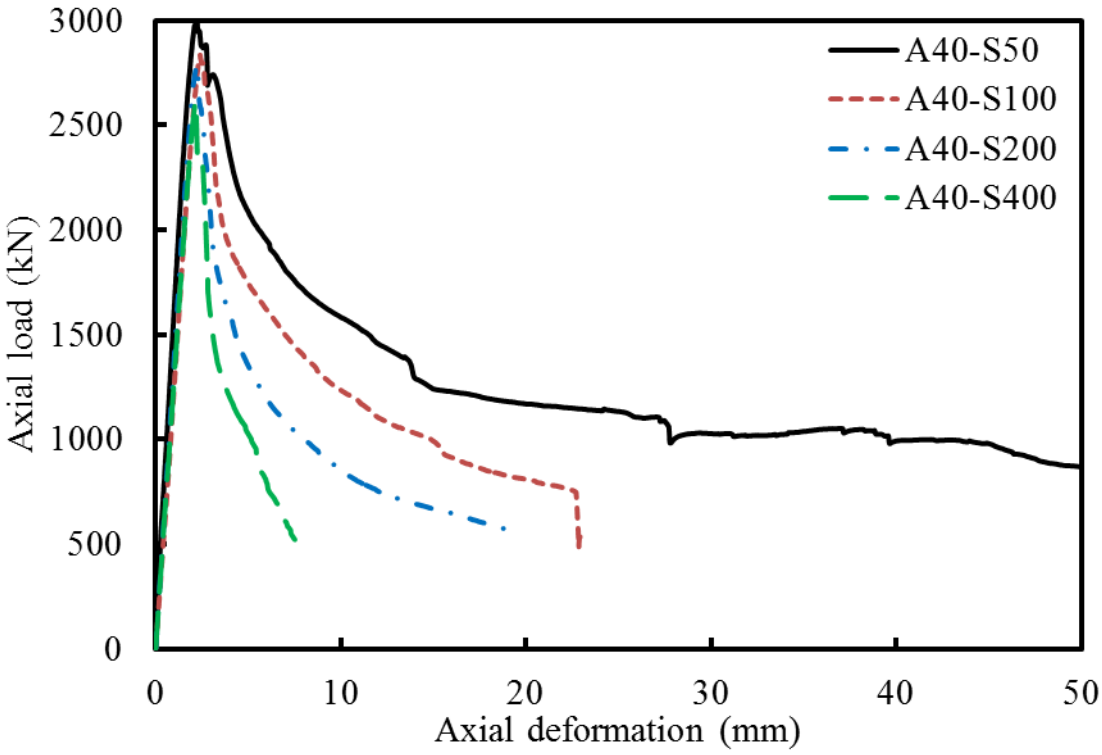

Figure 8.19 Axial load-axial deformation response of Group A40 specimens

8.4 Summary

In this chapter, the test results of 12 square HSC column specimens with 600 mm height reinforced longitudinally with either steel bars or SEA sections were reported to discuss the influence type of longitudinal reinforcements and spacing of transverse ties. The specimens were divided into three groups based on the type of longitudinal reinforcements (steel bars, A30 and A40 SEA sections). The test results such as load carrying capacities, axial deformations and ductilities of the tested specimens were presented.

Based on the test results presented in this study, it was found that the use of the SEA sections as longitudinal reinforcements in HSC column specimens led to significant improvements in the axial load carrying capacity and ductility compared to the corresponding HSC column specimens reinforced longitudinally with steel bars. Also, it can be reported that for specimens with transverse tie spacing of 400 mm, the use of the conventional steel bar as longitudinal reinforcement led to a premature failure of the specimen, while the use of the SEA sections as longitudinal reinforcement did not lead to premature failure of the specimen. This was because the buckling load (buckling length) of SEA sections was significantly higher than the buckling load (buckling length) of steel bars. The analytical evaluations of the tested specimens with 800 mm and 600 mm height are presented and discussed in the next chapter.

9 ANALYTICAL EVALUATIONS AND DISCUSSIONS

9.1 Introduction

In this chapter, the experimental maximum axial loads for specimens that were tested under concentric and eccentric axial loads are compared to the corresponding nominal axial loads. Also, the maximum spacing between transverse ties for specimens reinforced with SEA sections was investigated and compared with the column specimens reinforced with steel bars. This chapter also shows an analytical study aimed at investigating the suitability of using existing models in the literature to predict the axial load-axial deformation responses of square high strength concrete (HSC) columns reinforced longitudinally with SEA sections that were tested in this research study. The explanation of the procedure to predict the axial load-axial deformation behaviour of the tested columns are also presented. Afterwards, the experimental results are compared to analytical axial load-axial deformation behaviour based on a stress-strain model. The model used is based on the work by Cusson and Paultre (1995), which is applicable of predicting the behaviour of HSC columns under axial compression. The effects of buckling of either steel bars or SEA were not taken into account in the analytical model. The results of the twenty-one of thirty-two reinforced concrete columns tested in this study are investigated in this chapter.

9.2 Predicted Versus Tested Axial Load Capacity

9.2.1 Evaluation of Concentric Axial Load Capacity

In this section, The axial load capacity (P_o) for each column specimen was calculated using Australian Standard AS 3600 (2009), as presented in Equation (9.1). It is noted that the recommendation in AS 3600 (2009) is only applicable for conventional steel bar reinforced concrete. In this study, Equation (9.1) was used to calculate the axial load capacity for column specimens reinforced longitudinally with SEA sections to investigate whether AS 3600 (2009) based recommendations for steel bar reinforced concrete columns can be applied for the SEA reinforced concrete columns.

$$P_o = \alpha_1 f_c' \left(A_g - A_s\right) + f_y A_s \tag{9.1}$$

where A_g and A_s are the gross cross-sectional area of the column and the total area of longitudinal reinforcement, respectively; f_c' and f_y are the compressive strength of concrete and the yield tensile strength of the longitudinal reinforcement, respectively. The α_1 is a reduction factor that takes into account the differences in shape, concrete casting practice and size between standard concrete cylinders and concrete columns (Hognestad 1951; Ozbakkaloglu and Saatcioglu 2004; Afifi et al. 2013). In this study, the reduction factor is calculated according to AS 3600 (2009) as a function of the compressive strength of concrete.

$$\alpha_1 = 1 - 0.003 f_c' \qquad 0.72 \leq \alpha_1 \leq 0.85 \tag{9.2}$$

Figure 9.1 presents the ratios of experimental maximum axial load to the predicted axial load capacity (P_{max}/P_o) of the specimens with 800 mm height. Of the 20 Specimens, 5

Specimens with 800 mm height (R-S50-C, A30-S50-C, A30-S75-C, A40-S50-C and A40-S75-C) were tested under concentric axial loads. It was observed that the ratios of the experimental maximum axial load to predicated results P_{max}/P_o using Equation (9.1) ranged between 0.96 and 1.08. The highest P_{max}/P_o ratio was calculated for Specimen A30-S75-C. The P_{max}/P_o ratio was calculated as 1.03, 1.00, 1.08, 1.04 and 0.96 for Specimens R-S50-C, A30-S50-C, A30-S75-C, A40-S50-C and A40-S75-C, respectively. it can be noted that the P_{max}/P_o ratios are close to 1.00, which is indicated that the AS 3600 (2009) equation is accurate for predicting the nominal axial capacity of square HSC columns reinforced longitudinally with either steel bars or SEA sections.

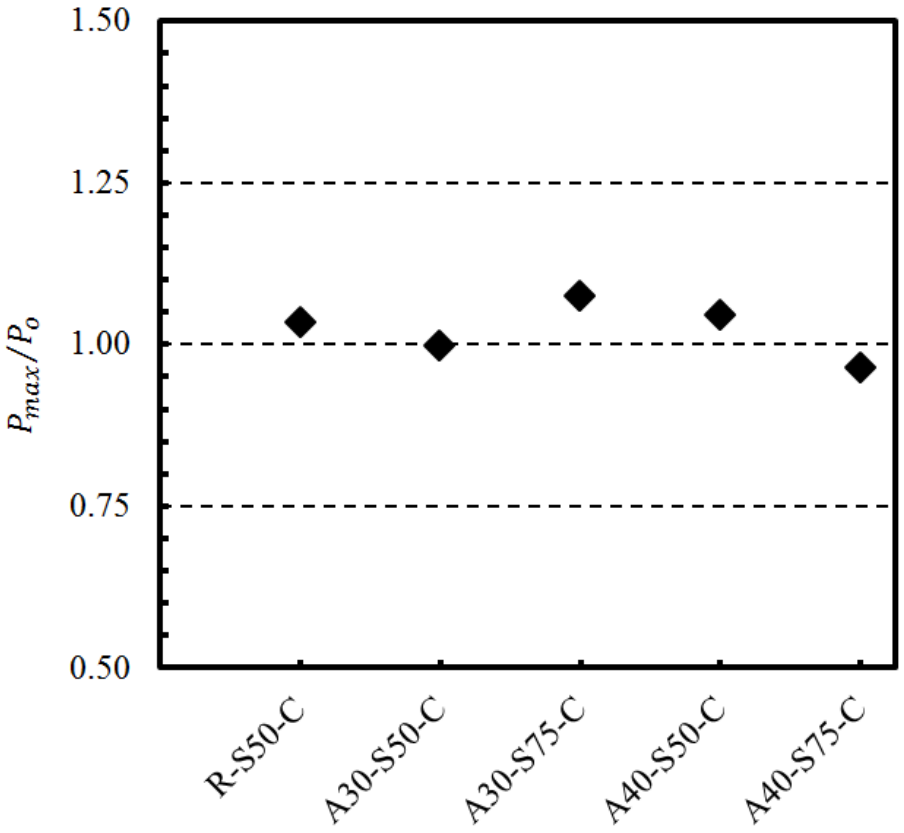

Figure 9.1 Experimental maximum axial loads to predicted axial load capacities of specimens with 800 mm height

Figure 9.2 presents the ratios of experimental maximum axial load to the predicted axial load capacity (P_{max}/P_o) of the specimens with 600 mm height, which included testing of 12 specimens under concentric axial load. For column specimens reinforced longitudinally with N12 steel bars, the ratios of P_{max}/P_o varies from 0.65 to 1.11. The P_{max}/P_o ratio was calculated as 1.11, 1.00, 0.91 and 0.65 for Specimens B-S50, B-S100 and B-S200 and B-S400, respectively. The reason of lowest P_{max}/P_o ratio of Specimen B-S400 was because premature failure occurred in Specimen B-S400 at an early stage of loading. The reason for the premature failure of Specimen B-S400 was due to large transverse tie spacing of 400 mm. Where the transverse ties in Specimen B-S400 with a large spacing of 400 mm resulted in buckling of longitudinal steel bars before reaching the yield tensile strength. It is noted that Equation (9.1) does not take into account the influence of lateral confinement provided by transverse ties. With the exception of Specimen B-S400, the P_{max}/P_o ratios indicated that the equation of AS 3600 (2009) provide accurate and reasonable predictions of the analytical concentric axial load capacity of the tested column specimens reinforced longitudinally with steel bars.

For column specimens reinforced longitudinally with A30 SEA sections, it was observed from Figure 9.2 that the ratio of P_{max}/P_o varied from 0.96 to 1.03. The highest P_{max}/P_o ratio was calculated for Specimen A30-S50. The P_{max}/P_o ratio was calculated as 1.03, 1.02, 0.97 and 0.96 for Specimens A30-S50, A30-S100, A30-S200 and A30-S400, respectively. The P_{max}/P_o ratios indicated that the equation of AS 3600 (2009) provide accurate and reasonable predictions of the analytical concentric axial load

capacity of the tested column specimens reinforced longitudinally with A30 SEA sections.

For column specimens reinforced longitudinally with A40 SEA sections, it can be seen from Figure 9.2 that the ratio of P_{max}/P_o varied from 0.92 to 1.06. The highest P_{max}/P_o ratio was calculated for Specimen A40-S50. The P_{max}/P_o ratio was calculated as 1.06, 1.00, 0.98 and 0.92 for Specimens A40-S50, A40-S100, A40-S200 and A40-S400, respectively. The P_{max}/P_o ratios of specimens reinforced longitudinally with SEA sections indicate that the equation of AS 3600 (2009) provided accurate and reasonable predictions of the analytical concentric axial load of column specimens reinforced longitudinally with A40 SEA sections.

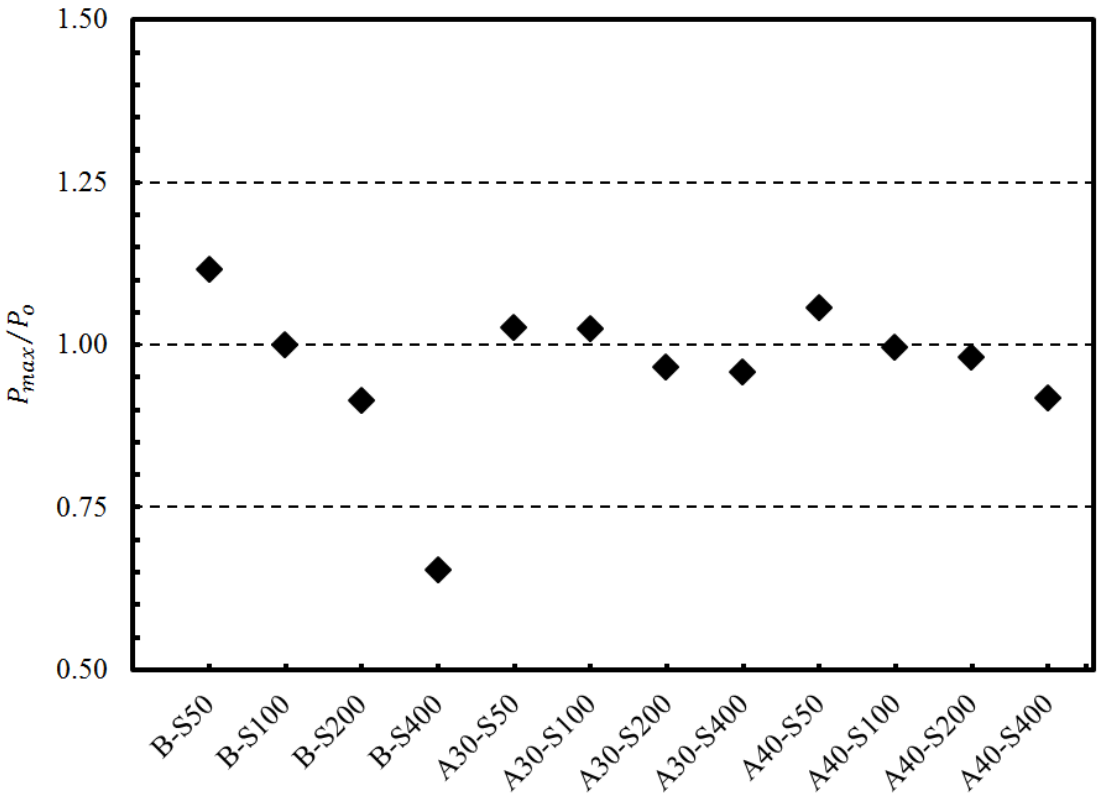

Figure 9.2 Experimental maximum axial loads to predicted axial load capacities of specimens with 600 mm height

9.2.2 **Evaluation of Eccentric Axial Load Capacity**

Ten of the twenty specimens with 800 mm height were cast and test under 25 mm and 50 mm eccentric axial loads. The predicted eccentric axial load capacity for the specimens tested under eccentric compression load was calculated using Equation (9.3). This equation was derived based on the experimental results to evaluate the influence of the applied load eccentricity on the columns (Afefy and El-Tony 2016).

$$P_{ecc} = P_o exp(-2.9\left(\frac{e}{b}\right)) \tag{9.3}$$

where P_o is the nominal concentric axial compression for the specimens tested under concentric axial load, e refers to the eccentricity (25 mm or 50 mm) and b refers to the side width of concrete column cross-section. The nominal concentric axial compression (P_o) was calculated based on the recommendations of AS 3600 (2009), as in Equation (9.1).

For column specimens tested under 25 mm eccentric axial load, it was shown from Figure 9.3 that the ratio of P_{max}/P_{ecc} varied from 0.93 to 1.06 with an average of 1.00. The highest P_{max}/P_{ecc} ratio was calculated for Specimen R-S50-E25. The P_{max}/P_{ecc} ratio was calculated as 1.06, 1.00, 1.01 and 0.93 for Specimens R-S50-E25, A30-S50-E25, A40-S50-E25 and A40-S75-E25, respectively. It can be observed that the P_{max}/P_{ecc} ratios are close to 1.00, which is indicated that the Equation (9.3) is valid for predicting the predicted axial capacity of square HSC columns reinforced longitudinally with either steel bars or SEA sections and tested under 25 mm eccentric axial load.

For column specimens tested under 50 mm eccentric axial load, it was presented from Figure 9.4 that the ratio of P_{max}/P_{ecc} varied from 0.98 to 1.04 with an average of 1.01. The highest P_{max}/P_{ecc} ratio was calculated for Specimen A40-S75-E50. The P_{max}/P_{ecc} ratio was calculated as 1.02, 0.98, 1.01, 1.02 and 1.04 for Specimens R-S50-E50, A30-S50-E50, A30-S75-E50, A40-S50-E50 and A40-S75-E50, respectively. The P_{max}/P_{ecc} ratios indicated that the Equation (9.3) provides accurate and reasonable predictions of the predicted eccentric axial load capacity of the square HSC column specimens reinforced longitudinally with either steel bars or SEA sections and tested under 50 mm eccentric axial load.

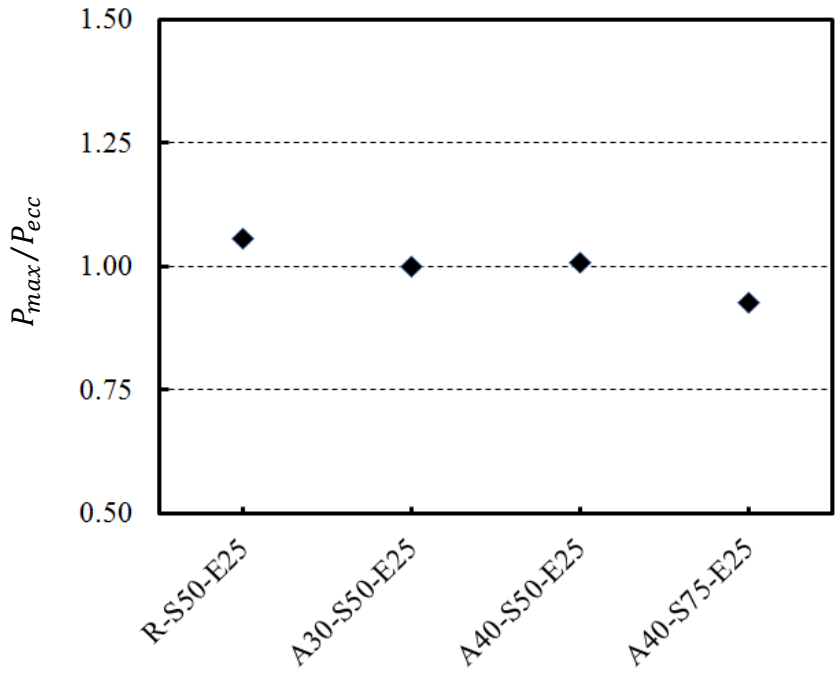

Figure 9.3 Experimental maximum eccentric axial loads to predicted eccentric axial load capacities of specimens tested under 25 mm eccentric axial load

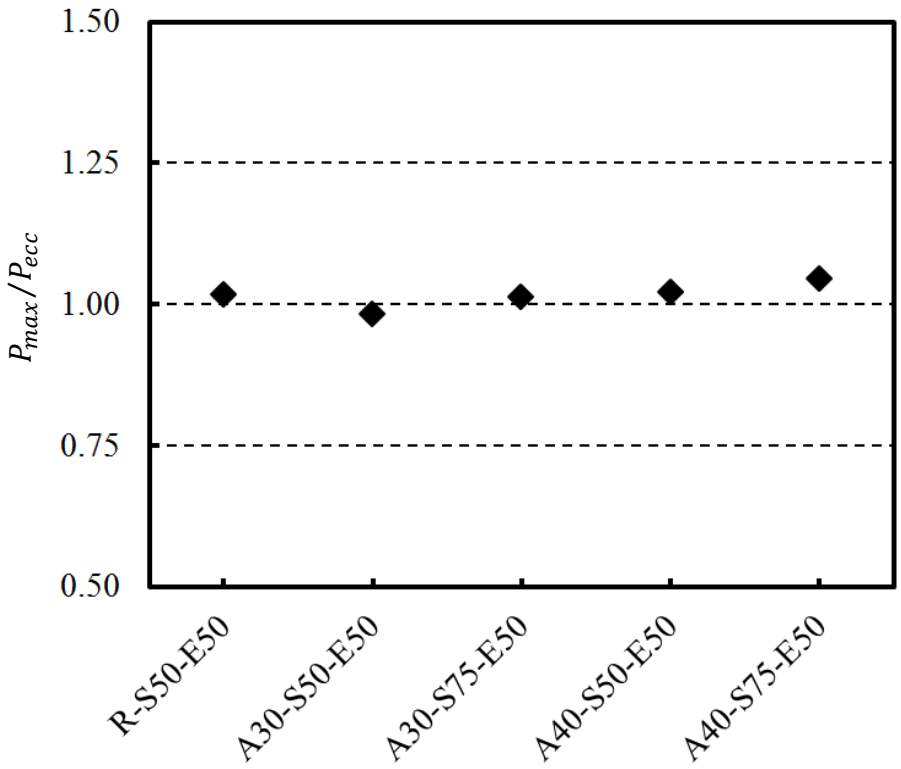

Figure 9.4 Experimental maximum eccentric axial loads to predicted eccentric axial load capacities of specimens tested under 50 mm eccentric axial load

9.3 Maximum Tie Spacing for RC Column Specimens

For reinforced concrete (RC) columns, the requirements of transverse tie spacing were provided by ACI (2014) to not exceed 16 times longitudinal bar diameters, 48 times transverse tie diameters or the smallest side dimension of the columns. It can observed that the transverse tie spacing can be related to the longitudinal reinforcement diameter (16 bar diameter) by a simplified model, which can be assumed that the longitudinal reinforcement is a compressive structure simply supported between the two supports supplied only by the transverse reinforcement (ties) and the transverse support provided

by the concrete cover is ignored (Zadeh and Nanni 2012). For such a member to reach a strain value without buckling, this relationship can be expressed as follows:

$$A_s E_s \varepsilon_s \geq \frac{\pi^2 E_s I_s}{s^2} \tag{9.4}$$

where s is the tie spacing, ε_s is the strain of longitudinal reinforcement, which was assumed the tensile yield strength equal to 0.002 for steel reinforcement to yield prior to buckling (Zadeh and Nanni 2012). A_s, E_s and I_s are the area, the modulus of elasticity and the second moment of area of longitudinal reinforcement, respectively. For longitudinal reinforcement with a rounded section (N12 steel bar) and a steel equal angle (A30 and A40) sections, the Equation (9.5) can be expressed as follows:

$$s_{max} = \sqrt{\frac{\pi^2 I_s}{A_s \, \varepsilon_s}} \tag{9.5}$$

Figure 9.5 shows the maximum tie spacing using Equation (9.5) for three different types of longitudinal reinforcement types (N12 steel bar, A30 or A40 SEA sections). It can be observed that when using N12 steel bars as longitudinal reinforcement, the maximum spacing between transverse ties was 211 mm, which is in good agreement with 16 N12 steel bar diameter, which is recommended by ACI 318 (2014). However, it was obtained that when using A30 SEA sections as longitudinal reinforcement, the maximum spacing between transverse ties was 410 mm, which is equivalent to about 34 N12 steel bar diameter. Also, it can be observed that when using A40 SEA sections as longitudinal reinforcement, the maximum spacing between transverse ties was 552 mm, which is equivalent to about 46 N12 steel bar diameter.

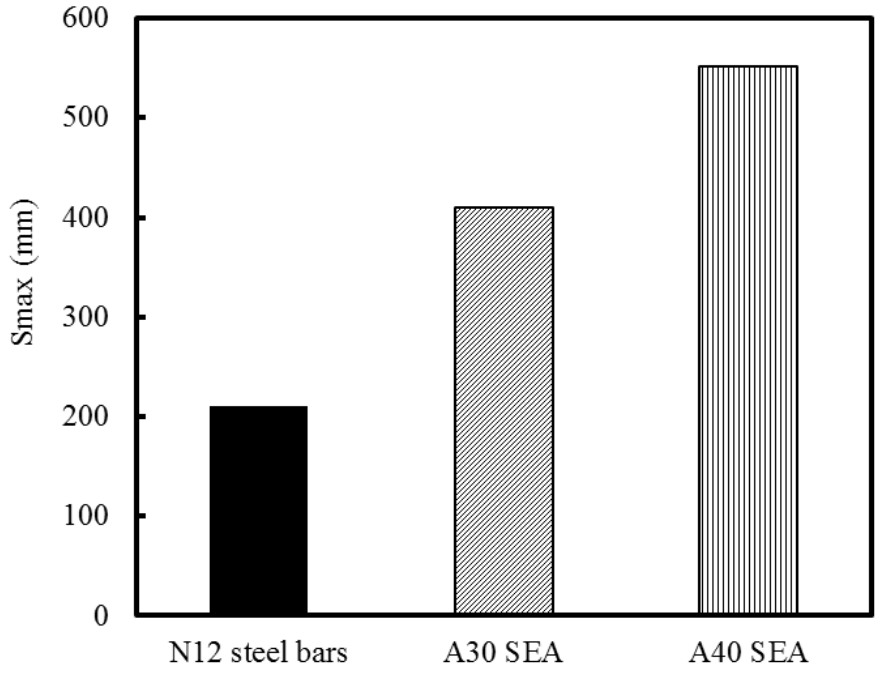

Figure 9.5 Maximum spacing of transverse ties for column specimens reinforced with N12 steel bars, A30 and A40 SEA sections

As mentioned above, the cross-sectional area of A30 SEA section was similar to the cross-sectional area of N12 steel bars. However, the average yield tensile strength of A30 SEA sections was 49% lower than the average yield tensile strength of N12 steel bars. Therefore, to investigate effects of the buckling length of longitudinal reinforcement (steel bars and SEA sections) on the strength and ductility of square HSC columns, specimens reinforced longitudinally with N12 steel bars compared with specimens reinforced longitudinally with A30 SEA sections with the spacing of transverse ties of 200 mm and 400 mm.

For example, if the experimental results of Specimens B-S200 (200 mm transverse tie spacing) and A30-S200 (200 mm transverse tie spacing) are compared, it can be observed that the maximum axial load (2399 kN) and ductility (1.5) of Specimen B-S200 were lower than the maximum axial load (2469 kN) and ductility (1.6) of Specimen A30-S200. Also, it can be seen from Figure 9.6 that for transverse tie spacing of 400 mm, the maximum axial load sustained by specimen B-S400 was 1717 kN, which is 42.5% less than Specimen A30-S400. Also, it was found that the maximum axial load of Specimen A30-S400 with the spacing of transverse ties of 400 mm was greater than the maximum axial load of Specimen B-S200 with the spacing of transverse ties of 200 mm. This is indicated that the maximum spacing of transverse ties for specimens reinforced longitudinally with SEA sections is much higher than the maximum spacing of transverse ties for specimens reinforced longitudinally with N12 steel bars. This means that the buckling length of longitudinal reinforcement was lager for specimens reinforced with SEA sections than for specimens reinforced with steel bars. In other words, if the same strength and ductility improvements are desired, N12 steel bar specimens shall require more amounts of transverse ties than those of the SEA specimens. In conclusion, the use of SEA sections as longitudinal reinforcements not only increase the performance of concrete columns but also decrease the cost of the construction of members.

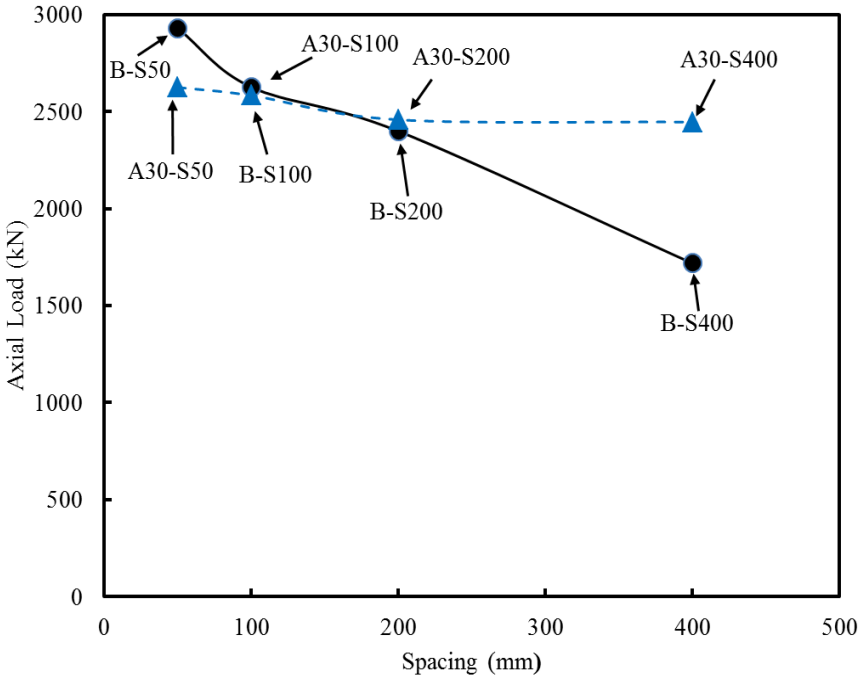

(a)

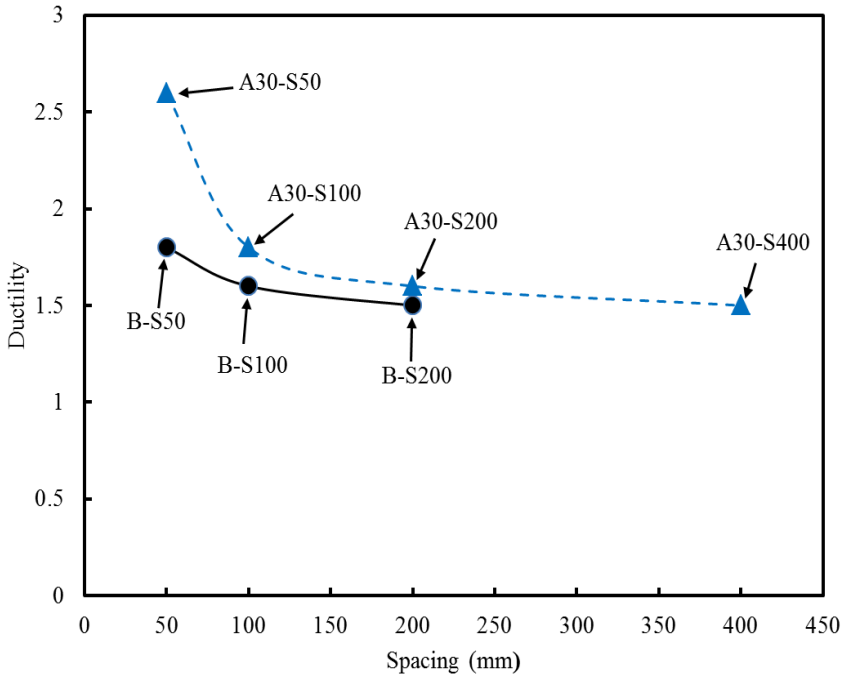

(b)

Figure 9.6 Influence of transverse tie spacing on (a) Maximum axial load and (b) Ductility

9.4 Concrete Column Confined by Tie Reinforcement

Under the application of axial compression, the concrete experience longitudinal shortens and laterally expands due to Poisson's effect. Transverse reinforcement can be used to restrain the lateral expansions of concrete that create a triaxle state of stress, which leads to improved compressive strength and axial deformation of the RC columns. In the case of square concrete reinforced with transverse ties, the effectively confined concrete core is smaller than the concrete core area (Mander et al. 1988b; Saatcioglu and Razvi 1992; Cusson and Paultre 1995; Foster 1999). The reduction in the effectively confined concrete core area due to the lateral pressure is non-uniform in the square columns, which leads to marginal strength improvement. The magnitude of reduction in the effectively confined concrete core area can be affected by the tensile strength, spacing, volumetric ratio of transverse reinforcement and also by the spacing and number of longitudinal reinforcement (Tobbi et al. 2014). Therefore, the concrete core area under axial compression can be divided into unconfined and confined areas. To define these areas, it was assumed that arching action had taken position laterally between longitudinal reinforcement and longitudinally between transverse reinforcement, as shown in Figure 9.7. The unconfined concrete core area between longitudinal reinforcement is assumed as a parabolic arch with a 45^{o} tangent slope (Sheikh and Uzumeri 1982).

The concept of Sheikh and Uzumeri (1982) was modified by Mander et al. (1988b) to formulate the confinement effectiveness coefficient (k_e), which represents the ratio of

the smallest effectively confined concrete core area to the nominal concrete core area. The expression of the relationship can be written as follows:

$$k_e = \frac{\left[1 - \frac{\sum w_i^2}{6c_x c_y}\right]\left[1 - \frac{s'}{2c_x}\right]\left[1 - \frac{s'}{2c_y}\right]}{1 - \rho_c} \tag{9.6}$$

where $\sum w_i^2$: is sum of the squares of the clear horizontal spacing (w_i) between the longitudinal reinforcement along the perimeter of the cross-section; *s'* is the clear vertical spacing between two layers of transverse bars of diameter *dh*; c is the lateral dimension of the column core (c_x and c_y apply to rectangular sections) and ρ_c is the area ratio of the longitudinal reinforcement to the column core section.

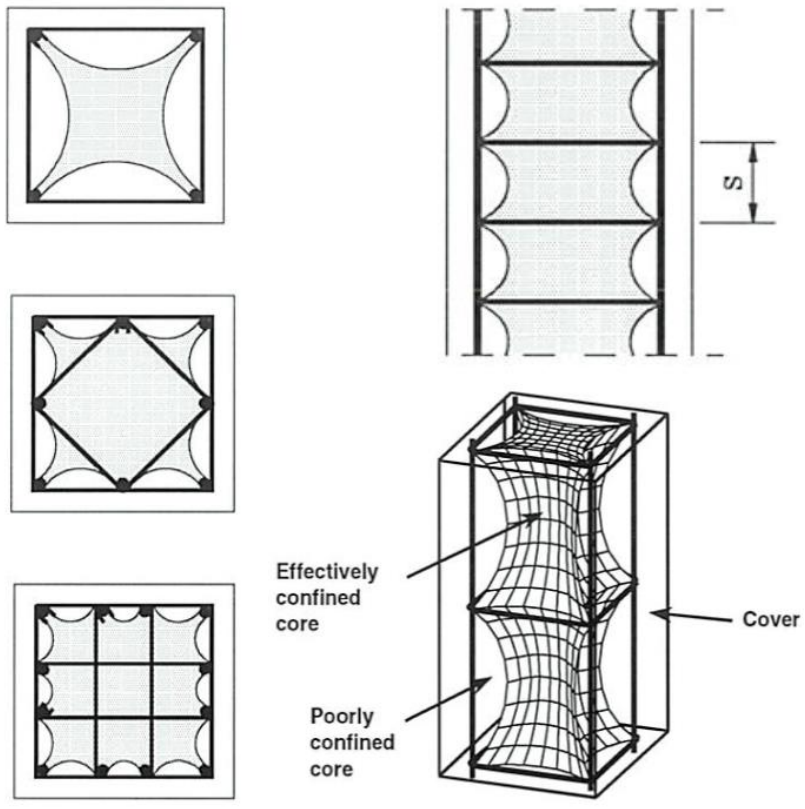

Figure 9.7 effectively confined area in tied reinforced concrete columns (Foster 1999)

9.4.1 **Influence of The SEA Sections on The Effectively Confinement of the Concrete Core**

For specimens reinforced longitudinally with SEA sections, a similar approach was assumed to predict the unconfined and confined concrete core areas. The difference between specimens reinforced longitudinally with steel bars and specimens reinforced longitudinally with SEA sections is only in the geometry of longitudinal reinforcement. In the case of specimens reinforced with steel bars, the longitudinal reinforcement has a round cross-section while in the case of specimens reinforced with SEA sections; the longitudinal reinforcement has an equal angle cross-section which leads to increase the volume of the effectively confined concrete core area, as shown in Figure 9.8.

The concrete arching action provided by the transverse ties and different types of longitudinal reinforcement (steel bars, A30 and A40 SEA sections) is presented in Figure 9.8. The advantage effect of steel equal angle (SEA) sections on the confinement of the concrete core can be observed by comparing Figure 9.8(a) and (b). It can be seen that the clear distance between longitudinal reinforcement reduces when using SEA sections as longitudinal reinforcement, which results in increasing k_e in calculating the effective transverse confining pressure of square HSC columns reinforced with SEA sections. It can be concluded that the synergies between the transverse and longitudinal arching action provide form and volume of the effectively confined concrete core area. Therefore, reduction spacing between transverse and longitudinal reinforcement leads to increased volume of the effectively confined concrete core area, leading to enhancement in both strength and ductility of columns.

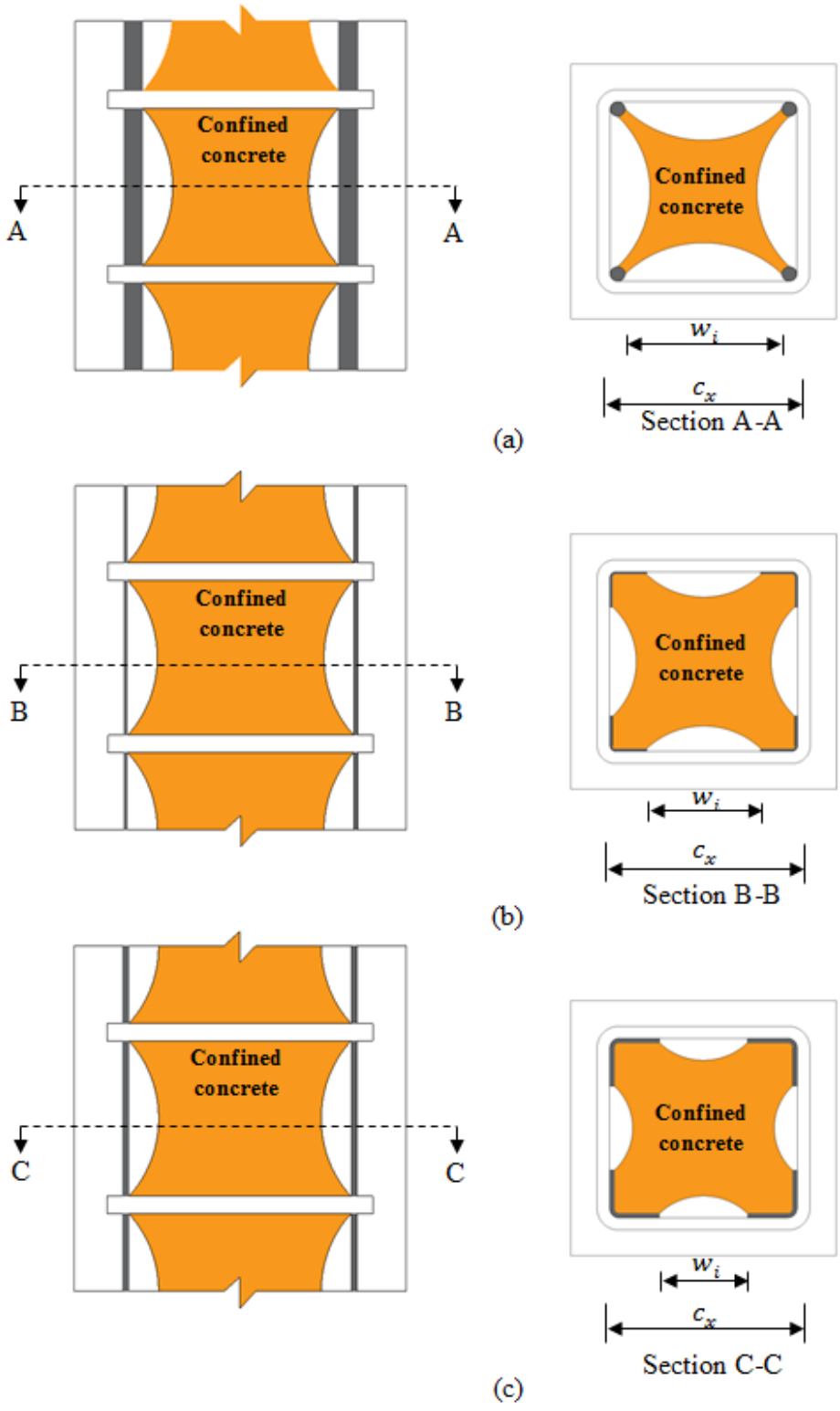

Figure 9.8 Arching action in confined concrete columns: (a) Transverse ties and N12 steel bars, (b) Transverse ties and A30 SEA sections and (b) Transverse ties and A40 SEA sections

9.5 Analytical Modelling

9.5.1 **Analytical Consideration of Material Properties**

The stress-strain models of the constituent materials used in this study are described in the following sections. The concrete cross-sectional area of each specimen can be divided into two parts: the unconfined concrete (concrete cover) and the confined concrete (concrete core). For both of two parts (the concrete cover and core), the stress-strain relationship for high strength concrete (HSC) proposed by Cusson and Paultre (1995) was used.

9.5.1.1 Stress-Strain Behaviour of Concrete

The analytical stress-strain model is classified into two parts (Figure 9.9). The first part is the ascending branch and the second part is the descending branch. The ascending branch is a relationship originally proposed by Popovics (1973) for normal strength concrete and later modified by Cusson and Paultre (1995) for high strength concrete (HSC), has been adopted in this study to model the compressive stress in the ascending branch of the specimen's stress-strain behaviour. The following equation was used to calculate the stress-strain curve in the ascending branch:

$$f_c = f_{cc}\left[\frac{k\left(\frac{\varepsilon_c}{\varepsilon_{cc}}\right)}{k-1+\left(\frac{\varepsilon_c}{\varepsilon_{cc}}\right)^k}\right] \qquad \varepsilon_c \leq \varepsilon_{cc} \qquad (9.7)$$

The k factor, which is controled the initial slope and the curvture of the ascending branch, is estimated by Equation (9.8).

where $$k = \frac{E_c}{E_c - \left(\frac{f_{cc}}{\varepsilon_{cc}}\right)} \quad (9.8)$$

where f_c and ε_c are compressive stress and the corresponding strain of the concrete, respectively. f_{cc} and ε_{cc} are compressive confined stress and the corresponding strain of the concrete, respectively. The elastic modulus of the concrete (E_c) was calculated according to ACI 363 R-10 (ACI 2010)

$$E_c = 6.9 + 3.32\sqrt{f_c'} \quad (9.9)$$

where f_c' is the unconfined concrete strength in MPa, which was obtained from a standard concrete cylinder test at 28-days.

The use of transverse reinforcements in concrete columns results in lateral restricting of the concrete core, leading to enhance in both strength and post-peak behaviour of concrete. In this study, the descending branch of the stress-strain response of square HSC columns confined by transverse ties is based on the stress-strain model was proposed by Cusson and Paultre (1995) for HSC columns. The following equation was used to calculate the stress-strain curve in the descending branch:

$$f_c = f_{cc}\, exp(k_1(\varepsilon_{c50c} - \varepsilon_{cc})^{k_2}) \qquad \varepsilon_c \geq \varepsilon_{cc} \quad (9.10)$$

where f_{cc}, ε_{cc} and ε_{c50c} are etimated by Equations (9.11), (9.12) and (9.13), respecively and the factors k_1 and k_2 are estimated by Equations (9.14) and (9.15), respectively.

$$f_{cc} = f_c' \left[1 + 2.1 \left(\frac{f_l'}{f_c'} \right)^{0.7} \right] \tag{9.11}$$

$$\varepsilon_{cc} = \varepsilon_{co} + 0.21 \left(\frac{f_l'}{f_c'} \right)^{1.7} \tag{9.12}$$

$$\varepsilon_{c50c} = 0.004 + 0.15 \left(\frac{f_l'}{f_c'} \right)^{1.1} \tag{9.13}$$

$$k_1 = \frac{ln0.5}{(\varepsilon_{c50c} - \varepsilon_{cc})^{k_2}} \tag{9.14}$$

$$k_2 = 0.58 + 16 \left(\frac{f_l'}{f_c'} \right)^{1.4} \tag{9.15}$$

where k_1 and k_2 are the coefficient affecting the slope and curvature, respectively, of the descending branch of the stress-strain curve. The effective lateral confining pressure f_l' is calculated by Equation (9.16).

$$f_l' = k_e f_l \tag{9.16}$$

where f_l is lateral confinement pressure on the confined concrete from transverse ties and k_e is the effective confinement coefficient, which represents the ratio of the smallest effectively confined concrete core area to the nominal concrete core area. The expression of the relationship can be written as follows:

$$k_e = \frac{\left(1 - \frac{\sum w_i^2}{6c_x c_y}\right)\left(1 - \frac{s'}{2c_x}\right)\left(1 - \frac{s'}{2c_y}\right)}{(1 - \rho_{cc})} \tag{9.17}$$

where w_i is the clear spacing between adjacent longitudinal reinforcement, $s'$is the clear spacing between transverse ties, c_x and c_y are the are the width of the concrete core parallel to the x- and y- axes, respectively and ρ_{cc} is the ratio of the longitudinal reinforcment area to the confined core area.

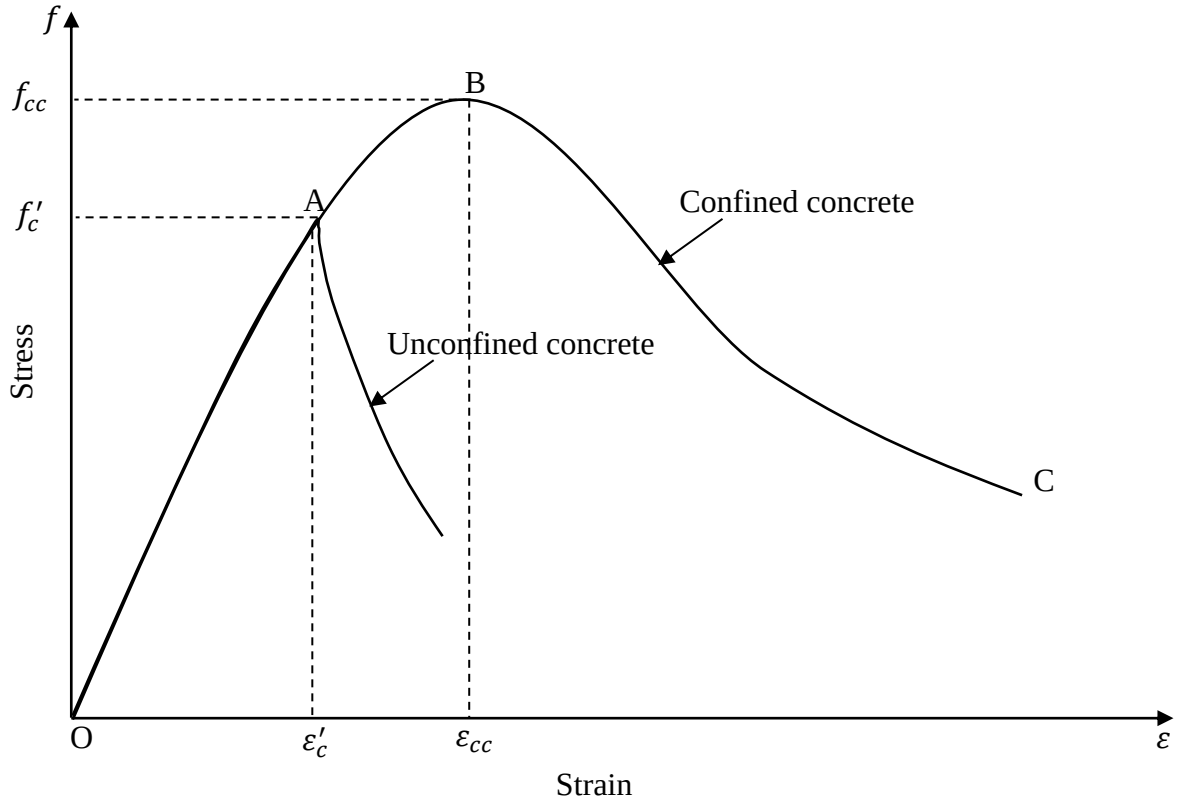

Figure 9.9 Stress-strain behaviour of concrete

9.5.1.2 Stress-Strain behaviour of Longitudinal Reinforcement

The stress-strain behaviour of the longitudinal reinforcements is assumed bilinear elastic-perfectly plastic behaviour for both steel bars and SEA sections, as shown in Figure 9.10. Therefore, the stress in the longitudinal reinforcements was calculated by the following equations:

$$f_s = \varepsilon_s E_s \qquad \varepsilon_s \leq \varepsilon_{sy} \tag{9.18}$$

$$f_s = f_{sy} \qquad \varepsilon_s > \varepsilon_{sy} \tag{9.19}$$

where f_s and ε_s are the tensile stress and the corresponding strain of the longitudinal reinforcements (steel bars and SEA sections). f_{sy} and ε_{sy} are the yield tensile stress and the coressponding strain of the longitudinal reinforcements (steel bars and SEA sections)

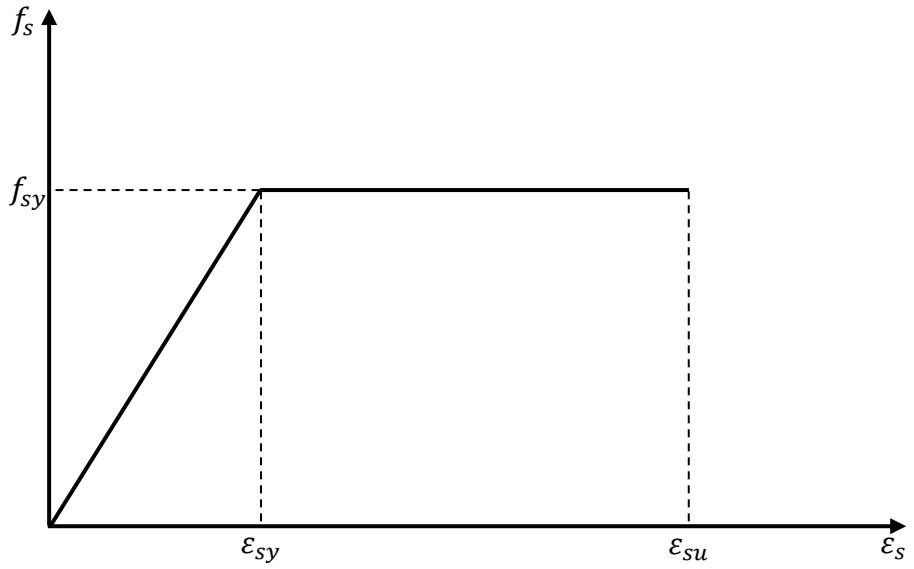

Figure 9.10 Stress-strain relationships of longitudinal reinforcement (steel bars and SEA sections)

9.6 Predicted Axial Load-Axial Deformation Behaviour of the Tested Specimens

The analytical stress-strain behaviour of the tested specimens converted into an axial load-axial deformation behaviour. The following assumptions were used to predict the analytical axial load-axial deformation behaviour of the tested specimens: The concrete during the ascending branch of stress-strain response is marginally affected by the transverse reinforcement (Paultre et al. 2010). Hence, the axial load of specimens was calculated by multiplying the stress of concrete during ascending branch (OA) of stress-strain curve (Figure 9.9) and the cross-section area of the specimen (concrete cover and core). After the maximum compressive strain of unconfined concrete (ε_{co}), it was assumed that the concrete cover spalling or crushing, which means that only the concrete core of specimens is effective. Therefore, the axial loads of specimens were calculated by multiplying the stress of concrete during the ascending branch (AB) and the area of the concrete core. In addition, the axial loads of specimens in the descending branch (BC) were calculated by multiplying the confined concrete stress and the area of the concrete core. Also, it was assumed that there is a perfect bond between the concrete and the longitudinal reinforcement (steel bars or SEA sections). The elastic-perfectly plastic stress-strain curve for longitudinal reinforcement was used, which means that the strain hardening of longitudinal steel reinforcement is neglected (Shin et al. 2016). This is because the local buckling of longitudinal reinforcement occurs earlier than the strain hardening at inelastic stage (Pantazopoulou 1998; Bai and Au 2011), consequently, the strain hardening in the compression longitudinal reinforcement is not considered. Also, it can be seen that the clear distance between longitudinal reinforcement reduces when using SEA sections as longitudinal reinforcement, which results in increasing the

confinement effectiveness coefficient (k_e) in calculating the effective transverse confining pressure of square HSC columns reinforced with SEA sections. Therefore, reducing the spacing between longitudinal reinforcement leads to increased volume of the effectively confined concrete core area, leading to enhancement in both strength and ductility of columns.

9.7 Comparison between Experimental and Analytical Axial Load-Axial Deformation Behaviour of The Tested Columns

The analytical axial load-axial deformation behaviours for the square HSC columns reinforced with either steel bars or SEA sections were established to complement the experimental results. Figures 9.11 to 9.15 presents comparisons between the experimental and analytical axial load-axial deformation behaviours of the tested column specimens with 800 mm height. Also, Figures 9.16 to 9.21 presents comparisons between the experimental and analytical axial load-axial deformation responses of the tested specimens with 600 mm height. The analytical axial load-axial deformation responses of the tested specimens were calculated based on the stress-strain model that was proposed by Cusson and Paultre (1995). The model was based on the square high strength concrete (HSC) columns with the spacing of transverse ties ranged between 23 mm and 100 mm. Therefore, only the experimental axial load-axial deformation behaviours of the tested specimens reinforced transversely with the spacing of 50 mm, 75 mm and 100 mm were compared with the analytical results using Cusson and Paultre'model.

9.7.1 **Column Specimens with 800 mm Height**

Of the 20 Specimens with 800 mm height, 5 Specimens (R-S50-C, A30-S50-C, A30-S75, A40-S50-C and A40-S75-C) were tested under concentric axial load. Figures 9.11 to 9.15 present comparisons between the analytical and experimental axial load-axial deformation behaviours of the tested specimens. It can be seen from these Figures that the ascending branches of the analytical axial load-axial deformation curves of the tested column specimens were nearly linear and similar to the ascending branches of the experimental axial load-axial deformation curves of the tested column specimens up to the maximum axial load. Also, it can be observed that analytical descending branch of axial load-axial deformation curve for Specimen R-S50-C that was reinforced longitudinally with steel bars match very well with the experimental descending branch of axial load-axial deformation curve. However, the analytical descending branches of the most specimens reinforced longitudinally with SEA sections are steeper than the experimental descending branches. This may be because Cusson and Pualtre's model adopted based on the square HSC columns reinforced longitudinally with steel bars. It is noted that the tested specimens that were reinforced longitudinally with SEA sections are more efficiency confined concrete core area than specimens reinforced longitudinally with steel bars, which showed higher descending branch slope compared to analytical results. In general, it can be concluded that there is a reasonable agreement between the analytical and experimental axial load-axial deformation behaviours for the tested specimens, particularly for specimens reinforced longitudinally with N12 steel bars.

Table 9.1 compares the analytical maximum axial load of Specimens R-S50-C, A30-S50-C, A30-S75, A40-S50-C and A40-S75-C with the corresponding experimental results. For specimens reinforced longitudinally with N12 steel bars, the analytical maximum axial load of Specimen R-S50-C was 95% of the experimental maximum axial load. For the specimens reinforced with A30 SEA sections, the analytical maximum axial loads of Specimens A30-S50-C and A30-S75-C were 103% and 90%, respectively, of the experimental maximum axial loads. For the specimens reinforced longitudinally with A40 SEA sections, the analytical maximum axial loads of Specimens A40-S50-C and A40-S75-C were 99% and 100%, respectively, of the experimental maximum axial loads. In general, the experimental maximum axial load obtained from tested specimens is very well matched with the maximum axial load calculated from Cusson and Pualtre's model.

Table 9.1 Analytical and Experimental results of Specimens with 800 mm height and tested under concentric axial loads

Specimen	Spacing of transverse ties (mm)	Maximum axial load (kN)		$\frac{\text{Analytical}}{\text{Experimental}}$ %
		Experimental P_{max}	Analytical P_{ana}	
R-S50-C	50	2716	2593	95
A30-S50-C	50	2548	2613	103
A30-S75-C	75	2749	2488	90
A40-S50-C	50	2977	2944	99
A40-S75-C	75	2747	2756	100

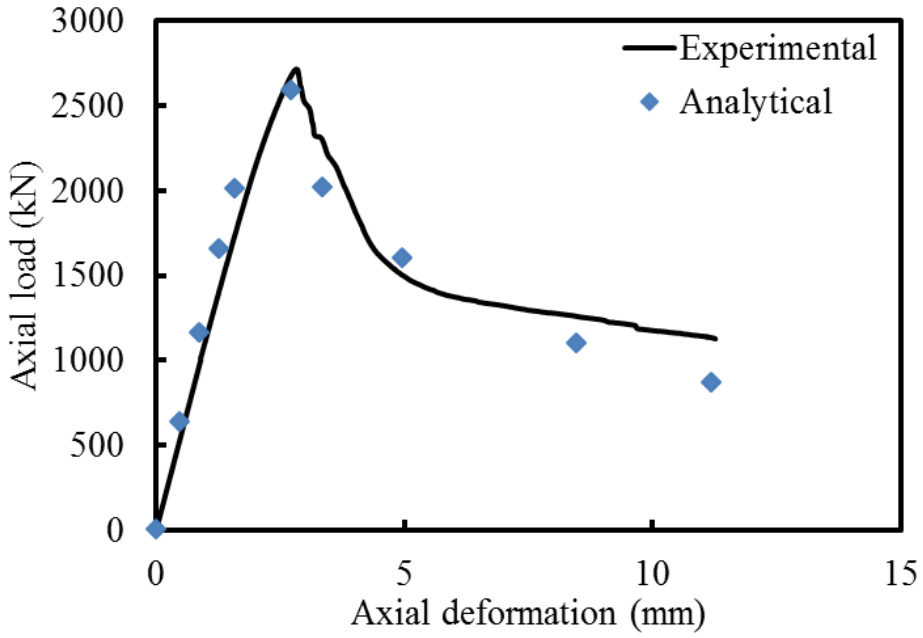

Figure 9.11 Comparison between analytical and experimental axial load-axial deformation behaviour of the tested Specimen R-S50-C

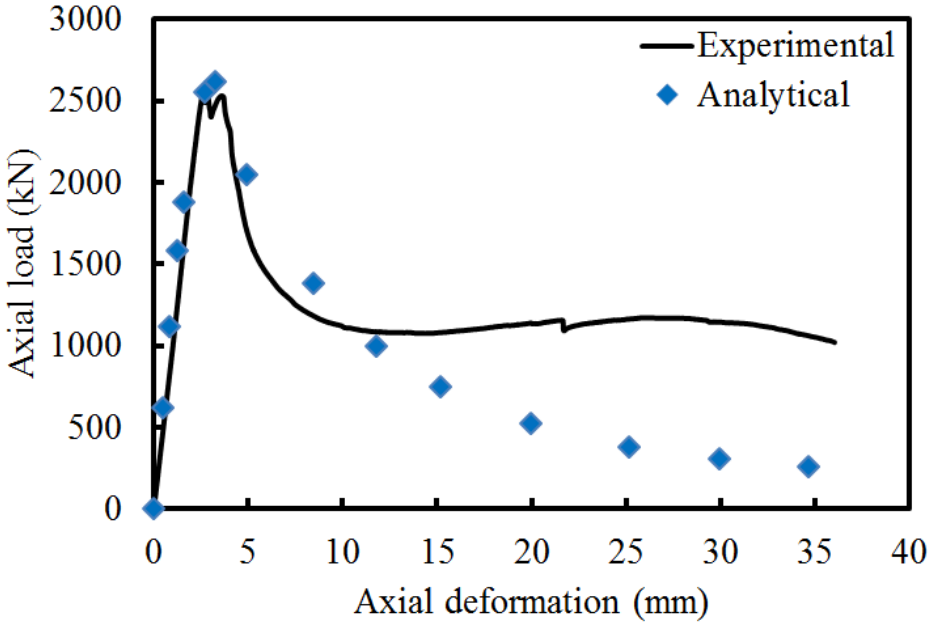

Figure 9.12 Comparison between analytical and experimental axial load-axial deformation behaviour of the tested Specimen A30-S50-C

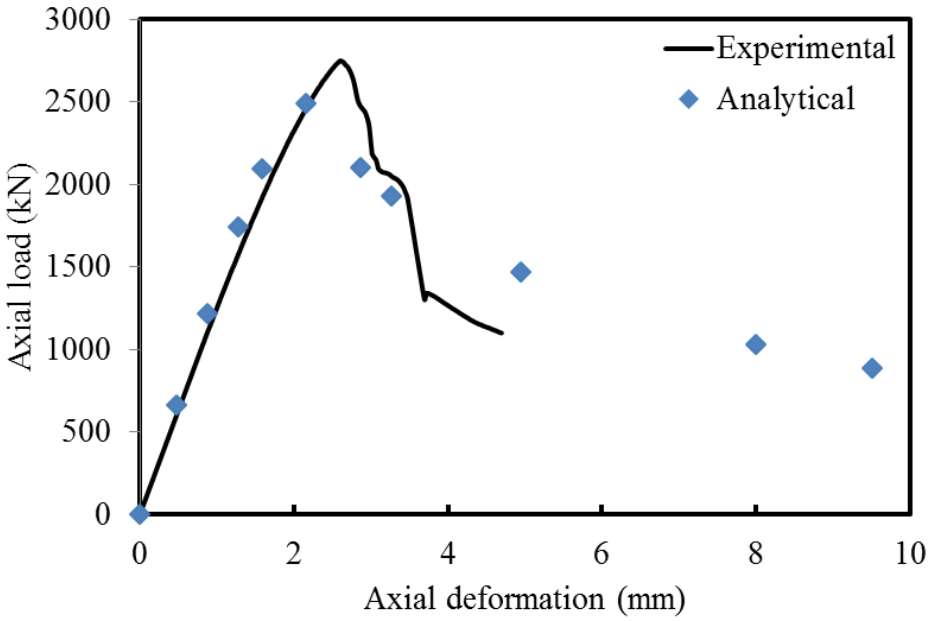

Figure 9.13 Comparison between analytical and experimental axial load-axial deformation behaviour of the tested Specimen A30-S75-C

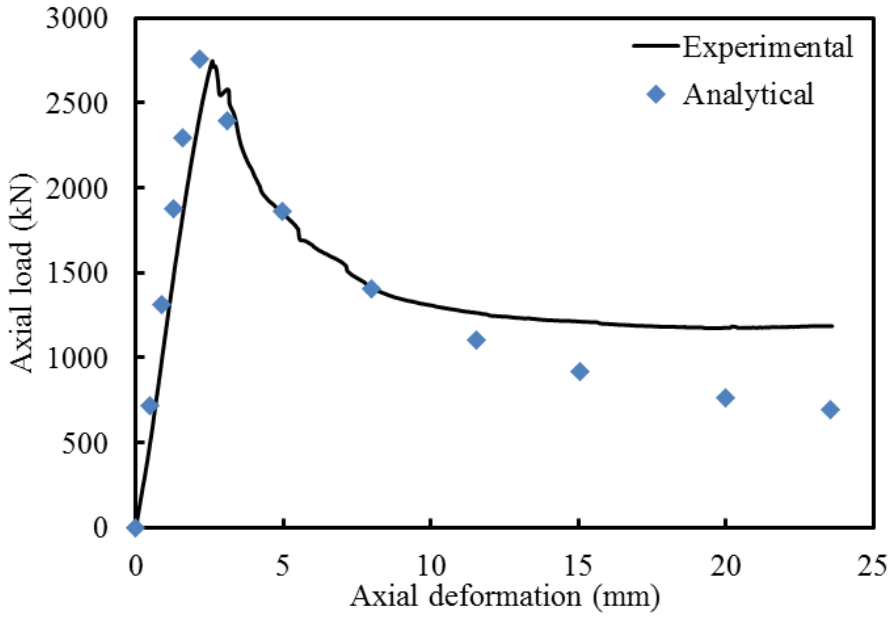

Figure 9.14 Comparison between analytical and experimental axial load-axial deformation behaviour of the tested Specimen A40-S50-C

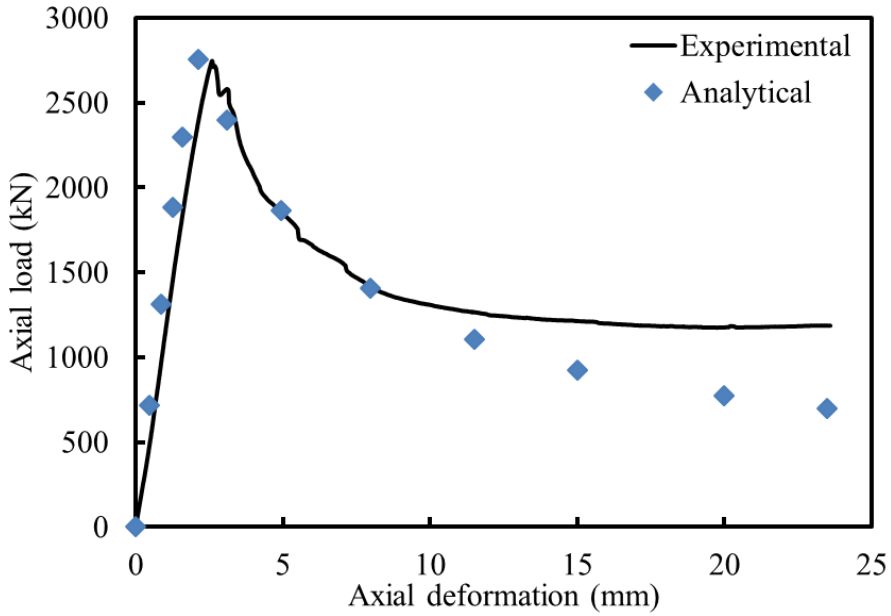

Figure 9.15 Comparison between analytical and experimental axial load-axial deformation behaviour of the tested Specimen A40-S75-C

9.7.2 **Column Specimens with 600 mm Height**

9.7.2.1 Column Specimens of the B Group

Figures 9.16 and 9.17 present the comparisons between the analytical and experimental axial load-axial deformation responses of Specimens B-S50 and B-S100, respectively. It was observed that the ascending branch of the analytical axial load-axial deformation behaviour of Specimen B-S50 was similar to the ascending branch of the experimental axial load-axial deformation behaviour. However, it was found that the slope of the ascending branch of the analytical axial load-axial deformation curve of Specimen B-S100 had a slightly greater stiffness than the slope of the ascending branch of the experimental axial load-axial deformation curve. This is because the longitudinal reinforcement in Specimen B-S50 with transverse tie spacing of 50 mm tends to fail by

yielding, whereas the longitudinal reinforcement in Specimens with transverse tie spacing of transverse of 100 mm tends to fail by buckling of longitudinal reinforcement. Also, it can be observed that the slope of the descending branches of the analytical axial load-axial deformation curves for Specimens B-S50 and B-S100 are less steep than the slope of the descending branches of the experimental axial load-axial deformation curves.

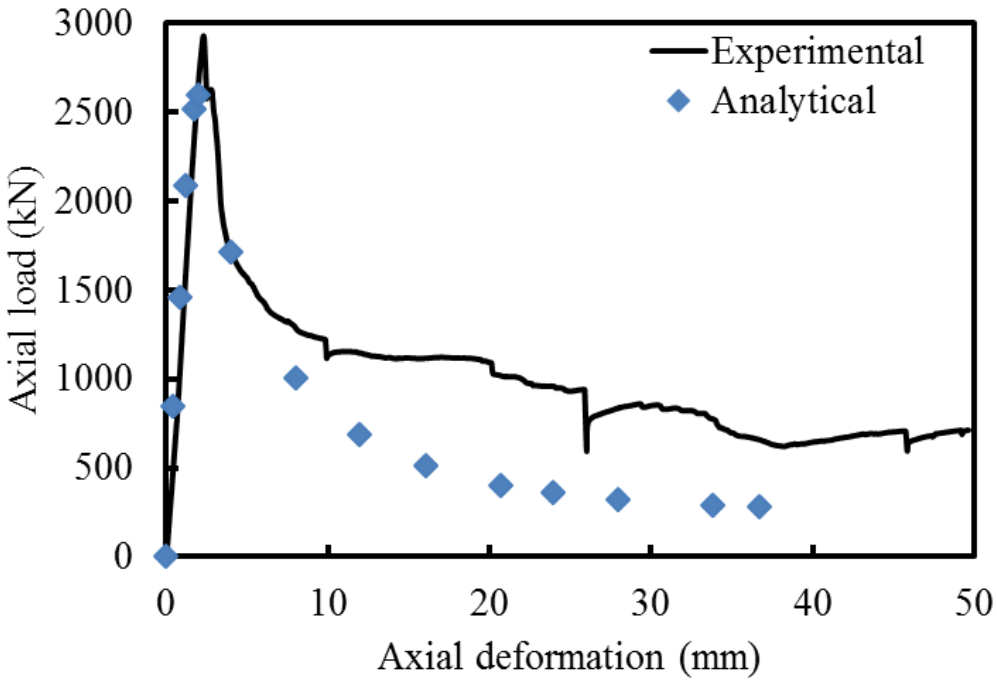

Figure 9.16 Comparison between analytical and experimental axial load-axial deformation behaviour of the tested Specimen B-S50

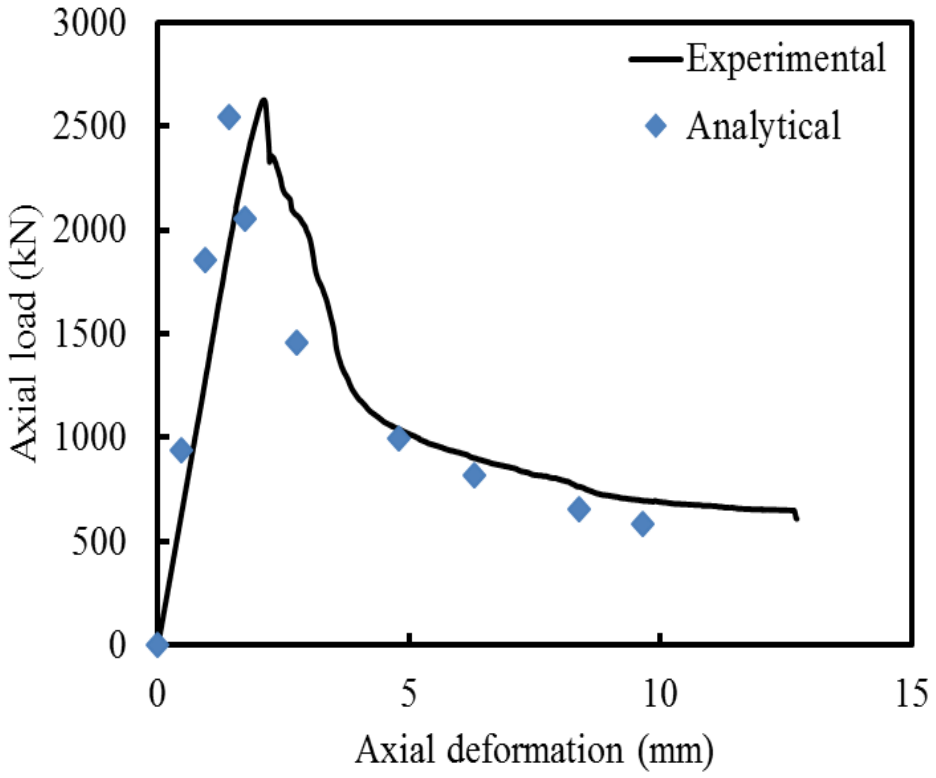

Figure 9.17 Comparison between analytical and experimental axial load-axial deformation behaviour of the tested Specimen B-S100

Table 9.2 compares the analytical maximum axial load of Specimens B-S50 and B-S100 with the corresponding experimental results. It was found that the analytical maximum axial load of Specimen B-S50 is 89% of the corresponding experimental maximum axial load. The reason for the difference between analytical and experimental maximum axial load of Specimen B-S50 is because the closer spacing of transverse ties (50 mm) in Specimen B-S50 created a separation plane between the concrete cover and the concrete core which resulted in instability of the concrete cover shell and cover spalling at an early stage. Consequently, the spalling of the concrete cover led to some reduction in axial load capacity of columns. Similar observations were reported by Razvi and Saatcioglu (1994) and Awati and Khadiranaikar (2012). Also, it was found that the

analytical maximum axial load of Specimen B-S100 was 97% of the corresponding experimental maximum axial load. This value is close to 100, which is indicated a good agreement between analytical and experimental results.

Table 9.2 Analytical and Experimental Results of Group B specimens

Group	Specimen	Spacing of transverse ties (mm)	Maximum axial load (kN)		$\frac{\text{Analytical}}{\text{Experimental}}$ %
			Experimental P_{max}	Analytical P_{ana}	
B	B-S50	50	2929	2593	89
	B-S100	100	2626	2544	97

9.7.2.2 Column Specimens of the A30 Group

Figures 9.18 and 9.19 present the comparisons between the analytical and experimental axial load-axial deformation behaviours of Specimens A30-S50 and A30-S100, respectively. It was observed that the ascending branches of the analytical axial load-axial deformation curves of the Specimens A30-S50 and A30-S100 are similar to the ascending branches of the experimental axial load-axial deformation curves. However, the descending branches of the analytical axial load-axial deformation curves of Specimens A30-S50 and A30-S100 are seriously less steep than the descending branches of the experimental axial load-axial deformation curves. This may be because the presence of SEA sections as longitudinal reinforcement resulted in increasing the

buckling length of the longitudinal reinforcement and provided good confinement of the concrete core in the post-peak behaviours.

Table 9.3 compares the analytical maximum axial load of Specimens A30-S50 and A30-S100 with the corresponding experimental results. It was reported that the analytical maximum axial loads of the Specimens A30-S50 and A30-S100 were 99% and 94%, respectively, of the experimental maximum axial loads. These values are close to 100, which is indicated a good agreement between analytical and experimental results.

Table 9.3 Analytical and Experimental Results of Group A30 specimens

Group	Specimen	Spacing of transverse ties (mm)	Maximum axial load (kN)		$\frac{\text{Analytical}}{\text{Experimental}}$ %
			Experimental P_{max}	Analytical P_{ana}	
A30	A30-S50	50	2626	2613	99
	A30-S100	100	2619	2466	94

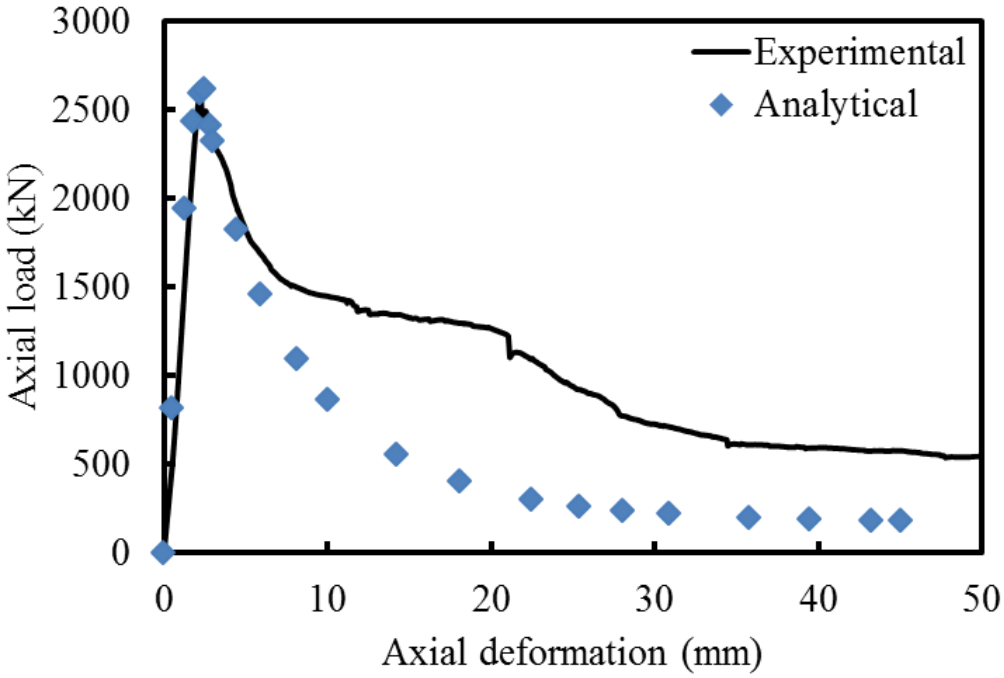

Figure 9.18 Comparison between analytical and experimental axial load-axial deformation behaviour of the tested Specimen A30-S50

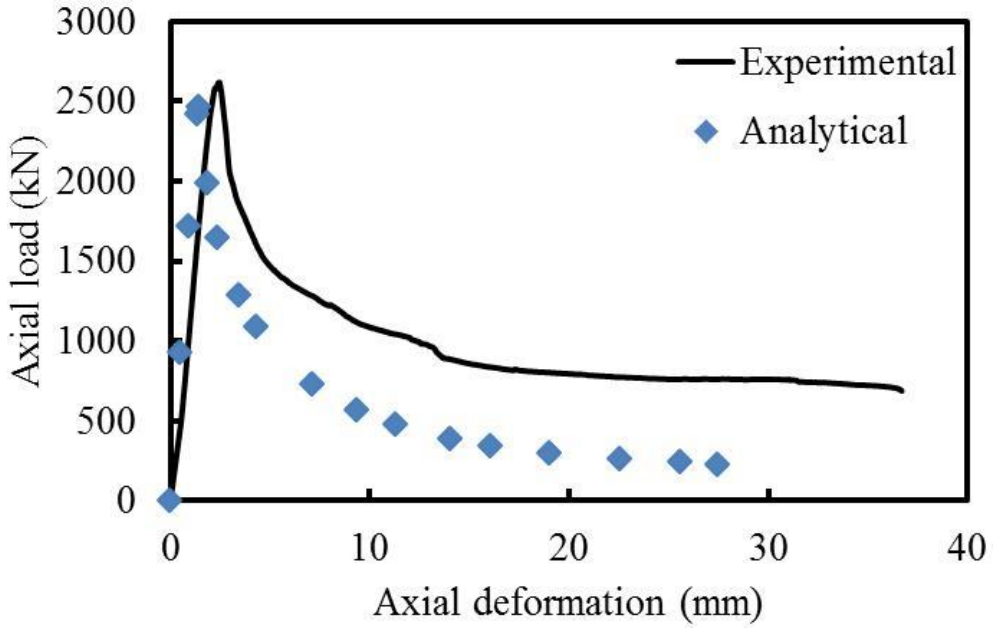

Figure 9.19 Comparison between analytical and experimental axial load-axial deformation behaviour of the tested Specimen A30-S100

9.7.2.3 Column Specimens of the A40 Group

Figures 9.20 and 9.21 present the comparisons between the analytical and experimental axial load-axial deformation behaviours of Specimens A40-S50 and A40-S100, respectively. It can be seen that the slope of the ascending of the analytical axial load-axial deformation curve of Specimen A40-S50 is similar to the corresponding slope of the branch of the experimental axial load-axial deformation curve. However, it was found that the slope of the ascending branch of analytical axial load-axial deformation curve of Specimen A40-S100 is slightly stiffer than the corresponding slope of the descending branch of the experimental descending branch of axial load-axial deformation curve. Also, it can be observed that the slope of the descending branches of the analytical axial load-axial deformation curves of Specimens A40-S50 and A40-S100 are is considerably steeper than the slope of the descending branches of the experimental axial load-axial deformation curves.

Table 9.4 compares the analytical maximum axial load of Specimens A40-S50 and A40-S100 with the corresponding experimental results. It can be observed that the analytical maximum axial load of Specimens A40-S50 and A40-S100 are 98% and 97%, respectively, of the corresponding experimental maximum axial load. This value is close to 100, which is indicated a good agreement between analytical and experimental results.

Table 9.4 Analytical and Experimental Results of Group A40 specimens

Group	Specimen	Spacing of transverse ties (mm)	Maximum axial load (kN)		Analytical / Experimental %
			Experimental P_{max}	Analytical P_{ana}	
A40	A40-S50	50	3009	2943	98
	A40-S100	100	2836	2747	97

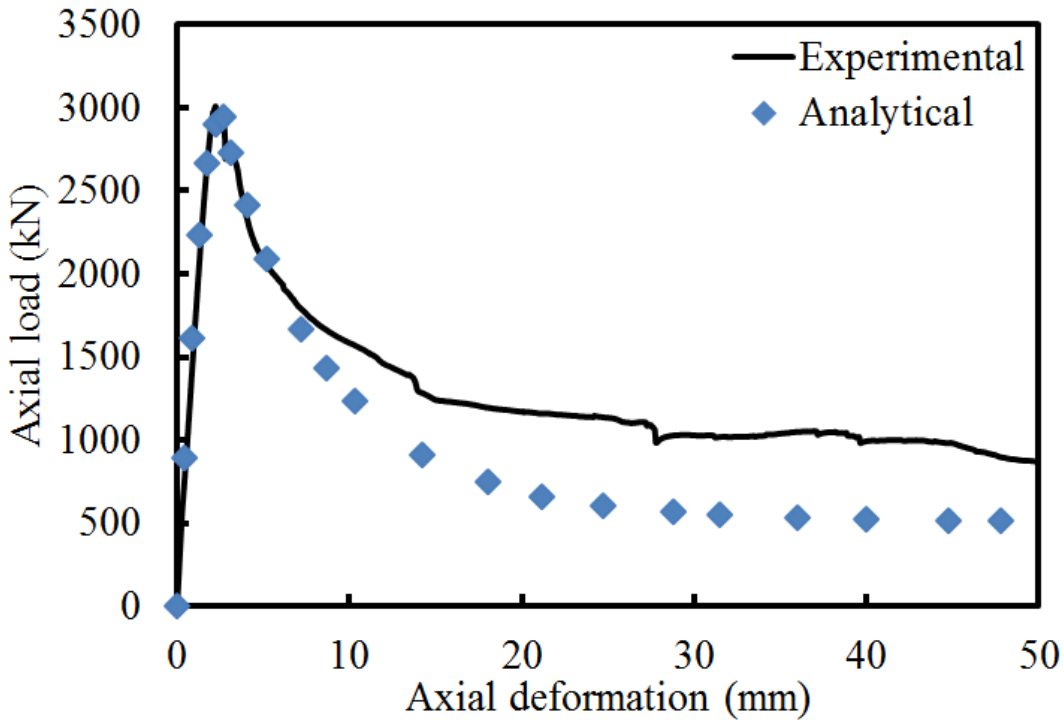

Figure 9.20 Comparison between analytical and experimental axial load-axial deformation behaviour of the tested Specimen A40-S50

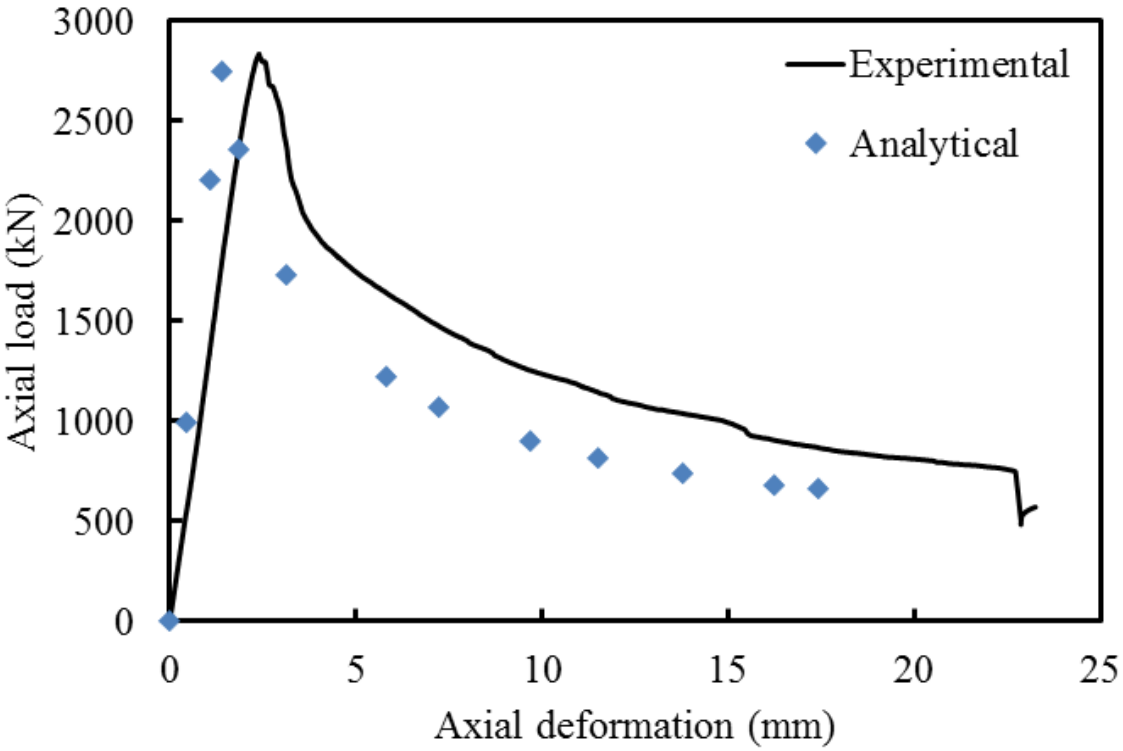

Figure 9.21 Comparison between analytical and experimental axial load-axial deformation behaviour of the tested Specimen A40-S100

9.8 Summary

In this chapter, the analytical results of 21 column specimens were evaluated and discussed. The nominal load carrying capacities of the specimens with 800 mm and 600 mm height that were tested under concentric and eccentric axial loads were presented and compared with the corresponding experimental results. The maximum spacing of transverse ties of specimens reinforced longitudinally with SEA sections was also presented and compared with the maximum spacing of transverse ties of specimens reinforced longitudinally with conventional steel bars. Furthermore, the analytical axial

load-axial deformation behaviours of the tested specimens with 800 mm and 600 mm height using an available stress-strain model were presented and compared with the experimental axial load-axial deformation curves.

Based on the comparisons between analytical and experimental results in this chapter, it is concluded that the nominal load carrying capacities of the tested specimens under concentric and eccentric axial loads are in good agreement with the experimental results. Also, the buckling load of longitudinal reinforcement was larger for specimens reinforced longitudinally with SEA sections compared to the specimens reinforced longitudinally with steel bars. Consequently, to achieve same strength and ductility, the specimens reinforced with steel bars need more amounts of transverse ties than those of the specimens reinforced longitudinally with SEA sections. Also, the analytical stress-strain model, which was used in this chapter, give reasonable estimates of the axial load-axial deformation behaviour.

The next chapter presents the experimental and analytical axial loads and bending moment interaction diagrams using the equivalent rectangular stress block method and the layer-by-layer numerical integration method, which are used to analyse square HSC specimen cross-sections.

10 AXIAL LOAD-BENDING MOMENT (*P-M*) INTERACTION DIAGRAMS

10.1 General

The main aim of this chapter is the examination of the axial load-bending moment (*P-M*) interaction diagrams for steel equal angle (SEA) reinforced concrete (RC) columns. To achieve this aim, a total of 20 specimens having 210 mm square cross-section and 800 mm height were tested under different loading conditions including concentric axial load, 25 mm eccentric axial load, 50 mm eccentric axial load and four-point bending (flexural bending). In this chapter, the axial load-bending moment (*P-M*) interaction analysis is conducted for square high strength concrete (HSC) columns reinforced longitudinally with either steel bars or steel equal angle (SEA) sections and laterally with R10 steel bars. The *P-M* interaction diagrams were constructed based on four points: firstly, the column specimens tested under concentric axial load. Secondly, the column specimens tested under 25 mm eccentricity. Thirdly, the column specimens tested under 50 mm eccentricity and fourthly the specimens tested under four-point bending (pure bending moment). Two analytical methods of predicting the *P-M* interaction diagram were used. The first method is based on the strain compatibility and force equilibrium (the equivalent rectangular stress block method). The second method is based on the cross section of the specimens divided into thin layers (layer-by-layer numerical integration method). Finally, the analytical *P-M* interaction diagrams are compared with the corresponding experimental *P-M* interaction diagrams.

10.2 Experimental *P-M* Interaction Diagrams

To describe the axial load and bending moment carrying capacity for tested specimens, an experimental axial load-bending moment *(P-M)* interaction diagrams were constructed based on four points. The first point on the *P-M* interaction diagram represents pure axial compression. The second and third points on *P-M* interaction diagram represent 25 mm and 50 mm eccentric axial loads, respectively. The fourth point on the *P-M* interaction diagram represents pure bending moment (four-point bending). The experimental *P-M* interaction diagrams were constructed by using experimental results, which collected during the test procedure. For 25 mm and 50 mm eccentrically loaded column specimens, the bending moment capacity (*M*) of the specimens was determined to value both the primary (M_1) and secondary (M_2) bending moments. The calculation of primary bending moment (M_1) was determined by multiplying the maximum concentric axial load and the applied initial eccentricity (e). The calculation of secondary bending moment (M_2) was also determined by multiplying the maximum concentric axial load and the summation applied initial eccentricity and lateral deformations (Δ) at mid-height of the column specimen at the maximum axial load. The experimental *P-M* interaction diagrams for the specimens are shown in Figure 10.1.

$$M = P(e + \Delta) \tag{10.1}$$

where M is the bending moment value, and P is the maximum load; e initial eccentricity (25 mm and 50 mm).

The bending moment capacity (M) of specimens tested as beams under four-point bending was calculated as:

$$M = \frac{P}{2}a \tag{10.2}$$

where P is the maximum load applied to the beam specimen with four-point bending apparatus; a is the length of the shear span, or the distance from the support to the closer loading point (in this study $a = 233$ mm).

The experimental axial load-bending moment (*P*-*M*) interaction diagrams of R-S50, A30-S50 and A30-S75 groups are presented in Figure 10.1. Specimen A30-S50-C exhibited only 6.6% smaller maximum axial load than Specimen R-S50-C. This lower maximum axial load may be attributed to the fact that N12 steel bars in Specimen R-S50-C had 49% higher yield tensile strength than A30 GSEA sections in Specimen A30-S50-C. The maximum axial load of Specimen A30-S50-E25 was 8.8% less than the maximum axial load of Specimen R-S50-E25. Specimen A30-S50-E50 achieved only 6.3% lower maximum axial load compared to Specimen R-S50-E50. Specimen A30-S50-E25 showed only 5.0% lower bending moment than Specimen R-S50-E25. Specimen A30-S50-E50 was 7.9% lower bending moment than Specimen R-S50-E50. It can be noted that the maximum axial load and bending moment of R-S50 specimens tested under concentric and eccentric axial loads were greater than those of A30-S50 specimens. This may be because N12 steel bars had 49% higher yield tensile strength than A30 SEA sections. However, Specimen A30-S50-F showed 7.1% greater bending moment than Specimen R-S50-F. This was because the bending stiffness of a SEA

section was greater than the bending stiffness of a steel bar for the similar cross-sectional area. In addition, the SEA section has a higher second moment of area and radius of gyration than the conventional steel bar for the same cross-sectional area.

Specimens A30-S75-C and R-S50-C had about the similar maximum axial loads. Specimen A30-S75-E50 showed only 3.3% less maximum axial load than Specimen R-S50-E50. This is because that the combination of different yield tensile strengths (N12 steel bars and A30 SEA sections) and different spacing of transverse ties (50 mm for R-S50-E50 and 75 mm for A30-S75-E50). Despite, the spacing of transverse ties in Specimen A30-S75-E50 was 75 mm and in Specimen R-S50-E50 was 50 mm, Specimens A30-S75-E50 and R-S50-E50 had about the similar bending moments. However, Specimen A30-S75-F showed 7.1% greater bending moment than Specimen R-S50-F because A30 SEA sections had higher bending stiffness than steel bars.

Specimen A30-S50-C was 7.9% less maximum axial load than Specimen A30-S75-C. This may be because the closer spacing of transverse ties in Specimen A30-S50-C led to the formation of a natural separation plane between the concrete core and the concrete cover, which can result in dropping in axial load resistance. A similar behaviour was observed in Saatcioglu and Razvi (1998) in which the test results of high strength concrete columns with square sections under concentric compression. The maximum axial load of Specimen A30-S50-E50 exhibited 2.9% lower than the maximum axial load of Specimen A30-S75-E50. Also, the decrease in the bending moment was 6.7% for Specimen A30-S50-E50 relative to the bending moment of Specimen A30-S75-E50. Specimen A30-S50-F and A30-S75-F had about the similar bending moments. This

may be attributed to that the confinement effect due to lateral reinforcement in the beams is not significant at peak load. Similar observations were reported in Rashid and Mansur (2005) and Kwan et al. (2006).

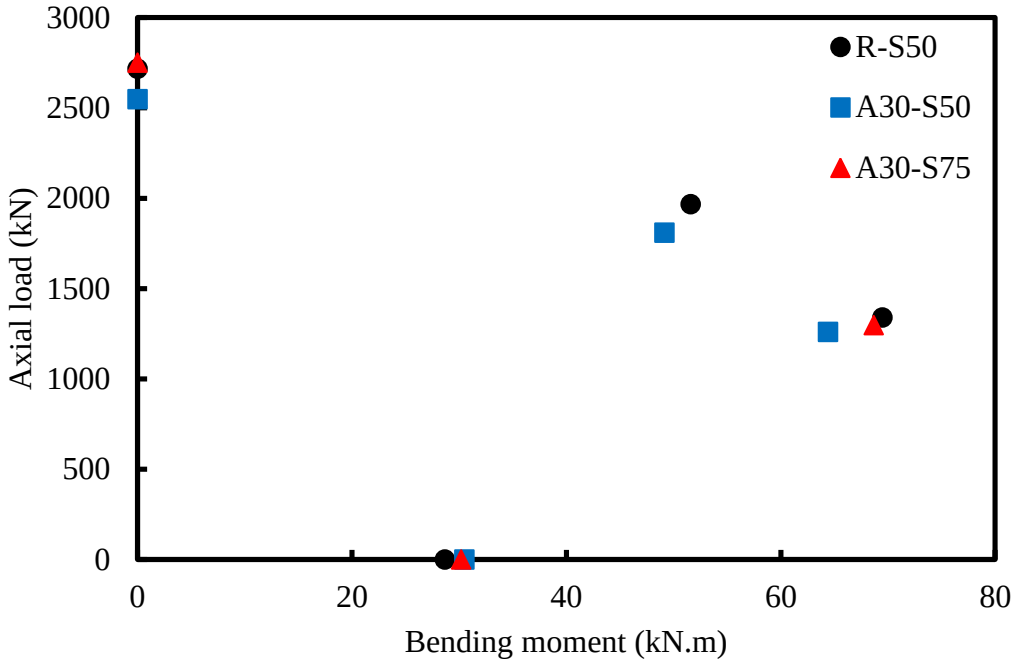

Figure 10.1 Experimental axial load-bending moment interaction diagrams of R-S50, A30-S50 and A30-S75 groups

The experimental axial load-bending moment (*P*-*M*) interaction diagrams of R-S50, A40-S50 and A40-S75 groups are also presented in Figure 10.2. Specimen A40-S50-C was 9.6% higher maximum axial load than Specimen R-S50-C. The maximum axial load of Specimen A40-S50-E25 was 3.3% greater than the maximum axial load of Specimen R-S50-E25. Specimen A40-S50-E50 exhibited 8.7% greater maximum axial load than Specimen R-S50-E50. The bending moment of Specimen A40-S50-E25 was 3.4% higher than the bending moment of Specimen R-S50-E25. Specimen A40-S50-E50 exhibited 12.0% greater bending moment than Specimen R-S50-E50. However,

Specimen A40-S50-F showed about 107% greater bending moment than Specimen R-S50-F. This is because A40 SEA sections had much higher bending stiffness than steel bars.

Specimens A40-S75-C and R-S50-C had about the similar maximum axial loads. Specimen A40-S75-E25 showed 5.4% smaller maximum axial load than Specimen R-S50-E25. Specimen A40-S75-E50 achieved 11.3% higher maximum axial load compared to Specimen R-S50-E50. Specimen A40-S75-E25 showed 2.5% smaller bending moment than Specimen R-S50-E25. However, Specimen A40-S75-E50 exhibited 12.9% higher bending moment than Specimen R-S50-E50. Also, the bending moment of Specimen A40-S75-F was about 107% higher than bending moment of Specimen R-S50-F. This is because A40 SEA sections in Specimen A40-S75-F had much higher bending stiffness than N12 steel bars in Specimen R-S50-F as well as the cross-sectional area of A40 SEA section higher than the cross-sectional area of N12 SEA sections.

Specimen A40-S50-C exhibited 8.4% higher maximum axial load than Specimen A40-S75-C. It is noted that the transverse tie spacing of Specimen A40-S75-C was 75 mm and transverse tie spacing of Specimen A40-S50-C was 50 mm. The increase in the maximum axial load was 8.8% for Specimen A40-S50-E25 maximum relative to the maximum axial load of Specimen A40-S75-E25. However, Specimen A40-S50-E50 exhibited only 2.4% smaller maximum axial load than Specimen A40-S75-E50. The bending moment of Specimen A40-S50-E25 was 6.0% higher than the bending moment of Specimen A40-S75-E25. Also, Specimen A40-S50-E50 and A40-S75-E50 had about

the similar bending moments than Specimen. Specimens A40-S50-F and A40-S75-F had about the similar bending moments.

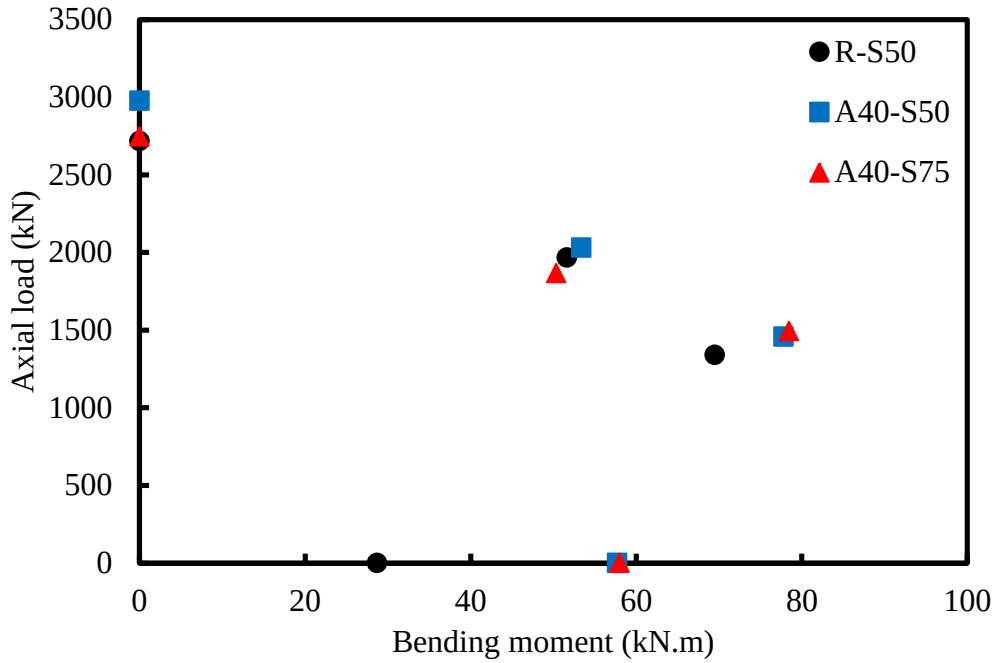

Figure 10.2 Experimental axial load-bending moment interaction diagrams of R-S50, A40-S50 and A40-S75 groups

10.3 Analytical Axial Load-Bending Moment (*P-M*) Interaction Diagrams

Analytical axial load-bending moment *(P-M)* interaction diagrams of R-S50, A30-S50, A30-S75, A40-S50 and A40-S75 groups were constructed using two methods. The first method is the equivalent rectangular stress block and the second method is the layer-by-layer integration. These two methods are explained in the following sections. To use the equivalent rectangular stress block and the layer-by-layer integration methods in

constructing the analytical *P-M* interaction diagrams of the reinforced concrete (RC) columns, the following assumptions were used:

1. The plane section remains plane after deformation and perpendicular to the neutral axis. Also, the distribution of concrete strain is assumed to be linear across the height of the section.

2. A perfect bond exists between concrete and steel reinforcement (steel bars and SEA sections).

3. The tensile strength of concrete is negligible.

4. Steel reinforcement (bars and SEA sections) behave as elastic-perfect plastic.

5. The confinement effect by the transverse reinforcement (ties) is neglected because the transverse reinforcement was assumed to increase only the ductility (Kim et al. 2012).

10.3.1 **Equivalent Rectangular Stress Block Method**

In this section, analytical axial load-bending moment *(P-M)* interaction diagrams were constructed to check whether the available analytical tools can predict the axial load-bending moment (*P-M*) interactions of HSC columns reinforced longitudinally with SEA sections. The *P-M* interaction diagrams were drawn based on the principles of strain compatibility and force equilibrium. This method is considered to construct *P-M* interaction diagrams for concrete specimens reinforced with steel bars. A similar procedure was applied to construct *P-M* interaction diagrams for concrete specimens reinforced longitudinally with SEA sections. The parameters of an equivalent rectangular stress block were calculated according to AS 3600 (2009). The stress

distributions are assumed to be uniform along the height of the cross section of column that having width of $\alpha_1 f_c'$ and depth of γd_n, as shown in Figures 10.3 and 10.4.

The *P-M* interaction diagrams can be generated based on four points (Warner et al. 2007). In this study, the *P-M* interaction diagrams of the tested specimens were drawn with four points, as shown in Figure 10.5. The first point (i) on the *P-M* interaction diagram represents pure axial compression. The second (ii) and third (iii) points on *P-M* interaction diagram represent 25 mm and 50 mm eccentric axial loads, respectively. The fourth point (iv) on the *P-M* interaction diagram represents pure bending moment (four-point bending). The axial load capacity of specimens under concentric axial load was calculated using Equation (10.3):

$$P_o = \alpha_1 f_c' \left(A_g - A_s\right) + f_y A_s \tag{10.3}$$

where A_g and A_s are the gross cross-sectional area of the column and cross-sectional area of longitudinal reinforcement, respectively; f_c' and f_y are the compressive strength of concrete and the yield tensile strength of the longitudinal reinforcement, respectively; and α_1 is the reduction factor, which was calculated according to Australian Standard AS 3600 (2009).

$$\alpha_1 = 1 - 0.003 f_c' \qquad 0.72 \leq \alpha_1 \leq 0.85 \tag{10.4}$$

The α_1 is a reduction factor that takes into account the differences in shape, concrete casting practice and size between standard concrete cylinders and concrete columns (Hognestad 1951; Ozbakkaloglu and Saatcioglu 2004; Afifi et al. 2013).

The compressive force C_c in the concrete is obtained the stress block method (AS 3600 2009).

$$C_c = \alpha_2 f_c' b \gamma d_n \tag{10.5}$$

$$\varepsilon_{sc} = \varepsilon_{cu} \frac{(d_n - d_{sc})}{d_n} \tag{10.6}$$

The strain in the compressive steel reinforcement was calculated as:

The stress in the compressive steel reinforcement was calculated as:

$$\sigma_{sc} = E_s \, \varepsilon_{sc} \qquad \varepsilon_{sc} < \varepsilon_{sy} \tag{10.7}$$

Or

$$\sigma_{sc} = f_{sy} \qquad \varepsilon_{sc} \geq \varepsilon_{sy} \tag{10.8}$$

Therefore, the force in the compressive steel reinforcement was calculated as:

$$C_s = \sigma_{sc} \, A_{sc} \tag{10.9}$$

Similarly, the stress in the tensile steel reinforcement was calculated as:

$$\sigma_{st} = E_s \, \varepsilon_{st} \qquad \varepsilon_{st} < \varepsilon_{sy} \tag{10.10}$$

Or

$$\sigma_{st} = f_{sy} \qquad \varepsilon_{st} \geq \varepsilon_{sy} \tag{10.11}$$

wheref_{sy}, ε_{sy} and E_s are the yield tensile stress, corresponding yield tensile strain and the modulus of elasticity of steel reinforcement. The tensile force in the tensile reinforcement can be calculated as:

$$T_s = \sigma_{st}\, A_{st} \tag{10.12}$$

The axial load capacity (P_u) and the bending moment (M_u) were calculated using Equations (10.13) and (10.14), respectively:

$$P_u = C_c + C_s - T_s \tag{10.13}$$

$$M_u = C_c\left(\frac{h}{2} - \frac{\gamma d_n}{2}\right) + C_s\left(\frac{h}{2} - d_{sc}\right) + T_s\left(d - \frac{h}{2}\right) \tag{10.14}$$

where C_c and C_s are the compressive force in concrete and longitudinal reinforcement, respectively, T_s is the tensile force in the tension reinforcement, h is the total high of the cross-section of the specimen. The factor γ was calculated based on the recommendations in AS 3600 (2009) ($\gamma = 1.05 - 0.007f_c'$ within the limit $0.67 \leq \gamma \leq 0.85$). The d_{sc} and d are distances from the extreme compression concrete fibre to the centroids of compressive longitudinal reinforcement and tensile longitudinal reinforcement, respectively. The d_n is the depth of the neutral axis.

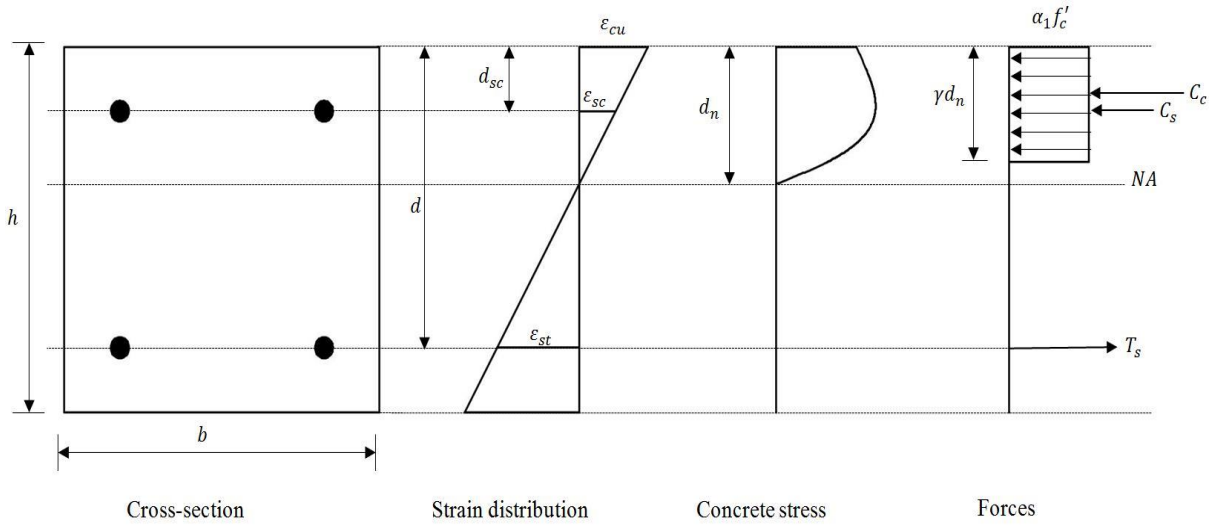

Figure 10.3 Stress-strain distribution and force equilibrium of steel bar specimens under eccentric axial compression

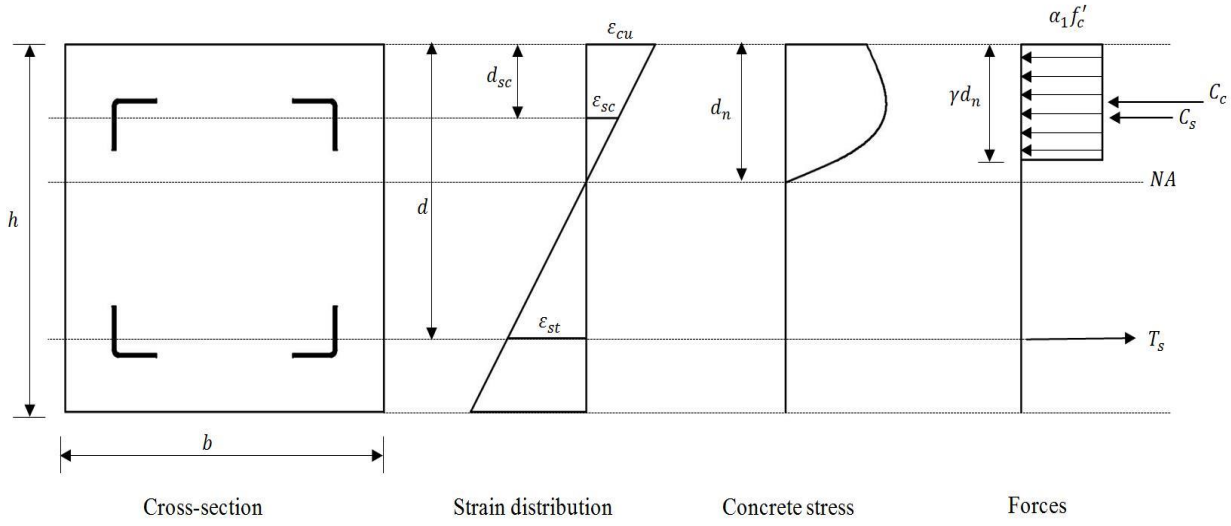

Figure 10.4 Stress-strain distribution and force equilibrium of SEA specimens under eccentric axial compression

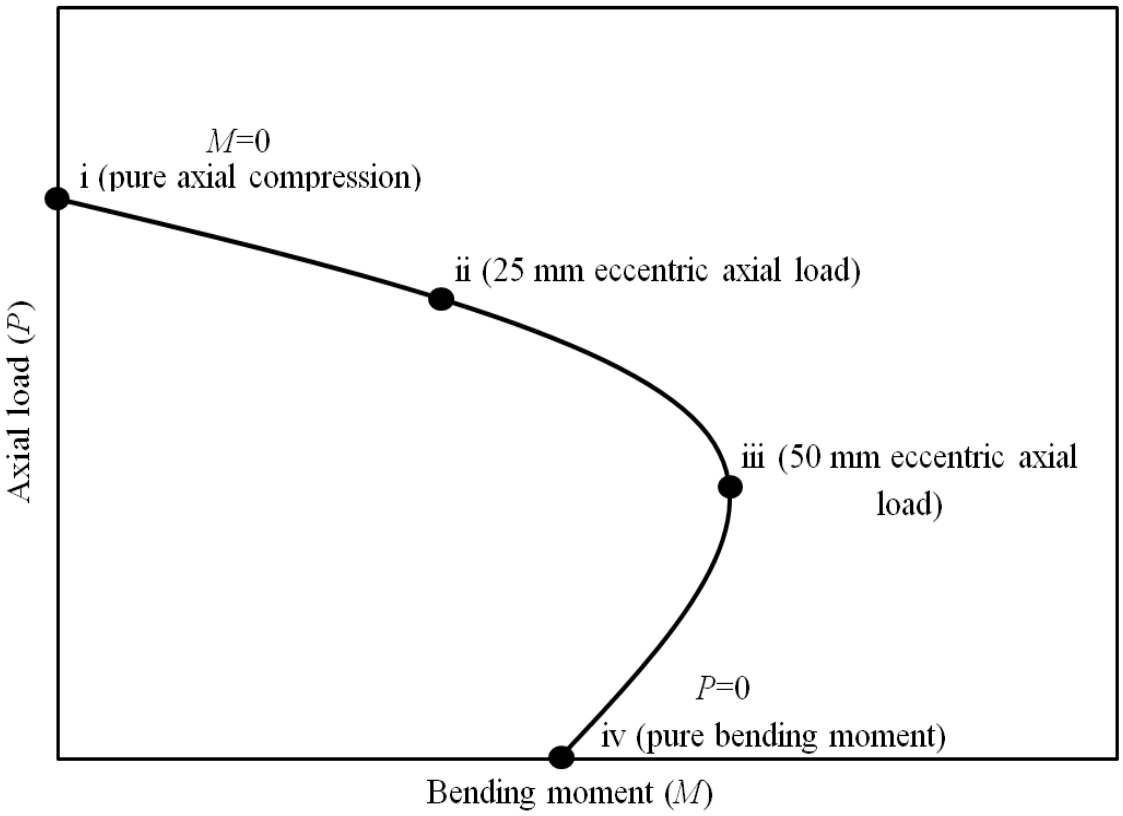

Figure 10.5 *P-M* interaction diagram

10.3.2 **The Layer-By-Layer Integration Method**

In this section, analytical axial load-bending moment *(P-M)* interaction diagrams were constructed based on the principles of layer-by-layer integration method. In the layer-by-layer integration method, the total depth (h) of the specimen is divided into layer-by-layer integration with a small thickness. The number of layers (n) was computed by divided the total depth of the cross section (h) by the thickness of each layer. In the present study, a value of 1 mm was selected as the thickness ($t_{cl,n}$) of each layer and 210 mm was taken as the width (b) of each layer (Figure 10.6). The nominal axial load capacity (P_o) of specimens tested under concentric axial load was determined according to AS 3600 (2009) as in Equation (10.3).

The strain in each concrete layer is assumed to be constant throughout the layer (Figure 10.6), which was calculated as shown in Equation (10.15). The ultimate compressive strain ε_{cu} at the extreme concrete fibre was assumed to be 0.003. The strain in the centre of each layer can be computed and the corresponding stress ($f_{cl,i}$) is estimated according to the unconfined high strength concrete stress-strain model proposed by Thorenfeldt et al. (1987) was used in this study to analyse the stress-strain behaviour of HSC under compressive strength. Then the force ($F_{cl,i}$) at the centre of each concrete layer was calculated by multiplying the stress and the area of concrete layer as shown in Equation (10.16). The bending moment ($M_{cl,i}$) of each layer was calculated by mutiplying the force ($F_{cl,i}$) in each concrete layer by the distance to the centrline of the corss section as shown in Equation (10.17)

$$\frac{\varepsilon_{cl,i}}{\varepsilon_{cu}} = \frac{d_n - \left(i * 1 - \frac{1}{2}\right)}{d_n} \tag{10.15}$$

$$F_{cl,i} = f_{cl,i} \times A_{cl,i} \tag{10.16}$$

$$M_{cl,i} = F_{cl,i}\left(\frac{h}{2} - \left(i * 1 - \frac{1}{2}\right)\right) \tag{10.17}$$

The stress-strain relationship for longitudinal reinforcement (steel bars and SEA sections) was assumed to be a simplified elastic-perfectly plastic. The force for each longitudinal reinforcement was calculated by multiplying the stress of longitudinal reinforcement by the cross sectional area of the longitudinal reinforcement

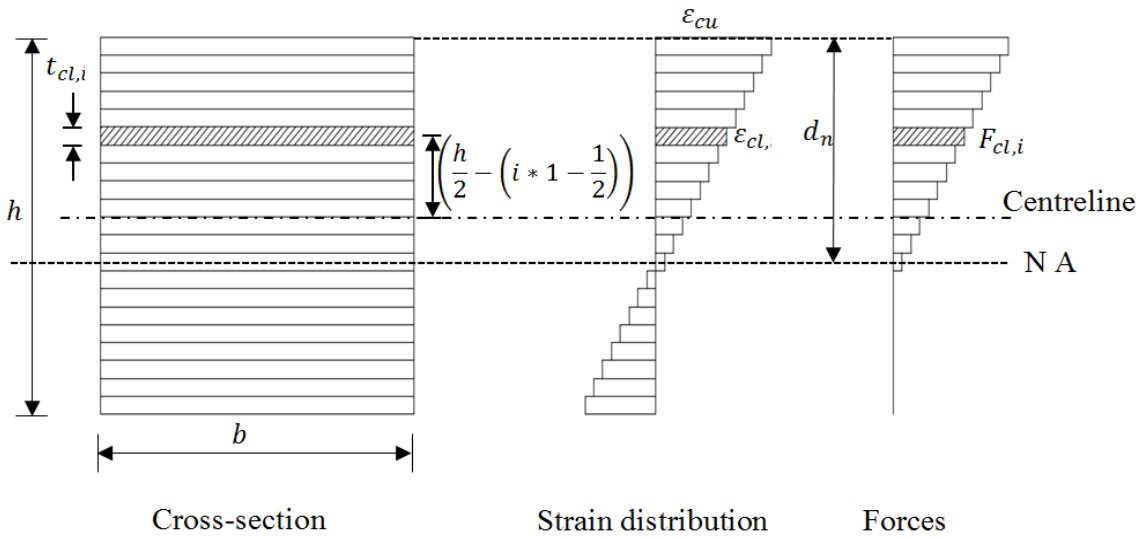

Figure 10.6 Strain distribution and force equilibrium of concrete under eccentric axial compression

10.4 Comparisons of Experimental and Analytical *P-M* Interaction Diagrams Using Equivalent Stress Block Method

In this section, the experimental axial load-bending moment (*P-M*) interaction diagrams were compared with the theoretical *P-M* interaction diagrams using the equivalent rectangular stress block method. The theoretical results based on the equivalent rectangular stress block method for Groups R-S50, A30-S50, A30-S75, A40-S50 and A40-S75 specimens are comparisons between the experimental and analytical *P-M* interaction diagrams are shown in Figures 10.7 to 10.11 and summarised in Table 10.1.

Figure 10.7 compares the Experimental and analytical axial load-bending moment (*P-M*) interaction diagrams of Group R-S50 specimens, which were reinforced longitudinally with four N12 steel bars and laterally with R10 steel bars at spaced 50

mm centre. Analytical maximum axial load of Specimen R-S50-C was 97% of the experimental maximum axial load. The analytical maximum axial loads of Specimens R-S50-E25 and R-S50-E50 were 101% and 104%, respectively, of the experimental maximum axial loads. Analytical bending moments of Specimens R-S50-E25 and R-S50-E50 were 97% and 100%, respectively, of the experimental bending moments. For specimen tested under four-point bending, the analytical bending moment of Specimen R-S50-F was 82% of the experimental bending moment. The reason for the differences between experimental and analytical bending moments under four-point bending was due to small shear span to depth ratio of the tested specimens. It can be noted that the analytical axial load-bending moment interaction diagrams match very well with the experimental axial load-bending moment interaction diagrams of R-S50 specimens.

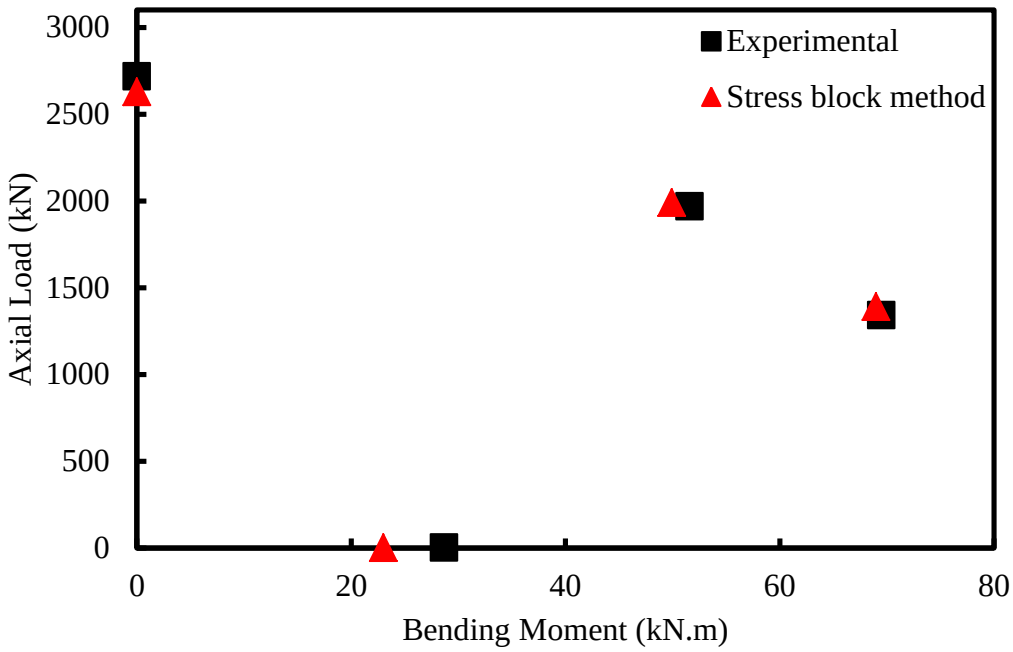

Figure 10.7 Comparison of analytical and experimental axial load-bending moment interaction diagrams for Group R-S50 specimens using equivalent rectangular stress block method

Figure 10.8 compares the experimental and analytical axial load-bending moment (*P-M*) interaction diagrams of Group A30-S50 specimens, which were reinforced longitudinally with our A30 steel equal angle (SEA) sections and laterally with R10 steel bars at spaced 50 mm centre. Analytical maximum axial load of Specimen A30-S50-C was 100% of the experimental maximum axial load. The analytical maximum axial loads of Specimens A30-S50-E25 and A30-S50-E50 were 107% and 106%, respectively, of the experimental maximum axial loads. Analytical bending moments of Specimens A30-S50-E25 and A30-S50-E50 were 98% and 105%, respectively, of the experimental bending moments. It can be observed that under concentric and eccentric axial load, the analytical results match well with the experimental of A30-S50 specimens. However, for specimen tested under four-point bending, the analytical bending moment of Specimen A30-S50-F was 63% of the experimental bending moment. The reason for the large differences between experimental and analytical bending moments under four-point bending was due to small shear span to depth ratio of the tested specimens. Another possible reason might be the analytical method did not adequately take into account the bending stiffness of the longitudinal reinforcement and also the analytical method originally derived for specimens reinforced longitudinally with conventional steel bars. Whereas, the bending stiffness of a steel bar is much lower than the bending stiffness of a SEA section with the similar cross-sectional area.

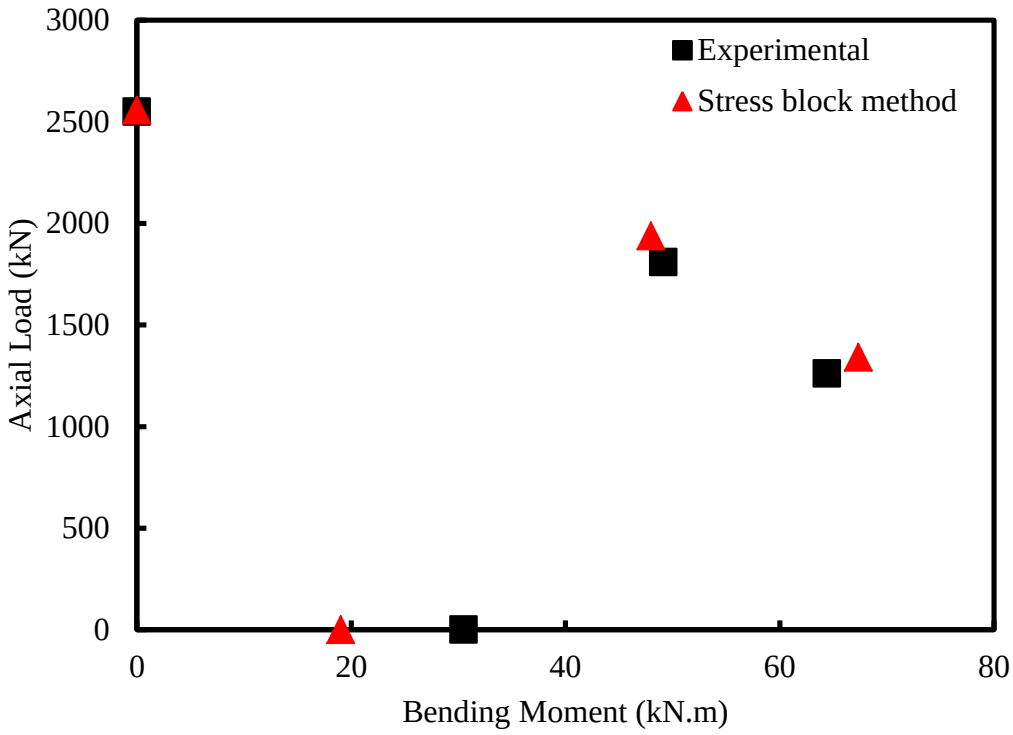

Figure 10.8 Comparison of analytical and experimental axial load-bending moment interaction diagrams for Group A30-S50 specimens using equivalent rectangular stress block method

Figure 10.9 compares the experimental and analytical axial load-bending moment (*P-M*) interaction diagrams of Group A30-S75 specimens, which were reinforced longitudinally with four A30 steel equal angle (SEA) sections and laterally with R10 steel bars at spaced 75 mm centre. Analytical maximum axial load of Specimen A30-S75-C was 93% of the experimental maximum axial load. The analytical maximum axial load of Specimen A30-S75-E50 was 103% of the experimental maximum axial load. Analytical bending moment of Specimen A30-S75-E50 was 97% of the experimental bending moments. However, for specimen tested under four-point bending, the analytical bending moment of Specimen A30-S75-F was 63% of the experimental bending moment.

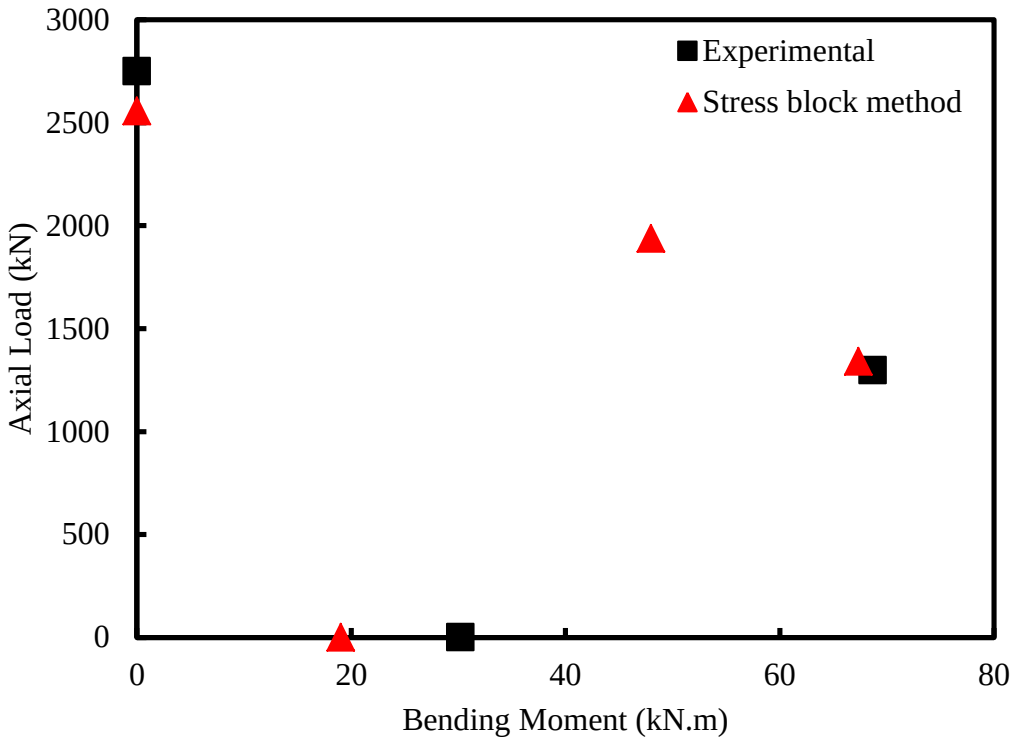

Figure 10.9 Comparison of analytical and experimental axial load-bending moment interaction diagrams for Group A30-S75 specimens using equivalent rectangular stress block method

Figure 10.10 compares the experimental and analytical axial load-bending moment (*P*-*M*) interaction diagrams of Group A40-S50 specimens, which were reinforced longitudinally with four A40 steel equal angle (SEA) sections and laterally with R10 steel bars at spaced 50 mm centre. Analytical maximum axial load of Specimen A40-S50-C was 96% of the experimental maximum axial load. The analytical maximum axial loads of Specimens A40-S50-E25 and A40-S50-E50 were 105% and 105%, respectively, of the experimental maximum axial loads. Analytical bending moments of Specimens A40-S50-E25 and A40-S50-E50 were 100% and 98%, respectively, of the experimental bending moments.

For specimen tested under four-point bending, the analytical bending moment of Specimen A40-S50-F was 71% of the experimental bending moment. The reason for the large differences between experimental and analytical bending moments under four-point bending was due to small shear span to depth ratio of the tested specimens. Another possible reason might be that the analytical method did not adequately take into account the bending stiffness of the longitudinal reinforcement and also the analytical method originally derived for specimens reinforced longitudinally with conventional steel bars. Whereas, the bending stiffness of a steel bar is much lower than the bending stiffness of a SEA section with the similar cross-sectional area.

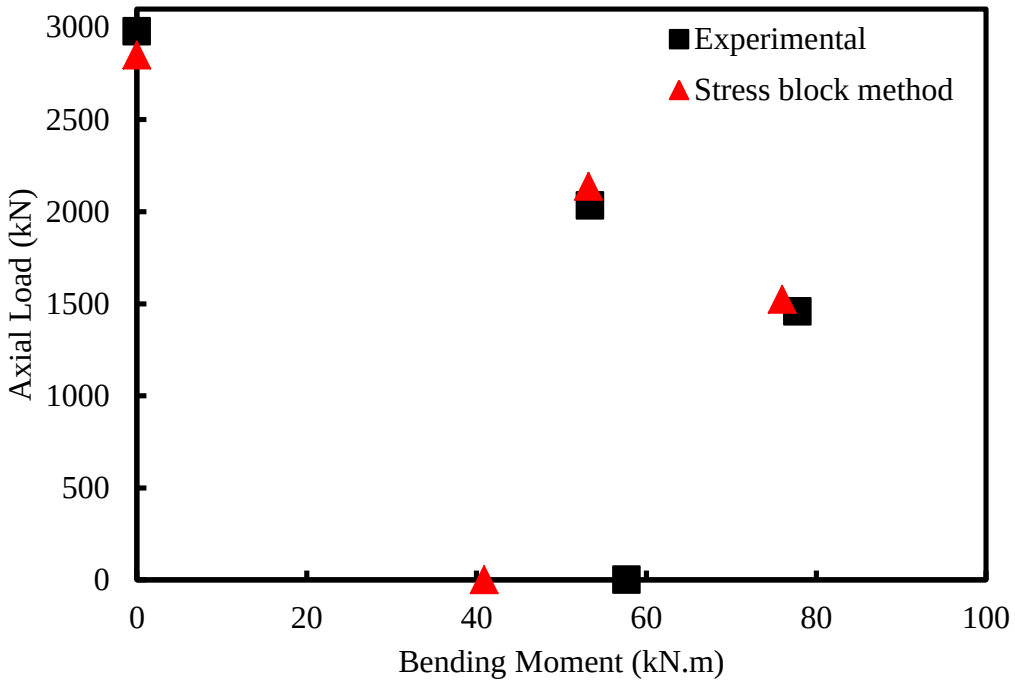

Figure 10.10 Comparison of analytical and experimental axial load-bending moment interaction diagrams for Group A40-S50 specimens using equivalent rectangular stress block method

Figure 10.11 compares the experimental and analytical axial load-bending moment (*P*-*M*) interaction diagrams of Group A40-S75 specimens, which were reinforced longitudinally with four A40 steel equal angle (SEA) sections and laterally with R10 steel bars at spaced 75 mm centre. Analytical maximum axial load of Specimen A40-S75-C was 104% of the experimental maximum axial load. The analytical maximum axial loads of Specimens A40-S75-E25 and A40-S75-E50 were 114% and 102%, respectively, of the experimental maximum axial loads. Analytical bending moments of Specimens A40-S75-E25 and A40-S75-E50 were 106% and 97%, respectively, of the experimental bending moments. However, for specimen tested under four-point bending, the analytical bending moment of Specimen A40-S75-F was 71% of the experimental bending moment.

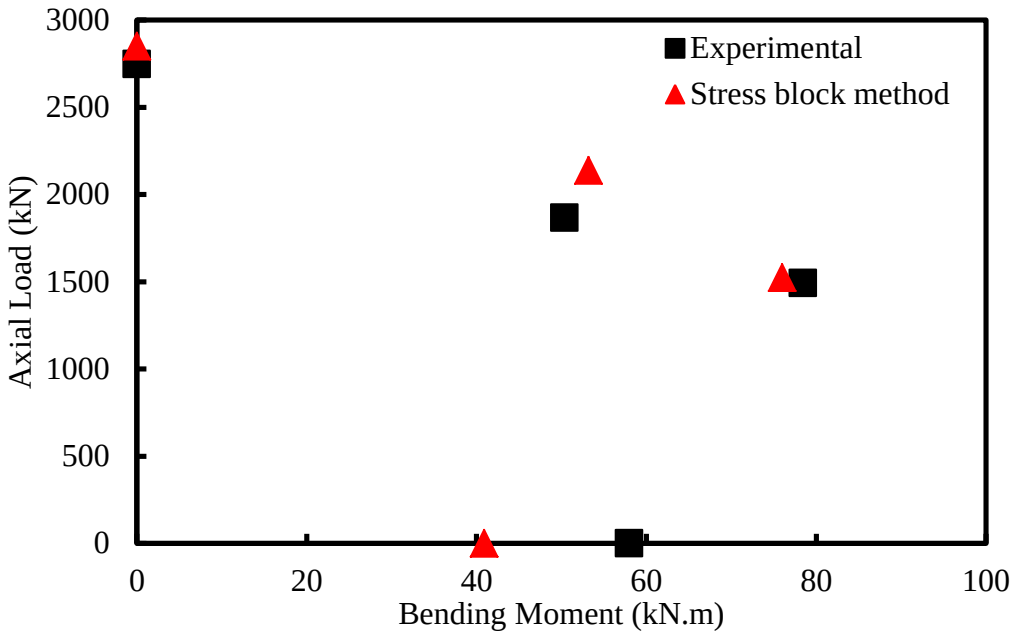

Figure 10.11 Comparison of analytical and experimental axial load-bending moment interaction diagrams for Group A40-S75 specimens using equivalent rectangular stress block method

Table 10.1 Experimental and Analytical Results Based on the Equivalent Rectangular Stress Block Method

Group ID	Specimen Labels	Experimental results		Analytical results		$\frac{\text{Analytical}}{\text{Experimental}}$	
		Maximum axial load (kN)	Bending moment (kN.m)	Maximum axial load (kN)	Bending moment (kN.m)	Maximum load %	Bending Moment %
R-S50	R-S50-C	2716	-	2627	-	97	-
	R-S50-E25	1967	52	1990	50	101	97
	R-S50-E50	1340	69	1389	69	104	100
	R-S50-F	244	28	-	23	-	82
A30-S50	A30-S50-C	2548	-	2557	-	100	-
	A30-S50-E25	1808	49	1937	48	107	98
	A30-S50-E50	1260	64	1340	67	106	105
	A30-S50-F	260	30	-	19	-	63
A30-S75	A30-S75-C	2749	-	2557	-	93	-
	A30-S75-E25	1457	-	1937	48	-	-
	A30-S75-E50	1297	69	1340	67	103	97
	A30-S75-F	257	30	-	19	-	63
A40-S50	A40-S50-C	2977	-	2849	-	96	-
	A40-S50-E25	2032	53	2137	53	105	100
	A40-S50-E50	1457	78	1523	76	105	98
	A40-S50-F	491	58	-	41	-	71
A40-S75	A40-S75-C	2746	-	2849	-	104	-
	A40-S75-E25	1867	50	2137	53	114	106
	A40-S75-E50	1492	78	1523	76	102	97
	A40-S75-F	493	58	-	41	-	71

10.5 Comparisons of Experimental and Analytical *P-M* Interaction Diagrams Using Layer-By-Layer Integration Method

In this section, the experimental axial load-bending moment (*P-M*) interaction diagrams were compared with the theoretical *P-M* interaction diagrams using the finite layer method. The theoretical results based on the finite layer method for Groups R-S50, A30-S50, A30-S75, A40-S50 and A40-S75 specimens are summarised in Table 10.2 and comparisons between the experimental and analytical *P-M* interaction diagrams are shown in Figures 10.12 to 10.16.

Figure 10.12 compares the experimental and analytical axial load-bending moment (*P-M*) interaction diagrams of Group R-S50 specimens, which were reinforced longitudinally with four N12 steel bars and laterally with R10 steel bars at spaced 50 mm centre. Analytical maximum axial load of Specimen R-S50-C was 97% of the experimental maximum axial load. The analytical maximum axial loads of Specimens R-S50-E25 and R-S50-E50 were 96% and 100%, respectively, of the experimental maximum axial loads. Analytical maximum bending moments of Specimens R-S50-E25, R-S50-E50 and were 91% and 98%, respectively, of the experimental maximum bending moments. For specimen tested under four-point bending, the analytical bending moment of Specimen R-S50-F was 87% of the experimental bending moment It is evident from Figure 10.12 that the results obtained from the analytical axial load-bending moment (*P-M*) interaction diagrams of Group R-S50 specimens were a good agreement with the experimental results.

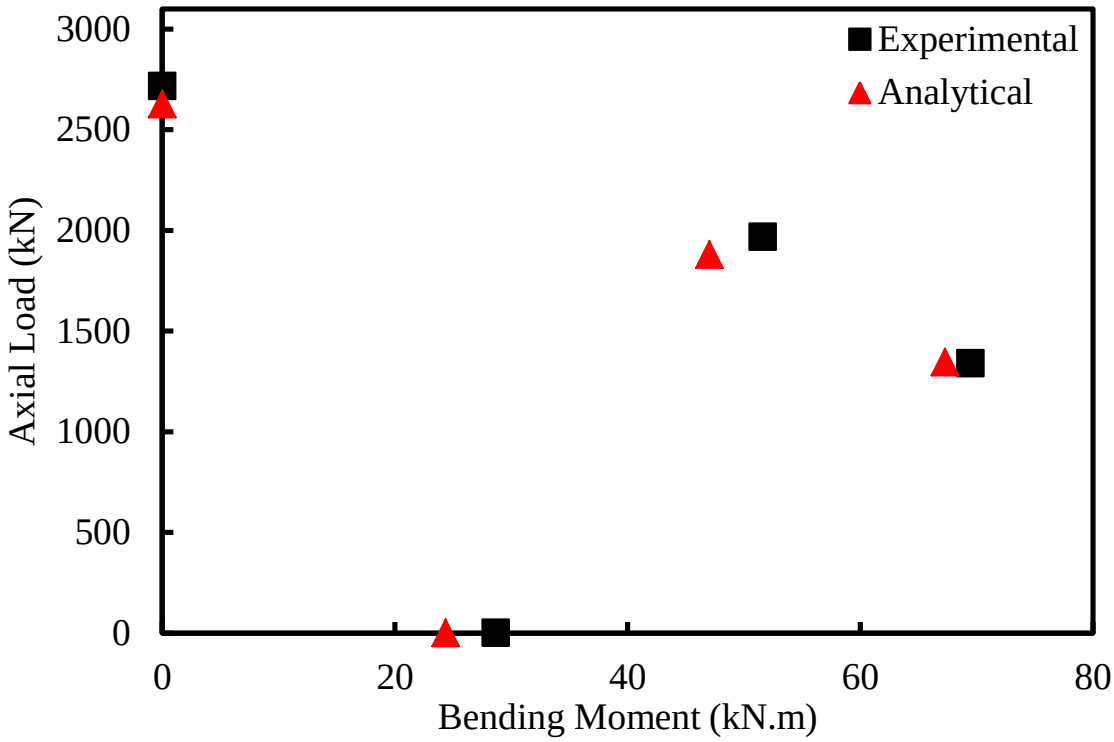

Figure 10.12 Comparison of analytical and experimental axial load-bending moment interaction diagrams for Group R-S50 specimens using layer-by-layer integration method

Figure 10.13 compares the experimental and analytical axial load-bending moment (*P-M*) interaction diagrams of Group A30-S50 specimens, which were reinforced longitudinally with our A30 steel equal angle (SEA) sections and laterally with R10 steel bars at spaced 50 mm centre. Analytical maximum axial load of Specimen A30-S50-C was 100% of the experimental maximum axial load. The analytical maximum axial loads of Specimens A30-S50-E25 and A30-S50-E50 were 103% and 106%, respectively, of the experimental maximum axial loads. Analytical bending moments of Specimens A30-S50-E25 and A30-S50-E50 were 95% and 103%, respectively, of the experimental bending moments. However, the analytical maximum bending moment of

Specimen A30-S50-F was 64% of the experimental maximum bending moment. The reason for the large differences between experimental and analytical bending moments under four-point bending was due to small shear span to depth ratio of the tested specimens. Another possible reason might be that the analytical method did not adequately take into account the bending stiffness of the longitudinal reinforcement and also the analytical method originally derived for specimens reinforced longitudinally with conventional steel bars. Whereas, the bending stiffness of a steel bar is much lower than the bending stiffness of a SEA section with the similar cross-sectional area.

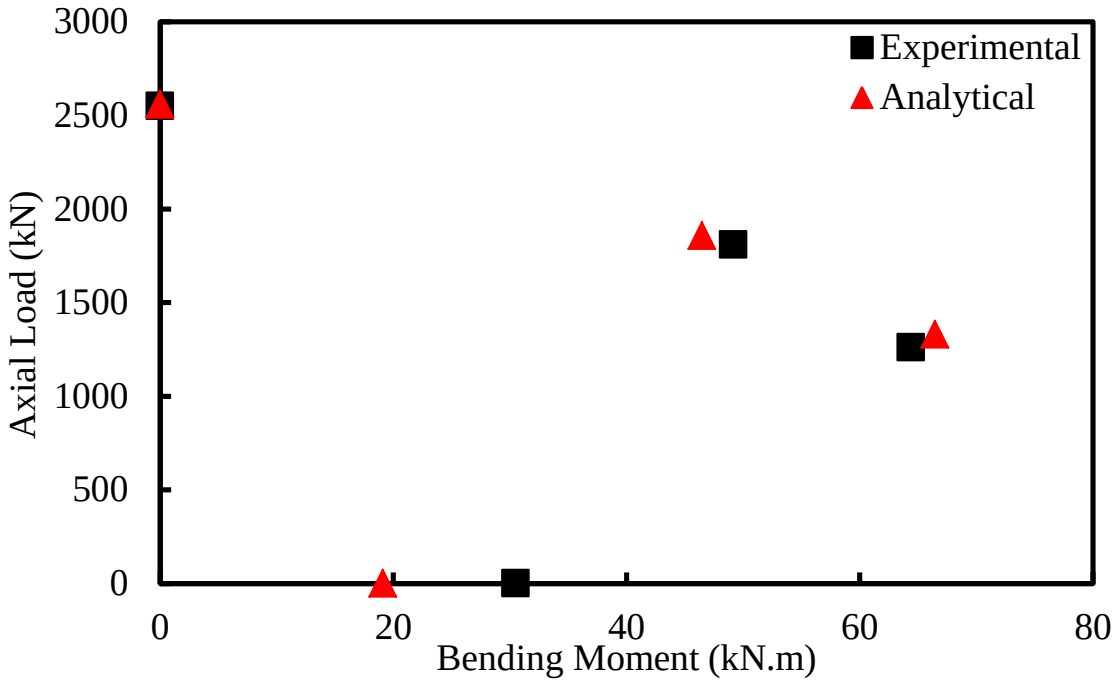

Figure 10.13 Comparison of analytical and experimental axial load-bending moment interaction diagrams for Group A30-S50 specimens using layer-by-layer integration method

Figure 10.14 compares the experimental and analytical axial load-bending moment (*P*-*M*) interaction diagrams of Group A30-S75 specimens, which were reinforced

longitudinally with four A30 steel equal angle (SEA) sections and laterally with R10 steel bars at spaced 75 mm centre. Analytical maximum axial load of Specimen A30-S75-C was 93% of the experimental maximum axial load. The analytical maximum axial load of Specimen A30-S75-E50 was 103%, respectively, of the experimental maximum axial load. Analytical bending moments of Specimens A30-S75-E50 and A30-S75-F were 96% and 64%, respectively, of the experimental bending moments. The reason for the large differences between experimental and analytical bending moments under four-point bending was due to small shear span to depth ratio of the tested specimens. Another possible reason might be that the analytical method did not adequately take into account the bending stiffness of the longitudinal reinforcement

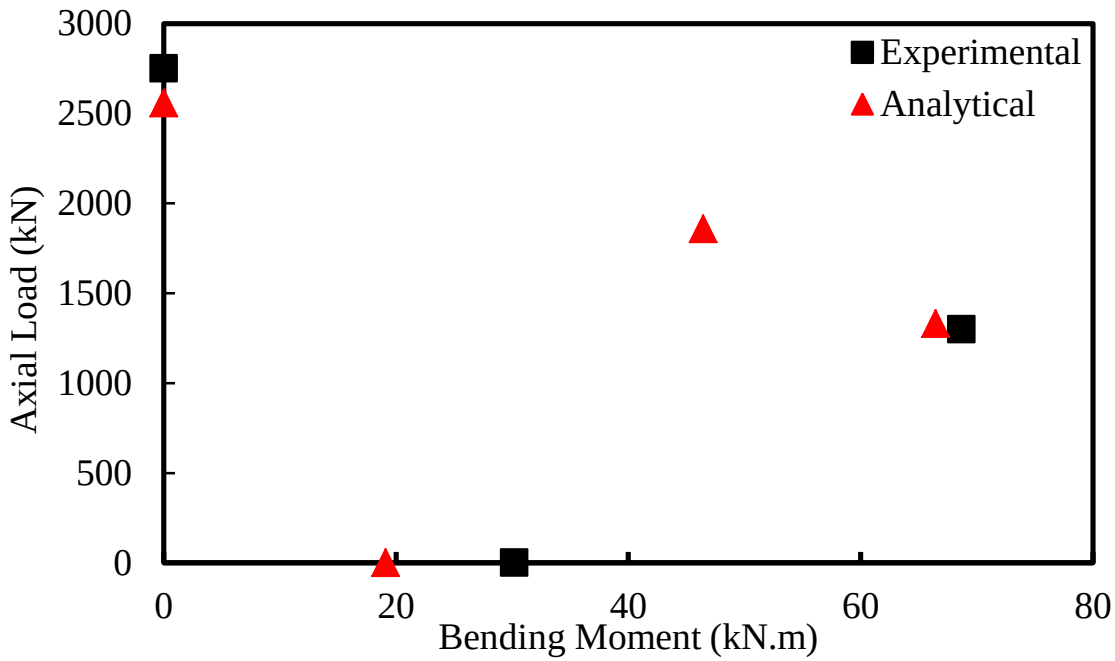

Figure 10.14 Comparison of analytical and experimental axial load-bending moment interaction diagrams for Group A30-S75 specimens using layer-by-layer integration method

Figure 10.15 compares the experimental and analytical axial load-bending moment (*P*-*M*) interaction diagrams of Group A40-S50 specimens, which were reinforced longitudinally with four A40 steel equal angle (SEA) sections and laterally with R10 steel bars at spaced 50 mm centre. Analytical maximum axial load of Specimen A40-S50-C was 96% of the experimental maximum axial load. The analytical maximum axial loads of Specimens A40-S50-E25 and A40-S50-E50 were 103% and 103%, respectively, of the experimental maximum axial loads. Analytical bending moments of Specimens A40-S50-E25 and A40-S50-E50 were 98% and 96%, respectively, of the experimental bending moments. The analytical maximum bending moment of Specimen A40-S50-F was 70% of the experimental maximum bending moment.

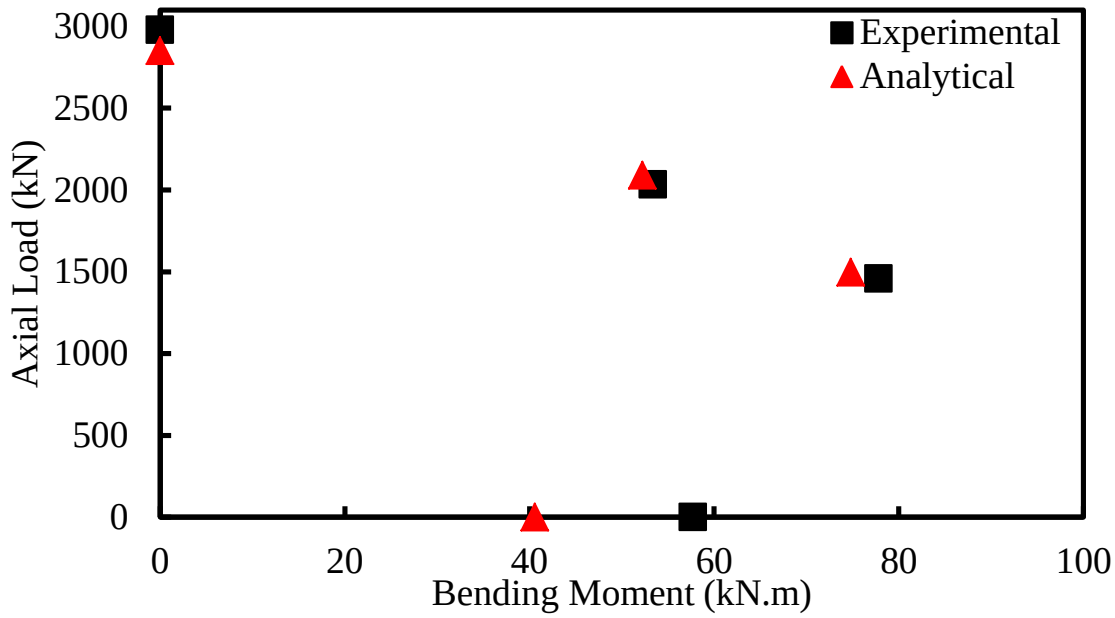

Figure 10.15 Comparison of analytical and experimental axial load-bending moment interaction diagrams for Group A40-S50 specimens using layer-by-layer integration method

Figure 10.16 compares the experimental and analytical axial load-bending moment (*P*-*M*) interaction diagrams of Group A40-S75 specimens, which were reinforced

longitudinally with four A40 steel equal angle (SEA) sections and laterally with R10 steel bars at spaced 75 mm centre. Analytical maximum axial load of Specimen A40-S75-C was 104% of the experimental maximum axial load. The analytical maximum axial loads of Specimens A40-S75-E25 and A40-S75-E50 were 112% and 100%, respectively, of the experimental maximum axial loads. Analytical bending moments of Specimens A40-S75-E25, A40-S75-E50 and were 104% and 95%, respectively, of the experimental maximum bending moments. However, the analytical maximum bending moment of Specimen A40-S75-F was 70% of the experimental maximum bending moment. The reason for the large differences between experimental and analytical bending moments under four-point bending was due to small shear span to depth ratio of the tested specimens. Another possible reason might be that the analytical method did not adequately take into account the bending stiffness of the longitudinal reinforcement

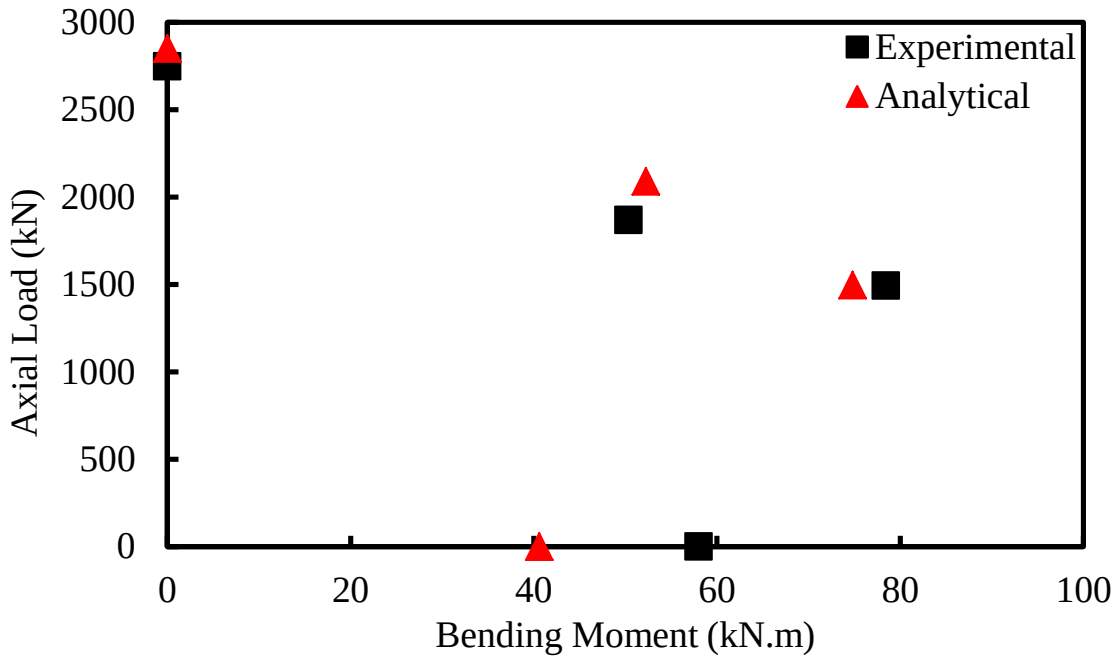

Figure 10.16 Comparison of analytical and experimental axial load-bending moment interaction diagrams for Group A40-S75 specimens using layer-by-layer integration method

Table 10.2 Experimental and Analytical Results Based on the Layer-By-Layer Integration Method

Group ID	Specimen Labels	Experimental results		Analytical results		$\frac{\text{Analytical}}{\text{Experimental}}$	
		Maximum axial load (kN)	Bending moment (kN.m)	Maximum axial load (kN)	Bending moment (kN.m)	Maximum axial load %	Bending moment %
R-S50	R-S50-C	2716	-	2627	-	97	-
	R-S50-E25	1967	52	1879	47	96	91
	R-S50-E50	1340	69	1345	67	100	98
	R-S50-F	244	28	-	24	-	87
A30-S50	A30-S50-C	2548	-	2557	-	100	-
	A30-S50-E25	1808	49	1857	46	103	95
	A30-S50-E50	1260	64	1331	66	106	103
	A30-S50-F	260	30	-	19	-	64
A30-S75	A30-S75-C	2749	-	2557	-	93	-
	A30-S75-E25	1457	-	1857	46	-	-
	A30-S75-E50	1297	69	1331	66	103	96
	A30-S75-F	257	30	-	19	-	64
A40-S50	A40-S50-C	2977	-	2849	-	96	-
	A40-S50-E25	2032	53	2089	52	103	98
	A40-S50-E50	1457	78	1496	75	103	96
	A40-S50-F	491	58	-	41	-	70
A40-S75	A40-S75-C	2746	-	2849	-	104	-
	A40-S75-E25	1867	50	2089	52	112	104
	A40-S75-E50	1492	78	1496	75	100	95
	A40-S75-F	493	58	-	41	-	70

10.6 Parametric Study

In this section, two parametric studies were carried out to investigate the effects of ratio and strength of longitudinal reinforcement on the axial load-bending moment (*P-M*) interaction diagrams of specimens reinforced with SEA sections tested under concentric and eccentric axial loads and four-point bending. The layer-by-layer integration method was adopted to calculate the parametric study in this section. All other parameters such as the compressive strength of concrete and the cross-sectional dimensions of square HSC specimens were kept the same.

10.6.1 **Effect of Longitudinal SEA Reinforcement Ratio**

The parametric study considered square HSC specimens reinforced longitudinally with three different sizes of SEA sections to explore the effect of longitudinal reinforcement ratio. In this parametric study, three nominal sizes of SEA sections were selected: 40 mm × 40 mm × 2.5 mm, 45 mm × 45 mm × 2.5 mm and 50 mm × 50 mm × 2.5 mm that were provided longitudinal reinforcement ratios of 1.65%, 1.87% and 2.09%, respectively. The reason for selected these sections was because they are already produced and available in providing a company of SEA sections, as well as they, had same nominal thickness and strength compared to the A30 SEA sections. The details of these three different sizes of SEA encased in square HSC specimens are shown in Figure 10.17. The *P-M* interaction diagrams of square HSC specimens with an increase in longitudinal reinforcement ratios of 1.11% (actual), 1.65%, 1.87% and 2.09% are presented in Figure 10.18(a). It was obtained from the parametric study results that increasing the longitudinal SEA reinforcement ratio from 1.11% to 2.09% in the square

HSC specimens affects the strength slightly (up to 6.6%) while significantly affects the maximum bending moments (up to 56.3%).

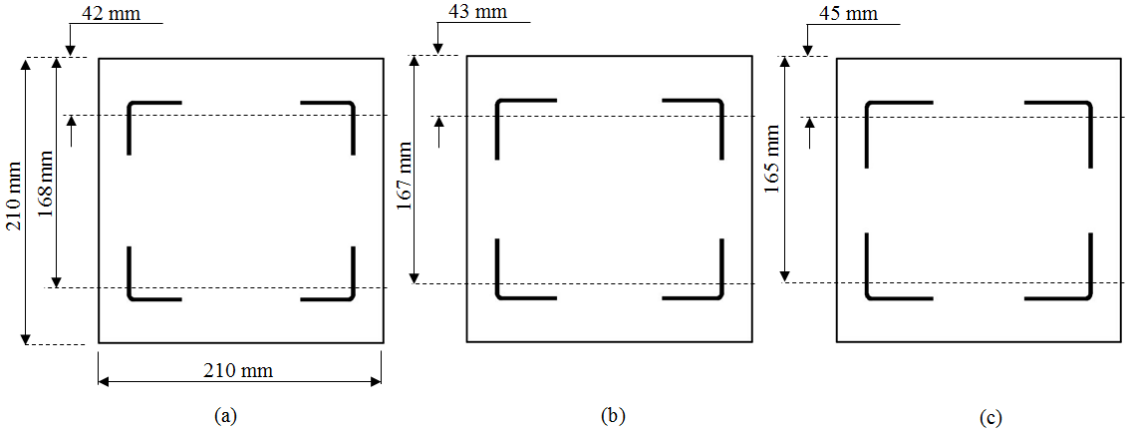

Figure 10.17 Dimensions and reinforcement for specimens reinforced with SEA sections: (a) 40 mm × 40 mm × 2.5 mm, (b) 45 mm × 45 mm × 2.5 mm and (c) 50 mm × 50 mm × 2.5 mm

10.6.2 **Effect of Longitudinal SEA Reinforcement Strength**

To evaluate the influence of varying longitudinal SEA sections strength on *P-M* interaction diagrams of square HSC specimens, four yield strengths of longitudinal A30 SEA 350 MPa, 374 MPa (actual), 400 MPa and 500 MPa were considered. Figure 10.18 (b) shows the *P-M* interaction diagrams for Specimens reinforced with different longitudinal A30 SEA reinforcement strengths. It was obtained that increase in the strength of longitudinal SEA sections from 350 MPa to 500 MPa in the square HSC specimens resulted in a slight increase in strength while significantly affects the maximum bending moments (up to 26.3%).

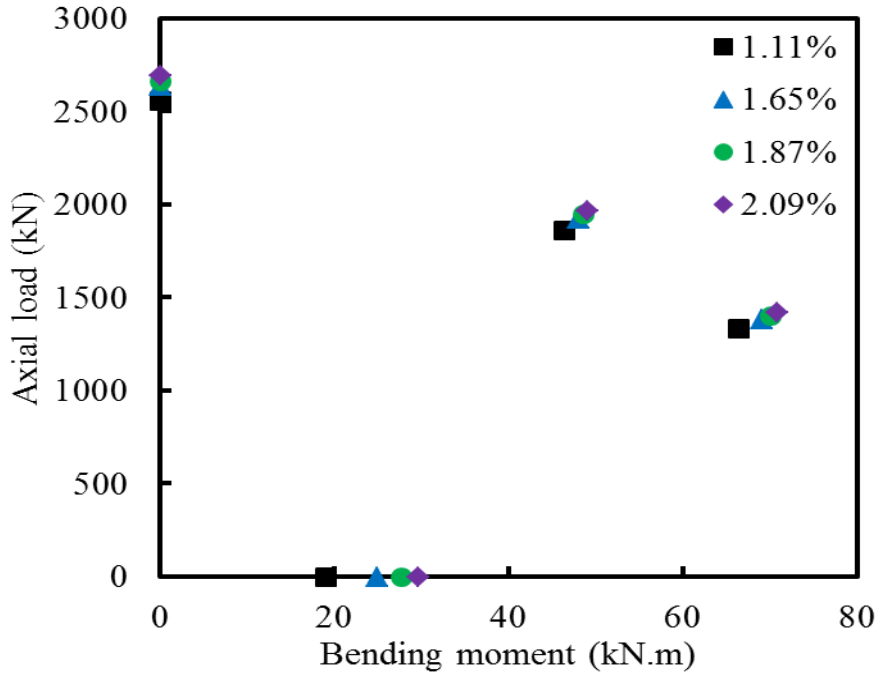

(a)

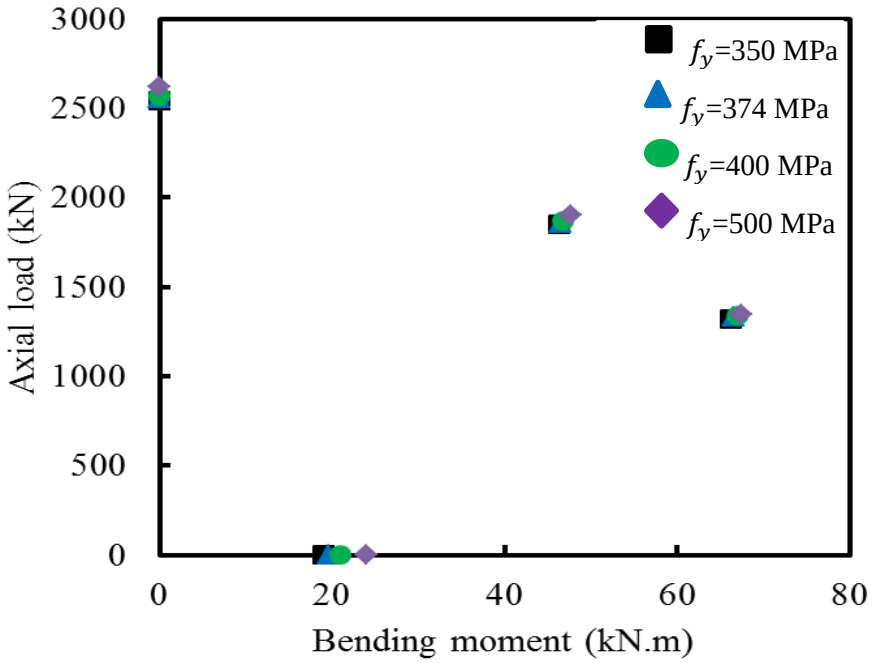

(b)

Figure 10.18 Effect of parametric studies on *P-M* interaction diagrams: (a) longitudinal SEA reinforcement ratio and (b) longitudinal SEA reinforcement strength

10.7 Summary

In this chapter, the experimental and analytical axial load-bending moment *(P-M)* interaction diagrams of steel bar reinforced concrete specimens and SEA reinforced concrete specimens were analysed and discussed. The analytical *(P-M)* interaction diagrams using the equivalent rectangular stress block and the layer-by-layer integration methods were constructed to compare with the experimental results. It can be observed that the analytical axial load-bending moment interaction diagrams match well with the experimental axial load-bending moment interaction diagrams.

For the equivalent rectangular stress block method, it can be seen that analytical maximum axial loads are within 93%-104% of experimental maximum axial loads for specimens reinforced with SEA sections tested under concentric axial load. Analytical maximum axial loads are within 105%-114% and 102%-106% of experimental maximum axial loads for specimens reinforced with SEA sections tested under 25 mm and 50 mm eccentric axial loads, respectively. Analytical maximum bending moments are within 98%-106% and 97%-105% of experimental maximum bending moments for specimens reinforced with SEA sections tested under 25 mm and 50 mm eccentric axial loads, respectively. However, the analytical maximum bending moments are within 63%-71% of experimental maximum bending moments for specimens reinforced with SEA sections tested under four-point bending.

For the layer-by-layer integration method, it can be seen that analytical maximum axial loads are within 93%-104% of experimental maximum axial loads for specimens

reinforced with SEA sections tested under concentric axial load. Analytical maximum axial loads are within 103%-112% and 100%-106% of experimental maximum axial loads for specimens reinforced with SEA sections tested under 25 mm and 50 mm eccentric axial loads, respectively. Analytical maximum bending moments are within 95%-104% and 95%-103% of experimental maximum bending moments for specimens reinforced with SEA sections tested under 25 mm and 50 mm eccentric axial loads, respectively. However, the analytical maximum bending moments are within 64%-70% of experimental maximum bending moments for specimens reinforced with SEA sections tested under four-point bending.

Based on the experimental and analytical axial load and bending moment interaction diagrams, It can see that as compared with the experimental results, the analytical results obtained by the layer-by-layer integration method is closer than the analytical results obtained by the equivalent rectangular stress block method. It can also be observed that both the equivalent rectangular stress block and the layer-by-layer integration methods show a good estimate of the specimen strengths. The analytical *(P-M)* interaction diagrams of tested specimens can be more accurately modelled using both of the equivalent rectangular stress block and the layer-by-layer integration methods. Based on the experimental and analytical results conducted in this study, the conclusions and recommendations of the thesis are summarised in the next chapter.

11 CONCLUSIONS AND RECOMMENDATIONS

11.1 Conclusions

The main objectives of this study were to investigate the behaviour of square high strength concrete (HSC) specimens reinforced longitudinally with steel equal angle (SEA) sections. A total of 32 square HSC specimens were cast and tested. The experimental work presented in this study consists of two sets.

In the first set, a total of 20 square HSC specimens were tested under concentric and eccentric axial loads and four-point bending to explore the behaviour of HSC specimens reinforced longitudinally with SEA sections. The main parameters examined included the type of longitudinal reinforcement (steel bars and SEA sections), the spacing of transverse ties (50 mm and 75 mm) and different loading conditions.

In the second set, a total of 12 square HSC specimens were tested under concentric axial loads. Eight of these specimens were reinforced longitudinally with SEA sections (A30 and A40) to investigate the effect of using SEA sections as longitudinal reinforcement with the different spacing of transverse ties (50 mm, 100 mm, 200 mm and 400 mm). For comparison purposes, four specimens were reinforced longitudinally with conventional steel bars and had the same spacing of transverse ties (50 mm, 100 mm, 200 mm and 400 mm).

A total of 15 pullout specimens were also tested to investigate the bond behaviour between reinforcing steel (steel bars and SEA sections) and surrounding concrete. it was observed that the proposed method (welding small steel bar pieces at embedded ends of SEA sections) to improve the pullout behaviour of plain SEA sections embedded in HSC can be enhanced pullout load capacity, which can decrease the impact of the absence of ribs in the SEA sections.

Analytical axial load-axial deformation responses of specimens reinforced longitudinally with SEA sections tested under axial compression were drawn and discussed. Two analytical methods were also carried out to draw the axial load-bending moment interaction diagrams of specimens reinforced with SEA sections. The following conclusions were drawn from the results of the analytical and experimental investigations on the 32 square HSC specimens.

11.1.1 **Conclusions for Specimens with 800 mm Height**

1. In general, the specimens reinforced with SEA sections under concentric and eccentric axial loads experienced two peak axial loads while the specimens reinforced with steel bars experienced one peak axial load. This indicates that the longitudinal SEA sections positively influenced the confinement of the concrete core after the spalling of concrete cover.

2. Specimens A30-S50-C, A30-S50-E25 and A30-S50-E50 carried about 6.6%, 8.8% and 6.4% lower maximum axial load than Specimens R-S50-C, R-S50-E25 and R-S50-E50, respectively. These slightly lower maximum axial loads were mainly because the

A30 SEA sections had 49% lower yield tensile strength than steel bars. In other words, the force contribution of A30 SEA sections was lower than the force contributions of N12 steel bars by about 27%. However, the ductilities of Specimens A30-S50-C, A30-S50-E25 and A30-S50-E50 were 56.3 %, 30.8% and 8.3%, respectively, higher than the ductility of the Specimens R-S50-C, R-S50-E25 and R-S50-E50. This indicates that the A30 SEA section more effectively confined the concrete core of the tested specimens.

3. For all loading conditions, specimens of Group A40-S50 exhibited higher maximum axial load and higher ductility than specimens of the reference Group R-S50 because of the more effective confinement provided by A40 SEA sections than the steel bars. Another possible reason is that the A40 SEA section had a higher cross-sectional area than the N12 steel bars.

4. All specimens reinforced with SEA sections that were tested under four-point bending showed higher maximum load and significantly higher ductility than the corresponding specimen reinforced with steel bars. This is because the SEA sections had higher bending stiffness than the steel bars.

5. Also, an analytical stress-strain model to predict the axial load-axial deformation behaviour was established for specimens tested under concentric axial loads. It was observed that the analytical axial load-axial deformation behaviours of the tested specimens agreed reasonably well with the experimental results.

6. The load carrying capacity and bending moment of the specimens reinforced longitudinally with SEA sections can be calculated by the same principles used for the conventional specimens reinforced longitudinally with steel bars. The analytical axial load-bending moment interactions for the tested specimens constructed using the equivalent rectangular stress block and the layer-by-layer numerical integration methods

are in good agreement with the experimental results, particularly for specimens tested under concentric and eccentric axial loads.

7. The analytical axial load-bending moment interaction diagram of the specimens were reasonably close to the experimental results. However, the experimental bending moment of the specimens tested under four-point bending was greater than the calculated results, particularly for specimens reinforced with the SEA sections. The reason for the differences between the experimental and the analytical bending moments under four-point bending was due to the small shear span to depth ratio of the tested specimens. Another possible reason might be that the analytical method did not adequately take into account the bending stiffness of the longitudinal reinforcement, where the bending stiffness of a SEA section was much greater than the bending stiffness of a steel bar for the same-cross sectional area.

11.1.2 **Conclusions for Specimens with 600 mm Height**

1. In general, the failure of the specimens reinforced with N12 steel bars was characterised by the buckling of longitudinal bars, which was followed by the fracture of transverse ties at welded points for 50 mm and 100 mm centre-to-centre spacing of transverse ties. However, for 200 mm and 400 mm centre-to-centre spacing of transverse ties, the failure of the specimen was characterised by buckling of longitudinal steel bars and the crushing of concrete core. The failure of specimens reinforced with A30 and A40 SEA sections was characterised by the buckling of longitudinal SEA sections, which was followed by the fracture of transverse ties at welded points for 50 mm centre-to-centre spacing of transverse ties. Whereas, in general, the failure of

specimens reinforced with A30 and A40 SEA sections with a centre-to-centre spacing of transverse ties of 100 to 400 mm was attributed to the buckling of longitudinal SEA sections and then cracking of the concrete core.

2. The maximum axial loads of Specimens B-S50 and B-S100 were 11.6% and 2.7%, respectively, greater than the maximum axial loads of Specimens A30-S50 and A30-S100. However, at the maximum axial load, the force contribution of the N12 steel bars in specimens reinforced longitudinally with the N12 steel bars was 27% higher than the force contribution of the A30 SEA sections in specimens reinforced longitudinally with the A30 SEA. The maximum axial loads of Specimens B-S200 and B-S400 were 2.5% and 52%, respectively, lower than the maximum axial loads of Specimens A30-S200 and A30-S400. At the same lateral tie spacing, all specimens reinforced with A30 SEA sections exhibited higher ductility compared to the reference specimens reinforced with N12 steel bars. This was because the use of the A30 SEA sections as longitudinal reinforcement in HSC column specimens increased the effective confinement of the concrete core of the specimens.

3. For the increase of the centre-to-centre spacing of transverse ties from 50 mm to 400 mm, the maximum axial load of the specimens reinforced with A30 SEA sections decreased by about 7.3%, while the maximum axial load of the specimens reinforced with N12 steel bars decreased by about 70.6%. This indicated that the buckling load for A30 SEA section in HSC specimens (Group A30) was significantly higher than the buckling load of N12 steel bars in the reference HSC specimens (Group B).

4. For the same centre-to-centre spacing of transverse ties, all specimens reinforced longitudinally with A40 SEA sections exhibited higher maximum axial load and ductility than the corresponding specimens reinforced longitudinally with N12 steel

bars. Increasing the spacing of transverse ties from 50 mm to 400 mm led to a decrease of 15.1% of the maximum axial load for specimens reinforced with A40 SEA sections. Also, Specimens A40-S50, A40-S100 and A40-S200 showed higher maximum axial load and ductility compared to Specimens A30-S50, A30-S100 and A30-S200, respectively. The reason for higher maximum axial load and ductility of specimens reinforced with A40 SEA sections was due to the combined effect of the increased confinement effectiveness of the concrete core and the greater cross section area of A40 SEA section

5. For specimens with lateral tie spacing of 400 mm, the use of the conventional steel bar as longitudinal reinforcement led to a premature failure of the specimen, while the use of the SEA sections as longitudinal reinforcement did not lead to premature failure of the specimen. This was because the buckling load of SEA sections was significantly higher than the buckling load of steel bars.

6. The experimental results also found that Specimen A30-S200 obtained higher maximum axial load and ductility than Specimen B-S100, although the spacing of transverse ties of Specimen A30-S200 was 200 mm and the spacing of transverse ties of Specimen B-S100 was 100 mm. Similarly, Specimen A30-S400 obtained higher maximum axial load and ductility than Specimen B-S200, although the spacing of transverse ties of Specimen A30-S400 was 400 mm and the spacing of transverse ties of Specimen B-S200 was 200 mm. This indicates that the use of SEA sections as longitudinal reinforcement provided high confinement to the concrete core of HSC columns as well as increased the buckling load of the longitudinal SEA sections compared to conventional steel bars for the same cross-sectional area. Consequently, based on the experimental and analytical results, the maximum spacing of transverse

ties for specimens reinforced longitudinally with SEA sections can be increased over the current requirements that were provided by AS 3600 (2009) and ACI 318-14 (2014).

On the basis of the experimental and analytical results presented in this study, the use of SEA sections as the longitudinal reinforcements in square HSC columns can provide higher maximum axial load and ductility compared to the HSC columns reinforced longitudinally with conventional steel bars. Also, the SEA sections considerably confined the concrete core of HSC columns, particularly after the spalling of the concrete cover. Hence, the use of SEA sections as longitudinal reinforcement in HSC specimens can be recommended to improve the performance of square HSC concrete columns.

11.2 Recommendations for Future Studies

Based on the examinations on the square high strength concrete (HSC) specimens reinforced longitudinally with steel equal angle (SEA) sections conducted in this study, below are recommendations for future studies:

1. Experimental research study on the behaviour of columns reinforced longitudinally with SEA sections under reverse-cyclic loads is recommended to validate the advantages of using SEA sections in improving the seismic performance of the specimens.

2. Influence of concrete strength can be examined on the behaviour and performance of concrete specimens reinforced longitudinally with SEA sections.

3. Experimental studies on SEA columns with different slenderness ratios and different sizes of SEA sections need to be investigated to assess the behaviour and performance of SEA sections as longitudinal reinforcement.

REFERENCES

ACI (American Concrete Institute). (2010). "Report on high-strength concrete." *ACI 363 R-10*, Farmington Hills, MI.

ACI (American Concrete Institute). (2014). "Building code requirements for structural concrete." *ACI 318-14*, Farmington Hills, MI.

Afefy, H. M., and El Tony, E.T. M. (2016). "Simplified Design Procedure for Reinforced Concrete Columns Based on Equivalent Column Concept." *International Journal of Concrete Structures and Materials.* 10(3), 393-406.

Afifi, M. Z., Mohamed, H. M., and Benmokrane, B. (2013). "Axial capacity of circular concrete columns reinforced with GFRP bars and spirals." *Journal of Composites for Construction.* 18(1), 04013017.

AISC (2005). "Specification for Structural Steel Buildings. American Institute of Steel Construction." *AISC 360-05*,, Inc: Chicago, IL.

Antonius, A., and Imran, I. (2012). "Experimental study of confined low-, medium-and high-strength concrete subjected to concentric compression." *Journal of Engineering and Technological Sciences.* 44(3), 252-269.

AS (Australian Standard). (1999). "Methods of testing concrete – Method 9: Determination of the compressive strength of concrete specimens." *AS 1012.9*, Sydney, Australia.

AS (Australian Standard). (2000). "Methods of testing concrete – Method 10: Determination of indirect tensile strength of concrete cylinders (‘Brazil’ or splitting test)." *AS 1012.10*, Sydney, Australia.

AS (Australian Standard). (2007). "Metallic materials tensile testing at ambient temperature." *AS 1391-2007*, Sydney, Australia.

AS (Australian Standard). (2009). "Concrete structures." *AS 3600-2009*, Sydney, Australia.

Attard, M., and Setunge, S. (1996). "Stress-strain relationship of confined and unconfined concrete." *ACI Materials Journal.* 93, 432-442.

Awati, M., and Khadiranaikar, R. (2012). "Behavior of concentrically loaded high performance concrete tied columns." *Engineering Structures.* 37, 76-87.

Bai, Z., and Au, F. (2011). "Effects of strain hardening of reinforcement on flexural strength and ductility of reinforced concrete columns." *The Structural Design of Tall and Special Buildings.* 20(7), 784-800.

Bastami, M. (2010). "Constitutive model for HSC confined by UHS and NS transverse reinforcements under cyclic and earthquake loadings." *Journal of Seismology and Earthquake Engineering.* 12(3), 131-141.

Bayrak, O., and Sheikh, S. A. (1998). "Confinement reinforcement design considerations for ductile HSC columns." *Journal of Structural Engineering.* 124(9), 999-1010.

Begum, M., Driver, R. G., and Elwi, A. E. (2013). "Behaviour of partially encased composite columns with high strength concrete." *Engineering Structures.* 56, 1718-1727.

Bhowmick, R., Sharma, U., and Bhargava, P. (2006). "Numerical simulation of confined concrete columns and a parametric study." *Asian Journal Of Civil Engineering (Building And Housing).* 7(3), 269-286.

Bing, L., Park, R., and Tanaka, H. (2001). "Stress-strain behavior of high-strength concrete confined by ultra-high-and normal-strength transverse reinforcements." *ACI Structural Journal.* 98(3), 395-406.

Bjerkeli, L., Tomaszewicz, A., and Jensen, J. (1990). "Deformation properties and ductility of high-strength concrete." *ACI Utilization of HighStrength Concrete—Second International Symposium, SP.* 121, 215-238.

Bresler, B., and Gilbert, P. (1961). "Tie requirements for reinforced concrete columns." *ACI Journal, Proceedings.* 58, 555-570.

Campione, G., and Minafò, G. (2010). "Compressive behavior of short high-strength concrete columns." *Engineering Structures.* 32(9), 2755-2766.

Canbay, E., Ozcebe, G., and Ersoy, U. (2006). "High-strength concrete columns under eccentric load." *Journal of Structural Engineering.* 132(7), 1052-1060.

Chan, W. (1955). "The ultimate strength and deformation of plastic hinges in reinforced concrete frameworks." *Magazine of Concrete Research.* 7(21), 121-132.

Chen, C., Wang, C., and Sun, H. (2014). "Experimental study on seismic behavior of full encased steel-concrete composite columns." *Journal of Structural Engineering.* 140(6), 04014024.

Chen, C. C., and Lin, N. J. (2006). "Analytical model for predicting axial capacity and behavior of concrete encased steel composite stub columns." *Journal of Constructional Steel Research.* 62(5), 424-433.

Chung, H.-S., Yang, K.-H., Lee, Y.-H., and Eun, H.-C. (2002a). "Strength and ductility of laterally confined concrete columns." *Canadian Journal of Civil Engineering.* 29(6), 820-830.

Chung, H. S., Yang, K. H., Lee, Y. H., and Eun, H. C. (2002b). "Stress–strain curve of laterally confined concrete." *Engineering structures.* 24(9), 1153-1163.

Cladera, A., and Mari, A. (2005). "Experimental study on high-strength concrete beams failing in shear." *Engineering Structures.* 27(10), 1519-1527.

Claeson, C. (1999). "Finite element analysis of confined concrete columns." *NORDIC Concrete Research-Publications.* 22, 1-20.

Cloyd, J. E. (1998). 'Investigation of Minimum Longitudinal Reinforcing Requirements for Concrete'. *M.S. Thesis*, The University of Texas at Austin,

CSA (Canadian Standards Association). (2004). "Design of concrete structures." *A23. 3-04*, Toronto.

Cusson, D., and Paultre, P. (1994). "High-strength concrete columns confined by rectangular ties." *Journal of Structural Engineering.* 120(3), 783-804.

Cusson, D., and Paultre, P. (1995). "Stress-strain model for confined high-strength concrete." *Journal of Structural Engineering.* 121(3), 468-477.

Dundar, C., Tokgoz, S., Tanrikulu, A. K., and Baran, T. (2008). "Behaviour of reinforced and concrete-encased composite columns subjected to biaxial bending and axial load." *Building and Environment.* 43(6), 1109-1120.

Ellobody, E., and Young, B. (2011). "Numerical simulation of concrete encased steel composite columns." *Journal of Constructional Steel Research.* 67(2), 211-222.

Eurocode, C. 1994. 4: "Design of composite steel and concrete structures."

Fafitis, A., and Shah, S. (1985). "Lateral reinforcement for high-strength concrete columns." *ACI SP-87.* 213-232.

Foster, S. J. (1999). 'Design and detailing of high strength concrete columns', Research report No. R-375. University of New South Wales, School of Civil Engineering, Sydney.

Foster, S. J., and Attard, M. M. (1997). "Experimental tests on eccentrically loaded high-strength concrete columns." *ACI Structural Journal.* 94(3), 295-303.

Foster, S. J., and Attard, M. M. (2001). "Strength and ductility of fiber-reinforced high-strength concrete columns." *Journal of Structural Engineering.* 127(1), 28-34.

Foster, S. J., Liu, J., and Sheikh, S. A. (1998). "Cover spalling in HSC columns loaded in concentric compression." *Journal of Structural Engineering.* 124(12), 1431-1437.

Hadi, M. N. S. (2006). "Behaviour of FRP wrapped normal strength concrete columns under eccentric loading." *Composite Structures.* 72(4), 503-511.

Hadi, M. N. S., Balanji, E. K., and Sheikh, M. N. (2017). "Behavior of Steel Fiber-Reinforced High-Strength Concrete Columns under Different Loads." *Structural Journal.* 114(4), 815-826.

Hadi, M. N. S., Karim, H., and Sheikh, M. N. (2016a). "Experimental Investigations on Circular Concrete Columns Reinforced with GFRP Bars and Helices under Different Loading Conditions." *Journal of Composites for Construction.* 04016009.

Hadi, M. N. S., Khan, Q. S., and Sheikh, M. N. (2016b). "Axial and flexural behavior of unreinforced and FRP bar reinforced circular concrete filled FRP tube columns." *Construction and Building Materials.* 122, 43-53.

Hadi, M. N. S., and Widiarsa, I. B. R. (2012). "Axial and flexural performance of square RC columns wrapped with CFRP under eccentric loading." *Journal of Composites for Construction.* 16(6), 640-649.

Hadi, M. N. S., and Youssef, J. (2016). "Experimental investigation of GFRP-reinforced and GFRP-encased square concrete specimens under axial and eccentric load, and four-point bending test." *Journal of Composites for Construction.* 93, 1-16.

Han, B. S., and Shin, S. W. (2006). "Confinement effects of high-strength reinforced concrete tied columns." *International Journal of Concrete Structures and Materials.* 18(2E), 133-142.

Ho, J., Lam, J., and Kwan, A. (2010). "Effectiveness of adding confinement for ductility improvement of high-strength concrete columns." *Engineering Structures.* 32(3), 714-725.

Hognestad, E. (1951). "A study of combined bending and axial load in reinforced concrete members", Bulletin Series No. 399, Engineering Experiment Station, University of Illinois, Urbana.

Hong, K. N., Han, S. H., and Yi, S. T. (2006a). "High-strength concrete columns confined by low-volumetric-ratio lateral ties." *JEST Engineering Structures.* 28(9), 1346-1353.

Hong, K. N., Han, S. H., and Yi, S. T. (2006b). "High-strength concrete columns confined by low-volumetric-ratio lateral ties." *Engineering Structures.* 28(9), 1346-1353.

Hsu, H. L., Jan, F. J., and Juang, J. L. (2009). "Performance of composite members subjected to axial load and bi-axial bending." *Journal of Constructional Steel Research.* 65(4), 869-878.

Hsu, L., and Hsu, C. T. (1994). "Complete stress—strain behaviour of high-strength concrete under compression." *Magazine of Concrete Research.* 46(169), 301-312.

Hunaiti, Y., Fattah, B. A., and Fattah, A. (1994). "Design considerations of partially encased composite columns." *Proceedings of the ICE-Structures and Buildings.* 104(1), 75-82.

Husem, M., Pul, S., Gorkem, S. E., and Demir, S. (2016). "The behaviour of high-strength reinforced concrete columns under low eccentric loading." *European Journal of Environmental and Civil Engineering.* 20(4), 486-502.

Jin, L., Du, M., Li, D., Du, X., and Xu, H. (2017). "Effects of cross section size and transverse rebar on the behavior of short squared RC columns under axial compression." *Engineering Structures.* 142, 223-239.

Junior, H. L., and Giongo, J. (2004). "Steel-fibre high-strength concrete prisms confined by rectangular ties under concentric compression." *Materials and structures.* 37(10), 689-697.

Kim, C. S., Park, H. G., Chung, K. S., and Choi, I. R. (2012). "Eccentric axial load testing for concrete-encased steel columns using 800 MPa steel and 100 MPa concrete." *Journal of Structural Engineering.* 138(8), 1019-1031.

Kottb, H. A., El-Shafey, N. F., and Torkey, A. A. (2015). "Behavior of high strength concrete columns under eccentric loads." *HBRC Journal.* 11(1), 22-34.

Kwan, A., Chau, S., and Au, F. (2006). "Improving flexural ductility of high-strength concrete beams." *Structures and Buildings.* 159(6), 339-347.

Kwan, A., and Ho, J. (2010). "Ductility design of high-strength concrete beams and columns." *Advances in Structural Engineering.* 13(4), 651-664.

Lam, J., Ho, J., and Kwan, A. (2009). "Flexural ductility of high-strength concrete columns with minimal confinement." *Materials and Structures.* 42(7), 909-921.

Lee, J. H., and Son, H. S. (2000). "Failure and strength of high-strength concrete columns subjected to eccentric loads." *Structural Journal.* 97(1), 75-85.

Leite, L., Bonet, J., Pallarés, L., Miguel, P. F., and Fernández-Prada, M. A. (2013). "Experimental research on high strength concrete slender columns subjected to compression and uniaxial bending with unequal eccentricities at the ends." *Engineering Structures.* 48, 220-232.

Li, B., Park, R., and Tanaka, H. (2000). "Constitutive behaviour of high strength concrete under dynamic loads." *ACI Structural Journal.* 97(4), 619-629.

Li, J., and Hadi, M. N. S. (2003). "Behaviour of externally confined high-strength concrete columns under eccentric loading." *Composite Structures.* 62(2), 145-153.

Lloyd, N. A., and Rangan, B. V. (1995). 'High strength concrete columns under eccentric compression', School of Civil Engineering, Curtin University of Technology.

Mander, J., Priestley, M., and Park, R. (1988a). "Observed stress-strain behavior of confined concrete." *Journal of Structural Engineering.* 114(8), 1827-1849.

Mander, J. B., Priestley, M. J., and Park, R. (1988b). "Theoretical stress-strain model for confined concrete." *Journal of Structural Engineering.* 114(8), 1804-1826.

Massone, L. M., and López, E. E. (2014). "Modeling of reinforcement global buckling in RC elements." *Engineering Structures.* 59, 484-494.

Mendis, P., Kovacic, D., and Setunge, S. (2000). "Basis for the design of lateral reinforcement for high-strength concrete columns." *Structural Engineering and Mechanics.* 9(6), 589-600.

Mendis, P., and Panagopoulos, C. (2000). 'Applications of high strength concrete in seismic regions'. 12 th World Conference on Earthquake Engineering (12WCEE), Auckland, New Zealand.

Mirza, S. A., Hyttinen, V., and Hyttinen, E. (1996). "Physical tests and analyses of composite steel-concrete beam-columns." *Journal of Structural Engineering.* 122(11), 1317-1326.

Munoz, P. R., and Hsu, C. T. T. (1997). "Behavior of biaxially loaded concrete-encased composite columns." *Journal of Structural Engineering.* 123(9), 1163-1171.

Nagashima, T., Sugano, S., Kimura, H., and Ichikawa, A. (1992). 'Monotonic axial compression test on ultra-high-strength concrete tied columns'. 10th world conference on earthquake engineering. 2983-2988.

OneSteel. (2010). "Know your steel: steel reference guide", Wollongong, NSW, Australia [www.onesteel.com].

Ozbakkaloglu, T., and Saatcioglu, M. (2004). "Rectangular stress block for high-strength concrete." *ACI Structural Journal.* 101(4), 475-483.

Pantazopoulou, S. J. (1998). "Detailing for reinforcement stability in RC members." *Journal of Structural Engineering* 124(6), 623-632.

Park, R., and Paulay, T. (1975). 'Reinforced concrete structures', John Wiley and Sons, New York, USA.

Paultre, P., Eid, R., Langlois, Y., and Lévesque, Y. (2010). "Behavior of steel fiber-reinforced high-strength concrete columns under uniaxial compression." *Journal of Structural Engineering.* 136(10), 1225-1235.

Paultre, P., and Légeron, F. (2008). "Confinement reinforcement design for reinforced concrete columns." *Journal of structural engineering.* 134(5), 738-749.

Pessiki, S., and Pieroni, A. (1997). "Axial load behavior of large-scale spirally-reinforced high-strength concrete columns." *ACI Structural Journal.,* 94(3), 304-313.

Polat, M. B. (1992). 'Behaviour of normal and high strength concrete under axial compression'. *Master of Applied Science*, Department of Civil Engineering, University of Toronto, Ottawa, Canada.

Popovics, S. (1973). "A numerical approach to the complete stress-strain curve of concrete." *Cement and concrete research.* 3(5), 583-599.

Rashid, M., and Mansur, M. (2005). "Reinforced high-strength concrete beams in flexure." *ACI Structural Journal.* 102(3), 462-471.

Razvi, S., and Saatcioglu, M. (1999). "Confinement model for high-strength concrete." *Journal of Structural Engineering.* 125(3), 281-289.

Razvi, S. R., and Saatcioglu, M. (1994). "Strength and deformability of confined high-strength concrete columns." *ACI Structural Journal.* 91(6), 678-687.

Richart, F. E., Brandtzæg, A., and Brown, R. L. (1929). 'The failure of plain and spirally reinforced concrete in compression', University of Illinois, Urbana, Ill.

Richart, F. E., Brandtzaeg, A., and Brown, R. L. (1928). "A study of the failure of concrete under combined compressive stresses", University of Illinois Bulletin No. 185.

Ricles, J. M., and Paboojian, S. D. (1994). "Seismic performance of steel-encased composite columns." *Journal of Structural Engineering.* 120(8), 2474-2494.

RILEM (1983). "Bond test for reinforcing steel. 2: Pullout test." *Recommendation RC 6, E&FN SPON*, London, 218-220.

Ros, P. S., Yazzar, S., and Calvo, A. C. (2003). "Influence of confinement on high strength concrete behavior." *Materials and Structures.* 36(7), 439-447.

Saatcioglu, M., and Razvi, S. R. (1992). "Strength and ductility of confined concrete." *Journal of Structural Engineering.* 118(6), 1590-1607.

Saatcioglu, M., and Razvi, S. R. (1998). "High-strength concrete columns with square sections under concentric compression." *Journal of Structural Engineering.* 124(12), 1438-1447.

Sato, H., and Yamaguchi, K. (2000). 'Stress-strain behavior of square confined concrete column'. Proc. 12th World Conf. on Earthquake Eng.

Shanmugam, N., and Lakshmi, B. (2001). "State of the art report on steel–concrete composite columns." *Journal of constructional steel research.* 57(10), 1041-1080.

Sharma, U., Bhargava, P., and Sheikh, S. (2007). "Tie-confined fibre-reinforced high-strength concrete short columns." *Magazine of Concrete Research.* 59(10), 757-769.

Sharma, U. K., Bhargava, P., and Kaushik, S. (2005). "Behavior of confined high strength concrete columns under axial compression." *Journal of Advanced Concrete Technology.* 3(2), 267-281.

Sheikh, M. N., and Legeron, F. (2014). "Performance based seismic assessment of bridges designed according to Canadian Highway Bridge Design Code." *Canadian Journal of Civil Engineering.* 41(9), 777-787.

Sheikh, S. A. (1982). "A comparative study of confinement models." *ACI journal.* 79(4), 296-306.

Sheikh, S. A., and Uzumeri, S. (1982). "Analytical model for concrete confinement in tied columns." *Journal of the Structural Division.* 108(12), 2703-2722.

Sheikh, S. A., and Yeh, C. (1992). "Analytical moment-curvature relations for tied concrete columns." *Journal of Structural Engineering.* 118(2), 529-544.

Sheikh, S. A., and Yeh, C. C. (1990). "Tied concrete columns under axial load and flexure." *Journal of Structural Engineering.* 116(10), 2780-2800.

Shih, T. H., Chen, C. C., Weng, C. C., Yin, S. Y. L., and Wang, J. C. (2013). "Axial strength and ductility of square composite columns with two interlocking spirals." *Journal of Constructional Steel Research.* 90, 184-192.

Shin, H. O., Yoon, Y. S., Cook, W. D., and Mitchell, D. (2016). "Enhancing the confinement of ultra-high-strength concrete columns using headed crossties." *Engineering structures.*, 127, 86-100.

Soliman, M., and Yu, C. (1967). "The flexural stress-strain relationship of concrete confined by rectangular transverse reinforcement." *Magazine of Concrete Research.* 19(61), 223-238.

Somma, G., and Pieretto, A. (2016). "Confinement effects on high strength concrete under axial load: evaluation of International Standards prescriptions." *Materials and Structures.* 49, 57-69.

Subramanian, N. (2011). "Design of confinement reinforcement for RC columns." *The IndIan Concrete Journal.* 1-9.

Suzuki, M., Akiyama, M., Hong, K. N., Cameron, I. D., and Wang, W. L. (2004). 'Stress-strain model of high-strength concrete confined by rectangular ties'.

Proceedings of the 13th world conference on earthquake engineering, Vancouver.

Thorenfeldt, E., Tomaszewicz, A., and Jensen, J. J. (1987). 'Mechanical properties of high-strength concrete and application in design'. Proc. of the Symposium on Utilization of High-Strength Concrete, Trondheim, Norway. Tapir, 149-159.

Tobbi, H., Farghaly, A. S., and Benmokrane, B. (2014). "Strength model for concrete columns reinforced with fiber-reinforced polymer bars and ties." *ACI Structural Journal*. 111(4), 789-798.

Tsai, W. T. (1988). "Uniaxial compressional stress-strain relation of concrete." *Journal of Structural Engineering.* 114(9), 2133-2136.

Wang, Q., Shi, Q., and Tao, Y. (2016). "Experimental and numerical studies on the seismic behavior of steel reinforced concrete compression-bending members with new-type section steel." *Advances in Structural Engineering.* 19(2), 255-269.

Warner, R. F., Foster, S. J., and Kilpatrick, A. E. (2007). 'Reinforced concrete basics : analysis and design of reinforced concrete structures', Pearson Prentice Hall, Frenchs Forest, N.S.W.

Weng, C., and Yen, S. (2002). "Comparisons of concrete-encased composite column strength provisions of ACI code and AISC specification." *Engineering Structures.* 24(1), 59-72.

Woods, J. M., Kiousis, P. D., Ehsani, M. R., Saadatmanesh, H., and Fritz, W. (2007). "Bending ductility of rectangular high strength concrete columns." *Engineering structures.* 29(8), 1783-1790.

Yang, K. H., and Kim, W. W. (2016). "Axial Compression performance of reinforced concrete short columns with supplementary V-shaped ties." *ACI Structural Journal.* 113(6), 1347-1356.

Yong, Y. K., Nour, M. G., and Nawy, E. G. (1988). "Behavior of laterally confined high-strength concrete under axial loads." *Journal of Structural Engineering.* 114(2), 332-351.

Zadeh, H. J., and Nanni, A. (2012). "Design of RC columns using glass FRP reinforcement." *Journal of Composites for Construction.* 17(3), 294-304.

Zhao, G., Zhang, M., and Li, Y. (2010). "Strength and behaviour of slender steel reinforced concrete composite columns." *Advances in Structural Engineering.* 13(2), 231-240.

Ziehl, P. H., Cloyd, J. E., and Kreger, M. E. (1998). 'Evaluation of minimum longitudinal reinforcement requirements for reinforced concrete columns',

Center for Transportation Research, Bureau of Engineering Research, University of Texas at Austin.